Studies on Mathematical Models for Characterizing Plume and Drift Behavior From Cooling Towers

Volume 3: Mathematical Model for Single-Source (Single-Tower) Cooling Tower Drift Dispersion

EPRI

EPRI CS-1683
Volume 3
Project 906-1
Interim Report
January 1981

Keywords:
Cooling Tower Plumes
Plume Dispersion
Multiple Plumes
Plume Model
Mathematical Model

Prepared by
University of Illinois
Urbana, Illinois
and Argonne National Laboratory
Argonne, Illinois

ELECTRIC POWER RESEARCH INSTITUTE

Studies on Mathematical Models for Characterizing Plume and Drift Behavior From Cooling Towers

Volume 3: Mathematical Model for Single-Source (Single-Tower) Cooling Tower Drift Dispersion

CS-1683, Volume 3
Research Project 906-1

Interim Report, January 1981
Work Completed, March 1980

Prepared by

UNIVERSITY OF ILLINOIS
Department of Mechanical and Industrial Engineering
Urbana, Illinois 61801

Principal Investigators
W. E. Dunn
P. Gavin
B. Boughton

ARGONNE NATIONAL LABORATORY
Division of Environmental Impact Studies
9700 South Cass Avenue
Argonne, Illinois 60439

Principal Investigators
A. J. Policastro
J. Ziebarth

Prepared for

Electric Power Research Institute
3412 Hillview Avenue
Palo Alto, California 94304

EPRI Project Manager
J. A. Bartz

Water Quality Control and Heat Rejection Program
Coal Combustion Systems Divis

ORDERING INFORMATION

Requests for copies of this report should be directed to Research Reports Center (RRC), Box 50490, Palo Alto, CA 94303, (415) 965-4081. There is no charge for reports requested by EPRI member utilities and affiliates, contributing nonmembers, U.S. utility associations, U.S. government agencies (federal, state, and local), media, and foreign organizations with which EPRI has an information exchange agreement. On request, RRC will send a catalog of EPRI reports.

NOTICE

Prepared by
University of Illinois
Urbana, Illinois
and
Argonne National Laboratory
Argonne, Illinois

ABSTRACT

This report presents a new salt-drift deposition model for single natural-draft cooling towers which has the advantages of improved theory and good performance with field data. Advantages to the model include:

1. a submodel for cooling-tower plume rise which has been calibrated and validated with laboratory and field data,
2. improved treatment of droplet evaporation which accounts for salt-concentration gradients within the drop, and
3. an option to employ a new drop breakaway criterion which allows a more continuous transition between plume and ambient environments for the drop.

The drift model performs well in terms of comparisons made of predictions to 1977 Chalk Point Dye Study data. Those data include measurements of sodium deposition flux, average diameter, number drop deposition flux, and liquid deposition flux at downwind distances of 0.5 and 1.0 km. The model is untested for distances greater than 1.0 km due to the lack of good-quality field data at those distances.

The model was developed as an improvement over existing theories which are evaluated theoretically and tested with Chalk Point data in this report. Sensitivity studies are presented which provide considerable insight as to the differences among existing formulations for droplet evaporation and droplet breakaway methods.

Blank Page

EPRI PERSPECTIVE

PROJECT DESCRIPTION

Argonne National Laboratory is performing an effort to develop, improve, and validate mathematical models of cooling tower plumes. Emphasis is being placed on prediction of visible plume trajectory and deposition of saline droplet drift from the tower. Visible plumes and saline drift are environmental impacts of cooling towers that must be considered in power plant siting studies and licensing. A validated mathematical model of plume dispersion provides the industry with the tool required to make an assessment of environmental impact of the cooling tower.

This interim report, in five volumes plus an executive summary, describes results accomplished to date:

Executive Summary--Overview
Volume 1--Review of European Research
Volume 2--Single-Source Model
Volume 3--Drift Modeling of Single Sources
Volume 4--Multiple-Source Model
Volume 5--Drift Modeling of Multiple Sources

In a continuing effort, emphasis is being placed on developing a master model that is user-oriented and designed specifically for siting and licensing studies.

PROJECT OBJECTIVES

The goal of this effort is to develop, improve, and validate mathematical models of cooling tower plume dispersion for individual and clustered mechanical- and natural-draft cooling towers. The overall goal is to provide the utility planner with a tool for studies involving the environmental impact of cooling tower plumes.

PROJECT RESULTS

A model that has been developed and validated has prediction capabilities that are superior to other available mathematical models of cooling tower plume dispersion.

For example, in 77 percent of all cases of single sources that were studied, the model predicted a visible plume rise within a specified accuracy. This was the best performance among all available models (over a dozen) that were investigated.

This effort has also produced a useful review and summary of European research on cooling tower plume dispersion (Volume 1). Workshops in the fall of 1981 and in 1982 are being planned to disseminate to the industry the computer code that is being developed.

This series of volumes should be of value to utility planning engineers concerned with the impact of cooling tower plumes on plant siting.

John A. Bartz, Project Manager
Coal Combustion Systems Division

ACKNOWLEDGMENTS

The authors of this report would first like to extend their appreciation for the cooperation of the modelers whose work was evaluated in Sections 2, 3, 4, and 7 of this report. We thank each modeler for taking the time to answer questions about his model. Special thanks go out to Dr. Steve Hanna of ATDL in Oak Ridge, Tennessee; Prof. Tom Wigley presently at the University of East Anglia in Norwich, England; Prof. Peter Slawson of the University of Waterloo in Waterloo, Ontario, Canada; Mr. Michael von Euw and Dr. Pierre Brog of Motor Columbus Consulting Engineers in Bade, Switzerland; Prof. Jorge Pena of Penn State University; Dr. Howard McLain and Mr. Mel LaVerne of Oak Ridge National Laboratory in Oak Ridge Tennessee; Mr. Steve Maas now at the Blacklands Research Center in Temple, Texas; Dr. Mike Wolf and Dr. W. George Slinn now at The Air Resources Center at Oregon State University; Mr. Ron Moore of Environmental Systems Corporation of Knoxville, Tennessee; Dr. Gunter Schrecker now at Science Applications, Inc. of McLean Virginia; and Prof. Tom Overcamp of Clemson University at Clemson, South Carolina. Their cooperation and assistance was very important to the success of our evaluation.

Also important were the people who assisted us by responding to our numerous questions concerning the Chalk Point field data. Among them were Dr. Ron Webb, Mr. Karl Wilbur and Mr. Ron Moore of Environmental Systems Corporation, Dr. Jim Meyer of the Applied Physics Laboratory in Silver Spring, Maryland and Dr. Richard Nietubicz, administrator of the Chalk Point Project.

We would also like to thank Professor Ken Beard of the Illinois State Water Survey in Urbana, Illinois for providing us with the photographs of evaporating drops used in Section 5.

We would also like to thank Dr. John Bartz of EPRI for his continued support and encouragement as technical monitor for the project. Finally, we would like to thank Dr. George McVehil for the many helpful comments and suggestions he made on a draft of this volume.

Blank

CONTENTS

ILLUSTRATIONS

SUMMARY

This report presents the development of an improved model for salt-drift deposition for single natural-draft cooling towers. Improvement is in terms of the new theoretical assumptions made along with good performance of model predictions to field data. The work is a continuation of an earlier study evaluating the state-of-the-art of drift deposition modeling.

The first part of the report (Sections 2, 3, and 4) provides an in-depth analysis and evaluation of the theory and performance of existing drift models. Predictions of ten models are compared with field data taken at Chalk Point in 1976 and 1977. The 1977 study was the Dye Tracer Study which separated salt deposition from stack and cooling-tower sources. With this latter data, we found that the ESC/Schrecker, Hosler-Pena-Pena (ANL), and Wigley-Slawson models compared most favorably with the ground-level sodium deposition flux data from the cooling tower and were generally within the error bounds of the data. However, most models predicted larger drop diameters at deposition than were measured. The ESC/Schrecker model predicted nearly within a factor of three for sodium deposition flux, liquid mass deposition rate, number drop deposition flux, and average diameter. It should be recognized that the Chalk Point Dye Study data were taken under special ambient conditions and the performance of all models tested cannot necessarily be extrapolated to significantly different environmental conditions. The 1977 Chalk Point data are also limited in the sense that only one survey was performed and only within 1.0 km from the tower. The 1976 Chalk Point data were of marginal value due to the small size samplers used. Model evaluation and improvement is best accomplished by relying on other relevant data not directly connected with the drift problem in order for significant advances to be made. We found that a separate study of each of the four component parts of a drift model (plume rise, breakaway, droplet evaporation, and droplet deposition) for possible improvements provided the best direction for improvement efforts. Chalk Point salt-deposition data could then be used for model validation purposes.

The plume rise portion of a drift model was studied in detail in Vol. 2 and the model developed there is sufficiently validated and calibrated to laboratory and

field data for use in drift predictions. That model serves as the plume rise portion of our improved drift model.

We carried out much work to evaluate and improve existing models' formulations for droplet evaporation. First, six formulations commonly used in predicting drift droplet evaporation were evaluated in terms of simplifying approximations made. The fundamental theory of droplet evaporation in an unsaturated atmosphere is reviewed and the different treatments of evaporation used by the models are compared with the exact formulation. The major discrepancies arise due to approximations to the droplet temperature. The best (nonexact) treatment of droplet evaporation of those tested is Mason's equation (employed in the Overcamp-Israel and Wigley-Slawson drift models) yielding differences from the exact solution which are generally less than 20%. The worst is the case of the drop temperature taken equal to the ambient dry-bulb temperature (employed in the Hanna drift model) yielding evaporation rates consistently too large by about 130%.

To determine the range of differences between the predictions of existing evaporation submodels, a sensitivity study comparing droplet trajectories was made for a hypothetical case of a salt-containing drop released from a fixed height. It was found that (a) significant differences can exist among model predictions of distance to deposition, final diameter and final settling velocity, (b) these differences are generally smaller for the larger drop sizes, (c) model predictions are quite sensitive to changes in relative humidity at relative humidities above 70%, but are fairly insensitive to changes below this value, and (d) larger ambient temperatures and lower drop salt concentrations lead to larger distances to deposition. That sensitivity study also revealed that initial drop diameter is the most important parameter in determining deposition history. Ambient relative humidity is important in determining the final state of the smaller drops. General rules of thumb are provided for extreme behaviors such as deposition with little evaporation and deposition after near instantaneous evaporation.

In all existing methods studied, the effect on drop evaporation of salt concentration gradients in the drop was not treated. Without such treatment, evaporation rates may be incorrectly computed and the final size of the droplet (after complete evaporation) may be wrongly determined.

Based upon the knowledge gained in the above-mentioned comparisons of existing evaporation submodels, we undertook the development of an improved analysis of

drop dynamics and thermodynamics which serves as a basis for our drift model (Section 5). Starting from sound physical principles and calling upon previous experimental studies of drop evaporation, we have developed an analysis which avoids the arbitrary simplifications inherent in most of the earlier models. Important features of this model are: (a) it treats all the dynamic and thermodynamic phenomena characterizing an evaporating drop, (b) it uses proven correlations for heat and mass transfer coefficients, (c) all properties are considered to be temperature, and if appropriate, salt concentration or vapor concentration dependent, (d) it considers salt gradients internal to the drop and their effects on evaporation, precipitation, and desiccation, and (e) the drop model permits fully three-dimensional ambient conditions to be utilized. For drops reaching their final state, the present model predicts the point of deposition further from the tower than any of the other existing models tested, owing to the fact that the final state is actually a porous particle that is hollow inside (an effect of salt gradients within the drop) instead of a commonly-assumed solid crystalline particle.

The third area of detailed evaluation and improvement is the treatment of droplet deposition (Section 6). A number of drift models employ the Ballistic-Gaussian approach to handle droplet dispersion in a field of ambient turbulence. Our study of those deposition formulations shows that most are unvalidated, do not conserve mass, and do not give the correct qualitative behavior when parameters such as wind speed are changed. Considering the above deficiencies in the available deposition formulations, the following advancements and improvements have been made: (a) a basic nondimensionalization of the deposition problem has been developed which reduces the number of parameters that must be considered and has allowed clearer insight into the effects of different variables and the problems with existing models, (b) a Monte Carlo simulation has been developed which will serve as a standard of comparison, and (c) a sensitivity study has been carried out with the Monte Carlo model in order to gain insight into the effect of non-dimensional parameters on deposition patterns. Our drift model will continue to employ the Ballistic approach until work on a cost-effective and accurate Ballistic-Gaussian methodology can be completed.

The fourth major part of a drift model that was analyzed in detail is the treatment of drop breakaway (Section 7 and 8). Four breakaway methods from the literature were identified and a fifth was developed by us. Our new method provides a continuous transition between plume and ambient environment for the drift drops.

Our single-tower NDCT plume model was coupled with our improved drop evaporation formulation allowing breakaway by any of the five methods under study. A sensitivity study was carried out to determine the differences among the five methods in predictions of breakaway location and deposition distances for individual drops (Section 7). We found that the five breakaway criteria tested provided significantly different predictions of droplet breakaway locations and resulting drop deposition distances for the intermediate range of droplet sizes, 100-850 μm. The breakaway criteria are least sensitive for the smallest (D_o < 100 μm) and largest droplets (D_o > 850 μm). Other than initial droplet size, the second most important parameter in determining breakaway location and deposition distance is ambient wind speed, not only on its effect on the plume (and therefore the drop), but also its effect on drop trajectory after breakaway. Two of the five criteria tested showed a level of insensitivity to some important variations such as ambient profile chosen (neutral, unstable, or stable) and wind speed.

We then completed our drift model by combining our single-tower NDCT plume model to our new droplet evaporation formulation for all drops (tentatively allowing all of the five breakaway criteria) and employing the Ballistic method for deposition. In this way, we could test the complete drift model with field data using any of the five breakaway criteria. The model was tested against the 1977 Chalk Point Dye data by running the model five times, once with each of the five breakaway criteria (Section 8). Results were tabulated and compared to field data for sodium deposition flux, liquid mass deposition flux, number drop deposition flux, and average diameter. Two of the five breakaway criteria which appeared most physically justifiable (from the sensitivity study) provided the best performance with the field data. The new method noted above performed as well as the "radius" criterion used in a number of existing models. It is the radius criterion, however, which is used in both our single and multiple-source drift models. The new method is presently an option only in our single-source drift computer code.

Section 1

INTRODUCTION

This report presents work carried out to improve mathematical models for salt-drift deposition from single natural-draft cooling towers. The objective of this portion of our overall study is twofold:

1. to assess the correctness of the assumptions made in the presently available models of drift deposition, and

2. to develop, through improvement of the best existing models, a new model which has strong theoretical support and which can accurately represent the range of experimental data available.

This work began as a continuation of the U.S. NRC sponsored work to evaluate the state-of-the-art of drift deposition modeling (1). The results of the earlier NRC study available as input to our work here were:

1. Field data on drift deposition at the Chalk Point cooling tower (1975 and 1976), organized in a common format and documented in sufficient detail for model verification.

2. Computer codes for the numerous (10) available models for drift dispersion, each operational at the ANL Computer Facility with input/output formats consistent with the data bank organization.

3. Comparisons of model predictions with field data and an evaluation of the applicability and adequacy of the models as currently formulated.

4. Limited sensitivity studies establishing the sensitivity of model predictions to uncertainties in measured input data.

5. A state-of-the-art report on drift modeling (1).

As can be seen, our previous model validation program was a natural first step toward the ultimate goal of generating a viable drift deposition model.

Our model improvement program began with a deeper investigation into the existing theories to determine areas best suited for improvement. Section 2 provides a

review of the existing theories of drift dispersion along with a review of model/data comparisons to 1975 and 1976 Chalk Point data.

Section 3 provides a detailed evaluation of the various droplet evaporation formulations employed in existing drift models. As will be seen, most employ simplifying assumptions which are not appropriate for drift droplet dispersion applications. Also, no methods treat the important effects of salt-concentration gradients within the drop.

Section 4 updates the previous validation work by testing the existing drift models with the present high-quality field data taken during the 1977 Chalk Point Dye Study. In addition, an analysis of the field data is undertaken.

Section 5 presents our improved droplet evaporation submodel. That model avoids the arbitrary simplifications inherent in most of the earlier models. Also, the model accounts for salt-concentration gradients in the drop which leads to the conclusion that drops which reach their final state in the evaporation process fall further from the tower than predicted by any of the other existing models; this conclusion results from the fact that the final state is actually a porous particle that is hollow inside (and of lower settling velocity) instead of a commonly-assumed solid crystalline particle.

Section 6 provides a study of the various deposition formulations in current use which aim at accounting for the effect of ambient turbulence on the trajectory and fall of drift droplets. It is found that most existing models are unvalidated, do not conserve mass, and do not always give the correct qualitative behavior when key parameters are varied.

Section 7 presents our drift model in which the ANL single-tower plume model is combined with our new evaporation submodel through different breakaway criteria. This section presents a sensitivity study which helps us to assess the effect different choices in breakaway criteria have on drop trajectory, distance to deposition, and drop size upon deposition. A new breakaway method is also introduced which provides a continuous transition between plume and ambient environments for droplets.

Section 8 compares predictions of our drift model (under different breakaway methods) to the 1977 Chalk Point Dye Data. The two breakaway methods with the

greatest physical appeal perform best. One of them, the "radius" criterion, was chosen for our single and multiple-source drift model due to its simplicity in application. The new breakaway method (which is one of the two) is our option in our ANL single-source drift model.

As will be seen, we have followed two basic points of philosophy in this report. First, the amount of high-quality field data available to test drift models are not extensive and are available only at ground level. As a consequence, we cannot make final judgements on specific modeling assumptions (such as plume rise, drop evaporation rates, etc.) solely from the available ground-level field data. Thus we concentrated our efforts to improve the four basic submodels of a drift model (plume rise, breakaway, drop evaporation, and deposition) separately through special studies and special data related indirectly to the drift problem in order to provide improved submodels. The Chalk Point data were then used only for validation (and not calibration) of the resulting model. The second point of philosophy relates to the fact that the high-quality field data from Chalk Point are at or within 1 km from the tower. No high-quality data exist at further distances. As a result, we must rely on theoretical considerations alone for such phenomena (drop dynamics/thermodynamics, ambient turbulence effects, etc.) which have effects at larger distances downwind than 1 km, until field data at those large distances are acquired.

REFERENCES

1. A. J. Policastro, W. E. Dunn, M. Breig, and J. Ziebarth. Evaluation of Mathematical Models for Characterizing Plume Behavior from Cooling Towers. Vol. 2. Salt Drift Deposition from Natural Draft Cooling Towers. U.S. Nuclear Regulatory Commission Report NUREG/CR-1581. February 1979.

Section 2

EVALUATION OF THEORY AND PERFORMANCE OF SALT-DRIFT DEPOSITION MODELS FOR NATURAL DRAFT COOLING TOWERS

This section reprints a paper we presented in May 1978 which provides a review of the formulations of existing drift models. These models are similar in development consisting of four components: plume rise, drop breakaway, drop evaporation, and effects of atmospheric turbulence. The models are also tested with the field data acquired at the Chalk Point cooling tower during 1976. The Chalk Point data taken in 1975 and 1976 by the Environmental Systems Corporation were mainly of qualitative value, because the ground-level samplers were too small in size and few in number and because stack and cooling tower contributions could not be distinguished. Comparisons of model predictions to the 1976 field data showed the ESC/Schrecker, Wigley-Slawson, Wolf I, Wolf II, and Overcamp-Israel Models performing most favorably. Sections 3 and 4 provide additional perspective on these results.

This validation work identified two important areas of needed model improvement. They were:

1. use of a plume model which accounts for full vertical ambient profiles of environmental variables. The plume model should be validated with plume rise data from cooling towers. The Briggs-type formulas are less desirable since (a) the formulas cannot account for local variations in ambient profiles, and (b) the formulas are developed from a theory which required special simplifications to provide a closed-form solution.

2. preparation of predictions are based on 10-min. or 30-min. averages of meteorological conditions. It has been common to average, say 4 hours of ambient conditions to provide one set of model input conditions for a single run of the model. Such treatment does not account for true ambient wind direction variations during a 4-hour period. Model calculations for each of 24 10-min. sub-periods or 8 30-min. sub-periods with a summation of results for each sampler provided a much closer representation of the actual distribution of ground measurements.

This paper also identifies two drift modeling areas in particular which are quite difficult to evaluate since specialized data are lacking. They are:

1. The breakaway criterion is defined in many different ways, yet no measurements are available to test alternative definitions. Complexities involve simulating the turbulent buoyant environment of the drop while in the plume and the effect of the wake of the tower on the motion of the plume. Clearly, from Section 4, the models were found to predict drop sizes upon deposition that were generally significantly larger than observed drop sizes. This systematic behavior implies that presently employed drop breakaway criteria are not permitting small drops to break from the plume early enough.

2. Droplet deposition in the presence of atmospheric turbulence should account for the local evaporation occurring for the drop. The models which account for atmospheric turbulence (Ballistic-Gaussian Models), important for the smaller drops, do so with a formulation that assumes a fixed drop size during dispersion. The deposition formulations are taken from the air pollution literature; they ignore local drop evaporation and attempt to correct this by using the "average" drop size during fall. The value of this simplification (made in all Ballistic-Gaussian models) is difficult to assess. We indeed can compare the various solutions of the convective-diffusion equation used by the models (for fixed size particles) and determine a superior formulation, yet the basic issue is the validity of that convective-diffusion equation in the first place in treating droplets which are evaporating as well as dispersing due to ambient turbulence.

Reprint of Paper #1:

"Evaluation of Theory and Performance of Salt-Drift Deposition Models for Natural-Draft Cooling Towers"

Anthony J. Policastro
William E. Dunn
Marvin Breig
Michael Ratcliff

Proceedings, Environmental Effects of Atmospheric Heat/Moisture Releases. Cooling Towers, Cooling Ponds, and Area Sources. Presented at the Second AIAA/ASME Thermophysics and Heat Transfer Conference. Palo Alto, California. May 24-26, 1978. Eds. Kenneth Torrance and Robert S. Watts. ASME publication. 1978.

EVALUATION OF THEORY AND PERFORMANCE OF SALT-DRIFT DEPOSITION MODELS FOR NATURAL-DRAFT COOLING TOWERS

Anthony J. Policastro
Division of Environmental Impact Studies
Argonne National Laboratory
Argonne, Illinois

William E. Dunn, Assistant Professor
Department of Mechanical and Industrial Engineering
University of Illinois at Urbana-Champaign
Urbana, Illinois

Marvin Breig*, Professor
Division of Environmental Impact Studies
Argonne National Laboratory
Argonne, Illinois

Michael Ratcliff
Division of Environmental Impact Studies
Argonne National Laboratory
Argonne, Illinois

ABSTRACT

Significant variability exists among the predictions of various mathematical models formulated to predict drift-deposition patterns surrounding large natural-draft cooling towers. This paper provides insights into which of the alternative formulations give the best results, although, in comparisons with field data acquired recently at the Chalk Point Power Plant, none of the existing models performed well. Areas for future improvement are identified.

NOMENCLATURE

A = a constant used in formulation of buoyancy flux,

C = volumetric drop concentration,

D = diffusivity of water vapor in air,

f(Re,Pr) = ventilation factor,

F_o = initial buoyancy flux,

g = acceleration of gravity,

H = release height,

i = Van't Hoff factor,

k = thermal conductivity of air,

K_y,K_z = eddy diffusivity for droplet transport,

L = latent heat of vaporization,

m = mass of solute in drop,

M_o = molecular weight of water,

M = molecular weight of salt,

p = pressure or vapor pressure,

Pr = Prandtl number,

r = drop radius,

R_o = tower radius,

R = gas constant,

Re = Reynolds number,

Sc = Schmidt number,

T = temperature,

U = wind speed,

V_d = deposition velocity,

V_s = settling velocity,

x,y,z = x downwind distance from tower; y lateral distance from x axis; z vertical distance from ground,

γ = entrainment coefficient,

σ = surface tension,

ρ = density,

ω = mixing ratio,

Subscripts

o = at tower top,

p = plume,

e = environment,

* = nondimensional value,

ℓ = liquid state,

v = vapor state.

*Permanent Address: Department of Physics, Eastern Illinois University, Charleston, IL 61920.

INTRODUCTION

Drift refers to the small droplets of liquid water released from a cooling tower along with the warm, moist plume. These droplets, ranging in size from a few to more than 1000μm in diameter, are transported through the atmosphere eventually evaporating totally or being deposited on the ground. If the droplets contain large concentrations of dissolved solids, as is particularly the case when brackish cooling water is used, then the drift deposition can damage vegetation and/or accelerate the corrosion and deterioration of structures. Therefore, predictions of anticipated drift-deposi-

tion rates are essential to an informed estimate of the environmental impact of a plant for which cooling towers are planned.

Once emitted from the tower, a drift drop moves under the combined influences of gravity and the aerodynamic drag force produced by the vector difference between the drop and local air velocities. Simultaneously, the drop experiences both heat and mass transfer. As a result, the drop temperature will approach the local wet-bulb temperature and evaporation will occur as long as the vapor pressure at the drop surface exceeds that of the local ambient. For a drop containing salt, evaporation will increase the concentration within the drop and thus lower the vapor pressure at the drop's surface. The salt concentration will continue to increase until either (a) the droplet vapor pressure exactly equals that of the local ambient after which evaporation will cease or (b) the salt becomes saturated within the drop after which salt particles will begin to precipitate out as evaporation proceeds. In the latter case, the drop will eventually become a dry particle, although it may strike the ground before reaching its final state. The purpose of a drift model, then, is to predict the number, size, and character of drops and/or particles striking the ground at any given location with respect to the emitting tower.

Numerous mathematical models have been formulated to predict drift plumes and drift-deposition patterns. However, the limits of reliability of these models is largely unknown since different models, even models that are conceptually similar, can give vastly different predictions of deposition rates. This paper provides a perspective on this issue by (1) reviewing alternative formulations to determine the level of approximation in each of the physical treatments; (2) determing the sensitivity of model predictions to differing assumptions and to changes in the input data; and (3) comparing model predictions with field data taken at the Chalk Point Power Plant located on the saline Patuxent River in Maryland.

EVALUATION OF MODEL FORMULATIONS

The features of the 11 models (1-9) considered in this paper are summarized in Table 1. Here, the models are divided according to whether their basic approach is ballistic, Gaussian, or ballistic-Gaussian. A model is classed as ballistic if only the influences of a steady wind, the plume updraft and the acceleration of gravity are considered. In contrast, Gaussian models treat the drift droplet concentration as a continuous variable satisfying a convective-diffusion conservation equation. Models are said to be ballistic-Gaussian if they combine a deterministic analysis of drop settling and advection by the wind with a Gaussian plume model to account for dispersion by ambient turbulence.

For convenience in discussion, the usual drift model can be broken down into four basic submodels which are labelled plume rise, breakaway, evaporation, and deposition in Table 1. We shall consider each of these individually.

Plume Rise

Predictions of plume dispersion are important in the calculation of drop dynamics, since a droplet's behavior depends on the local velocity, temperature and humidity fields which the drop encounters during its lifetime. Most models employ the Briggs plume rise formula (10) as modified by Hanna (15) for the prediction of plume trajectory and maximum plume rise. The Briggs formulae are an approximation to the closed-form solution of integral conservation equations, assuming that the plume moves horizontally at a vertically uniform wind speed and that the initial vertical velocity and initial plume radius are both zero. The Overcamp-Israel model employs a similar closed-form entrainment model for plume rise with a major difference being that the tower is a finite source of buoyancy and momentum rather than a point source of buoyancy as assumed by Briggs. Hanna, in his own drift model, employs different formulations of the Briggs theory for the calculation of different plume characteristics (see Table 1). In each of the above plume-rise treatments in the drift models, the atmosphere is assumed to have a uniform temperature gradient and the wind is idealized as uniform over the height of the plume. The key parameter in the Briggs/ Hanna-type analyses is the initial buoyancy flux F_o, which in general form can be written as

$$F_o = g R_o^2 W_o (T_{po} - T_{eo})/T_{po} + AL(\omega_{po} - \omega_{eo})/T_{po}$$

where R_o is the tower exit radius, W_o is the plume exit velocity, T_{eo} is the ambient dry-bulb temperature (at tower top), L is the latent heat of vaporization, ω_{po} is the plume exit mixing ratio, ω_{eo} is the ambient mixing ratio (at tower top), T_{po} is the plume exit temperature, and A is a constant. The first term represents the sensible heat component of the buoyancy flux, whereas the second term represents the latent heat contribution. In the drift models, three distinct interpretations are employed as follows:

a) A = 0 and T_{po} taken to be the dry-bulb temperature at exit. This method, yielding the lowest value of F_o, is that appropriate to dry plumes for which the Briggs formulae were originally developed. (The Hosler-Pena-Pena model uses this formulation).

b) A = 0 and T_{po} taken to be the virtual temperature of the plume at exit. This approach which represents an attempt to account for the smaller molecular weight of water vapor relative to dry air gives an increased value of F_o over (a) above. (The ORFAD, Wolf I, II, Hanna and Overcamp-Israel models use this formulation).

c) A ≠ 0 and T_{po} defined as the dry-bulb temperature of the plume at exit. This form gives too much buoyancy since the latent heat content of the plume is assumed to contribute fully to the buoyancy flux. (The MRI model uses this formulation with A = 1).

One major problem in the use of the Briggs/ Hanna-type formulae is that their simplicity requires much schematization of the ambient atmosphere in terms of temperature, humidity, and wind speed. The vertical variation in these quantities is often an important factor in determining plume characteristics. Even if one uses a vertical average over the height of the plume, such an average is difficult to calculate since the height of the plume is not known, a priori. Iterative schemes in which the plume heights and vertical averages are alternately calculated do not always converge.

A second problem of the Briggs/Hanna-type plume rise formulae is that the familiar "2/3-law" leads to an infinite updraft velocity at the tower. This singularity is due to the assumption that the

tower is a point source. One can avoid this difficulty by using the more complete expression

$$W_* = (W_{*_o} + F_{*_o} x_*)/(1 + W_{*o} x_* + F_{*o} x_*^2)^{2/3}$$

where $W_* = 3\gamma W/U$, $F_{*o} = 3\gamma F_o/U^3 R_o$, $x_* = x/R_o$, and W is the updraft velocity, U is the ambient wind speed, x is downwind distance, R_o is the tower exit radius and γ is the entrainment coefficient. Here, the tower is assumed to be a finite source of both momentum and buoyancy. Since F_{*o} is typically large, the above expression will quickly approach the value given by the 2/3-law for $x_* > 0$.

Two of the 11 drift models (Wigley-Slawson and ESC/Schrecker) numerically solve integral conservation equations for momentum and vapor rather than relying on formulae of the Briggs/Hanna type in an attempt to obtain a more accurate prediction of plume centerline trajectory and radius. Plume predictions such as these that can account for the vertical inhomogeneities of the atmosphere are generally preferred, although the Briggs equations do have the advantage of having been calibrated against dry plume data.

Breakaway

Droplets emitted from the tower initially move within the plume but eventually leave the plume influence and move in very nearly ambient air. Although it is not presently known exactly how this transition occurs, the usual treatment is to assume that the drift droplets are contained "within the plume" until a certain criterion, called the "breakaway criterion", indicates that they have "broken free" and are traveling through ambient air. Within this conceptualization, three major criteria are used to indicate drop breakaway as follows:

a) A drop breaks free when the updraft velocity at the plume centerline reduces to the drop settling velocity.
b) A drop breaks free when it has fallen, as a result of its settling velocity, a vertical distance below the centerline equal to the local plume radius.
c) A drop breaks free when its horizontal displacement from the plume centerline equals the initial plume radius.

In reality, breakaway is a very difficult problem. First, because drop settling velocities are low relative to the windspeed, small uncertainties in the droplet release height translate into very large differences in the deposition distance. Moreover, since the drops are typically evaporating as they fall, the type of drop striking the ground will be incorrectly predicted if the breakaway height is wrong. The treatment of breakaway is an important area for model improvement; however, there do not appear to be any clearly superior formulations at this time.

Evaporation

As a drift droplet moves first within the plume and then within the ambient, it experiences heat and mass transfer by virtue of vapor concentration and temperature differences between the drop surface and the local environment. Table 2 gives the three evaporation equations most commonly used.

The Fröessling equation (16) applies to droplet evaporation in an unsaturated atmosphere where the droplet temperature is approximately represented by the local ambient wet-bulb temperature. The Fletcher (17) and Mason (18) equations were developed for and are thus applicable to drop formation inside clouds. As a result, these equations were obtained under the assumptions of a very nearly saturated ambient and a small salt concentration within the drop. These assumptions are unrealistic for drift drops which usually move through subsaturated ambients and which often evaporate to dry particles or saturated-solution drops. Additional simplifications are made in the use of these equations by individual drift models. For example, several models ignore the temperature dependence of the transport and material properties (density, viscosity, etc.). Our experience is that this omission can lead to poor predictions of evaporation rates (all else being equal), particularly in the case of the mass diffusivity.

Three of the models considered here (Hosler, Pena, and Pena; ORFAD; and MRI) use the concept of equilibrium height as put forth by Hosler, Pena, and Pena to avoid a step-by-step numerical integration of the evaporation equation. Hosler, et al., integrated the approximation equations of Fletcher (17) for four different drop sizes, four different relative humidities and eight different ambient temperatures. These results were then summarized in terms of the equilibrium height h_e, which is defined as the height that a droplet falls before reaching its final radius. In the application of these results, the drop is assumed to decelerate uniformly from its initial settling velocity to its final velocity over a height of h_e. Under this assumption, the drop lifetime can be computed from simple kinematics and the downwind distance to deposition calculated as the product of that time with the wind speed. The advantage of this approach is that numerical calculations are simplified to the point at which they can be carried out by hand. It is doubtful whether the accuracy loss is justified, however, since computer codes are generally used in practice to make drift deposition calculations.

In order to calculate h_e, it is necessary to first determine the final drop disposition. Since the equilibrium relative humidity over saturated aqueous sodium chloride solution is roughly 76 percent, drops will eventually become dry salt particles in atmospheres of relative humidity less than this value. At relative humidities above 76 percent, the drop will evaporate (or acquire liquid water) until its vapor pressure (governed by its salt concentration) equals the ambient value. Since a drop may not have reached its equilibrium state before deposition, Hosler, Pena, and Pena give the following suggestions for use in practical calculations.

a) At ambient relative humidities above 90 percent, consider that the drop does not evaporate at all.
b) At ambient relative humidities below 90 percent but above 65 percent, consider that the drop is saturated solution at final velocity.
c) At ambient relative humidities below 65 percent, consider that the drop becomes a dry salt particle.

Clearly, these categories are only approximate.

We developed a computer code to independently confirm Hosler's calculations of h_e, from which we found

a) The criterion one uses to cut off the integration is important in the determination of h_e. We chose the equilibrium height to be the actual droplet fall distance when it

Table 1 Summary of Drift Model Formulations

MODEL	PLUME RISE		BREAKAWAY	EVAPORATION				DEPOSITION
	formulation	buoyancy flux		temperature dependent coefficients?	solute effects	time dependent aspect	saturated solution drops and dry particles?	formulation
Ballistic								
Hosler, Pena and Pena (1)	Briggs (10)	Sensible	A+++	Yes	DSA+	h_e concept	Yes	uniform over sector average
ORFAD (2)	Briggs (10)	Sensible-virtual	none	No	DSA+	h_e concept	Yes	"
Wolf I (3)	**Briggs (10)**	**Sensible-virtual**	C	No evaporation assumed				uniform over sector of size dependent on wind direction variation
Wolf II (3)	Briggs (10)	Sensible-virtual	C	Yes	No	interpolation of Beard-Pruppacher tables (14)	No	
Slinn I (4)	None	-	at tower	No evaporation assumed				uniform over sector average
Hanna (5)	Briggs*	Sensible-virtual	B	No	Yes	direct integration	Yes	"
Wigley-Slawson (6)	Wigley-Slawson (12)	-	B	No	No	direct integration	No	"
MRI (7)	Briggs (10)	Sensible + latent	A	No	DSA+	h_e concept	Yes	"
Gaussian								
Slinn II (4)	-	-	at max plume rise(500m)	No	No	instantaneous	dry particles only	source-image
Ballistic-Gaussian								
LSC/ Schrecker (8)	Winiarski-Frick (13)	-	A	some	Yes	direct integration	Yes	source only
Overcamp-Israel (9)	Simple closed-form integral entrainment model (assuming finite source)++	Sensible-virtual	A	No	Yes	direct integration	saturated solution drops only	image depletion

* Briggs 2/3 law (tower is point source of buoyancy) is used to determine downwind location of maximum plume rise but the formulation treating the importance of momentum and buoyancy (tower is point source of momentum and buoyancy) in the near-field plume is used to calculate centerline trajectory and upward velocity at the centerline (11). Plume radial growth used for drop breakaway is calculated assuming the tower is a finite source of buoyancy.

\+ Dilute solution approximation (DSA) assumes that the solute mass is much less than the droplet mass (See Table 2).

++ The maximum plume rise is calculated from (a) Briggs' neutral stability formula (10) for neutral and unstable conditions. or (b) the maximum of Briggs' neutral and stable condition formula (10) when stable ambient conditions occur.

+++ Categories A, B, and C for breakaway are discussed in text.

differs by more than 2% from the product of the total time of evaporation and the average fall velocity. This definition represents the philosophy of approximating the settling velocity versus fall height curve by two straight line segments. We found that different "reasonable" choices for cutting off the direct integration of the evaporation equation could give differences in h_e of up to 100 percent.

b) The Hosler graph for h_e was not entirely accurate since the time step used by Hosler, Pena, and Pena in their integration of the evaporation equation was too large. Our calculations in double precision arithmetic and with very small time steps indicated that the correct h_e is typically 27 percent larger than the published results.

c) Hosler's assumption that the same temperature correction factors apply for any relative humidity and initial drop size was not totally correct. Differences to 20 percent were found.

d) The dilute solution approximation is adequate only at lower relative humidities, where the Fletcher equation itself is suspect.

e) The h_e concept does not allow for vertical variation in ambient relative humidity and temperature which can produce errors in predictions of drop evaporation. Direct integration of the evaporation equation for each droplet can easily treat the effects of an inhomogeneous environment.

Our calculations of h_e (at 20C) given in Table 3 were obtained using a time step of 0.1 sec which is small enough to provide a time-step-size independent solution of the evaporation equation. Also given in Table 3 are h_e values obtained using the interpolating formulae of the ORFAD and MRI models.

In order to better define the differences among the various formulations for evaporation and settling, we developed a computer code to determine the trajectory of a drop released from a given height as predicted by each of the models under consideration. As a standard case, we chose a release height of 200m, a uniform wind speed of 4 m/s, a relative humidity of 70 percent, an ambient temperature of 10C and an initial salt concentration of 0.005 g-NaCl/g-solution. From this standard case, each of the significant parameters could be varied.

The results of the standard case prediction are given in Fig. 1. Plotted on the z axis is height above the ground. The x axis corresponds to the downwind distance and the curves represent droplet trajectories as predicted by the various models. Note that large differences exist in the models' predictions of final deposition distance. Note also that each trajectory can be divided into two parts--the first encompassing evaporation of the droplet to final size, and the second encompassing transport at final size, with no evaporation. Since no evaporation occurs in the second segment, drop transport follows a straight line of slope V_s/U where V_s is the final droplet settling velocity. It can be seen that the Hanna drop evaporates most rapidly for this case. An interesting feature here is that if all models had employed the same formula for final settling velocity (dry particle: Hanna, ESC/Schrecker; saturated droplet: Overcamp-Israel, HPP), those straight line segments would be parallel. Clearly, they are not; this is a result of the

Table 2 Droplet Evaporation Equation from Froessling, Fletcher, and Mason

Froessling (16): ... used in the Hanna, Wigley-Slawson, and ESC/Schrecker drift models

$$r\frac{dr}{dt} = D\frac{\rho_v}{\rho_L}\left(\frac{p_a - p_d}{p_a}\right) f(Re,Pr)$$

Fletcher (17): ... used in the h_e concept by Hosler, Pena, and Pena; ORFAD; and MRI drift models

$$r\frac{dr}{dt} = D\frac{\rho_v}{\rho_L}\frac{p_a - p_d}{p_a}(Re,Pr)\cdot\left[1 + \frac{D L^2 \rho_v M_o f(Re,Sc)}{R T^2 k f(Re,Pr)}\right]^{-1}$$

Mason (18): ... used in the Overcamp-Israel drift model

$$r\frac{dr}{dt} = \frac{\frac{p_a - p_d}{p_a} f(Re,Pr)}{\frac{L\rho_L}{RT}\left(\frac{L M_o}{RT} - 1\right) + \frac{P M_o}{p_s}}$$

$$p_d = p_s \exp\left[\frac{2\sigma M_o}{\rho_L RTr}\right]\left[1 + \frac{3i\,m\,M_o}{4\pi\rho_L r^3 (M - m)}\right]^{-1}$$

(where p_s denotes saturation vapor pressure)

$$\approx p_s\left[1 + \frac{2\sigma M_o}{\rho_L RT}\left(\frac{1}{r}\right) + \frac{3i\,m\,M_o}{4\pi\rho_L M}\left(\frac{1}{r^3}\right)\right]$$

(Dilute Solution Approximation)

In the Froessling equation, the drop temperature is represented by the ambient wet-bulb temperature while in the Fletcher and Mason equations, the drop temperature is taken to be the ambient dry-bulb temperature. However, in the Hanna and Wigley-Slawson application of the Froessling equation, the drop temperature was taken to be the ambient dry-bulb temperature.

Table 3 Comparison of h_e obtained from Hosler, Pena and Pena; ORFAD; and MRI Model with h_e from the Corrected Calculations (all calculations done at 20 C with C = 0.05 g/g)

RH (%)	Initial Droplet Radius (μm)	h_e (HPP) (m)	h_e (ORFAD) (m)	h_e (MRI) (m)	h_e (HPP')+ (m)	Error (%)++
90	50	17*	20	20	14	21
	100	130	127	121	145	9
	200	900	807	753	1160	22
	300	2200	2579	2195	2640	17
70	50	4*	6	6	5	20
	100	40	38	36	50	20
	200	290	239	225	347	31
	300	800	705	656	912	12
50	50	2*	3	3	3	-
	100	20*	22	21	33	33
	200	170	137	129	217	37
	300	400	405	374	570	29
30	50	1*	2	2	3	33
	100	10*	15	14	29	48
	200	100	95	89	191	50
	300	300	280	259	502	44

*Extrapolation necessary from graph of h_e from Hosler, Pena, and Pena.

+HPP' = HPP-corrected

++Error = $[(h_e)_{HPP} - (h_e)_{HPP'}]/(h_e)_{HPP'}$.

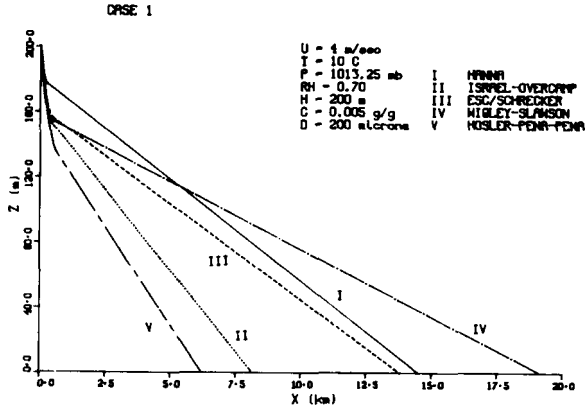

Fig. 1 Comparison of evaporation predictions for five drift deposition models for standard case

different expressions employed for settling velocity of saturated drops and dry particles used in the models. Notably, evaporation is completed rather rapidly--within the first 70m of fall.

Another interesting feature is that although the drop spends much of its time in its final state, the vertical position of the droplet when it first reaches final size is important in determining the final horizontal deposition distance. An example is the comparison of the HPP and Overcamp-Israel model predictions of final deposition distance (HPP: 6.2 km, O/I: 8.1km). Although each predicts evaporation to a saturated drop, the height of fall to saturation of the O/I drop is 48m while HPP predicts 66m. The difference in vertical height may appear small but it produces a difference in deposition distance of 1.9km. The large distance separating the HPP and O/I drops on the ground is the result of the large ratio of wind speed to saturation drop settling velocity acting on the O/I drop after the HPP drop has struck the ground. The difference in deposition distance becomes even more significant when dry particles are formed in the evaporation process. Thus, the vertical position of the droplet when evaporation is completed is very important in determining the downwind deposition distance. The need for accuracy in droplet evaporation rates is underscored by the above example.

Two areas thus seem very important in defining final drop variables (deposition distance, final diameter, and deposition velocity).

1. Droplet position and size at the end of droplet evaporation and
2. Droplet settling velocity during transport at final size.

The above observations on Case 1 apply to the other test cases as well.

Although Fig. 1 presents the results of droplet evaporation and kinematics for an emission height of 200m, the figure itself can be viewed as a sensitivity study to height of emission. For example, for a 50m height of emission, one simply views the vertical region from 200m to 150m. Deposition distances, diameters, and settling velocities are those at the 150m level (50m of fall).

The results of our study of evaporation formulations can be briefly summarized as follows:

a) The effect of increasing the salt concentration by a factor of 10 is to decrease the deposition distance by about four-fold and approximately double the final drop size. The relative distances to deposition among the models is altered, however, since assumptions on the final fate of the droplets differ. A wide variation in final drop diameter was noted.
b) Initial diameter has very significant effects. For the 1000μm drop, settling dominates over evaporation. As a result, the variation among model predictions is small and deposition is very close to the tower. For small drops in which evaporation is important, there are wide variations in final diameters and deposition distances. The final size of the droplet depends on whether the model considers the final fate to be a dry particle or a saturated solution droplet. Smaller droplets fall further from the tower due not only to their smaller initial settling velocity but also because the dry particle formed is smaller and thus has a lower settling velocity.
c) At relative humidities below 50 percent, model predictions are fairly insensitive to changes in humidity. At relative humidities above about 70 percent, predictions were seen to be quite sensitive; a wide variation in final droplet size was also seen.
d) Larger ambient temperatures produce greater distances to evaporation. This is due to the effects of temperature on saturation vapor pressure at the drop surface. Models that include the temperature dependency of the transport properties showed even greater variation.

It can be concluded that there are significant variations in models' predictions for identical conditions and also with changes in input quantities. This suggests that a deeper look into the physics of an evaporating drop in a unsaturated atmosphere is warranted. Comparisons of these models to one developed on a more fundamental basis would be useful to determine to what extent these simple models are valid and which one(s) perhaps is most accurate. An important and basic unknown is the evaporation rate and final character of large salt-containing droplets in an unsaturated atmosphere. A number of drift models use evaporation submodels based on evaporation formulae taken from cloud physics. These formulas are best applied to predict evaporation (or growth) rates for small droplets of very small solute content in a nearly saturated ambient environment. The validity of these cloud physics formulae as applied to drift drops needs to be ascertained.

Ambient Turbulence and Ground Deposition

A ballistic model typically assumes that the total mass emitted within a given droplet size range is uniformly deposited over an area on the ground formed by the intersection of a pie-shaped section (usually 22 1/2 degrees) centered about the wind direction and an annulus of inner and outer radii equal to the distances to deposition of the largest and smallest drops of that size range, respectively. Since the drop size ranges do not overlap, only one drop size strikes any single point on the ground. In reality, there is a wide variation in drop deposition sizes striking any given location because drift droplets are subject to the effects of local turbulence (plume and or atmosphere). Models that

consider such stochastic effects generally do so only after breakaway ignoring the dispersion effects of turbulence while the droplet is still within the plume itself.

One method used to handle atmospheric turbulence effects is based on solution of the convective-diffusion equation for the drop concentration C, assuming all drops of a given size are emitted from the point of breakaway. Thus,

$$U\frac{\partial C}{\partial x} = \frac{\partial}{\partial z}\left(K_z \frac{\partial C}{\partial z}\right) + \frac{\partial}{\partial y}\left(K_y \frac{\partial C}{\partial y}\right) + V_s \frac{\partial C}{\partial z} + Q_o\, \delta(x,y,z - H)$$

where K_y and K_z are coefficients of eddy diffusivity in the y- and z-directions, respectively; U is the wind speed; V_s is the drop settling velocity; and Q_o is the drift rate. The usual boundary conditions are: $C \to 0$ as $y \to \pm\infty$ and as $z \to +\infty$ and $V_d\, C = V_s\, C + K_z \cdot (\partial C/\partial z)$ at $z = 0$, where V_d is the deposition velocity. This equation has been solved by various analytical means under certain restrictions. For example, Ermak (22) gives the solution under the assumption that U, V_s, and V_d are constants. Horst (23) gives the solution for U constant and $V_s = 0$.

Slinn has developed a model intended to give a conservative estimate of the distance to deposition for any given droplet size. All drops are instantaneously evaporated to dry particles and then followed by a Gaussian plume model. The Slinn approach may be characterized as a source-image method since it builds on the solution of the convective-diffusion equation which can be gotten by the method of images when $V_s = V_d = 0$ and U is constant. This modified solution satisfies the convective-diffusion equation for V_s constant but does not satisfy the appropriate boundary condition at the ground. As a result, mass is not conserved in that total deposition at all downwind locations is not equal to the salt release rate.

Overcamp and Israel (9) build on the work of Csanady (24) in which an image-depletion approach is used. This approach utilizes an approximate solution of the convective-diffusion equation to which an x-dependent multiplier of the image term is added. Overcamp (19) states that this approach satisfies conservation of mass, although this statement is based on runs of the computer model rather than on an analytical result. The solution does not satisfy the convective-diffusion equation, however.

The approach taken in the development of the ESC/Schrecker model may be termed a source-only method since only the source term of the solution to the convective-diffusion equation is used. This leads to the result that the deposition velocity varies with downwind distance in an arbitrary way. In fact, the deposition velocity will eventually become negative unless $d\sigma_z/dx = 0$. To prevent negative deposition, the ESC/Schrecker model forces a constant σ_z from the point at which negative deposition would otherwise occur.

These three approaches certainly represent approximate solutions of the true convective-diffusion problem; however, the level of approximation is not well known at this time. The treatment of deposition appears to us to be an important one and one that warrants further investigation.

CHALK POINT SALT DRIFT DATA

The drift data (21) used herein for model validation were all acquired at the Chalk Point natural-draft cooling tower located on the Patuxent River, approximately 64km southeast of Washington, D.C. The tower at the Chalk Point site is 124m high and has a circulating water flow of 300,000 gpm. Salt droplets are also emitted from the 217m high power plant stack, located 138m to the east of the cooling tower, due to the use of salt water in the scrubber system. The data used in this paper were taken in June, 1976, by Environmental Systems Corporation; ambient meteorological measurements were made by the Applied Physics Laboratory of the Johns Hopkins University.

Drift rates from the cooling tower were determined using an instrument package suspended in a plane approximately 13.6m below the tower exit. The following measurements were made in this manner:

a) The drift droplet size spectrum was measured using sensitive paper and with a device based on scattering of infrared laser light (PILLS II-A, Particle Instrumentation by Laser Light Scattering).
b) The drift mineral mass flux was measured with a heated glass bead isokinetic (IK) sampling system.
c) The updraft air velocity (from which droplet velocity was determined) was measured using a Gill propeller-type anemometer.
d) The dry-bulb and wet-bulb exit temperatures of the plume were also measured.

The IK system sampled continuously during the traverse and yielded the sodium and magnesium mineral flux at the measurement plane. Updraft air velocities were acquired and averaged for each point. Grab samples of circulating water were also taken for chemical analysis of sodium and magnesium content. These two cations, which are present in the highest amounts in the water, were chosen as tracer elements for the IK measurements. Similar source measurements were made for the stack on two dates.

Ambient meteorological measurements were made using the Chalk Point 100m instrument tower which has wind and temperature instruments at three levels (7m, 50m, and 92m) and dew point sensors at two levels (7m and 92m). Half-hour averages of dry-bulb and dew-point temperature and wind speed were taken. To supplement the meteorological-tower measurements, rawinsonde flights were conducted at intervals of 1 to 2 hours in order to establish the short-term history of diurnal stability characteristics. Measurements of pressure (elevation), dry-bulb temperature, relative humidity, and wind speed (direction) were typically made every 10 to 20m vertically.

Concurrent with the sampling of drift releases from the cooling tower and stack, measurements of a number of drift parameters were made at ground level downwind of the cooling tower. Typically, four or five stations were used to measure the following ground-level drift quantities.

1. Sodium concentration in the air ($\mu g\text{-}Na/m^3$) using a rotating tungsten mesh.
2. Liquid droplet concentration as a function of droplet size ($g\text{-}H_2O/m^3$) using a rotating sensitive paper disk.
3. Liquid droplet deposition flux as a function of droplet size ($kg\text{-}H_2O/km^2\text{-month}$) using a stationary sensitive paper disk.
4. Sodium mass deposition flux ($kg\text{-}Na/km^2\text{-month}$) using a stationary funnel and bottle assembly.

Some ground-level stations were fixed in location and thus received drift only when the wind was blowing in the proper direction. Other stations were located beneath the cooling tower plume, being moved as the wind direction changed. For the purpose of model-data comparisons, we used the droplet number deposition flux measurements obtained using sensitive paper disks fixed to a petri dish. Droplet stains on the sensitive papers were first sized and counted and then the stain sizes were converted to droplet sizes using calibration data. Only drops greater than 100μm were considered in our model/data comparisons. In this way, we hoped to sidestep the difficult problem of accounting for blowout from the bottom of the cooling tower and sizing the small drops that result.

In order to place the reliability and quality of the data in better perspective, some of the difficulties encountered in acquiring the above drift data and some of the important questions that remain about the data will now be discussed.

i) The ground-level drift data include salt deposition originating from the power plant stack scrubber system and from the salt mist produced by the nearby Patuxent River. Although the water emission rate is eight times larger from the tower than from the stack, the salt emission from the tower is about 20 percent less than that from the stack. Dependent upon the location of the ground sampler with respect to the tower and stack, the stack may be a significant contribution to the droplet number deposition flux measurements. The problem of background contributions is compounded by the high efficiency of the drift eliminators at Chalk Point which limit the drift rate to 0.000717 percent of the cooling water flow rate in summer and 0.00035 percent in winter.

ii) The ground-level sensors employed by ESC were small in size and few in number. Questions as to statistical accuracy of the data arise since only small numbers of drops typically strike any given sampler. Larger numbers of samplers and samplers of much greater area can overcome this problem but greatly increase the cost of data reduction. A related problem is the statistical accuracy of droplet measurements in the cooling tower and stack for the larger drop sizes. A smaller number of such drops are actually observed yet these larger drops impact close to the tower where ESC has most of their ground samplers located.

iii) The time variation of ambient and tower conditions makes a deterministic model simulation difficult to validate. Detailed ambient profiles were made only hourly and the variable meteorology (which we noted from the time-dependent meteorological tower measurements) certainly affects plume rise and the drift deposition at any particular sampler location.

iv) The accuracy of the tower measurements is difficult to assess due to variations in the measured variables (updraft velocity, temperature, droplet size spectrum, liquid mass flux, etc.) with cross-tower location. Determinations of mineral mass emission rate from the IK measurements lead to values that are 2 to 4 times larger than those obtained if one integrates over the droplet size spectrum making the traditional assumption that all drops leave the tower with a solute concentration equal to that of the basin water. Experimental studies are being planned to determine if the drops under 50 μm (whose flux is difficult to measure with PILLS) contain a larger salt concentration than the basin water due to evaporation while in the tower.

Only further study can determine the significance of the above problems and the accuracy of the drift data.

MODEL VALIDATION

Drift predictions from the cooling tower were made for each of the models listed in Table 1 for seven dates in June, 1976. For two of those dates (June 22 and 23) source measurements were also made for the stack from which we also prepared drift predictions. Magnitudes of the ambient parameters measured at the 92m level of the meteorological tower were used as input to the models. The tower is located on a hill so that the 92m height is actually at the same horizontal plane as the tower top. Temperature lapse rates were determined from a best fit to the nearest (in time) rawinsonde temperature profile. Calculations of ground-level drift were made for each half-hour time period for which meteorological conditions were reported. These results were then summed over the several hours that ground-level measurements were made. For the one model that utilizes full ambient profiles (Wigley-Slawson), the rawinsonde profiles were used. Liquid mass emission from the tower (determined from PILLS-II) was used to obtain the drift rate instead of mineral mass emission given by the IK sampler, following the recommendation of ESC.

Table 4 summarizes the model/data comparisons for the seven sets of data and the 11 models. The ORFAD predictions are omitted because of several errors in the computer program provided to us by the model developers.

The model/data comparisons given in Table 4 support the following observations.

1. A number of comparisons show observed drift where none is predicted (June 18 a.m. and June 19, for example). For these cases, the 22 1/2-degree sector about the mean wind direction does not usually include any ground-level sensor during any half-hour period of meteorological observations. The cause of zero-prediction non-zero-measurement discrepancy is most likely due to either (a) a large standard deviation of wind direction for each half-hour meteorological observation period leading to a wider lateral dispersion than given by a 22 1/2 sector, or (b) the sometimes large vertical variation in the wind direction. This variation is sometimes larger than 22 1/2 degrees at the 92m level. None of the models consider variation of wind direction with height.
2. Most models show a large number (typically 50 percent) of predictions to be complete misses; that is, as in (1) above or the predicted number deposition is in error by a factor of 10 or more.
3. The models, in general, performed better for the two dates when stack and cooling tower contributions were predicted and

Table 4 Comparison of Predicted and Observed Ground-Level Drift Deposition for the Chalk Point Power Plant

Sampler	6-17 (Cooling Tower) # Drops/m^2-hr. -- 22.5° sector										
Distance (m)	Dir.	OBS.	1	2	3	4	5	6	7	8	9	10
240	213	1640	1952	1851	1120	4386	16603	0	4004	3634	2216	2549
610	221	605	10	869	1071	1451	249940	0	3379	652	72	619
620	211	288	28	981	1422	984	325000	0	4777	1151	120	670
740	213	1119	28	438	87	1203	252430	0	9191	549	120	764
870	210	394	22	165	19	761	150430	0	13650	525	172	301

Sampler	6-18 A.M. (Cooling Tower) # Drops/m^2-hr. -- 22.5° sector										
Distance (m)	Dir.	OBS.	1	2	3	4	5	6	7	8	9	10
260	222	2672	0	0	0	0	0	0	0	0	0	0
610	229	2550	0	0	0	0	0	0	0	0	0	0
620	212	4300	0	0	0	1092	0	0	4268	791	0	0
740	208	2407	35	196	20	344	52111	0	5740	754	49	423
1040	203	3552	63	406	123	144	82387	0	14390	576	5673	645

Sampler	6-18 P.M. (Cooling Tower) # Drops/m^2-hr. -- 22.5° sector										
Distance (m)	Dir.	OBS.	1	2	3	4	5	6	7	8	9	10
240	170		294	74	158	2182	591	0	134	132	482	149
300	149		333	171	566	2327	3098	0	2128	1403	1470	423
Totals		2016	314	124	368	2256	1881	0	1160	786	990	290
380	183		4	8	5	0	258	0	345	272	63	22
460	151		198	158	524	2120	4725	0	2579	1592	2726	468
Totals		616	108	89	284	1110	2663	0	1548	983	1497	262
520	182		9	20	22	0	1184	0	578	299	202	40
590	146		75	177	125	0	12354	0	3790	1460	2837	452
Totals		398	38	88	67	0	6044	0	1976	804	1348	219
710	182		1	10	55	0	15329	0	923	195	177	18
870	165		0	1	2	0	133	0	0	0	70	3
Totals		1073	1	7	36	0	9974	0	598	126	139	13
990	182		0	0	0	0	0	0	1318	73	0	0
990	167		0	0	0	0	0	0	0	0	0	0
Totals		256	0	0	0	0	0	0	693	38	0	0

Sampler	6-19 (Cooling Tower) # Drops/m^2-hr. -- 22.5° sector										
Distance (m)	Dir.	OBS.	1	2	3	4	5	6	7	8	9	10
240	145	2600	905	754	563	759	12235	0	3545	2913	2885	5610
370	178	2373	0	0	0	635	0	0	0	0	0	0
440	173	1820	0	0	0	1639	0	0	0	0	0	0
440	183	3381	0	0	0	0	0	0	0	0	0	0
460	164	1297	0	0	0	1464	0	0	0	0	0	0

Sampler	6-22 (Cooling Tower) # Drops/m^2-hr. -- 22.5° sector										
Distance (m)	Dir.	OBS.	1	2	3	4	5	6	7	8	9	10
240	188		2927	1245	1587	4622	14565	0	8049	6935	3280	8212
390	188		169	859	1089	1362	25581	0	5248	4366	3099	3425
550	182		407	998	431	2581	88808	0	7034	3415	3286	2903
570	196		41	282	94	759	85329	0	3655	1024	1250	978
Totals			173	540	215	1414	86580	0	4870	1884	1982	1670
570	192		180	575	192	1073	96850	0	4142	1320	2041	1829
770	183		82	341	517	908	104490	0	5751	1017	1137	1173

Sampler	6-22 (Stack) # Drops/m^2-hr. -- 22.5° sector										
Distance (m)	Dir.	OBS.	1	2	3	4	5	6	7	8	9	10
270	157		176	135	454	0	476	0	90	80	414	36
406	168		121	261	226	0	391	0	157	47	414	23
587	166		0	0	0	0	0	0	0	0	0	0
568	180		386	741	498	481	4612	0	465	336	1021	168
Totals			247	474	319	308	2953	0	298	215	654	108
569	178		423	783	538	478	4580	0	456	268	1138	177
786	173		87	430	197	95	1391	0	263	218	513	106

Sampler	6-22 (Cooling Tower and Stack) # Drops/m^2-hr. -- 22.5° sector										
Distance (m)	Dir.	OBS.	1	2	3	4	5	6	7	8	9	10
240(270)	188(157)	1681	3103	1380	2041	4622	15041	0	8139	6870	3694	8248
390(406)	188(168)	1286	290	1120	1315	1362	25972	0	4299	3820	3513	3448
550(587)	182(166)		407	998	431	2581	88808	0	7034	3415	3286	2903
570(568)	196(180)		427	1023	592	1240	88941	0	4120	1360	2271	1146
Totals		1138	420	1041	534	1722	89533	0	5168	2099	2636	1778
570(569)	192(178)	1024	612	1358	730	1551	101430	0	4598	1077	3179	2006
770(786)	183(173)	546	169	771	714	1003	105881	0	6014	1080	1650	1279

Sampler	6-23 (Cooling Tower) # Drops/m^2-hr. -- 22.5° sector										
Distance (m)	Dir.	OBS.	1	2	3	4	5	6	7	8	9	10
180	230		0	0	0	0	0	0	0	0	0	0
180	174		673	906	3150	6094	41365	0	4812	4068	1767	1679
Totals			318	428	1487	2874	19525	0	2271	1741	834	792
320	90		0	0	0	0	0	0	0	0	0	0
380	174		97	167	390	1399	276880	0	7660	1680	1582	1377
490	219		0	0	0	0	0	0	0	0	0	0
Totals			49	84	195	699	138440	0	3830	786	791	688
510	232		0	0	0	0	0	0	0	0	0	0
540	213		0	0	0	0	0	0	0	0	0	0
440	173		114	195	0	2592	295840	0	9522	1962	314	441
Totals			49	84	0	1112	126890	0	4084	842	135	189
540	173		16	151	0	0	159220	0	7715	805	326	353
620	214		0	0	0	0	0	0	0	0	0	0
Totals			*8*	*78*	*0*	*0*	*82440*	*0*	3995	417	*169*	*183*

LEGEND

1. Hanna
2. Hosler,Pena,Pena
3. Overcamp-Israel
4. Wigley-Slawson
5. Slinn-I
6. Slinn II
7. Wolf-I
8. Wolf-II
9. ESC/Schrecker
10. MRI

Table 4 Comparison of Predicted and Observed Ground-Level Drift Deposition for the Chalk Point Power Plant (Continued)

Sampler			6-23 (Stack) # Drops/m^2-hr. -- 22.5° sector									
Distance (m)	Dir.	OBS.	1	2	3	4	5	6	7	8	9	10
127	180		5979	609	13	5380	6634	0	654	596	1014	0
246	125		0	0	0	0	0	0	0	0	0	0
Totals			3157	322	7	2840	3503	0	345	296	535	0
458	91		0	0	0	0	0	0	0	0	0	0
427	155		840	1935	812	0	43802	0	1584	1422	4312	2009
427	204		0	0	0	0	0	0	0	0	0	0
Totals			420	968	406	0	21901	0	792	711	2156	1004
411	216		0	0	0	0	0	0	0	0	0	0
491	196		0	0	0	0	0	0	0	0	0	0
505	155		484	1419	388	0	11686	0	698	943	1170	1207
Totals			208	609	166	0	5012	0	299	404	502	518
584	160		530	2234	1156	0	22120	0	1015	925	2739	452
565	202		0	0	0	0	0	0	0	0	0	0
Totals			274	1157	599	0	11453	0	526	473	1416	752

Sampler			6-24 (Cooling Tower) # Drops/m^2-hr. -- 22.5° sector									
Distance (m)	Dir.	OBS.	1	2	3	4	5	6	7	8	9	10
270	220	1866	0	0	0	80	0	0	71	56	0	0
320	90	8956	0	0	0	0	0	0	0	0	0	0
630	205	1333	41	117	205	145	40086	0	1784	350	1483	211
630	218	715	0	0	0	0	0	0	128	30	0	0
650	212	146	10	23	71	147	4999	0	508	112	344	44

Sampler			6-23 (Cooling Tower and Stack) # Drops/m^2-hr. -- 22.5° sector									
Distance (m)	Dir.	OBS.	1	2	3	4	5	6	7	8	9	10
180(127)	230(180)		5974	609	13	5380	6634	0	654	560	1014	0
180(246)	174(125)		673	906	3150	6094	41365	0	4812	4068	1767	1679
Totals		6127	3475	750	1494	5714	23028	0	2616	2037	1369	792
320(458)	90(91)	2982	0	0	0	0	0	0	0	0	0	0
380(427)	174(155)		973	2102	1202	1399	320682	0	9244	3102	5894	3386
490(427)	219(204)		0	0	0	0	0	0	0	0	0	0
Totals		120	469	1052	601	699	160341	0	4622	1497	2947	1692
510(411)	232(216)		0	0	0	0	0	0	0	0	0	0
540(491)	213(196)		0	0	0	0	0	0	0	0	0	0
440(505)	173(155)		598	1614	388	2592	307526	0	10220	2905	1484	1648
Totals			257	693	166	1112	131902	0	4383	1246	637	707
540(584)	173(160)		546	2385	1156	0	181340	0	8730	1719	3065	1805
620(565)	214(202)		0	0	0	0	0	0	0	0	0	0
Totals		37	282	1235	599	0	93893	0	4521	890	1587	935

LEGEND

1. Hanna
2. Hosler,Pena,Pena
3. Overcamp-Israel
4. Wigley-Slawson
5. Slinn-I
6. Slinn II
7. Wolf-I
8. Wolf-II
9. ESC/Schrecker
10. MRI

summed for comparison to the field data. When samplers were located beneath the cooling tower plume, the cooling tower provided the most predominant contribution to the predicted number deposition flux. The same applies to the samplers located beneath the stack plume. Samplers located below the edges of both the cooling tower and stack plumes received significant contributions from both sources in terms of model predictions.

4. Six models appear to be competitive in terms of their predictive capability: ESC/Schrecker, MRI, Overcamp and Israel, Wigley and Slawson, and Wolf I, II. Two others--Hanna and Hosler, Pena, and Pena--are often far from the data and show a consistent tendency to underpredict number deposition. Their performance improved, however, in the cases where stack and tower runs were made. Three others--Slinn I and II, and ORFAD--performed very poorly. Although no ORFAD predictions are presented here, our study showed that it predicts too great a deposition distance and that it uses several unrealistic assumptions, e.g., drops never break away from the updraft velocity of the plume and only ground-level (not plume-level) ambient conditions are used. Comments that may be made about the performance of some of the individual models are:

Wigley-Slawson--The model generally underpredicts in the field cases where only cooling tower drift predictions were made. Although solute effects are not treated in the formulation for droplet evaporation, the samplers are close enough to the tower to permit small times to deposition and thus less time for evaporation to occur. The effect of neglecting solute in the drop is thus not shown to be very severe. As presently formulated, the Wigley-Slawson model should, however, generally overestimate evaporation and yield longer downwind distances to deposition for salt drops.

ESC/Schrecker--Although the model has a more advanced treatment of plume rise and drop evaporation than most other models, it condenses each drop size spectrum into exactly 8 bins. We found that this reduction in the ranges of the spectrum from $\tilde{\sim}$ 25 at Chalk Point to 8 adversely affected the performance of the model for these Chalk Point model/data comparisons. Noticeably better predictions resulted when the full spectrum was used for Chalk Point (not shown).

Slinn I--The assumptions of no evaporation at all and breakaway at the top of the tower lead to a very large deposition near the tower and low values far from the tower.

Slinn II--The assumptions of complete evaporation at tower exit and breakaway at maximum plume rise lead to deposition much too far from the tower. The models by Slinn were developed to give inner and outer bounds to

deposition distance. These bounds are not helpful in these particular cases, however.

Wolf I--The assumption of no evaporation leads to a larger predicted number deposition near the tower than is seen in the data. This model is designed to give a conservative estimate which, in fact, it does at these short distances from the tower. At larger distances from the tower than 1-2 km, the assumption of no droplet evaporation should, undoubtedly, begin to become a poor one.

Wolf II--This model also tends to overpredict droplet number deposition flux. However, farther from the tower, the neglect of solute effects in droplet evaporation should yield a more rapidly evaporating drop and deposition distances that are too large.

MRI--The model apparently has several conservative and optimistic assumptions whose effects offset each other. The inclusion of both sensible and latent heat components in the calculation of the buoyancy flux increases plume rise. The h_e errors (noted earlier) are not apparent here since they become less at ambient temperatures above 20 C as in these June data. The MRI model assumes a stable atmosphere independent of the measured lapse rate. The lapse rate and buoyancy flux assumptions appear to counterbalance. We suspect that data sets with ambient temperature below 20 C or with very stable or unstable atmospheres would provide a better test of the model.

Hanna--Model generally underpredicts deposition perhaps due to an overestimation of evaporation rates. The assumption of drop temperature equal to ambient dry bulb rather than wet bulb temperature will provide greater evaporation than actually occurs.

It should be noted that these data are not sufficiently strong to allow absolute conclusions about the models. The sensors used by ESC were too few (4-5 in number for field survey) and rather small (120 cm^2 each in area). Serious questions as to statistical significance of the data arise since only 10 to 50 droplets were typically obtained on the sensitive papers over a four-hour period. In spite of these shortcomings, these data are the best available at present. More definitive conclusions will be possible only upon the acquisition of more high quality field data.

ACKNOWLEDGMENTS

This work was funded by the Nuclear Regulatory Commission and the Electric Power Research Institute under separate contracts. The authors also wish to express their appreciation to the modelers whose work was utilized and to the Environmental Systems Corporation for their cooperation in completing this study.

REFERENCES

1 Hosler, C., Pena, J., and Pena R., "Determination of Salt Deposition Rates from Drift from Evaporative Cooling Tower", J. Eng. Power, Vol. 96, No. 3, 1974, p. 283.

2 LaVerne, M. E., "The Oak Ridge Fog and Drift Code (ORFAD) User's Manual", ORNL/TM-5021, 1977.

3 Wolf, M., Personal Communication, Battelle Pacific Northwest Laboratories, Richland, Wash., July 1976.

4 Slinn, W. G. N., Personal Communication, Battelle Pacific Northwest Laboratory, Richland, Wash., February 1977.

5 Hanna, S. R. "Fog and Drift Deposition from Evaporative Cooling Towers". Nuclear Safety. Vol. 15, No. 2. March-April 1974. pp. 190-196.

6 Slawson, P. R., and Kumar, A., "Cooling Tower Drift Deposition Program Guide to ENDRIFT II", Envirodyne Ltd., Tennessee Valley Authority Air Quality Branch, April 1976.

7 Maas, S. J., "Salt Deposition from Cooling Towers for the San Joacquin Nuclear Project", MRI 75-FR-1361, September 15, 1975.

8 Schrecker, G., and Rutherford, D., Personal Communication, Environmental Systems Corp., Knoxville, Tenn., 1976.

9 Overcamp, T., "Sensitivity Analysis and Comparison of Salt Deposition Models for Cooling Towers". Paper presented and published in Proceedings of the Conference on Waste Heat Management and Utilization. Miami Beach, Florida. May 9-11, 1977.

10 Briggs, G. A., Plume Rise, AEC Critical Review Series, USAEC Report TID-24635, 1969.

11 Briggs, G. A., "Some Recent Analyses of Plume Rise Observation", Proceedings of the Second International Clean Air Congress, Ed. by H. M. England and W. T. Berry, Academic Press, Inc., New York, 1971, pp. 1029-1032.

12 Slawson, P. R., and Wigley, T.M.L., "Cooling-Tower Drift Deposition: Application to the Tennessee Valley Authority Candidate Site at Phipps Bend, Tennessee", Envirodyne Ltd., Waterloo, Ontario, Canada.

13 Winiarski, L., and Frick, W., "A Cooling Tower Plume Model", Pacific Northwest Environmental Research Laboratory, The U.S. Environmental Protection Agency, Corvallis, Oregon, 1976.

14 Beard, K., and Pruppacher, H., "A Determination of the Terminal Velocity and Drag of Small Water Drops by Means of a Wind Tunnel", J. Atmospheric Sc., Vol. 26, 1969, p. 1066.

15 Hanna, S. R., "Rise and Condensation of Large Cooling Tower Plumes", Applied Meteorology, Vol. 11, 1972, pp. 793-799.

16 Froessling, N. Gerlands Beitr. Geophysiks. 52, 1938, p 170.

17 Fletcher, N. H., The Physics of Rainclouds, University Press, Oxford, England, 1971.

18 Mason, B. J., The Physics of Clouds, Clarendon Press, Oxford, England, 1971.

19 Overcamp, T., "A General Gaussian Diffusion Deposition Model for Elevated Point Sources", J. of Applied Meteorology, Vol. 15, No. 11, November 1976.

20 Briggs, G., "Diffusion Estimates for Small Emissions", ATDL Contribution No. 79, Atmospheric Turbulence and Diffusion Laboratory, Oak Ridge, Tenn., 1973.

21 "Environmental Systems Corporation Comprehensive Project Final Report for the Period October 1, 1975-June 30, 1976, Volumes 1 and 2, prepared by Engineering Projects Division, ESC for the State of Maryland Power Plant Siting Program, PPSP-CPCTP 12, October 1976.

22 Ermak, D. L., "An Analytical Model for Pollutant Transport and Deposition from a Point Source", Atmospheric Environment, Vol. 11, 1977, pp. 231-237.

23 Horst, T. W., "A Surface Depletion Model for Deposition from a Gaussian Plume", Atmospheric Environment, Vol. 11, 1977, pp. 41-46.

24 Csanady, G. T., "Dispersal of Dust Particles from Elevated Sources", Aust. J. Phys., Vol. 8, 1955, pp. 545-550.

Section 3

EVALUATION OF DROPLET EVAPORATION FORMULATIONS EMPLOYED IN DRIFT DEPOSITION MODELS

This reprint provides special insight into the droplet evaporation formulations used in the drift models tested in Sections 2 and 4.

Among the droplet evaporation treatments tested here, the use of the Mason formulation was found to be the most correct and preferable to the Fletcher or the Frössling equation in which the drop temperature is taken to be the ambient wet bulb (ESC/Schrecker Model) or the ambient dry bulb temperature (Hanna, KUMULUS Models). In all methods evaluated, the effect on drop evaporation of salt concentration gradients in the drop is not treated. Without such treatment, evaporation rates may be incorrectly computed and the final size of the droplet (after complete evaporation) may be wrongly determined (see Section 5).

Also presented here is a determination of the range of differences among the predictions of the evaporation models for typical drift drops. That evaluation was carried out by means of a comparison of droplet trajectories predicted by the models for a hypothetical case of a salt-containing drop released from a fixed height. It was found that (a) significant differences can exist among model predictions of distance to deposition, final diameter and final settling velocity, (b) these differences are generally smaller for the larger drop sizes, (c) model predictions are quite sensitive to changes in relative humidity at the relative humidities above 70%, but are fairly insensitive to changes below this value, (d) larger ambient temperatures and lower drop salt concentrations lead to larger distances to deposition.

It was found that initial drop diameter is the most important parameter in determining deposition history. Ambient relative humidity is important in determining the final state of the smaller drops. General rules of thumb are provided for extreme behaviors such as deposition with little evaporation and deposition after near instantaneous evaporation. Based partly upon the results of this investigation, an improved droplet evaporation formulation was developed under this project and is presented in Section 5.

Reprint of Paper #2:

"Evaluation of Droplet Evaporation Formulations
Employed in Drift Deposition Models"

William Dunn
Bruce Boughton
Anthony Policastro

Proceedings, Cooling Tower Environment -- 1978. A symposium on Environmental Effects of Cooling Tower Emissions. May 2-4, 1978. Published by the Water Resources Research Center, University of Maryland.

EVALUATION OF DROPLET EVAPORATION FORMULATIONS EMPLOYED IN DRIFT DEPOSITION MODELS

William Dunn*
Bruce Boughton**
Anthony Policastro***

ABSTRACT

Six models commonly used to predict drift deposition from evaporative natural-draft cooling towers are evaluated in terms of their formulation for droplet evaporation. The fundamental theory of droplet evaporation in an unsaturated atmosphere is reviewed and the different treatments of evaporation used by the models are compared with the exact formulation. The major discrepancies arise due to approximations to the droplet temperature. The best (nonexact) treatment of droplet evaporation of those tested is Mason's equation (employed in the Overcamp-Israel and Wigley-Slawson models) yielding differences from the exact solution which are generally less than 20%. The worst is the case of the drop temperature taken equal to the ambient dry-bulb temperature (employed in the Hanna drift model) yielding evaporation rates consistently too large by about 130%.

To determine the range of differences between the predictions of the evaporation models for drift drops, a comparison is made of droplet trajectories as predicted by the models for a hypothetical case of a salt-containing drop released from a fixed height. It was found that (a) significant differences can exist among model predictions of distance to deposition, final diameter and final settling velocity, (b) these differences are generally smaller for the larger drop sizes, (c) model predictions are quite sensitive to changes in relative humidity at the relative humidities above 70%, but are fairly insensitive to changes below this value, (d) larger ambient temperatures and lower drop salt concentrations lead to larger distances to deposition.

It was found that initial drop diameter is the most important parameter in determining deposition history. Ambient relative humidity is important in determining the final state of the smaller drops. General rules of thumb are provided for extreme behaviors such as deposition with little evaporation and deposition after near instantaneous evaporation.

NOMENCLATURE

A = coefficient dependent on temperature and relative humidity

B = coefficient dependent on salt concentration

C = droplet salt concentration

---

*Assistant Professor, Dept. of Mech. and Ind. Engr., Univ. of Ill., Urbana.
**Research Assistant, Dept. of Mech. and Ind. Engr., Univ. of Ill., Urbana.
***Engineer, Div. of Environmental Impact Studies, Argonne National Lab.

C_p = specific heat of the drop fluid

$C_{\infty,sat}$ = saturated vapor concentration at ambient dry bulb temperature at T_∞

C_∞ = ambient vapor concentration

D = coefficient of diffusion of water vapor in air

D_o = initial drop diameter

h_{fg} = latent heat of vaporization of the drop

i = van't Hoff factor

k = thermal conductivity of air

m = mass of droplet

M_o = molecular weight of water

m_s = mass of salt in the drop

M_s = molecular weight of salt

Nu = Nusselt number based on diameter

r = droplet radius

Pr = Prandtl number

R = universal gas constant

Re = Reynolds number based on diameter

RH = ambient relative humidity (also λ)

Sc = Schmidt number

Sh = Sherwood number based on diameter

T = ambient dry-bulb temperature

t = time

T_B, T_s, T_{WB}, T_{DB} = temperature: subscript B = bulk temperature, s = surface temperature, WB = ambient wet bulb temperature and DB = ambient dry bulb temperature.

T_∞ = ambient dry-bulb temperature

U = ambient wind speed

V_s = droplet settling velocity

ζ = nondimensional drop/ambient vapor concentration difference

λ = ambient relative humidity (also RH)

INTRODUCTION

This paper compares and contrasts alternative formulations of the droplet evaporation equations as related to the prediction of drift deposition from cooling towers. The objectives of this study are to (1) Ascertain the amount of variability among alternative formulations in an effort to understand differences among model predictions; (2) Determine which aspects of the formulation are most important in affecting deposition distance and final state; and (3) Gain new insights into the role of evaporation in

determining deposition parameters as a first step toward model improvement.

The study is carried out by comparing predictions of 6 formulations extracted from currently available drift models. Although these models share similar origins, the disparity between predictions can be great. Thus, the differences must be attributed to differing implementations of the same concept; i.e., to various simplifications and/or modifications introduced by the developers of the drift model.

EVAPORATION FUNDAMENTALS

The basic equation of mass transfer from a drop surface is

$$\frac{dm}{dt} = -ShD(2\pi r)(C_s - C_\infty), \tag{1}$$

where m is the drop mass, t is time, Sh is the Sherwood number, D is the coefficient of diffusion of water vapor in air, r is the drop radius, C_s is the vapor concentration at the drop surface and C_∞ is the ambient vapor concentration. Similarly, the basic equation of heat transfer is

$$mC_p \frac{dT_B}{dt} = -Nu\ k(2\pi r)(T_B - T_\infty) + h_{fg}\ dm/dt, \tag{2}$$

where T_B is the bulk drop temperature, C_p is the specific heat of the drop fluid, Nu is the Nusselt number, k is the thermal conductivity of air, T_∞ is the ambient dry-bulb temperature and h_{fg} is the latent heat of vaporization of the drop fluid.

These equations can be integrated as an initial-value problem in time if (a) expressions are found for Nu and Sh and (b) the vapor concentration at the drop surface C_s can be determined. Although over twenty semi-empirical correlations have been developed for heat and mass transfer from drops and spheres, the most widely used are those of Frössling[1],

$$Nu = 2 + 0.552\ Re^{1/2}\ Pr^{1/3}$$
$$Sh = 2 + 0.552\ Re^{1/2}\ Sc^{1/3}$$

Ranz and Marshall[2],

$$Nu = 2 + 0.6\ Re^{1/2}\ Pr^{1/3}$$
$$Sh = 2 + 0.6\ Re^{1/2}\ Pr^{1/3}$$

and Beard and Pruppacher[3],

$$Sh = 2.0 + 0.216\ Re\ Sc^{2/3} \qquad (Re \leq 2)$$
$$Sh = 1.56 + 0.616\ Re^{1/2}\ Sc^{1/3} \qquad (Re \geq 2)$$

Here, Re is the drop Reynolds number, and Pr and Sc are the Prandtl and Schmidt numbers of air, respectively.

Much greater variety exists among the different methods of determining vapor concentration at the drop surface. In principle, the dependency of saturated vapor concentration on temperature is governed by the Clausius-Clapeyron equation. In actuality, the vapor pressure over pure water deviates from this behavior and most modelers use one of the several semi-

empirical curve fits to the vapor-pressure/temperature relationship that are available in the literature.

For an ideal solution, the vapor pressure reduction due to the presence of solute (salt in this case) is governed by Raoult's Law. Again, salt water, especially with large salt concentrations, deviates from ideal-solution behavior. Some correction can be made for this deviation through the use of the van't Hoff factor which is meant to account for the fact that not all the salt is dissociated into ions. For an ideal solution, the van't Hoff factor would be 2.0, indicating that each sodium chloride molecule separates into 2 ions. For sodium chloride solutions, the van't Hoff factor actually varies from about 1.6 to 2.4 depending on the concentration of the solution. The fact that the van't Hoff factor exceeds 2.0 for some concentrations is the result of the interplay of complex intermolecular forces between the polar water molecules and charged salt ions. The introduction of the van't Hoff factor buys little simplification since one merely transfers the problem of finding the vapor pressure reduction as a function of concentration to one of finding the van't Hoff factor. Most modelers, in fact, use a constant van't Hoff factor, ignoring its dependence on concentration.

After the functional dependency of vapor concentration on the temperature and salt concentration of water is established, it remains only to relate the surface temperature and concentration to their corresponding bulk values. It is typically assumed that the surface and bulk temperatures are equal owing to circulations internal to the drop and the fact that the Biot modulus for the drop (Nuk/k_{water}) is small[2] (less than 0.1). Experimental measurements of droplet evaporation rates[2] support this assumption.

It is also common to assume that the bulk and surface salt concentrations are equal although the validity of this assumption is questionable. The Biot-modulus equivalent for salt diffusion inside the drop ($Sh\ D/D_{salt\text{-}water}$) is quite large ($>10^4$) indicating that internal concentration gradients may be large as well. In fact, experimental data[2] show that precipitation of salt begins on the drop surface and that the dry particle is actually a porous conglomeration of tiny crystals rather than one large crystal formed at the drop center as the models assume. We are currently studying the effect of salt gradients within evaporating drops more thoroughly to ascertain the possible impact on drift deposition modeling.

Analysis of the heat transfer equation reveals that the drop bulk temperature relaxes to its equilibrium value in a matter of a few seconds which is typically a small fraction of the total lifetime of a drift droplet. Therefore, the heat transfer equation may be eliminated from consideration if it assumed that $dT_B/dt = 0$. Under this assumption, and letting $T_S = T_B$ as noted above, Eqs. 1 and 2 can be combined to yield

$$(T_s - T_\infty) = \frac{-Sh}{Nu} \left(\frac{Dh_{fg}}{k}\right) (C_s - C_\infty) \qquad (3)$$

which can be solved for C_s once the exact form of the vapor-concentration/temperature/salt-concentration relationship is given.

Fletcher[4] and independently Mason[5] have given approximate solutions to

Eq. (3) under the following conditions

1. The difference in the saturation vapor pressure between the temperature at the drop surface and the ambient is given by the Clausius-Clapeyron equation.
2. The effect of solute is given by Raoult's Law as modified by the van't Hoff factor.
3. $\zeta = (C_s - C_{\infty,sat})/C_{\infty,sat}$ is much less than 1.

This last assumption may be expected to be quite good inside clouds where $C_s \approx C_\infty$ which are the conditions for which the Mason and Fletcher solutions were derived. It is, however, questionable for drift droplets moving in ambients of low humidity. We shall see the effect of this assumption shortly.

From assumptions 1 and 2, we may write

$$\frac{C_s}{C_{\infty,sat}} = \frac{T_\infty}{T_s} \exp\left[\frac{h_{fg} M_o}{RT_s T_\infty}(T_s - T_\infty)\right] \cdot \left[1 + i \frac{M_o}{M_s} \frac{m_s}{m - m_s}\right]^{-1}, \quad (4)$$

where

$C_{\infty,sat}$ = saturation vapor concentration at temperature T_∞,

M_o = molecular weight of water,

M_s = molecular weight of salt,

m_s = mass of salt in the drop,

i = van't Hoff factor,

and

R = universal gas content.

Substituting Eq. 3 into 4, we have

$$\zeta = \frac{T_\infty}{T_s} [\exp(-A\lambda\zeta)] B - 1, \quad (5)$$

where

$$\zeta = (C_s - C_{\infty,sat})/C_{\infty,sat}, \quad (6)$$

$$A = \frac{h_{fg}^2 D M_o Sh C_{\infty,sat}}{RT_s T_\infty k\, Nu} \approx \frac{h_{fg}^2 D M_o Sh C_{\infty,sat}}{RT_\infty^2 k\, Nu}, \quad (7)$$

and

$$B = \left[1 + i\,(M_o/M_s)\frac{m_s}{m - m_s}\right]^{-1}. \quad (8)$$

Fletcher 4 and Mason 5 derive approximate solutions to Eq. (5) assuming ζ is small. These solutions are respectively:

Fletcher: $\zeta = (B - \lambda)/(1/\lambda + A)$ (9)

Mason: $\zeta = (B - \lambda)/(1 + A)$ (10)

Figs. 1 and 2 compare these approximate solutions with the exact solution of Eq. (5). The relative error in the value of the mass transfer rate is plotted as a function of relative humidity for a dilute solution (B = 0.998) in Fig. 1 and a concentrated solution (B = 0.85) in Fig. 2. The relative error is also a function of ambient temperature, but

the variation is only a few percent over the range of 0 to 20C. Shown along with the Fletcher and Mason approximations are curves obtained assuming $T_S = T_{DB}$ (as is done by Hanna) and $T_S = T_{WB}$ (as is done by ESC/Schrecker). The following general observations can be made.

(a) The approximation due to Mason gives fairly accurate values over the entire range of relative humidities for both dilute and concentrated solutions.

(b) The approximation due to Fletcher gives good results at high relative humidities, but significantly underpredicts evaporation rate at lower relative humidities.

(c) The assumption that $T_S = T_{WB}$ gives good results for dilute solutions but is decidedly poor for a concentrated solution at relative humidities above 0.70. Thus, it appears that the effects of solute cannot be ignored for these cases.

(d) The spikes seen in all approximations around the point $\lambda = B$ is the direct result of the fact that the true solution is tending to zero. The very strong effects seen here help explain the sensitivity of model predictions to relative humidity between 0.70 and 1.0.

INDIVIDUAL MODEL FORMULATIONS

In this section, we wish to summarize how each of the drift models implements its particular evaporation formula within the context of the general framework set forth above. The specific models considered are those of Hosler[6], Pena, and Pena[9], Overcamp and Israel[7], Hanna[8], Wigley and Slawson[10], ESC/ Schrecker[5], and Wolf II[11]. Table 1 summarizes each of the evaporation submodels in terms of its major components. Compared in the table are the treatments of solute effects, effects of temperature, etc. Each formulation is also summarized below.

The Hosler-Pena-Pena[6] model employs the Fletcher evaporation equation. The dilute solution approximation is made to determine the vapor pressure reduction due to salt presence. These modelers determine the final state of the drop from the ambient relative humidity. Over the range of 0.65 to 0.90, saturated solution drops are assumed. Below 0.65, dry particles are assumed. The temperature dependency of all physical properties is considered.

Overcamp and Israel[7] use the Mason equation as given above but only allow the drops to go to saturated solution. Also, the code supplied to us by the model developers does not consider the temperature dependency of the physical properties.

Hanna[8] uses Eq. 1, but assumes that $T_S = T_B = T_\infty$. This gives an evaporation rate which is proportional to $(B - \lambda)$ and is thus much too large under nearly all conditions as evidenced by Fig. 1 above. The computer code supplied to us by Hanna from which the evaporation submodel was extracted does not include the temperature dependency of the physical properties such as mass diffusivity and viscosity. Hanna's code further uses a constant drop density of 1000 kg/m^3 regardless of the drop salt concentration or the presence of a precipitate particle. Evaporation ceases when the drop strikes the ground or an equilibrium is reached between the drop and ambient

vapor pressures or the drop diameter reaches that of a particle of crystalline salt equal in mass to the amount of salt in the drop. In the last case, the particle immediately assumes the density of crystalline salt thus producing a discontinuous increase in the drop settling velocity.

The ESC/Schrecker[9] model uses the basic mass transfer equation, but takes the drop temperature equal to that of the ambient wet bulb. The effect of this approximation is illustrated in Figures 1 and 2. The temperature dependency of all but the mass diffusivity of vapor in air is considered.

Wigley and Slawson[10] employ the basic mass transfer equation with approximations to the drop temperature similar in concept to that of Mason. Solute effects are not considered; thus, the integration is terminated when the drop strikes the ground or when the drop radius reaches 10 μm at which point it is assumed to evaporate completely. The model was developed for prediction of drift deposition at fresh-water towers where salt concentrations are very low. Its inclusion in our study is for comparative purposes only.

The Wolf model[11] evaluates dm/dt as a function of drop radius, temperature and relative humidity by interpolating data tabulated by Beard and Pruppacher[5]. These data are limited to a radius range of 20 to 600 μm, a temperature range of 0 to 40C, and a salt concentration of zero. Beyond these ranges, the model is not applicable. Wolf suggests, however, that the model can be used for drops containing salt. For the case of salt solution drops, Wolf states that evaporation will continue until the mass of the drop (as pure water) equals the mass of salt in the original drop. After this point, the particle becomes crystalline salt.

COMPARATIVE STUDY OF PREDICTIONS OF DROP EVAPORATION FORMULATIONS

In order to better define the differences among the various formulations for evaporation and settling, we wrote a computer code to calculate the trajectory of a drop released from a given height as predicted by each of the models under consideration. For the Hanna, ESC/Schrecker and Wigley-Slawson models, the evaporation codes were extracted directly from the drift computer programs provided to us by these modelers. For the Wolf II and Hosler-Pena-Pena models, we developed a computer code for their evaporation submodels in consultation with the modelers themselves. As a standard case, we chose a release height of 200 m, a uniform wind speed of 4 m/s, a relative humidity of 0.70, an ambient temperature of 10 C and an initial salt concentration of 0.005 g-NaCl/g-solution. From this standard case, the initial diameter, salt concentration, ambient temperature, and relative humidity were varied.

The results of the standard case prediction are given in Fig. 3. Plotted on the ordinate is height above the ground. The abscissa corresponds to the downwind distance and the curves represent droplet trajectories as predicted by the various models. Note that large differences exist in the predictions of final deposition distance. Note also that each trajectory can be divided into two parts--the first encompassing evaporation of the droplet to final size, and the second encompassing transport at final size,

with no evaporation. Since no evaporation occurs in the second segment, drop transport follows a straight line of slope V_s/U where V_s is the final droplet settling velocity. An interesting feature here is that two of the models (Overcamp-Israel and HPP) predict saturated solution drops as final state and thus land considerably closer than the three other models (Hanna, ESC/Schrecker, and Wolf) which predict dry particles as the final state. Notably, the assumed final state is reached within the first 70 m of fall.

Another interesting feature is that although the drop spends much of its time in its final state, the vertical position of the droplet when it first reaches final size is important in determining the final horizontal deposition distance. An example is the comparison of the HPP and Overcamp-Israel model predictions of final deposition distance (HPP: 6.4 km, O/I: 8.1 km). Although each predicts evaporation to a saturated drop, the distance of fall to saturation of the O/I drop is 48 m, while HPP predicts 66 m. Yet, this small difference in vertical height produces a difference in deposition distance of 1.7 km. The large distance separating the HPP and O/I drops on the ground is the result of the large ratio of wind speed to saturation drop settling velocity. The difference in deposition distance is also significant when dry particles are formed in the evaporation process. For example, the Hanna drop evaporates most rapidly and thus lands further from the point of release. Thus, the vertical position of the droplet when evaporation is completed is very important in determining the downwind deposition distance.

Thus, for this case, predictions depend on the rate of evaporation, the cutoff used to determine when final state is reached, the final state assumed for the particle (saturated solution drop, dry salt particle, or total evaporation) and the velocity of the particle at final state.

Although Fig. 3 presents the results of droplet evaporation and kinematics for a emission height of 200 m, the figure itself can be viewed as a sensitivity study to height of emission. For example, for a 50 m height of emission, one simply views the vertical region from 200 m to 150 m. Deposition distances, diameters, and settling velocities are those at the 150 m level (50 m of fall).

Figures 4-15 present comparisons of the models predictions for cases in which only one parameter is varied from the standard case. Among the variations in initial parameters shown are initial drop salt concentration C = 0, 0.005, 0.05 g-NaCl/g-soln.; initial drop diameter D_o = 50, 100, 200, 400, 600, 1000 μm; ambient temperature, T = -10, 0, 10, 20 C; and ambient relative humidity, RH = 0.3, 0.7, 0.8, and 0.9. Table 1 summarizes final drop variables at the point of deposition (or at the point of complete evaporation if deposition does not occur).

The results of our study of evaporation formulations can be briefly summarized as follows:

(a) The effect of increasing the salt concentration by a factor of 10 is to decrease the deposition distance by about four-fold and approximately double the final drop size. Doubling of the final drop size may be explained as follows. Since, for each model, the test drop struck the ground after evaporation had been completed,

increasing the salt concentration by a factor of 10 increased the final mass of the droplet (saturated solution or dry particle) also by a factor of 10. Since diameter is related to the 1/3-power of the mass, the expected diameter change would be by a factor of $10^{1/3}$ or about 2. Since drop settling velocity for small drops is proportional to the square of the diameter and since the drop traveled at its final size through most of its fall, the time of fall and therefore downwind deposition distance should be reduced by $10^{2/3}$ or about 4. The case of zero salt concentration revealed rapid evaporation in all models with the drop evaporating completely before striking the ground. The results for that case are included in Table 2 although no figure is presented

(b) Initial diameter has a very significant effect. For the 1000 μm drop, settling dominates over evaporation. As a result, the variation among model predictions is small and deposition is very close to the tower. For drops in which evaporation is important, there are wide variations in final diameters and deposition distances. The deposition distance and final size of the droplet depends heavily on whether the model considers the final state to be a dry particle or a saturated solution droplet. Smaller droplets fall further from the tower due not only to their smaller initial settling velocity but also because the dry particle formed is smaller and thus has a lower settling velocity.

For the height of release of 200 m, droplets of diameter 100 μm and less evaporate very rapidly to their final state and are transported at that state for nearly all of their fall to the ground. They may be approximated as drops of their final state (saturated solution or dry particles) from the point of fall. In contrast, droplets 600 μm and larger fall to the ground from 200 m high with almost no evaporation. Only for sizes in between (100 μm $\leq D \leq$ 600 μm) is the distance to evaporation an important consideration, for this release height.

We can generalize these results as follows. For $H^2/D_o^5 < 10^{-8}$, where H is release height in meters and D_o is initial diameter in micrometers, the drop will strike the ground almost as if no evaporation had occurred regardless of relative humidity. For $H/D_o^4 > 10^{-6}$, the drop will fall almost as if it were in its final state for the entire fall. In this case, the final state depends on ambient relative humidity. Below 0.76, the final state is a dry particle; above 0.76, the final state occurs where the droplet vapor pressure (as reduced by solute effects) equals the ambient vapor pressure.

(c) At relative humidities below 0.50, model predictions are fairly insensitive to changes in humidity. The RH = 0.70 results differ little from the 0.30 results except for the Hosler-Pena-Pena predictions where the assumed final state has changed from dry particles (RH = 0.30) to saturated solution drops (RH = 0.70). At relative humidities above about 0.70, predictions were seen to be quite sensitive to changes in relative humidity. Remarkable sensitivity in all drop variables is seen between relative humidities of 0.80 and 0.90.

(d) Larger ambient temperatures produce greater distances to deposition

This is due to the effects of temperature on saturation vapor pressure at the drop surface. Models that include the temperature dependency of the transport properties showed even greater effects.

IMPLICATIONS FOR DRIFT FIELD MEASUREMENTS

In spite of the often large differences in models predictions, several conclusions are apparent which aid in the collection of drift data at an operating natural-draft evaporative cooling tower. First, droplets of diameter less than about 300 μm do not contribute to deposition if samplers are located within the first 1-2 km downwind of the tower under normal ambient conditions. Consequently, special care should be exercised to measure mass efflux rates for droplets larger than 300 μm in diameter. At Chalk Point, for example, there has been difficulty in measuring mass emission in that range since the frequency at which large drops move through the sampling volume is small and the statistics are generally poor. The only alternative by which to study the behavior of the smaller drops is to locate the samplers further from the tower. However, measurements here would be made difficult by the small number of droplets striking per unit area and by the relatively greater amount of background.

Second, the measurement of the pertinent ambient conditions needs to be quite reliable especially for relative humidities between 0.70 and 1.00. Owing to the sensitivity of model predictions to relative humidity variations over that range, it is clear that accurate vertical ambient profiles are necessary. Yet, accuracy of a few percent in relative humidity is very difficult to achieve in the field.

ACKNOWLEDGMENTS

This work was funded by the Electric Power Research Institute. The authors also wish to express their appreciation to the modelers whose work was utilized and for their cooperation.

REFERENCES

1. Frössling, N. Gerlands Beitr. Geophysiks. 52, p. 170, 1938.

2. Ranz, W. E. and W. R. Marshall. Evaporation from Drops--Parts I and II, Chem. Eng. Progress, 48, p 141 and p 173, 1952.

3. Beard, K., and Pruppacher, H., "A Determination of the Terminal Velocity and Drag of Small Water Drops by Means of a Wind Tunnel", J. Atmospheric Sc., Vol. 26, p. 1066, 1969.

4. Fletcher, N. H., The Physics of Rainclouds, University Press, Oxford, England, 1971.

5. Mason, B. J. The Physics of Clouds, Clarendon Press, Oxford, England, 1971.

6. Hosler, C., Pena, J., and Pena R., "Determination of Salt Deposition Rates from Drift from Evaporative Cooling Tower", J. Eng. Power, Vol.

96, No. 3, 1972, p. 283.

7. Overcamp, T. "Sensitivity Analysis and Comparison of Salt Deposition Models for Cooling Towers". Paper presented and published in Proceedings of the Conference on Waste Heat Management and Utilization. Miami Beach, Florida. May 9-11, 1977.

8. Hanna, S. R. "Fog and Drift Deposition from Evaporative Cooling Towers". Nuclear Safety. Vol. 15, No. 2. March-April 1974. pp. 190-196.

9. Schrecker, G., and Rutherford, D., Personal Communication, Environmental Systems Corp., Knoxville, Tenn., 1976.

10. P. R. Slawson and T. M. L. Wigley. "Calculation of Cooling Tower Drift Deposition", Ch. 8 in Power Generation: Air Pollution Monitoring and Control. Ed. by K. E. Noll and W. T. Davis, Ann Arbor Science Publications, 1976.

11. Wolf, M. Personal Communication, Battelle Pacific Northwest Laboratories, Richland, Washington, July 1976.

Table 1.

Summary of Characteristics of Six Evaporation Submodels Employed in Drift Modeling.

Model	Evaporation Formula	Temperature-dependent Physical Constants	Drop Temperature	Evaporation to Saturated Solution and Dry Particles	Treatment of Solute Effects: Included	Treatment of Solute Effects: Method	Treatment of Solute Effects: DSA*	Treatment of Solute Effects: Internal Concentration Gradients	Precipitation	Treatment of Surface Tension Effects
Hosler, Pena, Pena[6]	Fletcher[4] (Eq. (1) and (9))	Yes	Approximation to drop wet-bulb temperature	Yes	Yes	Raoult's Law	Yes	No	solid crystal surrounded by saturated solution	Yes
Overcamp-Israel[7]	Mason[5] (Eq. (1) and (10))	No	Approximation to drop wet-bulb temperature	saturated solution drops only	Yes	Raoult's Law	No	No	None	Yes
Hanna[8]	Eq. (1) and $T_S = T_{DB}$	No	Ambient dry-bulb temperature	Yes	Yes	Raoult's Law	No	No	solid crystal surrounded by saturated solution++	Yes
ESC/Schrecker[9]	Eq. (1) and $T_S = T_{WB}$	All but coefficient of diffusion of water vapor	Ambient wet-bulb temperature	Yes	Yes	Raoult's Law	No	No	solid crystal surrounded by saturated solution	No
Wigley-Slawson[10]	Mason[5] modified (Eq. (1) and (10))	Yes	Approximation to drop wet-bulb temperature	No	No	-	-	-	-	-
Wolf[11]	Interpolation of Beard-Pruppacher[3] tables**		Ambient dry-bulb temperature	dry particles only	No+	-	-	-	-	No

* Dilute solution approximation (DSA) assumes that the solute mass is much less than the droplet mass.

** Wolf uses experimental data on the evaporation of pure water drops from Beard and Pruppacher. Evaporation rate is dependent upon droplet radius and ambient relative humidity and drop temperature.

\+ Droplet evaporation stops when droplet mass is reduced to mass of solute in initial drop.

++ Recomputation of drop density is not made during droplet evaporation calculation. Hanna assumes that droplet always has density of pure water, 1000 kg/m^3, until dry particle mass is achieved at which time the density jumps to 2165 kg/m^3.

Table 2.

Summary of predictions for distance to deposition, final diameter, and final settling velocity as determined from six drift evaporation submodels.

DISTANCE TO DEPOSITION (KM)

PARAMETER VARIED	Diameter						Drop Salt Concentration			Ambient Relative Humidity				Ambient Temperature			
Case No.	4	5	1	6	7	8	3	1	2	9	1	10	11	12	13	1	14
	D-50	D-100	D-200	D-400	D-600	D-1000	C-0.0	C-0.005	C-0.05	RH-0.30	RH-0.70	RH-0.80	RH-0.90	T-10	T-0	T-10	T-20
HANNA	257	63.7	14.5	1.59	0.37	0.22	0.23*	14.5	3.25	15.5	14.5	13.6	4.61	9.10	12.9	14.5	15.3
OVERCAMP & ISRAEL	161	39.5	8.13	0.58	0.35	0.20	0.47*	8.13	2.21	9.27	8.13	7.12	4.04	5.50	7.28	8.13	8.58
ESC/SCHRECKER	273	67.0	13.8	0.61	0.35	0.22	0.45*	13.8	3.15	15.8	13.8	12.0	6.43	8.35	11.8	13.8	15.0
WIGLEY & SLAWSON	0.08*	0.16*	0.40*	0.50	0.30	0.19	0.40*	0.40*	0.40*	0.24*	0.40*	0.64*	1.20*	1.12*	0.64*	0.40*	0.32*
HOSLER, PENA & PENA	48.7	8.31	6.40	0.56	0.35	0.20	0.60*	6.40	1.76	12.3	6.40	5.44	2.09	1.64	4.91	6.40	7.11
WOLF II	272	66.1	12.6	0.57	0.35	0.20	0.57*	12.6	3.12	15.2	12.6	10.3	3.31	1.70	10.2	12.6	13.8
NO EVAPORATION	10.3	2.58	1.12	0.50	0.33	0.20	1.13	1.12	1.09	1.12	1.12	1.12	1.12	1.12	1.12	1.12	1.12

FINAL DIAMETER (μM)

PARAMETER VARIED	Diameter						Drop Salt Concentration			Ambient Relative Humidity				Ambient Temperature			
CASE NO.	4	5	1	6	7	8	3	1	2	9	1	10	11	12	13	1	14
	D=50	D=100	D=200	D=400	D=600	D=1000	C=0.0	C=0.005	C=0.05	RH=0.30	RH=0.70	RH=0.80	RH=0.90	T=-10	T=0	T=10	T=20
HANNA	6.69	13.4	26.8	53.5	469	936	16.1*	26.8	57.6	26.8	26.8	26.8	35.5	26.8	26.8	26.8	26.8
OVERCAMP & ISRAEL	12.6	25.3	50.5	284	542	971	18.8*	50.5	109	50.5	50.5	50.3	50.5	50.5	50.5	50.5	50.5
ESC/SCHRECKER	6.61	13.2	26.4	277	542	970	25.8*	26.4	57.0	26.4	26.4	26.4	26.4	26.4	26.4	26.4	26.4
WIGLEY & SLAWSON	9.60*	17.2*	12.2*	278	544	970	12.2*	12.2*	12.2*	3.61*	12.2*	12.8*	17.9*	19.9*	18.2*	12.2*	18.5*
HOSLER, PENA & PENA	12.6	25.2	50.5	317	557	978	24.9*	51.0	117	27.7	51.0	51.0	65.8	84.1	51.0	51.0	50.9
WOLF II	6.61	13.2	26.4	299	545	972	14.5*	26.4	57.0	26.4	26.4	26.4	26.4	76.4	26.4	26.4	26.4
NO EVAPORATION	50	100	200	400	600	1000	200	200	200	200	200	200	200	200	200	200	200

FINAL VELOCITY (M/S)

PARAMETER VARIED	Diameter						Drop Salt Concentration			Ambient Relative Humidity				Ambient Temperature			
CASE NO.	4	5	1	6	7	8	3	1	2	9	1	10	11	12	13	1	14
	D=50	D=100	D=200	D=400	D=600	D=1000	C=0.0	C=0.005	C=0.05	RH=0.30	RH=0.70	RH=0.80	RH=0.90	T=-10	T=0	T=10	T=20
HANNA	0.0031	0.012	0.050	0.20	1.86	3.68	0.0083*	0.050	0.023	0.050	0.050	0.050	0.130	0.050	0.050	0.050	0.050
OVERCAMP & ISRAEL	0.0049	0.020	0.079	1.11	2.17	3.88	0.011*	0.079	0.33	0.079	0.079	0.079	0.079	0.079	0.079	0.070	0.079
ESC/SCHRECKER	0.0029	0.012	0.047	1.06	2.17	3.75	0.020*	0.047	0.21	0.047	0.047	0.047	0.047	0.050	0.048	0.047	0.046
WIGLEY & SLAWSON	0.029*	0.041*	0.033*	1.29	2.23	3.92	0.020*	0.093	0.41	0.052	0.033*	0.026*	0.025*	0.031*	0.036*	0.033*	0.050*
HOSLER, PENA & PENA	0.0049	0.020	0.079	1.28	2.23	3.92	0.020*	0.093	0.41	0.052	0.093	0.930	0.150	0.23	0.095	0.093	0.093
WOLF II	0.0029	0.012	0.04	1.18	2.18	3.89	0.0065*	0.047	0.22	0.047	0.047	0.047	0.047	0.18	0.047	0.047	0.047
NO EVAPORATION	0.078	0.31	0.71	1.60	2.40	4.01	0.71	0.71	0.73	0.71	0.71	0.71	0.71	0.71	0.71	0.71	0.71

* Drop evaporates before striking ground. The value in table is at point of evaporation.
Note: D = initial droplet diameter (μm), T = ambient dry bulb temperature (°C), C = droplet salt concentration (g-NaCl/g-soln.), and RH = ambient relative hunidity (fraction).

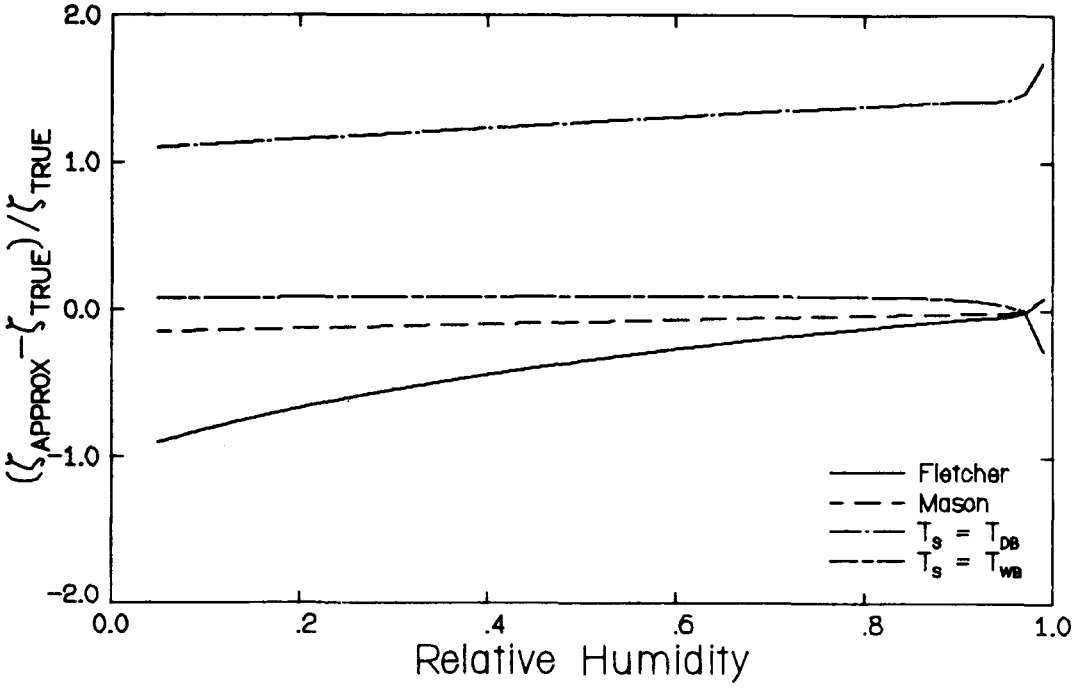

Fig. 1. Comparison of Evaporation Rates from Four Models for Drops with Dilute Solution (B = 0.998); at T_∞ = 10C.

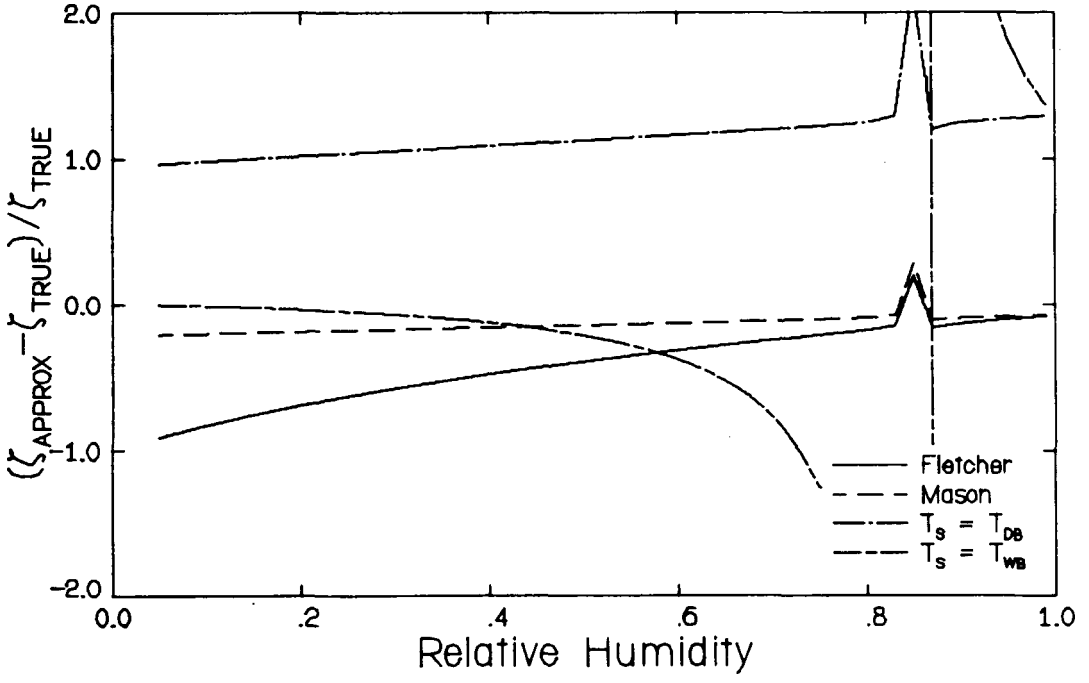

Fig. 2. Comparison of Evaporation Rates from Four Models for Drops with High Salt Concentration (B = 0.85); at T_∞ = 10C.

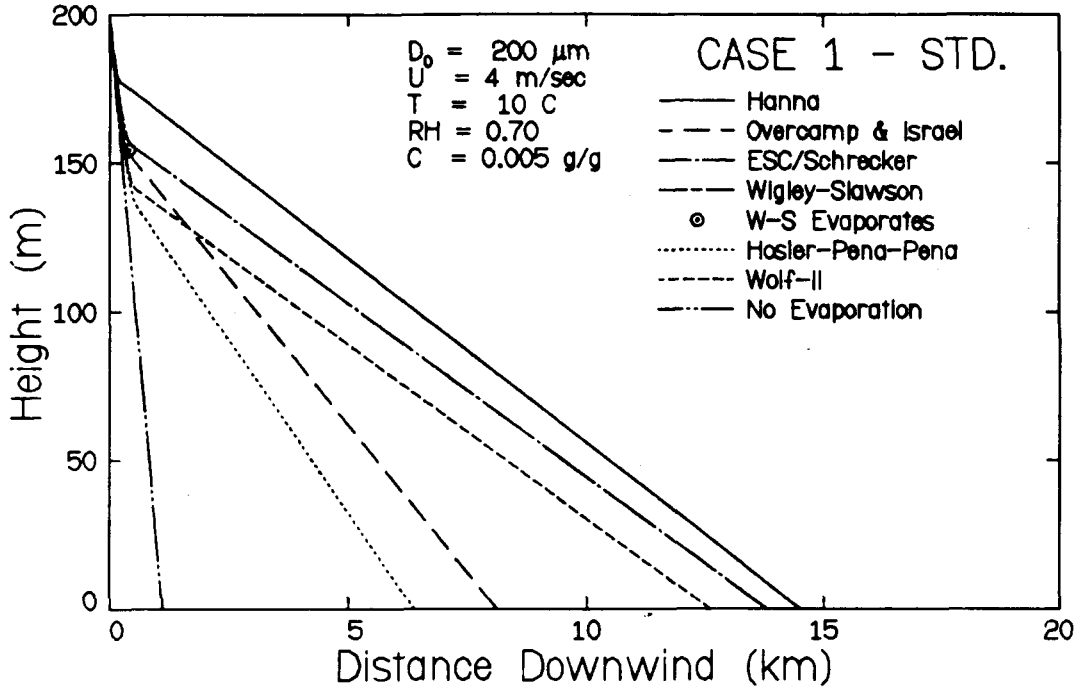

Fig. 3. Comparison of Six Droplet Evaporation Submodels for Standard Case .... Case 1.

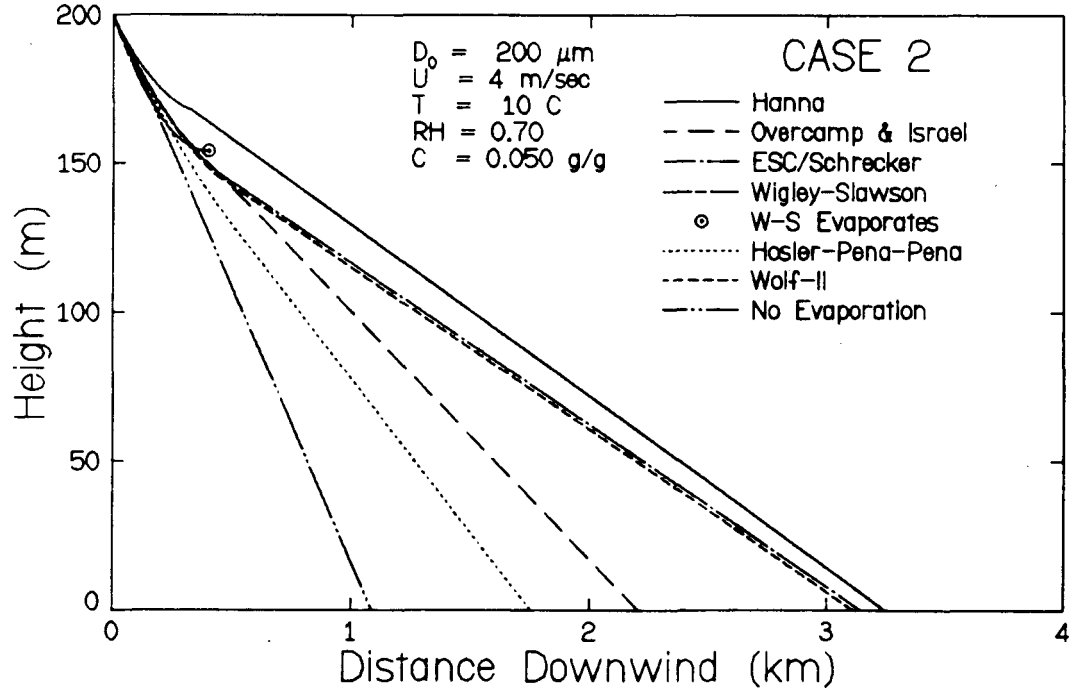

Fig. 4. Case 2 .... Standard Case Except C = 0.05.

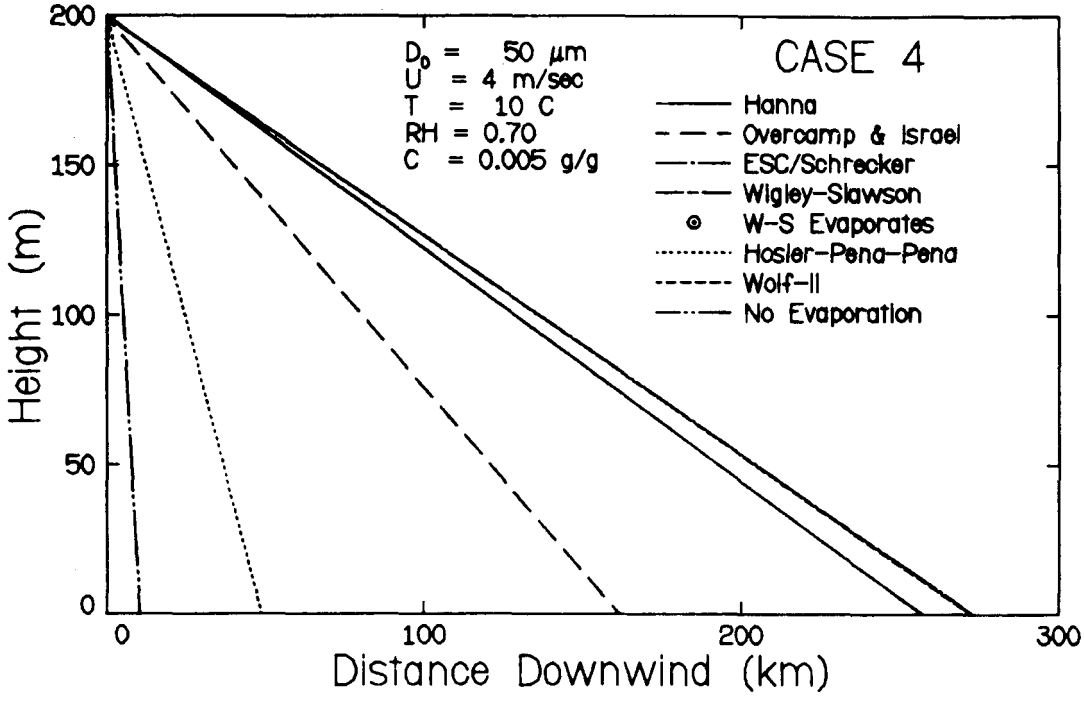

Fig. 5. Case 4 .... Standard Case Except D = 50.0 μm.

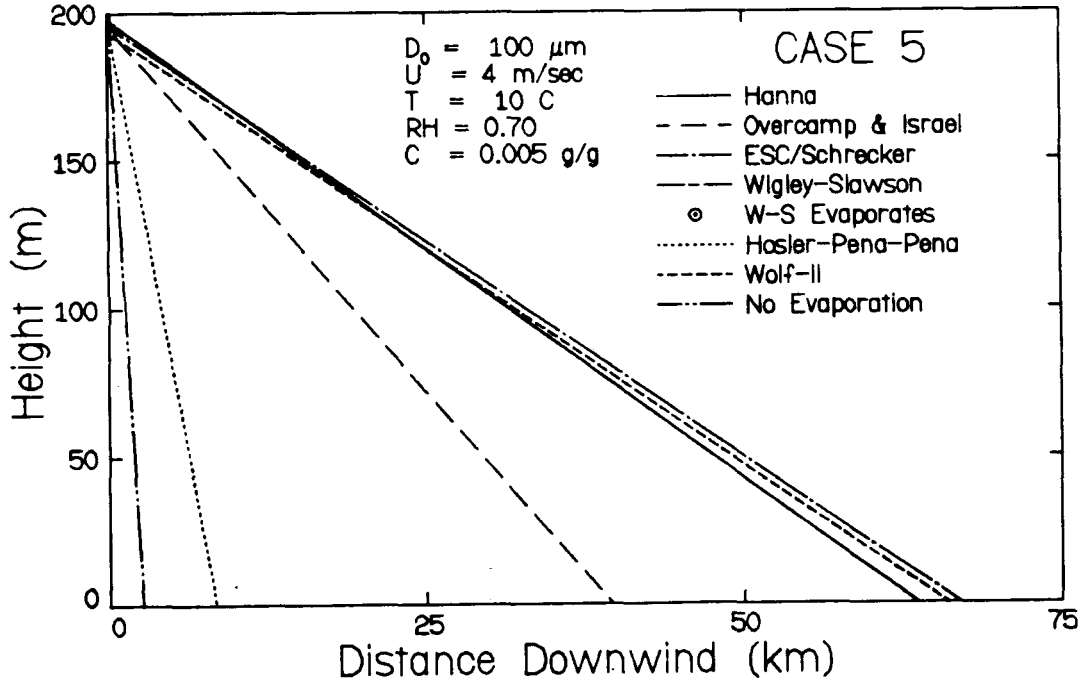

Fig. 6. Case 5 .... Standard Case Except D = 100 μm.

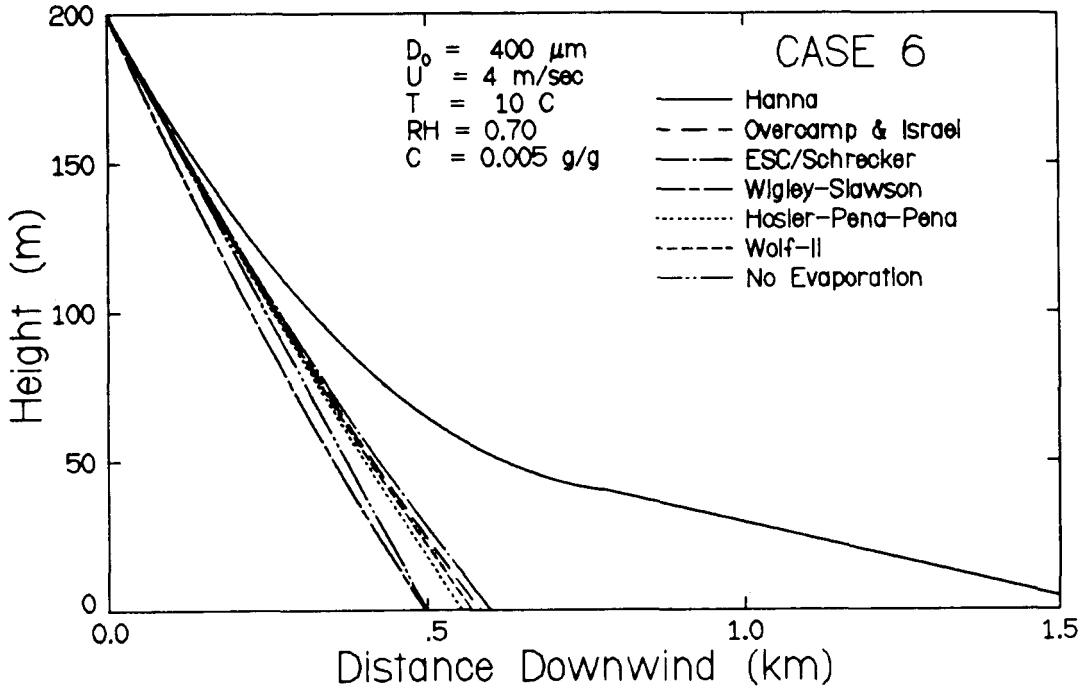

Fig. 7. Case 6 .... Standard Case Except D = 400 μm.

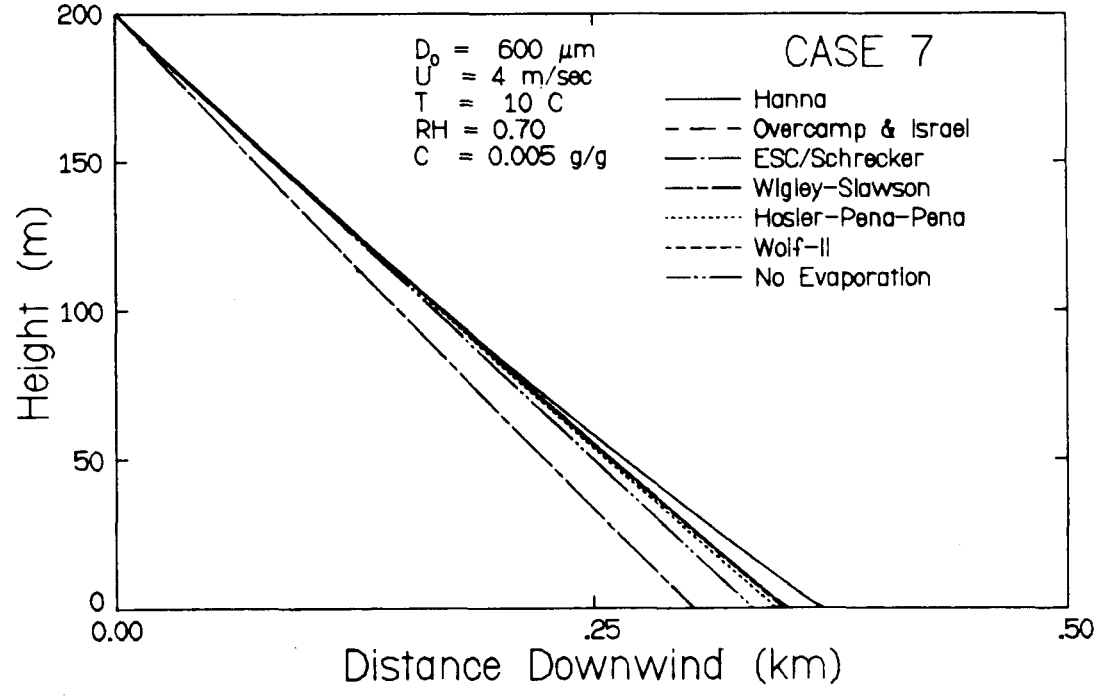

Fig. 8. Case 7 .... Standard Case Except D = 600 μm.

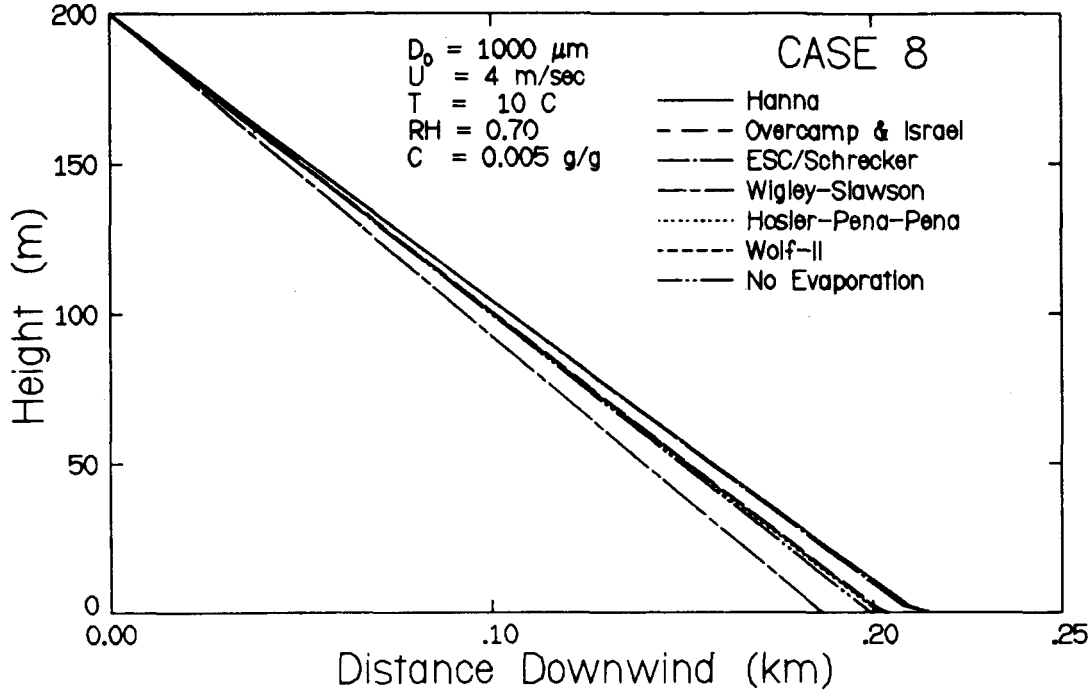

Fig. 9. Case 8 .... Standard Case Except D = 1000 μm.

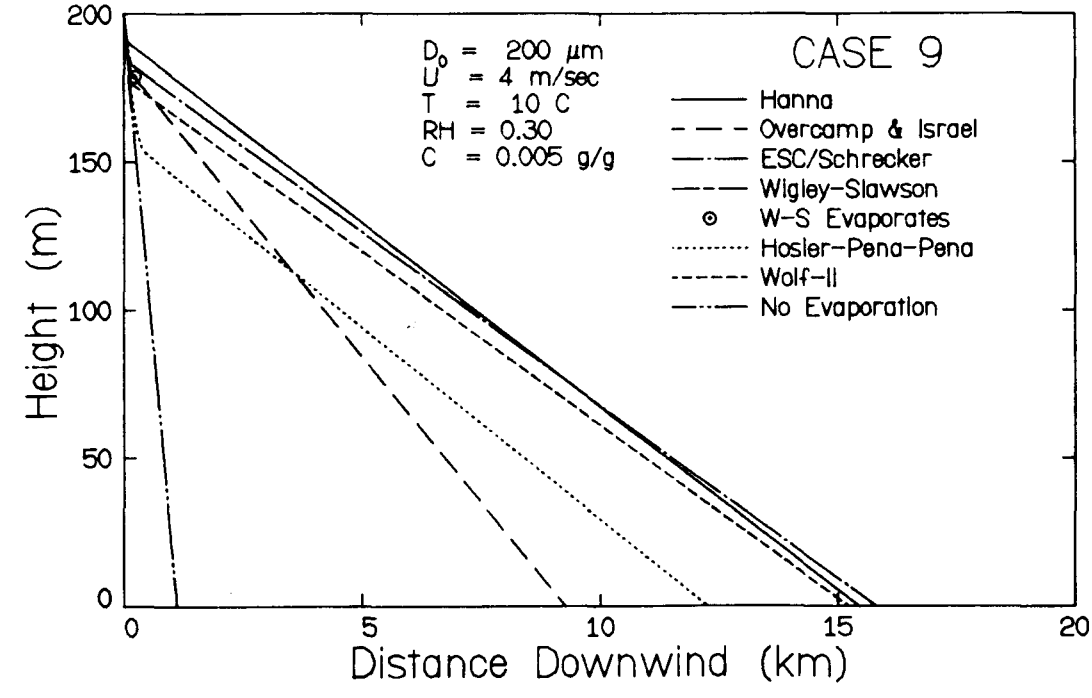

Fig. 10. Case 9 .... Standard Case Except RH = 0.30

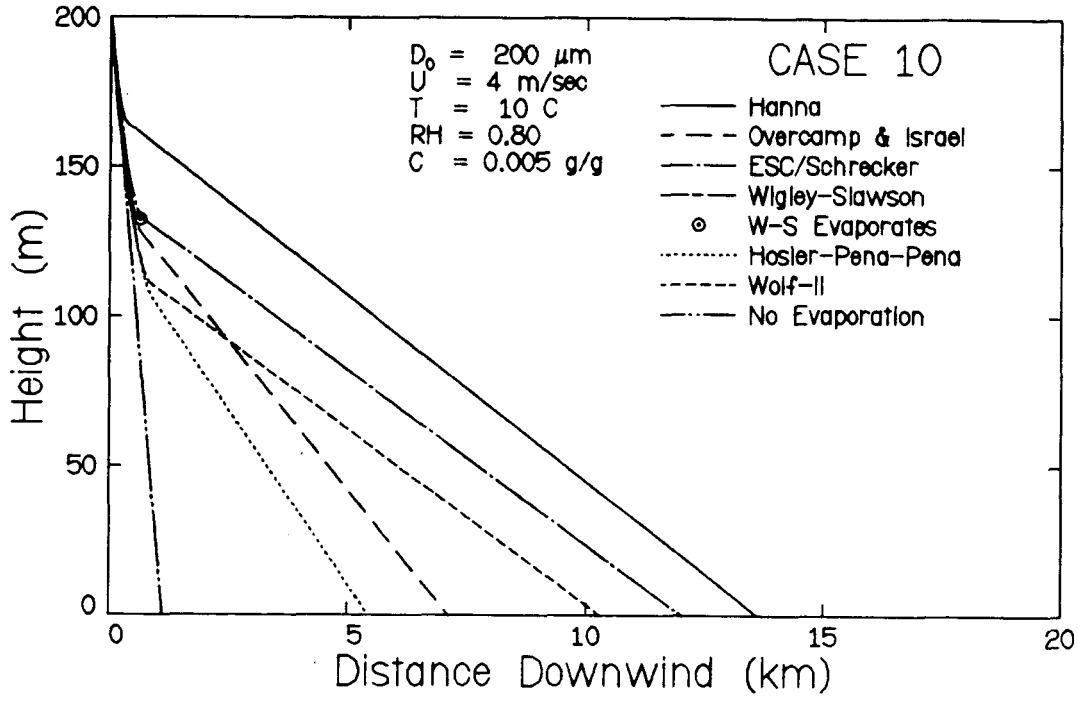

Fig. 11. Case 10 .... Standard Case Except RH = 0.80.

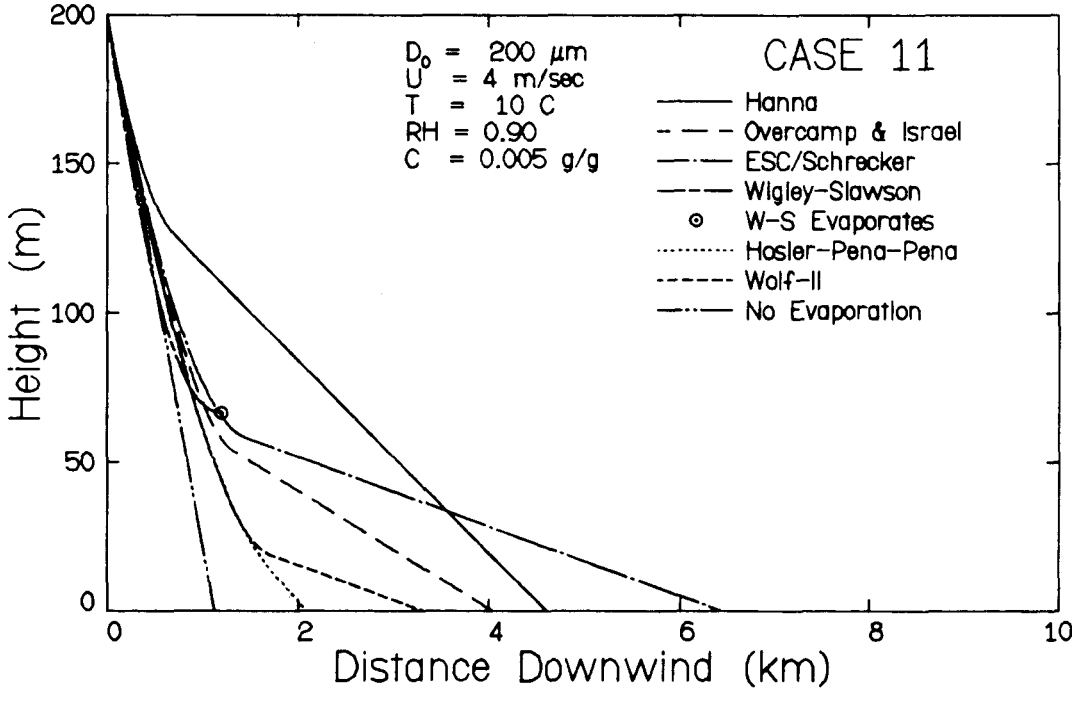

Fig. 12. Case 11 .... Standard Case Except RH = 0.90.

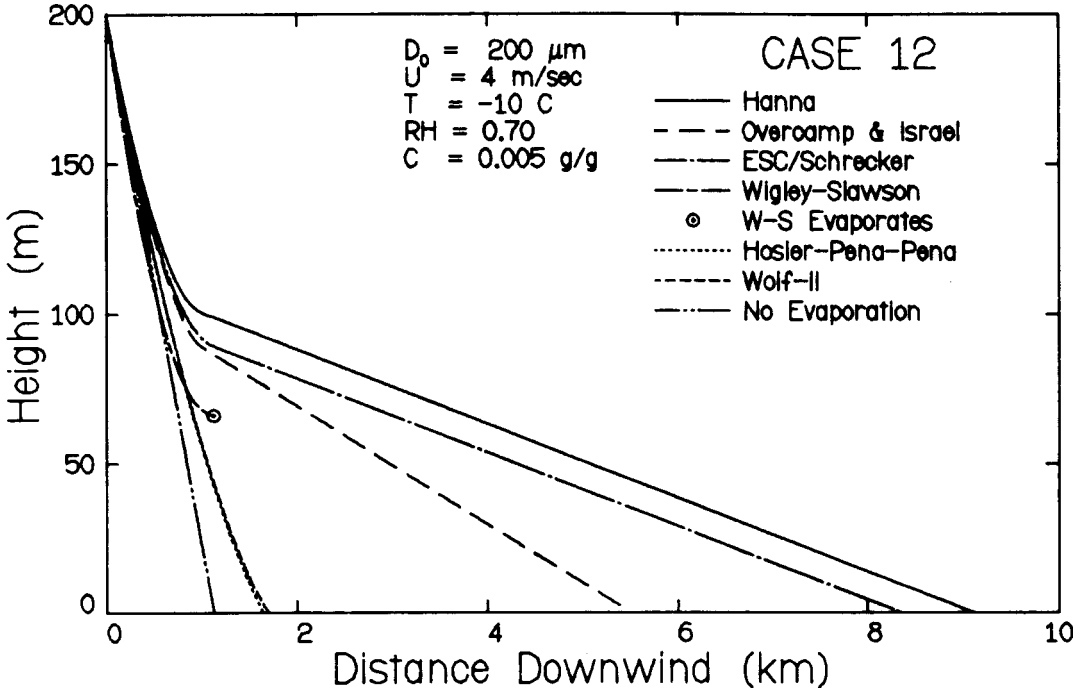

Fig. 13. Case 12 .... Standard Case Except T = -10C.

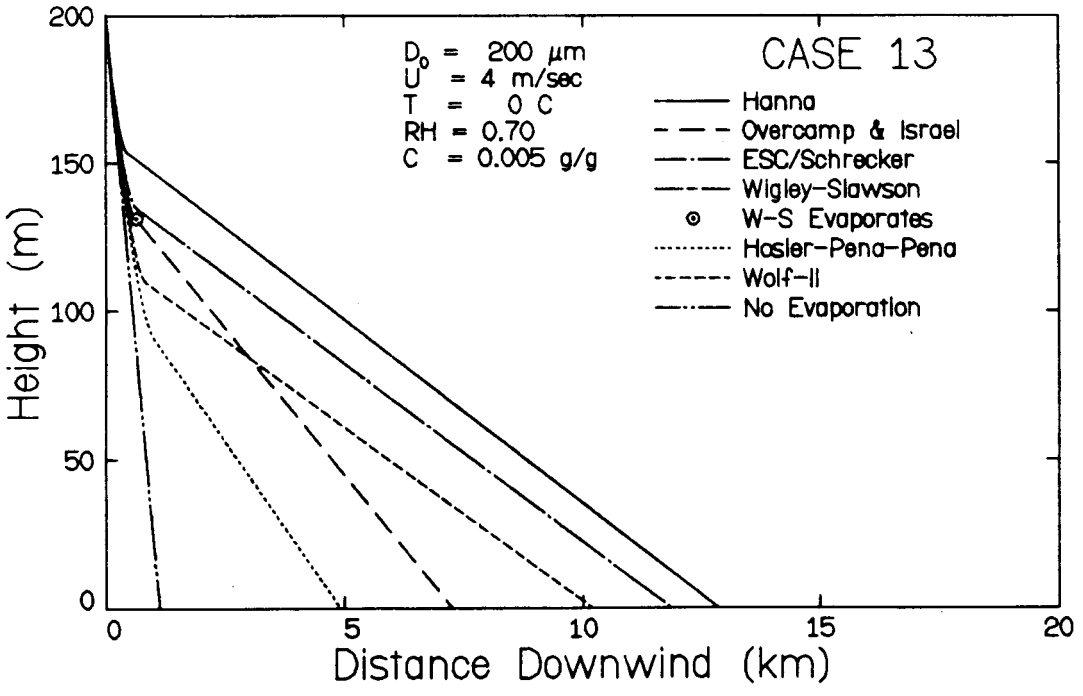

Fig. 14. Case 13 .... Standard Case Except T = 0C.

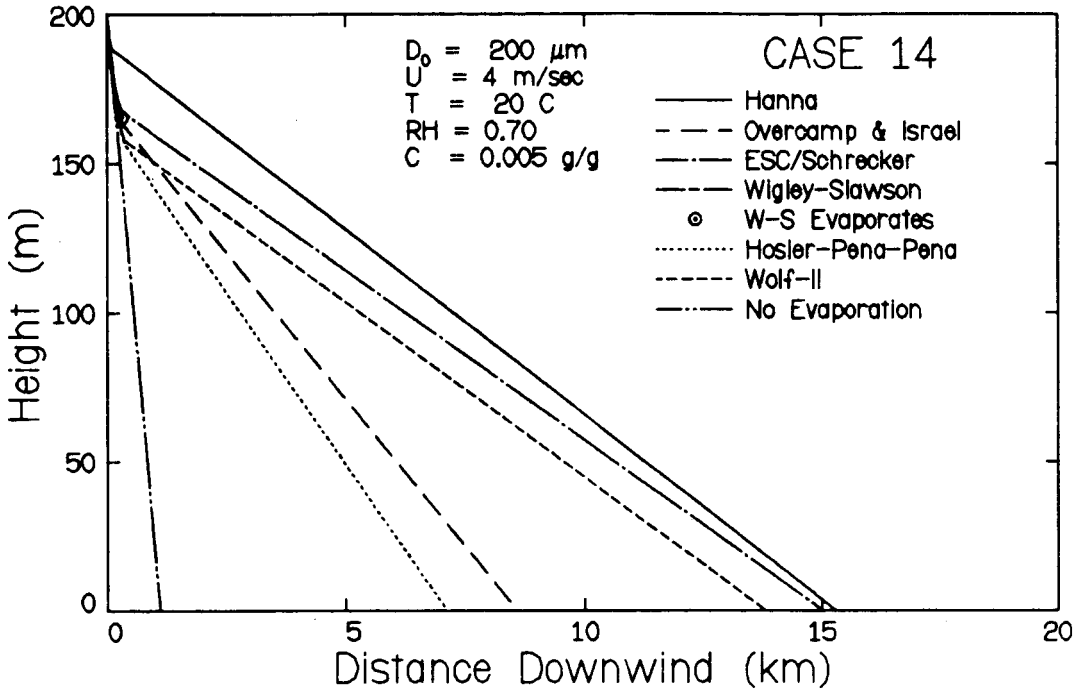

Fig. 15. Case 14 .... Standard Case Except T = 20C.

Blank

Section 4

THE CHALK POINT DYE TRACER STUDY: VALIDATION OF MODELS AND ANALYSIS OF FIELD DATA

This section provides a detailed study of field data on salt-drift deposition acquired at the Chalk Point Power Plant in Maryland in 1977. Rhodamine dye was used as a tracer in the tower cooling water in order to allow separation of tower and stack deposition contributions at ground level. Systematic behavior of the data was identified where possible. That data analysis was helpful in the evaluation of existing models as well as providing a basis for model improvement. The performance of existing models with these Chalk Point data are presented. These data are limited in that they represent only high humidity conditions, strong stability, and distances of only 0.5 and 1.0 km from the tower. In addition, the data lack good statistics in droplet fluxes for drops emitted from the tower larger than 300 μm. Despite these deficiencies, the 1977 Chalk Point Dye Study represents an excellent opportunity to test the predictive performance of models.

Indeed, much insight was gained in those model/data comparisons. Of the ten models tested with these data, the ESC/Schrecker model predicted most favorably, nearly within a factor of three for sodium deposition flux, liquid mass deposition rate, number drop deposition flux, and average diameter. The Hosler-Pena-Pena (ANL) and Wigley-Slawson models also compared favorably with the data, and, in terms of sodium deposition flux measurements at 0.5 km and 1.0 km distances downwind, were generally within the error bounds of the data. These data, however, were taken under high humidity, very stable and moderately windy conditions. The model performances can not necessarily be extrapolated to significantly differing environmental conditions.

This paper reconfirms some important areas of needed model improvement which were mentioned in Section 2. They are:

1. use of a plume model which accounts for full ambient profiles of environmental variables. The plume model should be validated with plume rise data for cooling towers. The Briggs-type formulas are

less desirable since (a) the formulas cannot account for local variations in ambient profiles, and (b) the formulas are developed from a theory which required special simplifications to provide a closed-form solution.

2. preparation of predictions based on 10-min. or 30-min. averages of meteorological conditions. It has been common to average, say, 4 hours of ambient conditions to provide one set of model input conditions for a single run of the model. Such treatment does not account for true ambient wind direction variations during a 4-hour period. Model calculations for each of 24 10-min. sub-periods or 8 30-min. sub-periods with a summation of results for each sampler provided a much closer representation of the actual distribution of ground measurements.

Model/data comparisons also support the modeling needs noted in Section 2. Most notable is the need to evaluate and perhaps better define the breakaway criterion and its effect on drift drop deposition.

Reprint of Paper #3:

"The Chalk Point Dye Tracer Study: Validation of Models and Analysis of Field Data"

A. J. Policastro
W. E. Dunn
M. L. Breig
J. P. Ziebarth

Published in Proceedings of the Second Conference on Waste Heat Management and Utilization. Miami Beach, Florida. December 4-6, 1978. Eds. Samuel S. Lee and Subrata Sengupta. University of Miami, Coral Gables, Florida.

THE CHALK POINT DYE TRACER STUDY: VALIDATION OF MODELS AND ANALYSIS OF FIELD DATA

A. J. Policastro*
W. E. Dunn□
M. L. Breig●
J. P. Ziebarth○

ABSTRACT

Predictions of ten models are compared with field data taken during the Chalk Point dye tracer study of June 1977. The ESC/Schrecker, Hosler-Pena-Pena, and Wigley-Slawson models compared most favorably with the deposition data from the cooling-tower alone and are generally within the error bounds of the data. Most models predict larger drop diameters at deposition than were measured. No model predicted each of the deposition parameters consistently within a factor of three. Predictions of stack deposition compared rather poorly with the stack deposition data probably due to the lack of good information on exit conditions.

A comparison of Johns Hopkins University (JHU) and Environmental Systems Corporation (ESC) ground-level drift data showed that the JHU data had larger drop counts in both the smallest and largest drop size ranges yet both sets of data agreed quite well in the intermediate drop size range. The JHU methodology appears superior since their data were more internally consistent and their technique of using large sensitive paper samplers and counting all drops on the paper yields a greater statistical accuracy.

INTRODUCTION

Drift refers to the small droplets of liquid water released from a cooling tower along with the warm, moist plume. These droplets, ranging in size from a few to more than 1000 microns in diameter, are transported through the atmosphere eventually evaporating totally or being deposited on the ground. If the droplets contain large concentrations of dissolved solids, as is particularly the case when brackish cooling water is used, then the drift deposition may damage vegetation and/or accelerate the corrosion and deterioration of structures.

---

*Engineer, Div. of Environmental Impact Studies, Argonne National Lab.
□Asst. Professor, Dept. of Mech. & Ind. Engr., Univ. of Ill., Urbana.
●Visiting Scientist, Div of Environmental Impact Studies, Argonne Nat. Lab.; Perm. Add.: Dept. of Physics, Eastern Ill. Univ., Charleston.
○Engineer, Div. of Environmental Impact Studies, Argonne National Lab.

Therefore, predictions of anticipated drift-deposition rates are essential to an informed estimate of the environmental impact of a plant for which cooling towers are planned.

Once emitted from the tower, a drift drop moves under the combined influences of gravity and the aerodynamic drag force produced by the vector difference between the drop and local air velocities. Simultaneously, the drop experiences both heat and mass transfer. As a result, the drop temperature will approach the drop wet-bulb temperature and evaporation will occur as long as the vapor pressure at the drop surface exceeds that of the local ambient. For a drop containing salt, evaporation will increase the concentration within the drop and thus lower the vapor pressure at the drop's surface. The salt concentration will continue to increase until either (a) the droplet vapor pressure exactly equals that of the local ambient after which evaporation will cease or (b) the salt becomes saturated within the drop after which salt particles will begin to precipitate out as evaporation proceeds. In the latter case, the drop will eventually become a dry particle, although it may strike the ground before reaching its final state. The purpose of a drift model, then, is to predict the number, size, and character of drops and/or particles striking the ground at any given location with respect to the emitting tower.

Numerous mathematical models have been formulated to predict drift plumes and drift-deposition patterns. Although each of these models has a number of theoretical limitations, good quality field data have been lacking to determine the limits of reliability of these models. Field data taken at the Chalk Point Power Plant in 1975 and 1976 by the Environmental Systems Corporation suffered from several inherent deficiencies: ground samplers were too small in size and few in number, no separation of cooling tower and stack drift was made, etc. Those data provided a rough test of the models, yet the limitations of those data did not allow definitive conclusions to be made about the field performance of the models tested.

The field data taken at Chalk Point in June, 1977 by the Environmental Systems Corporation (ESC) [1] and independently by the Johns Hopkins University (JHU) [2,3] represent a significant improvement in the data collection methods and the culmination of more than three years of experience in drift data collection. The data, taken as a whole, are of good quality and sufficient to provide a true test of the models' capability. In fact, these data are presently the only good-quality field data on drift deposition available in the literature. The purpose of this paper then is to evaluate the performance of 10 drift models [4-11] with respect to these data and to provide an analysis of the data themselves to uncover special trends. Moreover, the ground-level data taken simultaneously by the two groups (ESC and JHU) will be intercompared as a test of their measurement and data reduction methods. It is important that such data be studied in detail due to the uniqueness of these good-quality data as well as the difficulty and expense of acquiring new data.

It must be noted that while these data are the best available and were obtained only through a very carefully executed measurement program, the data were obtained at only two radial distances from the tower. Thus the data encompass only one of several possible regimes of droplet behavior.

THE FIELD EXPERIMENT

The Chalk Point Unit No. 3 cooling tower and stack effluent scrubber produce salt water drift because of the saline Patuxent River water used for the cooling tower circulating water and the stack particulate scrubbing agent. Previous drift measurements at Chalk Point have used sodium as a tracer and consequently separation of cooling tower and stack drift was not possible. To provide a positive identification of the drift deposition from the individual sources, JHU used a water soluble fluorescent dye (Rhodamine WT) as a tracer in the cooling tower circulating water. The photolytically unstable dye required that the experiment be performed at night. The drift dye tracer experiment was conducted during a four-hour period on June 16 and 17, 1977.

The instrumentation used by JHU consisted of 10.5 inch diameter modified deposition funnels for sodium and dye concentration measurements and 10.5 inch diameter Millipore HA type filter papers for measurement of total chloride and dyed drift droplet deposition. Three filter papers per sampling station were used for the deposition measurement of all water droplets (water sensitive filter paper), chloride containing droplets (plain filter paper) and dyed drift droplets (plain filter paper). A sketch of the sampler is shown in Fig. 1. The sampler consisted of a post with rectangular and triangular brackets for holding the funnel and sample bottle, and a filter paper holder plate with a can type candle heater. Filter paper heaters were required because of night time condensation which could affect the drop size measurements. The filter papers were photographed for fluorescent droplets using ultraviolet light. In this way, droplets deposited from the cooling tower could be identified. The water sensitive filter papers were used to define total drops deposited from all sources (stack and cooling tower). A calibration curve for droplet sizes was used to relate drop deposit size to falling drop size. The funnel samples were corrected to a standard volume (after being washed with distilled water) and split into two parts. One part was analyzed for sodium using an atomic absorption spectrophotometer while the other part was concentrated by boiling and analyzed for dye by fluorometry. The funnels could then give sodium deposition rate from all sources (tower and stack) by analyzing total sodium content of the sample. The funnels could also determine the part contributed by the tower alone by pro rating the dye deposited in the funnel to the ratio of the sodium to dye concentration in the basin water.

Fig. 1 also shows the Chalk Point power plant area and the JHU array of 8 stations on the 0.5 km arc (40 m apart) and 14 stations on the 1.0 km

arc (40 m apart). Each sampling station consisted of three samplers (see Fig. 1) to ensure at least one good sample in case of accidents or contamination during sample collection and for good statistics. A total of 26 sampling stations were used by JHU on the night of the dye test. Each sampling station used during the experiment by JHU is identified with a number.

A number of drift parameters were measured at ground level downwind of the cooling tower by ESC. Typically, ESC uses four or five stations to measure the following ground-level drift quantities.

1. Sodium concentration in the air (micrograms-Na/m^3) using a rotating tungsten mesh.

2. Liquid droplet concentration as a function of droplet size (g-water/m^3) using a rotating sensitive paper disk.

3. Liquid droplet deposition flux as a function of droplet size (kg-water/km^2-month) using a stationary sensitive paper disk.

4. Sodium mass deposition flux (kg-Na/km^2-month) using a stationary funnel and bottle assembly.

The ESC sampling stations for the dye study are also located in Fig. 4 (denoted E1-E4). Some of the ESC ground-level stations were fixed in location and thus received drift only when the wind was blowing in the proper direction. Other stations were located beneath the cooling tower plume, being moved as the wind direction changed. For the purpose of model-data comparisons with the ESC data, we used the droplet number deposition flux measurements obtained using sensitive paper disks fixed to a petri dish and the sodium mass deposition flux obtained using the stationary funnel and bottle assembly. In addition to the ground-level measurements, source and ambient conditions were also measured by ESC.

Drift rates from the cooling tower were determined by ESC using an instrument package suspended in a plane approximately 13.6 m below the tower exit. The following measurements were made:

1. The drift droplet size spectrum was measured using sensitive paper and with a device based on scattering of infrared laser light (PILLS II-A, Particle Instrumentation by Laser Light Scattering).

2. The drift mineral mass flux was measured with a heated glass bead isokinetic (IK) sampling system.

3. The updraft air velocity (from which droplet velocity was determined) was measured using a Gill propeller-type anemometer.

4. The dry-bulb and wet-bulb exit temperatures of the plume were also measured.

The IK system sampled continuously during the traverse and yielded the sodium and magnesium mineral flux at the measurement plane. Updraft air velocities were acquired and averaged for each point. Grab samples of circulating water were also taken for chemical analysis of sodium and magnesium content. These two cations, which are present in the highest amounts in the water, were chosen as tracer elements for the IK measurements. No source measurements were made for the stack however.

Ambient meteorological measurements were made using the Chalk Point 100 meter instrument tower which has wind and temperature instruments at three levels (7 m, 50 m, and 92 m) and dew point sensors at two levels (7 m and 92 m). Ten minute averages of dry bulb and dew point temperature and wind speed were taken. Due to the location of the meteorological tower on a hill, the 92 meter level on the meteorological tower was at the same vertical elevation as the cooling tower exit plane. To supplement the meteorological tower measurements, rawinsonde flights were conducted at intervals of 1 hour by JHU in order to establish the short-term history of diurnal stability characteristics. Measurements of pressure (elevation), dry-bulb temperature, relative humidity, and wind speed (and direction) were made every 10 to 20 meters vertically.

ANALYSIS OF FIELD DATA AND COMPARISON OF JHU AND ESC DATA

The published presentation [2,3] of the JHU data revealed several interesting facts. A histogram plot of the total water and fluorescent droplet size distributions for the approximate cooling tower plume centerline sampling stations, 0.5 km/355 deg. and 1.0 km/350 deg., indicates a bimodal distribution (see Fig. 2). One peak occurs at about the 40-60 micron droplet size and the other between 200 to 400 microns. The second peak is expected from model calculations while the first one is not. Meyer and Stanbro [2,3] suggest that the source of these droplets is most probably blowoff from the cooling tower fill. The droplet distribution data for the other 22 sampling stations in the JHU net has yet to be reduced. Figure 3 presents the above droplet distribution data as percent mass fraction. The smaller droplets with their greater number contribute less than 1% to the total mass fraction. Note also that the fluorescent droplet distibution peak is separated from the total water peak by approximately 80 microns. The shift in the peaks between fluorescent and total drops is probably due to larger droplets originating in the stack. Also shown in Fig. 3 is a comparison of salt deposition contributions from the cooling tower and stack at near centerline locations 0.5 km and 1.0 km downwind of the tower. Note that each distribution is nearly bell-shaped and due, we believe, to the variation in wind direction with time during the measurement campaign. Also, the distinction between the contributions of the two sources is clearly seen at the 0.5 km distance and gets less distinct further from the tower as may be seen by the comparison at the 1.0 km location.

Figure 4 shows the placement on the ground of the four ESC and the two JHU samplers which have data reduced in the form of droplet size ranges. J1 and J2 indicate the two samplers of JHU, and E1 through E4 represent the locations of the appropriate ESC samplers.

The first parameter we studied for each of the six samplers was the drop size spectrum measured at particular sampler locations. Figure 4 gives the drop size distributions reported for the JHU and ESC data. The JHU spectra are clearly bimodal with a large peak of small drops (up to 100 microns) and a second peak of larger drops (approximately 250-280 microns). The ESC spectra also show bimodal tendencies, but the small drop count is smaller for samplers E2, E3, and E4.

Figure 5 shows the same data replotted in terms of mass distribution. Here, we see that very little mass is contributed by drops less than 100 microns in diameter. The largest drops also contribute very little except for ESC sampler E1 in which one drop contributed 8% of the total liquid mass. Problems with a few large drops contributing a significant fraction of the mass were evident in the 1976 ESC data as well.

It is instructive to examine next the average drop size measured at each of the ESC and JHU samplers. Defining an average drop size poses some interesting questions as several alternatives are possible.

1. Mass Mean Diameter - d_{MM}

   $$d_{MM} = \left(\Sigma C_i \; d_i^3 \; / \Sigma C_i \right)^{1/3}$$

   where C_i is the number of drops in an interval and d_i is the corresponding drop diameter.

2. Mass Median Diameter - $\bar{d}$

   $\bar{d}$ is selected such that 50% of the total mass is contributed by drops larger than $\bar{d}$ and 50% by drops less than $\bar{d}$.

3. Count Mean Diameter - d_{CM}

   $$d_{CM} = \Sigma C_i \; d_i \; / \; \Sigma C_i$$

4. Mass Peak Diameter - d_{MP}

   d_{MP} is the diameter at which the greatest mass contribution occurs.

5. Count Peak Diameter - d_{CP}

   d_{CP} is the drop diameter with the highest recorded count.

Listed in Table 1 are the values of these characteristic diameters computed from the JHU and ESC drop size distributions shown in Fig. 5.

The mass mean and mass median diameters are fairly representative of the corresponding distribution with the mass mean being roughly 40 to 50 microns smaller than the mass median. The mass peak diameter is intermediate between these two. The count mean is much smaller reflecting the large counts of small drops. The count peak diameter is not unique.

Among these, either the mass mean diameter or mass median diameter is preferable; however, neither of these is totally satisfactory. The mass mean diameter can be greatly affected by errors in the small drop data (large count, small mass). In contrast, the mass median diameter is sensitive to errors in the large drop data (small count, large mass). Since the greater uncertainty appears to be in the small drop counts for the 1977 data, we have chosen to use the mass median diameter to characterize these data.

Figure 6 shows how mass median diameter varies with distance from the tower. A trend of decreasing drop size with increasing distance from the tower is evident, but Sampler E4 does not follow the trend. This may be due to a greater influence of the stack. Recall that the JHU investigators found that the stack distribution has a greater number of larger drops. As shown in Fig. 4, Sampler E4 experiences a stronger stack influence than do the other samplers.

A fourth test of the data concerns the consistency between the four independent measurements: sodium deposition flux, liquid deposition flux, sodium concentration and liquid concentration. We can calculate from the data <u>apparent droplet salt concentration</u> and <u>deposition velocity</u>.

1. Apparent Droplet Concentration

$$C_{DD} = \begin{bmatrix}\text{Apparent concentration} \\ \text{from deposition data}\end{bmatrix} = \frac{\text{Sodium deposition flux}}{\text{Liquid deposition flux}}$$

$$C_{CD} = \begin{bmatrix}\text{Apparent concentration} \\ \text{from concentration data}\end{bmatrix} = \frac{\text{Sodium concentration}}{\text{Liquid concentration}}$$

2. Apparent Deposition Velocity

$$V_{SD} = \begin{bmatrix}\text{Apparent velocity}\\ \text{from sodium data}\end{bmatrix} = \frac{\text{Sodium deposition flux}}{\text{Sodium concentration}}$$

$$V_{LD} = \begin{bmatrix}\text{Apparent velocity}\\ \text{from liquid data}\end{bmatrix} = \frac{\text{Liquid deposition flux}}{\text{Liquid concentration}}$$

Table 1 summarizes the comparison of these calculated quantities. (Note that the basin-water salt concentration (for the tower) was 0.014 g/g.) The agreement here is within a factor of 2 with one exception, suggesting some consistency among the ESC data. Also, the magnitudes given are not unreasonable. Notably, C_{CD} is consistently larger than C_{DD}, and V_{LD} is consistently larger than V_{SD}. This may be fortuitous as a suitable explanation is presently lacking.

As it happens, Samplers J1 and E3 are within 26 meters of one another. Thus, we may compare almost directly the measurements obtained independently by these two different groups. Figure 6 compares the count and mass distributions as functions of drop diameter. The following observations can be made. First, the JHU sampler shows a greater droplet count both below about 100 microns and above about 300 microns, (although agreement above 600 microns is good). Second, the JHU mass distribution is clearly shifted toward greater diameters, although agreement above 550 microns is good. Despite this discrepancy, the mass median diameter computed from the JHU distribution is 400 microns whereas that computed from the ESC distribution is 336 microns, which is less than a 25% difference. It is possible, although unlikely, that the JHU sampler received a larger contribution of drops from the stack than did the ESC sampler.

MODEL VALIDATION WITH JHU DATA

Critical reviews of the 10 models tested appear in References 12 and 13. Described below are the major features of the methodology used to make the model/data comparisons in this study.

1. Model predictions were made using the 10-minute averages of meteorological conditions acquired at the time of the dye study in order to better account for the variability of these conditions on deposition predictions. Predictions were made for each 10-minute period and the results summed over the four-hour duration of the study.

2. A 15 degree sector was chosen over the more common 22 1/2 degree sector due to the short duration of the averaging period.

3. For nine models, the 92-m level on the meteorological tower was used to provide the needed input. For one model (Wigley-Slawson), radiosonde profiles were used as well since that model has an option to accept full profiles.

4. At first, only the cooling tower was simulated and only the deposition acquired from the dye was used in the model/data comparisons. Sodium deposition rate, liquid mass deposition rate, number droplet deposition rate, and average diameter were computed by the models and also extracted from the data. The sodium deposition rate included contributions from all sizes; the other three ground-deposition variables were computed only from droplets of diameter greater than 100 microns. Average diameter was computed using the liquid mass deposition rate (droplets greater than 100 microns only) and number drop deposition rate (greater than 100 microns only). It should be noted that, although sodium deposition data were available from 8 locations along the 0.5 km arc and 12 locations along the 1.0 km arc, the data on droplet counts were reduced and made available only for the 0.5 km/355 deg. and 1.0 km/350 deg. locations. Thus data for number droplet deposition flux, liquid mass deposition rate and average diameter are available at only those two ground locations. We also made calculations for the stack separately and also combined cooling tower plus stack contributions at each sampler. No measurements at the stack were made during the dye study so we estimated the droplet size spectrum, liquid mass emission rate, exit temperature and velocity from measurements made in the stack during the previous study June, 1976. We will discuss those results later. The total of stack and cooling tower contributions were then compared with the plain filter paper results of JHU.

The results of the model/data comparisons for the cooling tower alone are given in Figs. 7 and 8 and Table 2. In Figs. 7 and 8, the model predictions of sodium deposition are plotted with respect to angle along the 0.5 km (Fig. 7) and 1.0 km arcs (Fig. 8) downwind of the tower. Tabular results of sodium deposition with angular position and distance from tower are listed in Table 2. Error estimates for the data are also shown. Notably, the plot of the observed sodium deposition rate is a bell-shaped curve on the angular range for which salt-drift data were acquired. Note also that the model predictions represent generally bell-shaped curves themselves. This is due to the variation in wind direction for the 10-minute averages of meteorological data. The usual procedure of averaging meteorological conditions over a four-hour period would provide only a single average value of deposition rate for the full four-hour period. Clearly then, wind direction variation with time is a likely explanation of the bell-shaped distribution of drift.

Some other general characteristics of the comparisons are noteworthy. First, wide variations among the predictions is striking. The Slinn I

predictions of sodium deposition rate are too large to fit on the scales of Figures 7 and 8. Second, the models tend to underpredict sodium deposition at the left and right end of the 0.5 km and 1.0 km arcs. This underprediction may be due, in part, to our choice of a 15 degree sector. A larger angle for sector-averaging may partially mitigate the discrepancy. Third, two predictions were made for both the ESC/Schrecker and Wigley-Slawson models in order to study the effects of changes in the input data on predictions. The second prediction of the ESC/Schrecker model, labeled "ESC/ Schrecker (limited)", was made by reducing the measured drop size spectrum from 25 to 8 intervals. Clearly, this modification of the spectrum led to a significant overprediction of sodium deposition in this case. The first prediction of the Wigley-Slawson model, labeled "Wigley-Slawson (profiles)", was made using the full ambient profiles as recorded by radiosonde flights with wind direction obtained from the meteorological tower. The second prediction was made using the met-tower data alone as was done for each of the other models. Here again, performance is degraded as the detail of the input data is degraded.

A few models, notably ESC/Schrecker, Wolf II, and Wigley-Slawson appear to be most accurate over the range of comparisons in Figs. 7 and 8. Observations on the performance of individual models will now be presented.

The ESC/Schrecker model (full spectrum) is rather good in its prediction of sodium deposition except at angles between 340 and 345 degrees on the 1 km arc, where the prediction is rather low. The predictions at 0.5 km are excellent. However, the prediction of number drop deposition (Table 2) at 1 km from the tower is too small by a factor of 3. This underprediction is carried through to the liquid mass deposition rate which is also too small by a factor of about 3. The prediction of final droplet diameter is quite good at both the 0.5 and 1.0 km distances from the tower.

The Wolf I and II model predictions are very similar at 0.5 km from the tower since evaporation is rather insignificant due to the high ambient relative humidity and the short time to deposition. Wolf II provides excellent predictions of sodium deposition except between angles of 330 and 335 degrees where low predictions occur. A larger difference between the predictions of the two Wolf models occurs at 1 km, where Wolf II now predicts noticeable evaporation; the effect of evaporation is to distribute the drift at the ground further downwind from the tower. The Wolf II predictions of final droplet diameter and liquid deposition rate give results that are low compared with the data probably due to excess evaporation predicted owing to the omission of solute effects in the model. Although the Wolf II predictions of sodium deposition are quite good at 0.5 and 1 km from the tower, the Wolf I model (which assumes no evaporation) overpredicts deposition.

The MRI model predicts sodium deposition reasonably well at both the 0.5 km and 1.0 km distance from the tower. However, the model underpredicts

number droplet deposition flux by a factor of 4 at 0.5 km from the tower and a factor of 5 at 1.0 km. No final drop size or liquid mass deposition is computed since the model is based on the equilibrium height concept which does not allow the computation of the final state of the drop. The model permits only two categories of relative humidity, greater than 50% and less than or equal to 50%. The case here of high relative humidity, approximately 93%, is perhaps not well represented by the formulas. The prediction of the Wigley-Slawson model with full ambient profiles is, overall, superior to the prediction of the model without profiles.

The Slinn I and II models were developed to provide upper and lower bounds on deposition. Clearly they do so. The Slinn II model predicts deposition just beginning to occur at 1 km. The prediction at 0.5 km is nearly zero. The Slinn I prediction for sodium deposition varies between a factor of 3 to 7 too large (see Table 2). Interestingly, the Slinn I prediction of average diameter at deposition is too small perhaps because the larger droplets have already deposited closer to the tower.

The Hanna model underpredicts sodium deposition probably due to the overprediction of evaporation in the model [14]. Predictions of number drop deposition rate and liquid mass deposition rate are also too low.

The Hosler-Pena-Pena model has in our previous model/data comparisons [12,13] underpredicted salt deposition rates (near the tower) but usually provided larger values than predicted by the Hanna model. Here, it does predict larger deposition rates than Hanna's model and performs quite well with the sodium ground flux data. The model, however, continues to underpredict the number drop deposition flux, here by factors of 2.5 and 3.6 at 0.5 and 1.0 km, respectively.

The Overcamp-Israel model underpredicts sodium deposition flux at 0.5 km from the tower. In addition, the deposition peak is shifted to the right. There is underprediction also at 1 km but only slightly. There is an underprediction in droplet number deposition rate and an overprediction in droplet size. In total, there is a consequent underprediction of liquid mass deposition flux by factors of 2.1 at 0.5 km and 2.7 at 1 km.

A few general comments should also be made. First, from Table 4, the models generally overpredict droplet diameter at deposition. Second, the peak deposition for sodium predicted by the models is generally coincident or nearly coinident with the observed peak along the two arcs. Third, it should be recalled that the sodium flux predicted and measured included droplets of all sizes, whereas, our droplet number deposition flux, average diameter, and liquid mass deposition rate include droplets only above 100 microns in size. We would expect the observed sodium deposition rate to be slightly larger than the predicted deposition rate since it includes some sodium coming from blow-off from the tower fill. The 100 micron cutoff for other deposition quantities

was set because it is difficult to accurately count drops less than this value and also it eliminates most of the blow-off droplets which are not considered by the models.

The models have also been run for the stack input data with results given in Figures 9 and 10 and Table 3. Combined results of model predictions from cooling tower and stack appear in Figs. 11 and 12 and Table 4. Field data taken from the water sensitive paper were used for comparison with model predictions. Some observations follow.

1. In the angular range (at 0.5 and 1.0 km distances) where the tower has a predominant effect, the models perform in a reasonable manner. However, in the angular range 350 to 365 degrees, the stack contribution becomes important and the tower contribution becomes insignificant (at 0.5 km). At 1.0 km, the stack contribution is about 3-4 times the tower contribution. From Figs. 11 and 12 and Table 4, the models overpredict by a factor of 5-15 in the angular range of 350-365 degrees. The poor comparison of models with stack plus tower data may be due to the use of average stack parameters from the year before. Among the unknowns for the stack exit were: (a) drop size spectrum, (b) liquid mass emission rate, (c) drop concentration at exit (we assumed saturated drops following ESC [15], 0.26 g/g), and (d) stack exit velocity and temperature.

2. The model predictions for the stack are quite consistent among themselves. One of the reasons may be our assumption that the drops are saturated with salt and evaporate only little out to the deposition samplers.

3. The cooling tower contribution to total deposition can be easily distinguished from the stack contribution at the 0.5 km distance but not as easily for the 1.0 km distance. Perhaps our assumed drop spectrum had too large a mass fraction in the large drop sizes.

4. In terms of total deposition there is less discrepancy between model predictions and data for the 1.0 km distance than for the 0.5 km distance. Here, the stack contributes 2-3 times more drift than does the cooling tower; in total, the predictions are about four times larger than observed. As expected from the earlier tower comparisons, the ESC/Schrecker (Limited) and Slinn I and II models perform very poorly.

5. It is interesting that the Wolf I and II predictions for the stack are very similar at both 0.5 and 1.0 km in contrast to the increasing effect of evaporation from 0.5 to 1.0 km seen for drift drops from the cooling tower. The similarity in predictions for Wolf I and II for the stack is due to the slower rate of evaporation which occurs for the larger size stack-emitted drops which fall from the stack plume to the nearby samplers at 0.5 and 1.0 km downwind of the tower.

VALIDATION OF MODELS WITH ESC DATA

The locations of the ESC sensors are given in Fig. 4. Unfortunately, the data for only 4 of the 9 samplers ESC placed at the site were reduced. Tables 5 and 6 provide a comparison of the model predictions with the data in terms of sodium deposition rate, number deposition rate, liquid mass deposition rate, and average diameter (mass averaged). Clearly, significant discrepancies exist between the model predictions and the data. Notably the predicted averaged deposited diameter is 50-100% larger than that measured. Clearly then, the mass of salt in the predicted drop should then be about 2.3-4 times that in the observed drops. Also, the droplet deposition flux is predicted to be about twice as large as observed (considering only drops of size greater than 100 microns). In total, the deposited sodium mass should be predicted as 5-8 times observed. Actually an average value of overprediction of salt deposition flux is more like 10-13. The overprediction of deposition at these near-tower sensors may be due in part to the questionable assumptions we had to make concerning the conditions at the stack exit. However, in view of the fact that the models overpredict deposition due to the tower contribution alone (compared to the total observed deposition from tower and stack), the problem is much more disturbing. ESC uses a smaller sensitive paper (122 cm^2) than the JHU sampler (700 cm^2) leading to a less statistically significant sample. Moreover, ESC does not count all drops on the paper. In their method of data reduction, two squares are drawn on the 122 cm^2 area, the larger one to size the larger drops and the smaller one to size the smaller drops. JHU, on the other hand, sizes all drops on the full area of their sampler. This difference in data reduction methods may be at the root of the difference between ESC and JHU measurements. It would be advisable for each group to count the droplets on the other's samplers to judge the potential differences in data reduction methods.

CONCLUSIONS

The field data acquired in the Chalk Point Dye Study represent the best thus far available for validation of salt-drift deposition models. Sodium deposition measurements taken on the ground along arcs 0.5 km and 1.0 km from the tower showed a bell-shaped profile. This shape was also evident in the model predictions when 10-minute average meteorological data were used and total deposition predictions were obtained by summing predictions made for each 10-minute period. Variation in wind direction thus appears to be a satisfactory explanation of the lateral distribution seen along arcs on the ground.

Comparison of JHU and ESC data yielded interesting results. The JHU measurements of drop size spectrum at ground locations yielded a clear bimodal distibution while the ESC measurements were at best weakly bimodal. The JHU measurements yielded a large peak of small drops (up to 100 microns and a second peak of larger drops (approximately 250-280 microns). The peak of small drops is thought to be due to blow-off from

the fill section of the tower and represents only a small fraction of the total mass deposited at any sampler. For a JHU and ESC sampler located close together (26 m apart), the following observations were made. The JHU sampler showed a greater droplet count both below 100 microns and above about 300 microns with reasonable agreement in between. In addition, the JHU mass distribution is clearly shifted toward greater diameters although agreement above 600 microns is good. The median diameters were only 25% different (JHU: 400 microns; ESC: 336 microns). Consistency checks on the ESC data revealed a factor of 2 difference between different methods of calculating droplet salt concentrations and droplet settling velocity at the ground sampler locations. In general, the JHU measurements were of better quality in terms of methodology of measurement, data reduction, and internal consistency. The general trends in ESC and JHU measurements agree although they differ in details. These details may be important in specific cases.

Ten drift-deposition models are compared with the JHU and ESC field data. For the cooling tower taken alone, a wide range in predictions occurs for sodium deposition flux, number drop deposition flux, liquid mass deposition flux, and average diameter. A number of models predicted very poorly; most, however, were not far off from the data, at least in terms of the sodium deposition predictions. The ESC/Schrecker, Hosler-Pena-Pena, and Wigley-Slawson Models compare best with the sodium deposition flux measurements and are generally within the error of the data. Those models which degrade the level of input data (e.g., use readings from one location on a meteorological tower rather than full profiles, or degrade the spectrum from 25 to 8 bins) lose accuracy in their predictions. Most models predict larger drop diameters at deposition than were measured. This may be due to an incorrect treatment of breakaway in which, in reality, smaller drops are breaking away from the plume sooner. The wind moving past the tower causes a wake or cavity effect with a resultant downdraft on the plume; this effect combined with complex internal circulations within the plume may be causing earlier breakaway. It should be noted that the comparative levels of performance of the models apply only to this special case: high relative humidity, moderate to large wind speed, very stable atmosphere. One cannot a priori extend the specific accuracy of any model to more general environmental conditions without further testing.

For the stack, calculations were made with average June conditions of the previous year since no stack parameters were measured on the date of the dye test. Average values from measurements on the previous June had to be used instead for model input; they were: droplet size spectrum, liquid mass emission rate, exit temperature and velocity. Also, the drops were assumed to be saturated at exit. Model/data comparisons yielded large overprediction of deposition by the models at 0.5 km but more realistic predictions at 1.0 km. In any case, the stack parameters need to be measured on any particular date calculations are required; this is due to the fact that a significantly larger discrepancy existed between stack plus tower predictions and data than with just tower

predictions and data. An important unknown is the salt concentration of droplets leaving the stack. Such exit conditions for the stack need to be measured because the impact of the stack can be as great as the tower, at least in terms of salt emitted.

ACKNOWLEDGMENTS

This work was funded by the Electric Power Research Institute. The authors also wish to express their appreciation to the modelers whose work was utilized for their cooperation.

REFERENCES

1. Environmental Systems Corporation. Cooling Tower Drift Dye Tracer Experiment. Chalk Point Cooling Tower Project, PPSP-CPCTP, August, 1977, pp.92-95.

2. J. H. Meyer and W. D. Stanbro. Cooling Tower Drift Dye Tracer Experiment. Johns Hopkins University Applied Physics Laboratory. Chalk Point Cooling Tower Project, PPSP-CPCTP-16, Volume 2, August, 1977, pp 6-18 through 6-26.

3. Meyer, J. H. and Stanbro, W. D., "Separation of Chalk Point Drift Sources Using a Fluorescent Dye." IN: Cooling-Tower Environment - 1978, A Symposium on Environmental Effects of Cooling Tower Emissions, May 2-4, 1978. Chalk Point Cooling Tower Project Report PPSP-CPCTP-22. WRRC Special Report No. 9. Baltimore, Maryland. May, 1978.

4. Hosler, C., Pena, J., and Pena, R., "Determination of Salt Deposition Rates from Drift from Evaporative Cooling Tower," J. Eng. Power, Vol. 96, No. 3, 1974, p. 283.

5. Wolf, M., Personal Communication, Battelle Pacific Northwest Laboratory, Richland, Washington, July, 1975.

6. Slinn, W. G. N., Personal Communication, Battelle Pacific Northwest Laboratory, Richland, Washington, February, 1977.

7. Hanna, S. R., "Fog and Drift Deposition from Evaporative Cooling Towers." Nuclear Safety. Vol. 15, No. 2. March-April, 1974. pp. 190-196.

8. Slawson, P. R. and Kumar, A., "Cooling Tower Drift Deposition Program ENDRIFT II," Envirodyne Ltd., Tennessee Valley Authority Air Quality Branch, April, 1975.

9. Maas, S. J., "Salt Deposition from Cooling Towers for the San Joaquin Nuclear Project," MRI 75-FR-1361, September 15, 1975.

10. Schrecker, G. and Rutherford, D., Personal Communication, Environmental Systems Corp., Knoxville, Tennessee, 1976.

11. Overcamp, T., "Sensitivity Analysis and Comparison of Salt Deposition Models for Cooling Towers." Paper presented and published in Proceedings of the Conference on Waste Heat Management and Utilization. Miami Beach, Florida. May 9-11, 1977.

12. Policastro, A. J., Dunn, W. E., Breig, M., Ziebarth, J., and Ratcliff, M. Evaluation of Mathematical Models for the Prediction of Salt-Drift Deposition from Natural-Draft Cooling Towers (in preparation). Division of Environmental Impact Studies, Argonne National Laboratory, Argonne, Illinois. 1978.

13. Policastro, A. J., Dunn, W. E., Breig, M., and Ratcliff, M. "Evaluation of Theory and Performance of Salt-Drift Deposition Models for Natural- Draft Cooling Towers." IN: Environmental Effects of Atmospheric Heat/ Moisture Releases, presented at the Second AIAA/ASME Thermophysics and Heat Transfer Conference. Palo Alto, California. May 24-26,. 1978. (available from ASME, New York City).

14. Dunn, W. E., Boughton, B., and Policastro, A. J. "Evaluation of Droplet Evaporation Formulations Employed in Drift Deposition Models." IN: Cooling-Tower Environment - 1978, A Symposium on Environmental Effects of Cooling Tower Emissions, May 2-4, 1978. Chalk Point Cooling Tower Project Report PPSP-CPCTP-22. WRRC Special Report No. 9. Baltimore, Maryland. May, 1978.

15. Environmental Systems Corporation. Chalk Point Cooling Tower Project. Comprehensive Project Final Report for the Period October 1, 1975-June 30, 1976. Volume 2. PPSP-CPCTP-12. October 1976.

Table 1a.

Comparison of Average Diameter (by Several Definitions) for the ESC and JHU Samplers.

Sampler	d_{MM}	$\bar{d}$	d_{CM}	d_{MP}	d_{CP} (micron)
JHU-J1	320	360	207	360	60,280
JHU-J2	240	280	152	280	40,180,240
E1	353	500	199	375	80,375
E2	268	326	195	285	80,285
E3	291	336	237	285	65,285
E4	289	344	238	285	35,225

Table 1b.

Comparison of Apparent Droplet Concentration and Droplet Settling Velocity at the ESC and JHU Samplers.

Sampler	C_{DD} (gm/gm)	C_{CD}	V_{SD} (m/s)	V_{LD}
JHU J1	0.029	-	-	-
JHU J2	0.019	-	-	-
ESC E1	0.006	0.009	1.29	1.76
ESC E2	0.011	0.022	0.69	1.47
ESC E3	0.018	0.020	1.41	1.53
ESC E4	0.031	0.052	1.57	2.63

Table 2.

Comparison of Predictions of 10 Drift Deposition Models to Ground-Level Measurements of Sodium Deposition Flux, Number Drop Deposition Flux, Average Deposited Diameter, and Liquid Mass Deposition Flux . . . Cooling Tower Contribution at JHU Samplers. .

Sampler		JHU Dye Data June 16-17, 1977 Sodium Deposition Flux Tower mg/m^2-4 hours												
Distance (m)	Dir.	OBS.	1	2	3	4	5	6	7	8	9	10	11	12
500	330	1.9 ± .5	0.00	0.00	0.00	0.00	0.00	0	0.00	0.00	0.00	0.00	0.00	0.00
500	335	2.7 ± .7	1.11	3.22	0.08	0.00	10.8	0	1.66	1.48	3.50	1.57	2.19	5.59
500	340	4.7 ± 2.1	1.98	5.65	0.39	3.50	18.9	0	9.24	8.66	6.22	3.95	4.22	10.2
500	345	8.9 ± 2.6	3.97	10.0	0.76	5.65	32.8	0	13.7	12.3	10.8	6.74	7.46	18.3
500	350	10.9 ± 2.7	5.41	11.2	2.49	11.04	35.8	0	13.8	11.7	12.1	9.27	9.06	21.5
500	355	7.7 ± 2.5	5.25	9.88	3.18	10.53	29.5	0	12.9	11.0	10.4	7.83	7.78	18.8
500	0.0	6.1 ± 2.4	3.07	4.32	3.13	6.34	10.7	0	5.38	4.95	4.77	4.30	3.81	8.82
500	5.0	1.9 ± .8	0.93	1.37	1.28	3.55	2.64	0	0.89	0.74	1.35	1.12	0.95	2.52

Sampler		JHU Dye Data June 16-17, 1977 Sodium Deposition Flux Tower mg/m^2-4 hours												
Distance (m)	Dir.	OBS.	1	2	3	4	5	6	7	8	9	10	11	12
1000	340	1.4 ± .4	0.6	1.71	1.29	0.61	4.54	0.10	4.28	2.52	0.40	1.45	1.29	1.85
1000	342.5	3.6 ± .9	0.7	1.72	1.46	1.08	5.24	0.13	4.96	2.72	0.53	1.67	1.49	2.36
1000	345.0	2.4 ± .4	0.9	2.35	1.99	1.12	8.26	0.19	6.55	3.33	1.04	2.26	2.14	3.75
1000	347.5	3.3 ± .8	1.0	2.34	2.02	2.30	9.50	0.22	6.30	3.12	1.40	2.44	2.20	5.09
1000	350.0	2.4 ± 1.2	1.0	2.19	1.65	2.32	11.3	0.20	6.25	2.95	1.99	2.26	2.18	6.25
1000	352.5	2.4 ± 1.2	0.8	1.73	1.42	1.74	10.0	0.19	6.59	2.90	3.00	2.09	1.94	7.67
1000	355.0	1.2 ± .3	0.8	1.29	1.16	2.11	9.86	0.17	5.79	2.75	2.28	1.82	1.70	7.51
1000	357.5	1.2 ± .3	0.6	1.21	0.90	1.51	8.51	0.11	3.92	1.66	2.09	1.50	1.41	7.11
1000	0.0	1.4 ± .4	0.4	0.64	0.40	1.46	5.84	0.05	2.63	1.08	1.73	0.92	0.86	5.98
1000	5.0	.51 ± .1	0.1	0.01	0.10	1.65	1.52	0.01	0.36	0.16	0.45	0.26	0.22	1.65
1000	7.5	0.0	0.0	0.00	0.00	0.00	0.00	0.00	0.00	0.00	0.00	0.00	0.68	0.00
1000	10.0	.55 ± .2	0.0	0.00	0.00	0.00	0.00	0.00	0.00	0.00	0.00	0.00	0.00	0.00

Sampler		JHU Dye Data June 16-17, 1977 Tower												
Distance (m)	Dir.	OBS.	1	2	3	4	5	6	7	8	9	10	11	12
		# Drops/m^2-hour												
500	355	6300	590	2475	408	4793	55737	-	6393	4706	4066	1495	2388	7143
1000	350	7208	231	2019	537	2788	100240	-	15100	4432	2113	1505	1530	8066
		Average Diameter (μm)												
500	355	310	519	-	607	424	262	-	376	334	359	-	484	398
1000	350	241	354	-	411	307	157	-	225	119	241	-	367	231
		Liquid Mass Deposition Flux mg/m^2-4 hours												
500	355	393	173	-	191	768	2104	-	706	367	526	-	567	915
1000	350	204	21	-	78	169	806	-	360	15	62	-	159	209

LEGEND

1. Hanna
2. Hosler-Pena-Pena
3. Overcamp-Israel
4. Wigley-Slawson (profiles)
5. Slinn I
6. Slinn II
7. Wolf I
8. Wolf II
9. ESC/Schrecker
10. MRI
11. Wigley-Slawson
12. ESC/Schrecker (limited)

Table 3.

Predictions of 10 Drift Deposition Models of Ground-Level Sodium Deposition Flux, Number Drop Deposition Flux, Average Deposited Diameter, and Liquid Mass Deposition Flux . . . Stack Contribution at JHU Samplers.

Sampler		JHU Dye Data June 16-17, 1977 Sodium Deposition Flux Stack mg/m^2-4 hours												
Distance (m)	Direction	OBS.	1	2	3	4	5	6	7	8	9	10	11	12
589.5	319		0.0	0.0	0.0	0.0	0.0	0.0	0.0	0.0	0.0	0.0	0.0	0.0
580.7	323		0.0	0.0	0.0	0.0	0.0	0.0	0.0	0.0	0.0	0.0	0.0	0.0
571.4	327		0.0	0.0	0.0	0.0	0.0	0.0	0.0	0.0	0.0	0.0	0.0	0.0
561.5	332		0.0	0.0	0.0	0.0	0.0	0.0	2.41	2.14	0.0	0.0	0.0	0.0
551.1	336		18.3	18.0	24.0	0.0	21.2	0.0	13.0	15.6	26.8	18.9	8.26	24.2
540.3	340		24.3	22.5	29.0	0.0	26.6	0.0	45.5	44.9	31.6	25.0	11.0	30.7
529.1	345		51.2	46.7	63.1	0.0	53.4	0.0	80.4	87.1	61.7	48.1	21.8	61.9
517.6	350		54.4	56.8	54.1	31.6	75.3	0.0	70.6	75.6	71.8	52.6	29.0	61.7

Sampler		JHU Dye Data June 16-17, 1977 Sodium Deposition Flux Stack mg/m^2-4 hours												
Distance (m)	Direction	OBS.	1	2	3	4	5	6	7	8	9	10	11	12
1064.8	333		0.74	2.13	0.67	0.0	3.49	0	0.39	0.18	1.03	0.77	0.36	4.62
1059.6	335.6		2.59	7.19	2.27	0.0	12.3	0	2.11	1.94	2.83	2.79	1.36	16.5
1054.3	338		3.32	9.03	2.95	0.0	15.0	0	3.15	3.34	3.63	3.72	1.84	21.0
1048.8	340.3		3.63	9.99	3.12	0.0	17.1	0	5.99	5.96	4.17	4.40	2.32	23.1
1043.3	343		4.96	15.1	4.74	0.0	24.1	0	7.59	7.09	6.45	6.19	2.93	27.0
1037.6	345		6.47	19.6	6.29	0.0	31.4	0	10.1	9.57	8.39	8.75	3.98	38.3
1031.9	347		7.84	21.2	7.52	0.0	33.4	0	12.0	10.7	9.10	10.1	4.79	42.5
1026.1	350		8.12	21.3	8.44	4.25	31.1	0	11.0	9.34	9.81	10.7	5.05	39.1
1020.2	352.2		7.65	19.5	8.18	5.99	26.8	0	11.2	9.60	9.19	9.95	5.23	33.6
1008.3	357.1		5.55	11.4	6.15	5.28	16.9	0	7.96	6.00	6.06	7.87	4.65	22.7
1002.3	359.6		4.55	8.02	5.06	5.44	10.1	0	5.58	4.11	4.57	5.98	4.15	16.6
992.3	2.1		2.52	3.28	2.93	5.99	4.99	0	4.28	2.86	4.96	3.28	2.96	4.52

Sampler		JHU Dye Data June 16-17, 1977 Stack												
Distance (m)	Direction	OBS.	1	2	3	4	5	6	7	8	9	10	11	12
		# Drops/m^2-hour												
540.2	340		578	1166	824	0	1390	-	862	800	762	555	404	889
1043.3	343		572	4994	553	0	9952	-	827	585	1527	620	525	4599
		Average Diameter (μm)												
500	355		699	-	630	0	463	-	605	556	651	-	551	504
1000	350		431	-	419	0	233	-	359	222	308	-	380	329
		Liquid Mass Deposition Flux mg/m^2-4 hours												
540.3	340		310	-	325	0	217	-	300	216	300	-	106	292
1043.3	343		72	-	64	0	197	-	60	10	61	-	28	257

LEGEND

1. Hanna
2. Hosler-Pena-Pena
3. Overcamp-Israel
4. Wigley-Slawson (profiles)
5. Slinn I
6. Slinn II
7. Wolf I
8. Wolf II
9. ESC/Schrecker
10. MRI
11. Wigley-Slawson
12. ESC/Schrecker (limited)

Table 4.

Comparison of Predictions of 10 Drift Deposition Models to Ground-Level Measurements of Sodium Deposition Flux, Number Drop Deposition Flux, Average Deposited Diameter, and Liquid Mass Deposition Flux . . . Contribution of Cooling Tower and Stack at JHU Samplers.

Sampler		JHU Dye Data June 16-17, 1977 Tower and Stack Sodium Deposition Flux mg/m^2-4 hours												
Distance (m)	Direction	OBS.	1	2	3	4	5	6	7	8	9	10	11	12
500(589.5)	330(319)	1.96 ± .26	0.0	0.0	0.0	0.0	0.0	0.0	0.0	0.0	0.0	0.0	0.0	0.0
500(580.7)	335(323)	5.16 ± .43	1.1	3.22	0.08	0.0	10.8	0.0	1.66	1.48	3.50	1.57	2.19	5.59
500(571.4)	340(327)	2.88 ± .96	1.98	5.65	0.39	3.50	18.9	0.0	9.24	8.66	5.43	3.95	4.22	10.2
500(561.5)	345(332)	5.44 ± .75	3.97	10.0	0.76	5.65	32.6	0.0	16.1	14.4	10.8	6.74	7.48	18.3
500(551.1)	350(336)	8.91 ± .44	23.7	29.2	26.4	11.0	56.4	0.0	26.8	27.3	38.9	28.2	17.3	45.7
500(540.3)	355(340)	7.99 ± .45	29.6	32.4	31.8	10.5	56.1	0.0	58.4	55.9	42.0	32.9	18.8	49.5
500(529.1)	0.0(345)	8.63 ± .78	54.3	51.0	66.1	6.34	64.1	0.0	85.8	92.1	66.5	52.4	25.6	70.7
500(517.6)	5.0(350)	12.6 ± .98	55.3	58.2	55.4	35.2	77.9	0.0	71.5	76.3	73.2	53.7	30.0	64.2

Sampler		JHU Dye Data June 16-17, 1977 Tower and Stack Sodium Deposition Flux mg/m^2-4 hours												
Distance (m)	Direction	OBS.	1	2	3	4	5	6	7	8	9	10	11	12
1000(1064.8)	340(333)	2.00 ± .32	1.34	3.84	1.96	0.61	8.03	0.10	4.67	2.70	1.43	2.22	1.65	6.51
1000(1059.6)	342.5(335.6)	2.98 ± .26	3.29	8.91	3.73	1.08	17.5	0.13	7.07	4.66	3.36	4.46	2.85	18.9
1000(1054.3)	345(338)	2.98 ± .34	4.22	11.4	4.94	1.12	23.3	0.19	9.70	6.67	4.67	6.00	3.98	24.8
1000(1048.8)	347.5(340.3)	3.67 ± .07	4.63	12.3	5.14	2.30	26.6	0.22	12.3	9.08	5.57	6.84	4.52	28.2
1000(1043.3)	350(343)	5.71 ± .15	5.96	17.3	6.39	2.32	35.4	0.20	13.8	10.0	8.44	8.45	5.11	35.3
1000(1037.6)	352.5(345)	5.18 ± .30	7.27	21.3	7.71	1.74	42.0	0.19	16.7	12.5	11.4	10.8	5.92	46.0
1000(1031.9)	355(347)	4.31 ± .12	8.64	22.5	8.68	2.11	43.3	0.17	17.8	13.5	11.4	11.9	6.49	50.0
1000(1026.1)	357.5(350)	4.81 ± .14	8.72	22.5	9.34	5.76	39.6	0.11	14.9	11.0	11.9	12.2	6.46	46.2
1000(1020.2)	0.0(352.2)	4.98 ± .095	8.05	20.1	8.58	7.45	32.6	0.05	13.8	10.7	10.9	10.9	6.09	39.6
1000(1008.5)	5.0(357.1)	4.72 ± .22	5.65	11.4	6.25	6.93	18.2	0.01	8.52	6.16	6.51	8.04	4.87	24.4
1000(1002.3)	7.5(359.6)	2.87 ± .51	4.55	8.02	5.06	5.44	10.1	0.0	5.58	4.11	4.57	5.98	4.81	16.6
1000(996.3)	10.0(2.1)	5.49 ± .68	2.32	5.28	2.93	5.99	4.99	0.0	4.28	2.86	4.96	5.28	2.96	4.52

Sampler		JHU Dye Data June 16-17, 1977 Tower and Stack												
Distance (m)	Direction	OBS.	1	2	3	4	5	6	7	8	9	10	11	12
		# Drops/m^2-hour												
500(540.3)	355(340)	7595	1168	3641	1232	4793	57127	-	7255	5506	4828	2050	2792	8032
1000(1043.3)	350(343)	7311	803	7013	1090	2788	110192	-	15927	5017	3440	2125	1855	12665
		Average Diameter (μm)												
500	355	358	582	-	584	425	269	-	405	370	434	-	486	419
1000	350	280	381	-	396	307	163	-	233	134	258	-	364	260
		Liquid Mass Deposition Flux mg/m^2-4 hours												
500(540.3)	355(340)	728	483	-	514	768	2321	-	1006	583	827	-	675	1257
1000(1043.3)	350(343)	358	93	-	142	169	1003	-	420	25	125	-	187	466

LEGEND

1. Hanna
2. Hosler-Pena-Pena
3. Overcamp-Israel
4. Wigley-Slawson (profiles
5. Slinn I
6. Slinn II
7. Wolf I
8. Wolf II
9. TSC/Schrecker
10. MRI
11. Wigley-Slawson
12. TSC/Schrecker (limited)

Table 5.

Comparison of Predictions of 10 Drift Deposition Models to Ground Level Measurements of Sodium Deposition Flux and Number Drop Deposition Flux . . . Contribution of Cooling Tower and Stack at ESC Samplers.

Sampler		ESC Dye Data (Evening) June 16-17, 1977 Sodium Deposition Rate Tower and Stack mg/m^2-4 hours												
Distance (m)	Direction	OBS.	1	2	3	4	5	6	7	8	9	10	11	12
230(261)	181(212.9)	0.02	0.0	0.0	0.0	0.0	0.0	0.0	0.0	0.0	0.0	0.0	0.0	0.0
300(346)	357(334)	6.58	62.0	75.5	42.6	24.2	105	0.0	65.6	62.0	83.5	56.4	80.2	58.5
400(461)	347(330)	1.34	12.2	15.9	4.56	17.3	36.4	0.0	21.5	20.2	35.4	14.4	7.24	40.3
500(547)	352(338)	4.24	29.1	32.4	31.4	7.56	52.8	0.0	37.7	37.3	42.9	29.1	19.3	49.6
750(778)	358(348)	NR	17.3	21.4	16.9	1.01	37.6	.002	16.4	12.3	29.1	17.5	18.1	30.8
750(800)	348(339)	NR	8.93	12.4	7.73	3.56	26.1	.003	16.1	12.2	11.6	10.5	9.93	5.68
1050(1110)	342(335)	NR	2.61	7.75	3.54	0.44	13.9	0.17	5.79	3.98	4.81	3.63	1.92	24.3
980(1023)	350(343)	NR	5.19	14.28	5.31	2.32	31.1	0.15	14.3	9.85	7.13	7.90	4.79	33.5
1740(1756)	0(356)	NR	3.05	8.91	3.54	2.44	11.0	0.89	6.41	4.57	8.70	4.98	0.04	0.52

Sampler		ESC Dye Data (Evening) June 16-17, 1977 Tower and Stack # $Drops/m^2$-hr.												
Distance (m)	Direction	OBS.	1	2	3	4	5	6	7	8	9	10	11	12
230(261)	181(212.9)	0	0	0	0	0	0	0	0	0	0	0	0	0
300(346)	357(334)	10766	2454	3020	3039	3064	14178	0	5055	4682	4460	2833	4672	4600
400(461)	347(330)	2101	1237	2480	584	5373	33508	0	7294	6485	4058	2222	1650	4468
500(547)	352(338)	3630	1164	3648	1213	3312	53317	0	7319	5373	4862	1953	2748	7958
750(778)	358(348)	NR	1208	4278	1392	983	67187	0	6011	3189	5610	1837	2654	1735
750(800)	348(339)	NR	812	4150	826	3214	90883	0	8398	4425	5630	1859	2364	1067
1050(1110)	342(335)	NR	424	4023	744	519	51377	0	11368	5289	3610	1371	892	15921
980(1023)	350(343)	NR	699	5557	788	2844	101393	0	14006	4925	3223	1873	1777	13146
1740(1756)	0(356)	NR	605	8255	1127	1203	37684	0	8531	1572	5500	1523	44	390

LEGEND

1. Hanna
2. Hosler-Pena-Pena
3. Overcamp-Israel
4. Wigley-Slawson (profiles)
5. Slinn I
6. Slinn II
7. Wolf I
8. Wolf II
9. ESC/Schrecker
10. MRI
11. Wigley-Slawson
12. ESC/Schrecker (limited)

NR - Not Reduced by ESC.

Table 6.

Comparison of Predictions of 10 Drift Deposition Models to Ground Level Measurements of Average Deposited Diameter and Liquid Mass Deposition Flux . . . Contribution of Cooling Tower and Stack at ESC Samplers.

Sampler		ESC Dye Data (Evening) June 16-17, 1977 Average Diameter (μm) Tower and Stack												
Distance (m)	Direction	OBS.	1	2	3	4	5	6	7	8	9	10	11	12
300(346)	357(334)	360	652	-	732	650	509	-	658	638	679	-	663	662
400(461)	347(330)	306	678	-	622	482	334	-	475	461	652	-	535	659
500(547)	352(338)	310	610	-	563	431	274	-	410	377	437	-	482	422

Sampler		ESC Dye Data (Evening) June 16-17, 1977 Liquid Mass Deposition Flux Tower and Stack mg/m^2-4 hours												
Distance (m)	Direction	OBS.	1	2	3	4	5	6	7	8	9	10	11	12
230(261)	181(212.9)	0	0.0	-	0.0	0.0	0.0	0	0.0	0.0	0.0	-	0.0	0.0
300(346)	357(334)	1047	1422	-	2485	1762	3914	0	3022	2542	2966	-	2848	2794
400(461)	347(330)	126	806	-	294	1261	2604	0	1639	1327	2352	-	528	2675
500(547)	352(338)	226	552	-	504	551	2301	0	1056	608	851	-	660	1253
750(778)	358(348)	NR	298	-	308	74	1196	0	491	147	498	-	361	299
750(800)	348(339)	NR	213	-	187	259	1146	0	471	173	391	-	370	57
1050(1110)	342(335)	NR	52	-	102	32	353	0	276	101	145	-	79	696
980(1023)	350(343)	NR	79	-	111	169	967	0	516	106	114	-	183	476
1740(1756)	0(356)	NR	25	-	44	36	183	0	144	4	92.3	-	3	6

LEGEND

1. Hanna
2. Hosler-Pena-Pena
3. Overcamp-Israel
4. Wigley-Slawson (profiles)
5. Slinn I
6. Slinn II
7. Wolf I
8. Wolf II
9. ESC/Schrecker
10. MRI
11. Wigley-Slawson
12. ESC/Schrecker (limited)

NR - Not Reduced by ESC.

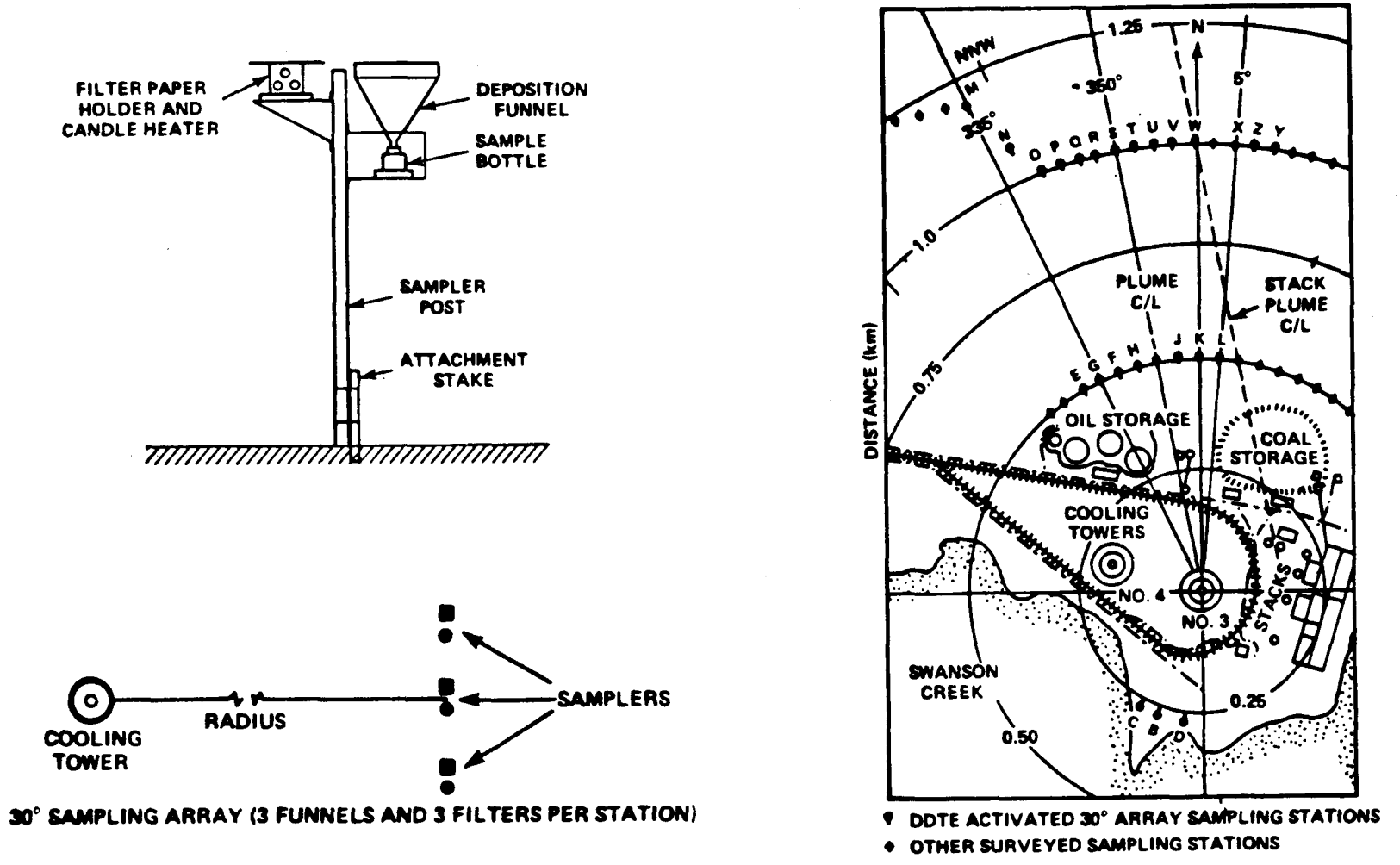

Fig. 4-1. (upper left) Sketch of Position of JHU Samplers at Typical Sampling Station. (lower left) Relative Position of Duplicate Samplers at a Sampling Location. (right) JHU and ESC Sampling Arrays at Chalk Point. (Adapted from Ref. 2).

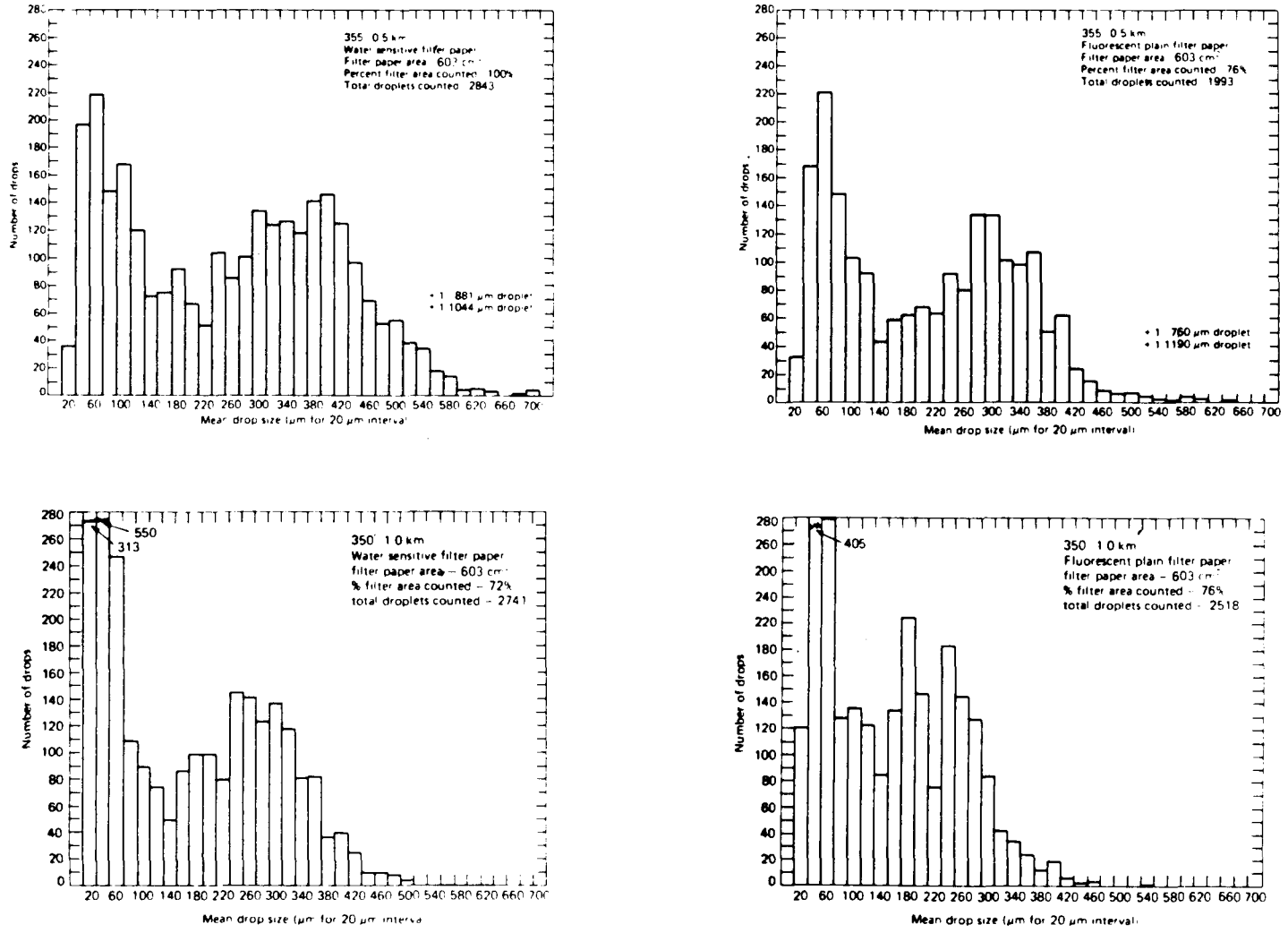

Fig. 4-2. Histogram Plots of Total Water and Fluorescent Droplet-Size Distribution for Sampling Stations Near Cooling Tower Plume Centerline. (Adapted from Ref. 2).

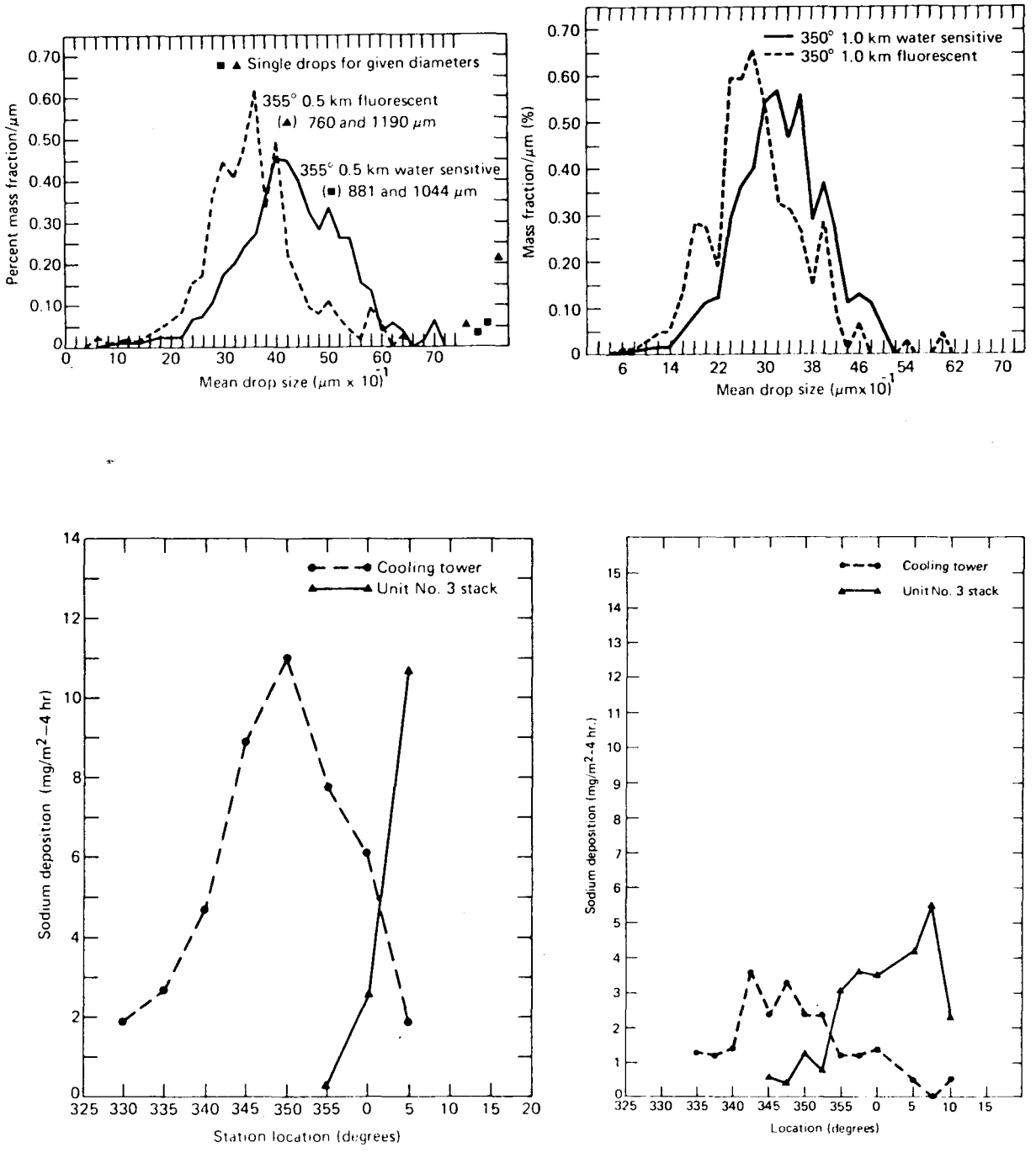

Fig. 4-3. (top) Percent Mass Fraction as a Function of Mean Drop Size at Two JHU Samplers. (bottom) Separation of Tower and Stack Sources of Sodium Deposition at the 0.5 km and 1.0 km Arcs. (Adapted from Ref. 2).

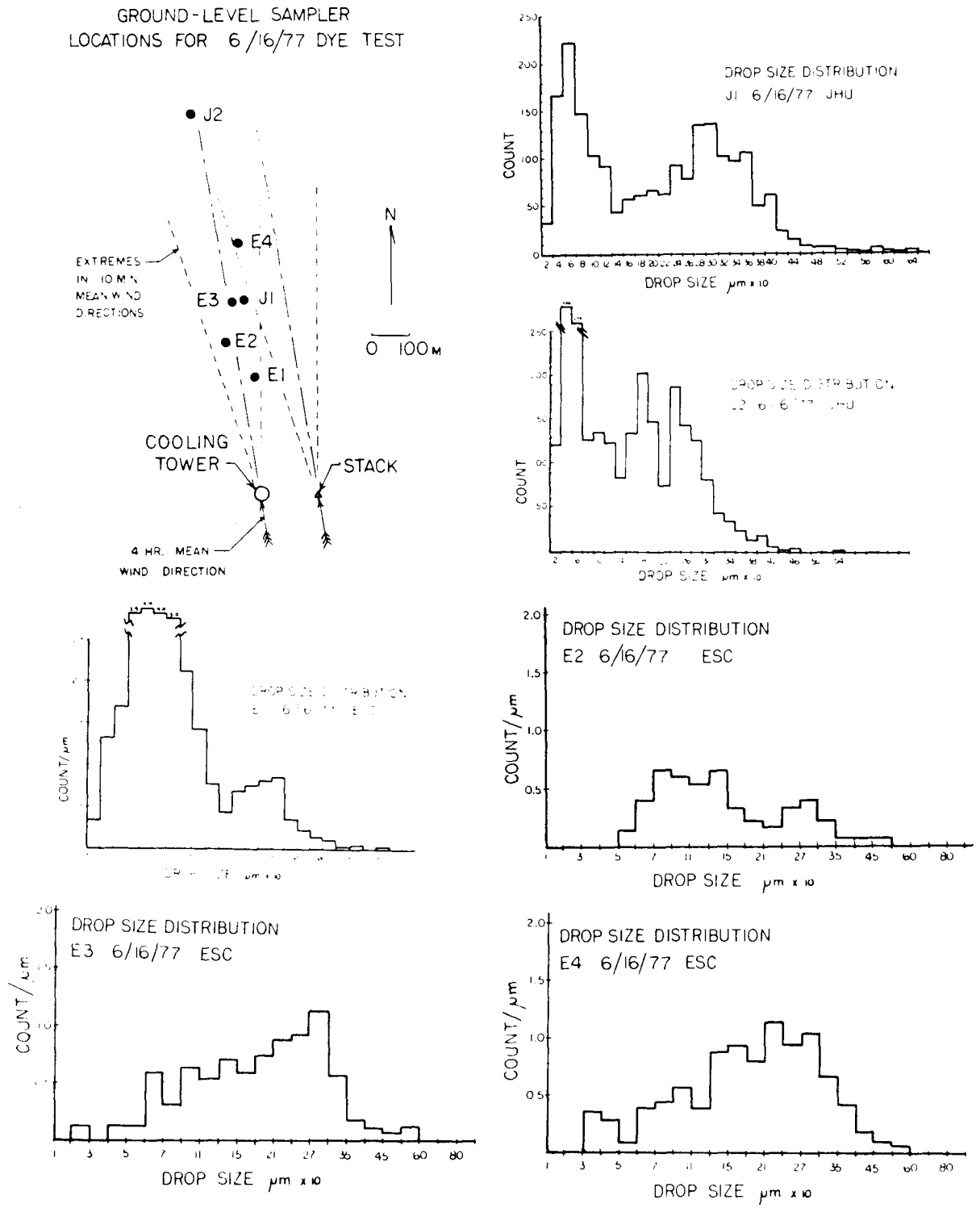

Fig. 4-4. (upper left) Location of 4 ESC and 2 JHU Samplers at which Drop Size Distributions were Measured. (lower left and right) Droplet Count as a Function of Droplet Size for All 6 Samplers.

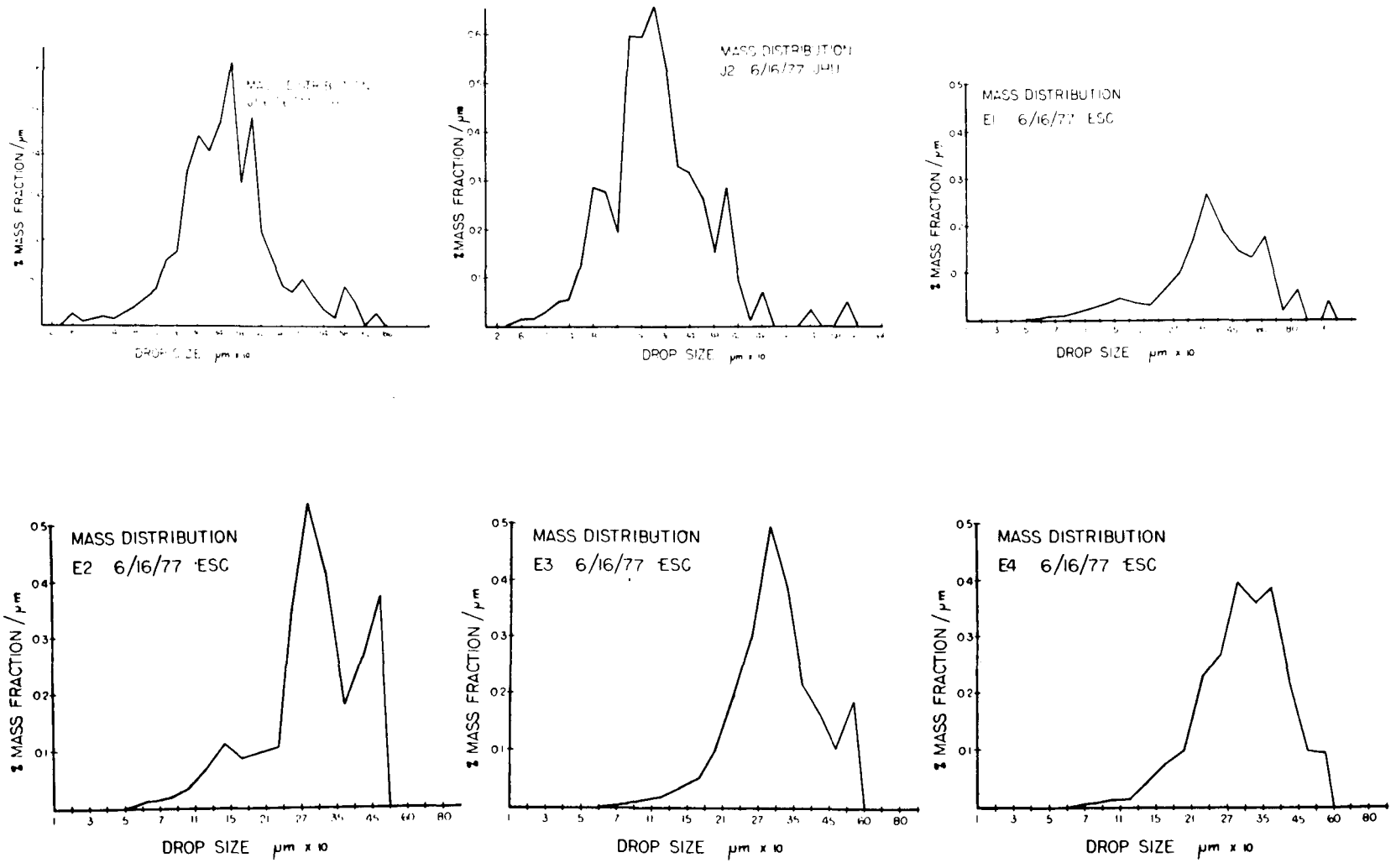

Fig. 4-5. Percent Mass Fraction as a Function of Droplet Size for the 4 ESC and 2 JHU Samplers.

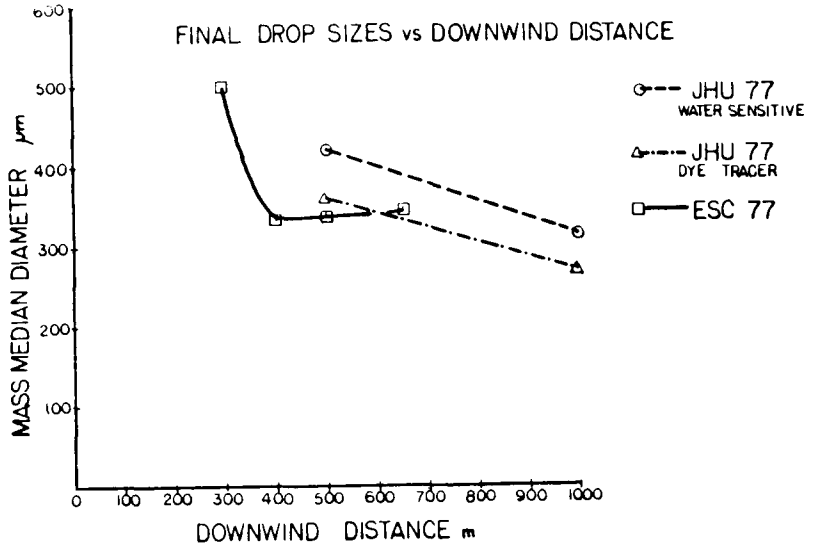

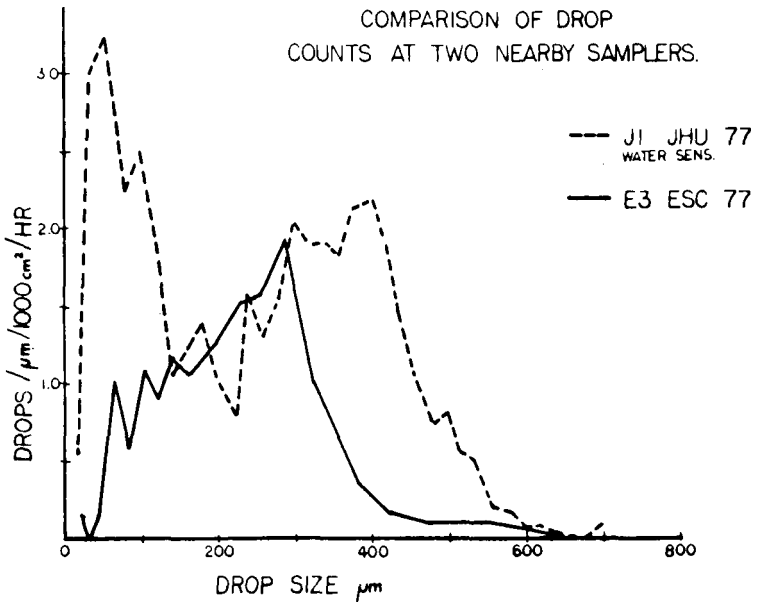

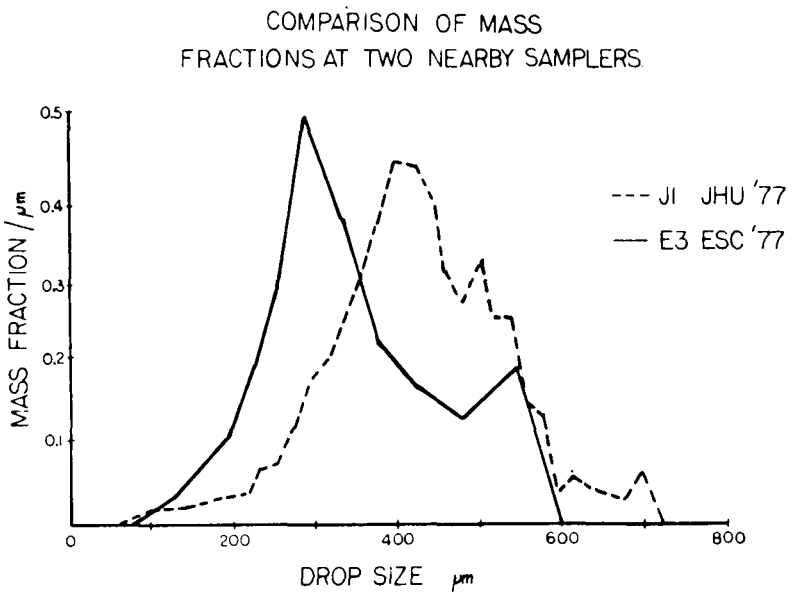

Fig. 4-6. (upper left) Variation of Mass Median Diameter with Distance from the Tower. (lower left) Comparison of Mass Fractions at Two Nearby Samplers. (above) Comparison of Drop Counts at the Same Two Nearby Samplers.

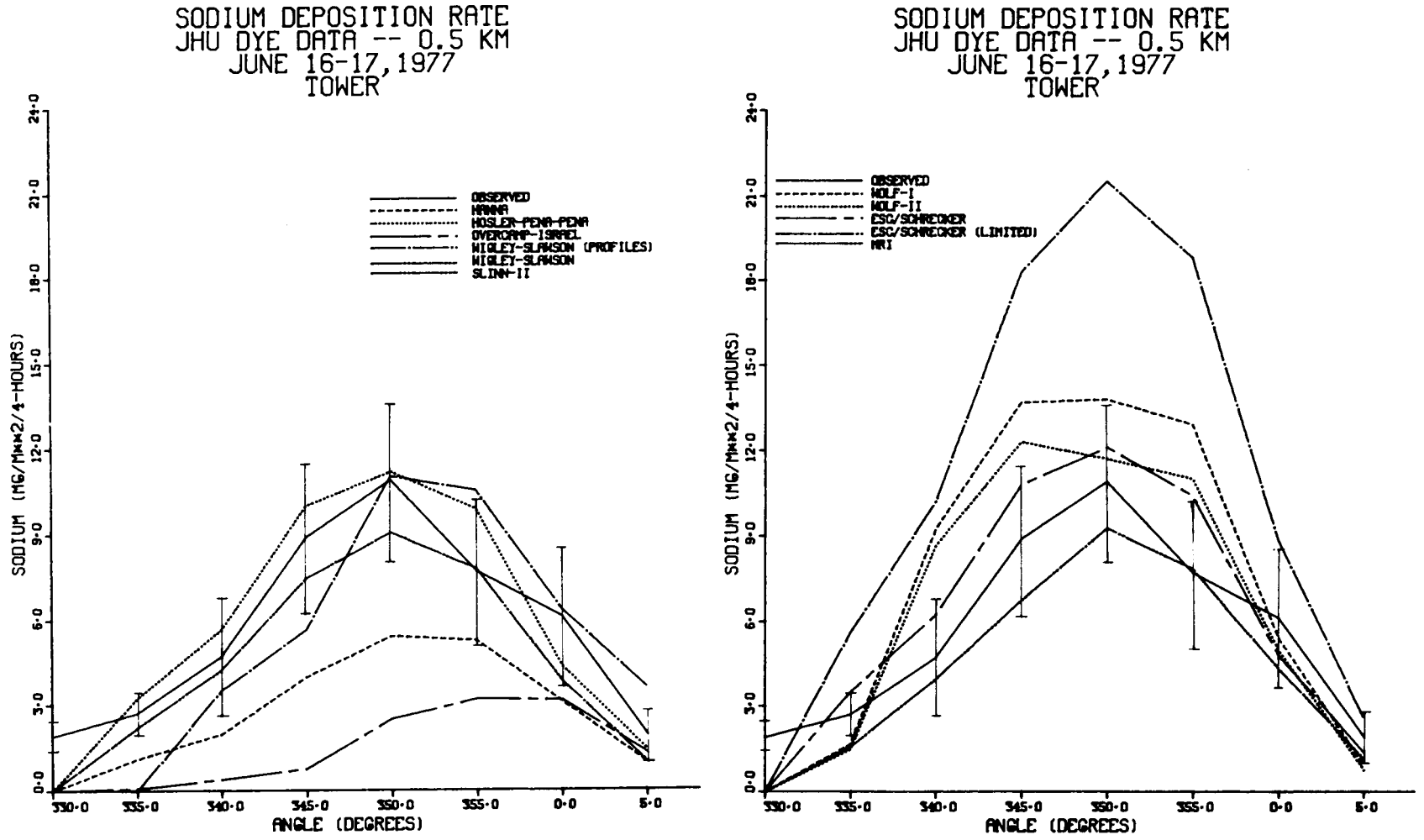

Fig. 4-7. Comparison of Predictions of 10 Drift Deposition Models to Sodium Deposition Flux Measurements at 8 Locations Along the 0.5 km Arc . . . Cooling Tower Contribution Alone.

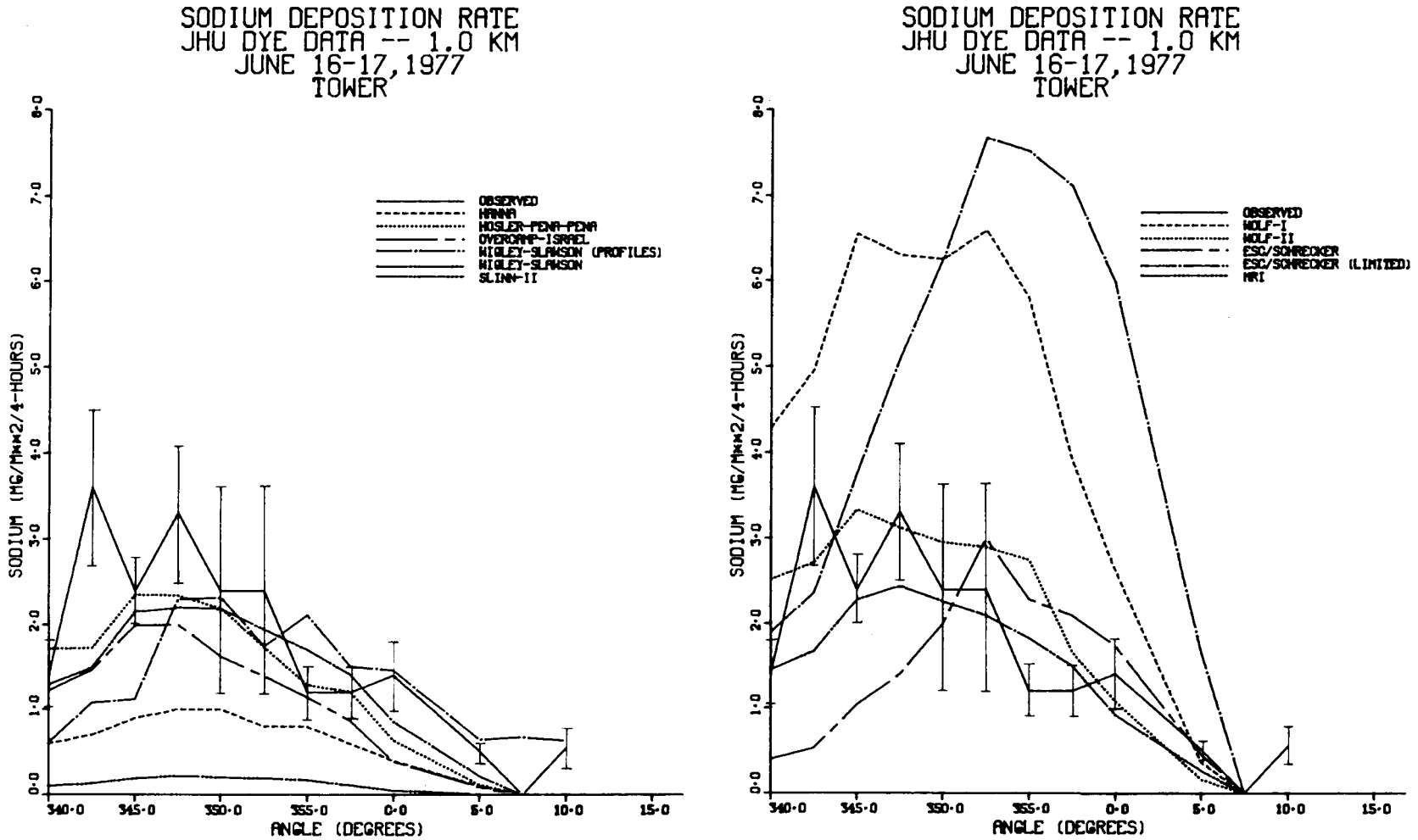

Fig. 4-8 Comparison of Predictions of 10 Drift Deposition Models to Sodium Deposition Flux Measurements at 8 Locations Along the 1.0 km Arc . . . Cooling Tower Contribution Alone.

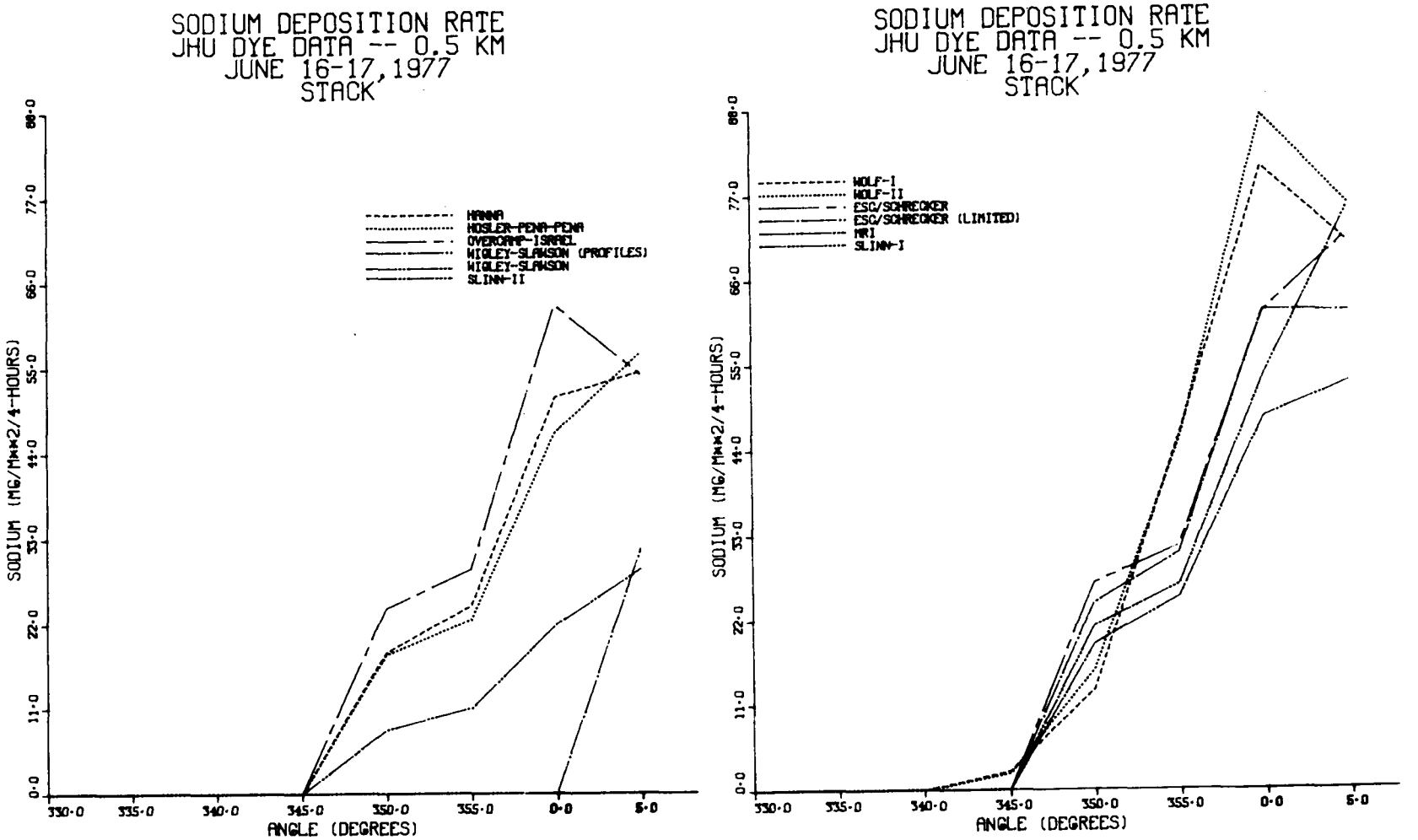

Fig. 4-9. Comparison of Predictions of 10 Drift Deposition Models of Sodium Deposition Flux at 8 Locations Along the 0.5 km Arc . . . Stack Contribution Only.

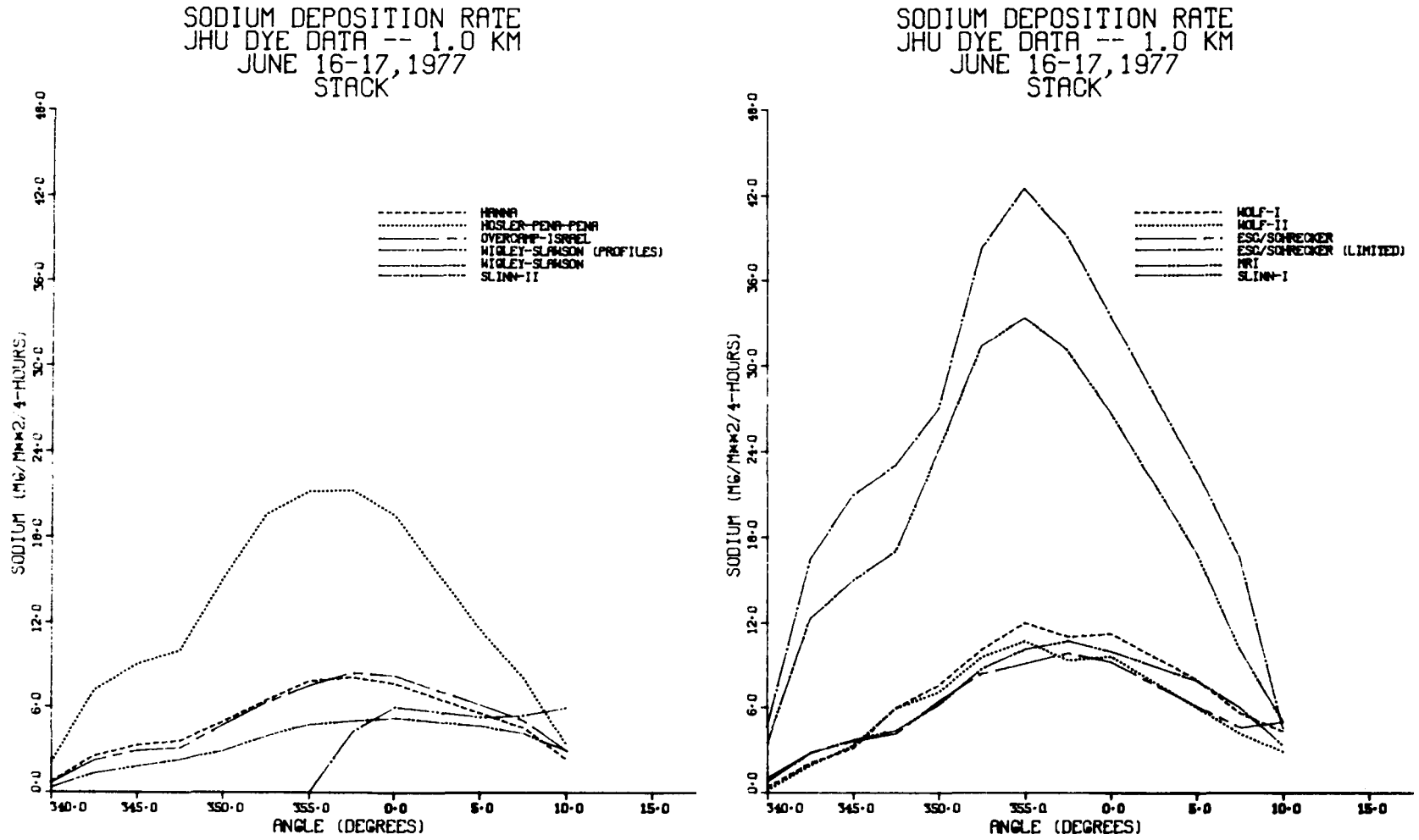

Fig. 4-10. Comparison of Predictions of 10 Drift Deposition Models of Sodium Deposition Flux at 8 Locations Along the 1.0 km Arc . . . Stack Contribution Only.

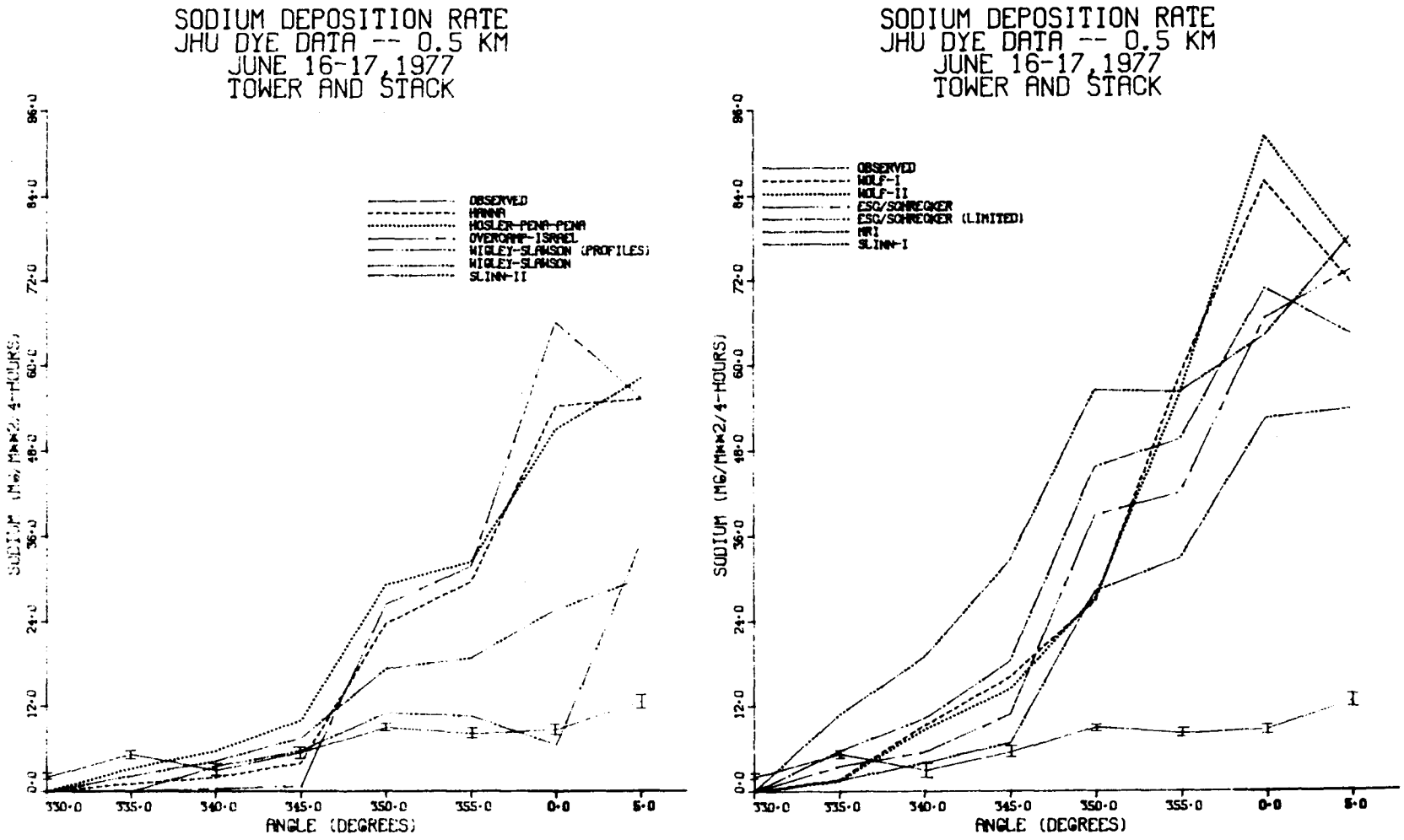

Fig. 4-11. Comparison of Predictions of 10 Drift Deposition Models to Sodium Deposition Flux Measurements at 8 Locations Along the 0.5 km Arc . . . Cooling Tower and Stack Contributions.

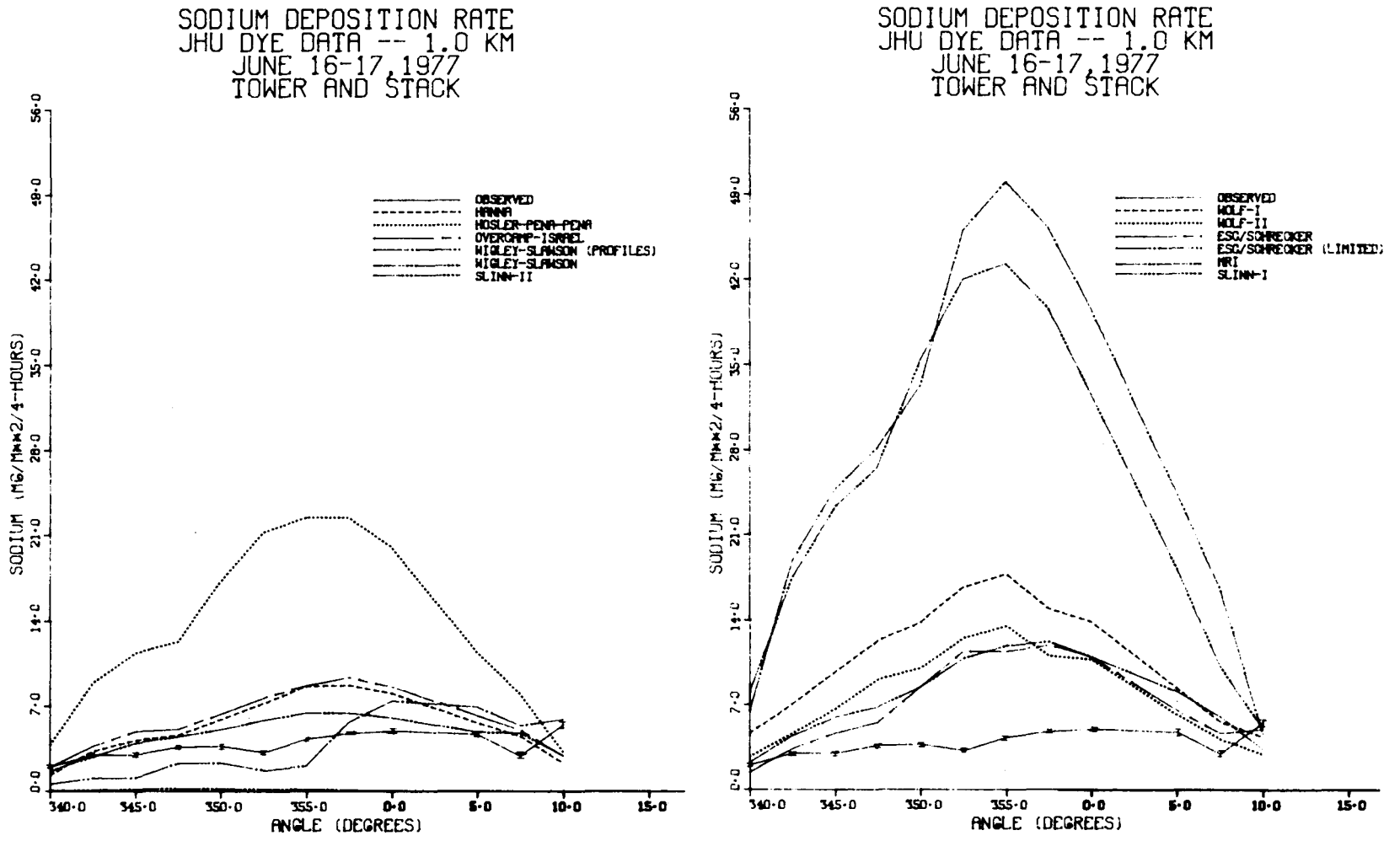

Fig. 4-12. Comparison of Predictions of 10 Drift Deposition Models to Sodium Deposition Flux Measurements at 8 Locations Along the 1.0 km Arc . . . Cooling Tower and Stack Contributions.

Blank

Section 5

THE DROP SUBMODEL

This section outlines the drop submodel used to predict the behavior of an evaporating drift drop. The model is developed from basic principles and attempts to treat the important physical processes influencing the drop, such as evaporation and precipitation of salt within the drop. The model has been tested independently of the overall drift model and has been found to provide excellent agreement with all available data.

The model takes as given the initial condition of the drop (i.e., its release height and diameter) and the spatial distribution of wind speed, temperature, and humidity in the ambient. The latter is closely related to the breakaway criterion in which one set of local conditions ("plume") is used prior to breakaway and a second set of conditions ("ambient") is used after the breakaway point is reached. More discussion of the breakaway problem will be given in Section 7.

As the droplet moves through the air and experiences different local environments, liquid will evaporate from and heat will be transferred to the drop surface, thus changing the mass and diameter of the drop. Correspondingly, the trajectory of the particle will be determined by the diameter/mass history and the local wind speed and direction. As evaporation proceeds, dissolved impurities in the drop may begin to precipitate, and eventually the drop may become a totally dry particle. The goal of the drop submodel is to use appropriate dynamic and thermodynamic analyses to predict the diameter/mass history and trajectory of a falling drift drop.

NOMENCLATURE

English Symbols

A_c	Drop cross-sectional area
A_s	Drop surface area
C	Solute concentration (mass of solute per unit volume of solution)
$\overline{C}$	Average solute concentration (total mass of solute in solution divided by total volume of solution)
C_D	Drag coefficient ($F_D/\frac{1}{2}\rho_g V^2 A_c$)

C_s	Solute concentration at drop surface
C_v	Vapor concentration
C_{va}	Vapor concentration in surrounding gas
C_{vs}	Vapor concentration at drop surface
$\bar{c}_p$	Mass-averaged drop specific heat at constant pressure
$c_{p\ell}$	Specific heat at constant pressure of liquid solution
c_{ps}	Specific heat at constant pressure of pure solute
D_{eff}	Effective diffusivity of vapor through gas within solute cap
D_s	Mass diffusivity of solute in solvent
D_v	Mass diffusivity of vapor in gaseous surroundings
d	Drop outside diameter
d_c	Diameter of solute core
d_i	Inside diameter of solute cap
d_o	Outside diameter of solute cap
d_v	Diameter of gas bubble at center of drop
$\vec{e}_D$	Unit vector defining the line of action of the drag force
F	Force
F_D	Drag force
f_A	Fraction of cap radial area occupied by pore openings
f_v	Volume fraction of solute cap occupied by pores
G	Nondimensional evaporation intensity $[-(d/4D_s)\ (dd/dt)]$
g	Acceleration of gravity
h_k	Convection coefficient for heat transfer
h_D	Convection coefficient for mass transfer
h_{fg}	Latent heat of vaporization
$\vec{i}, \vec{j}, \vec{k}$	Unit vectors in the x-, y-, and z-directions, respectively
k	Thermal conductivity of gaseous surroundings
k_c	Empirical crystallization coefficient
L	Tortuous path length through solute cap
M	Molecular weight of vapor
m	Drop mass
m_c	Mass of crystallized solute
m_s	Mass of solute in drop
$\dot{m}_v$	Mass flowrate of vapor through solute cap
Nu	Nusselt number $(h_k d/k)$
n_c	Empirical crystallization coefficient
Pr	Prandtl number (ν/γ)
P_s	Vapor pressure over solution
P_v	Vapor pressure over pure liquid

p	Ratio of tortuous path length to radial path length in solute cap
Re	Reynolds number (Vd/ν)
R_c	Convective mass transfer resistance
R_d	Solute cap diffusional mass transfer resistance
R_u	Universal gas constant
r	Radial position inside drop
Sc	Schmidt number (ν/D_v)
Sh	Sherwood number ($h_D d/D_v$)
T	Drop temperature
T_a	Dry-bulb temperature of gaseous surroundings
t	Time
U	Drop velocity
U_a	Ambient gas velocity
U_{rel}	Velocity of mass leaving the drop relative to the drop
u, v, w	Drop velocity components in x-, y-, and z-directions, respectively
u_a, v_a, w_a	Ambient gas velocity components in x-, y-, and z-directions, respectively
V	Magnitude of ambient gas velocity relative to drop, i.e., $V = \lvert\vec{U} - \vec{U}_a\rvert$
W	Drop weight
$\vec{X}$	Drop position relative to origin of coordinate system
x, y, z	Drop position coordinates (z-axis points vertically upward)

Greek Symbols

α	Solute mass fraction (mass of solute per unit mass of solution)
$\bar{\alpha}$	Average solute mass fraction (total mass of solute in solution divided by total mass of solution)
α_s	Solute mass fraction at drop surface
α_{sat}	Solute mass fraction in a saturated solution
β	Nondimensional parameter used in development of expression for surface-to-average concentration ratio
γ	Thermal diffusivity of surrounding gas
λ	Heat evolved per unit mass of solute crystallized from solution
ν	Kinematic viscosity of surrounding gas
ρ	Density of solution
ρ_c	Density of solute cap
ρ_g	Density of surrounding gas
ρ_s	Density of pure solute
σ	Absolute supersaturation ($\alpha/\alpha_{sat} - 1$)
ϕ_a	Ambient relative humidity

Convention

$\rightarrow$	Over a symbol denotes a vector quantity

PREVIOUS DRIFT MODELS

The various drift models already in existence, e.g., (1-4), were developed before reliable experimental drift data became available. Since 1976, drift measurements have been made at the cooling tower of the Chalk Point power plant near Washington, D. C. Policastro et al. (5) used the Chalk Point drift data to evaluate the performance of several available drift models and found some significant discrepancies between model predictions and the field data. Dunn et al. (6) have compared droplet trajectories predicted by the existing drift models for a number of different droplet sizes, salt concentrations, and ambient conditions. Differences of a factor of two or three in the droplet deposition distances predicted by different models under the same initial and ambient conditions are not uncommon.

Thus, presently available drift models produce results which are at odds with experimental data; substantial disagreement exists among the droplet trajectory predictions of the various models. In an effort to explain these discrepancies, Dunn et al. (6) have conducted an extensive investigation of the dynamic and thermodynamic formulations used by the models. They point out that many of the models are based on formulae taken from the cloud physics literature, such as the works of Fletcher (7) and Mason (8), which were developed to analyze drop formation inside clouds under the assumption that the atmosphere seen by the drops is very nearly saturated. Moreover, the formulae were designed to handle only drops with very low salt concentrations; a uniform distribution of solute within a given drop is assumed. Policastro et al. (5) note that the temperature dependence of the transport and material properties of the drop and the surrounding air is often ignored by the previous drift models.

The effects of the various analytical simplifications made in the previous drift models cannot be clearly defined until a new model is developed which avoids these simplifications and treats the drift modeling problem from a more fundamental viewpoint. The formulation of such a model is the primary goal of the work presented here.

Extensive studies of heat and mass transfer from pure liquid droplets, with results summarized in experimentally based correlations, have been presented in the engineering literature. Evaporation of drops containing dissolved solids has also received attention, particularly in the chemical engineering literature. By making use of the results of these studies, a drop model based on sound physical principles can be developed. It is hoped that such a model will help expose the underlying reasons for the inaccuracy of and the wide variations in the predictions of previous models.

STUDIES OF EVAPORATING DROPS

Numerous studies relating to heat, mass, and momentum transfer from single component and multicomponent drops have been conducted; and the results of such studies may be found in the literature of several disciplines including, but not limited to, spray drying, spray combustion, cloud physics, spray cooling, and particle technology. Overviews are given by Masters (9) for spray drying; Sirignano and Law (10), Williams (11), and Faeth (12) for spray combustion; Pruppacher and Klett (13) for cloud physics; Drake (14) for spray cooling; and Clift et al. (15) for particle technology. These references not only summarize and analyze past activity but also serve to illustrate the range of time and space scales, the types of drops and environments, and the dominant physical processes in each application area. For example, spray combustion studies focus on small, low temperature drops injected into high temperature surroundings, a situation in which rapid transient behavior is of importance. In contrast, spray cooling applications deal with larger, initially hot drops drying in lower temperature surroundings. Owing to this widespread interest and diversity of application, the droplet literature is vast in extent. Consequently, we shall restrict ourselves only to those studies which have immediate impact on the development of our drop model for use in drift deposition prediction.

Using analytical or numerical techniques, numerous investigators have attempted to solve the basic fluid mechanics equations, in either full or boundary-layer form, for a single drop moving in unbounded surroundings. These analyses are generally too complicated for practical use in our drop submodel. Of greatest interest to us are those studies in which semi-empirical correlations for heat, mass, and momentum transfer coefficients are parameterized in terms of the gross properties of the drop and its surroundings. Specifically, we wish to have expressions for the drag coefficient, heat transfer coefficient, and mass transfer coefficient as functions of drop Reynolds number. These can then be used in time-dependent ordinary differential equations to obtain quantitative predictions of drop behavior.

SINGLE COMPONENT DROPS

In 1949, Gunn and Kinzer (16) measured the terminal velocity of water drops by first charging the drops as they were formed and then measuring the elapsed time between the two voltage pulses caused by the passage of the drops through two inducing rings separated vertically by a distance of between 0.3 and 1 m. More recently, Beard and Pruppacher (17) measured the terminal velocity of water drops by suspending the

drops in a vertical air stream at saturated humidity and determining drop size photographically. Agreement with the results of Gunn and Kinzer was quite good. Either of these two sets of data can be used to deduce a drag coefficient versus Reynolds number relationship for predicting the dynamic behavior of drops, even under transient conditions.

The classic reference on heat and mass transfer from drops is that of Ranz and Marshall (18, 19), who suspended water and benzene drops from a capillary in a vertical air stream of known velocity. Evaporation rates were determined by monitoring the flow of liquid through the capillary required to maintain a constant drop diameter of 477 μm. Drop and air temperature and air flow rate were monitored; the air stream was assumed to be dry. More recently, Beard and Pruppacher (20) measured mass transfer rates by suspending water drops with diameters between 54 and 750 μm in a vertical air stream. Overall, the agreement between the results of Beard and Pruppacher and those of Ranz and Marshall is excellent; however, the former did find discrepancies of as much as 16% in the transfer coefficients for the smallest drops. Based on the experimental results and an asymptotic analytical solution at small Reynolds number, Beard and Pruppacher proposed a correlation which is preferable to that of Ranz and Marshall for Reynolds numbers less than 2. In addition, various authors have stated that the Ranz-Marshall analysis is invalid for drops larger than about 1 mm in diameter due to oscillation of the drop surface. However, Dunn (21) concluded that while oscillation is clearly present, the Ranz-Marshall results, if properly applied, provide excellent predictions of drop cooling rates for drops up to 6 mm in diameter. Thus, prediction of evaporation rates of pure liquid drops can be made with engineering accuracy using available technology.

MULTICOMPONENT DROPS

The situation for multicomponent drops, especially those containing nonvolatile species, is quite different, however. As the discussion below indicates, evaporation of multicomponent drops is a far more complicated process than evaporation of pure liquid drops. Thus, although some research on this topic has been performed, our understanding of the physics of multicomponent droplet evaporation is presently incomplete.

In order to facilitate description of the evaporation history and the analyses that have been advanced for multicomponent drops, we shall divide the drop lifetime into three phases. For simplicity, we phrase the following discussion in terms of a drop containing two components, component 1 and component 2, where component 1 is the volatile component. The period during which both components remain in solution is designated as Phase I. During this phase, the basic modeling problem is determination of surface vapor pressures and, in turn, internal concentration profiles. Charlesworth and Marshall (22), Schlünder (23), Gardner (24), and Gavin (25) have sought to determine the correct concentration profiles within the drop by solving the convective diffusion equation in spherically symmetric geometry. Other modelers, for example Hosler et al. (1), Schrecker (2), and El Golli et al. (26), have ignored these distributional effects and have instead based surface vapor pressure on bulk concentration. The fundamental difference between these two treatments of Phase I is highlighted in Fig. 5-1a. Note that the first alternative predicts nonuniform concentration profiles of components 1 and 2 within the drop, whereas the second alternative neglects internal distributional effects and thus assumes uniform concentration profiles of both components.

As mass transfer proceeds, both bulk and surface concentrations will change, until the drop evaporates completely or comes into equilibrium with the ambient. In many cases of practical interest, the point of insolubility will be reached; precipitation of a solid phase within the drop will begin. We designate the period during which separation of components is occurring as Phase II.

The customary approach for analyzing Phase II is to assume that separation occurs in the drop interior and that the solution on the drop surface is saturated. The analyses of Hosler et al. (1), Schrecker (2), and El Golli et al. (26) are examples of this approach. Because the separating or precipitating component is usually visualized as being located at the drop center and surrounded by saturated solution, we refer to this description as the core scenario of Phase II. Figure 5-1b illustrates the basic features of the core scenario.

From their work with aqueous solutions and suspensions, Ranz and Marshall (18, 19) and Charlesworth and Marshall (22) conclude that precipitation or aggregation of solute begins on the drop surface and spreads over the surface to form a cap. The following qualitative description of an evaporating sodium chloride solution drop is given by Ranz and Marshall (19):

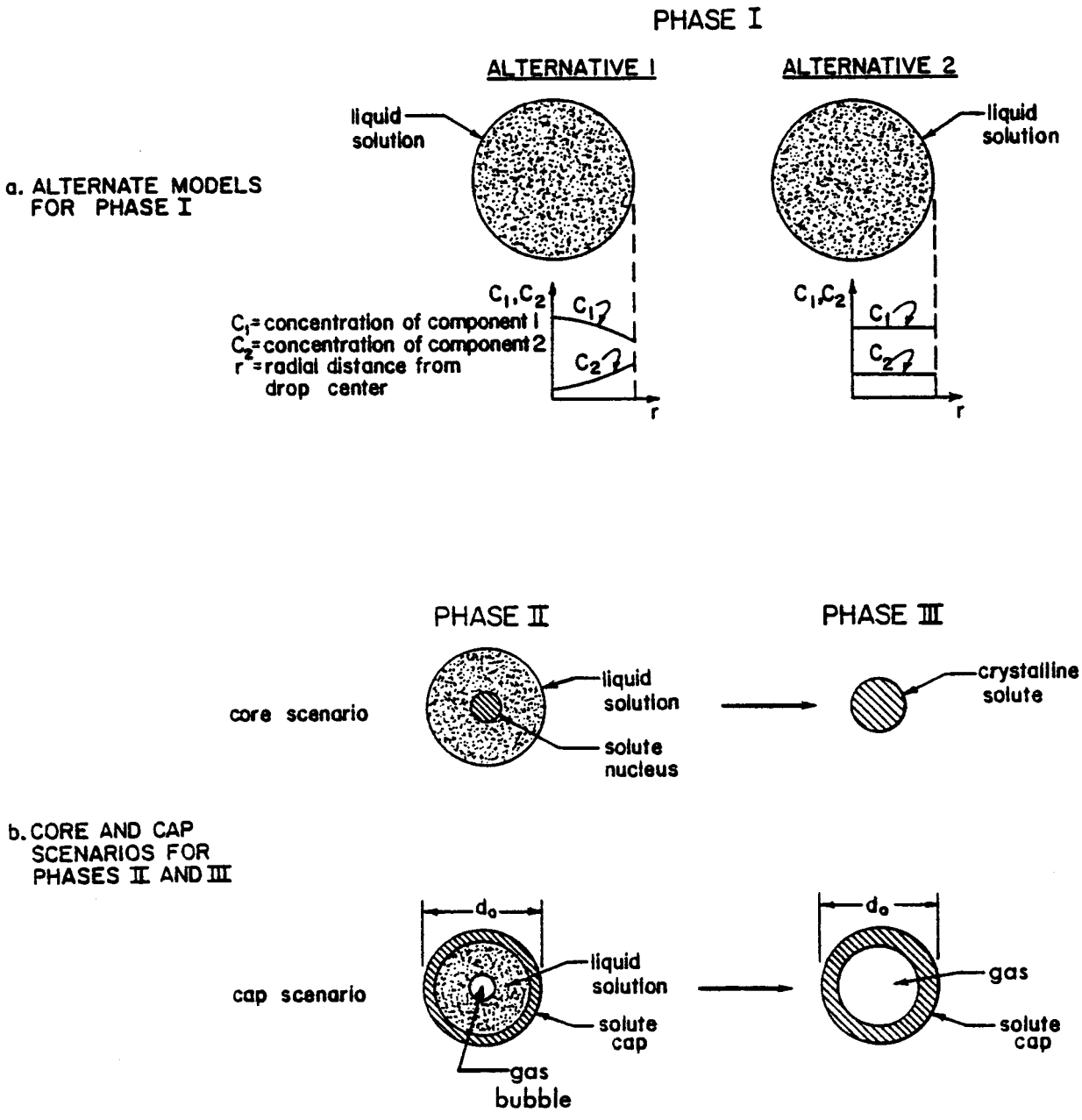

Figure 5-1. Modeling of evaporation phases of a two-component drop.

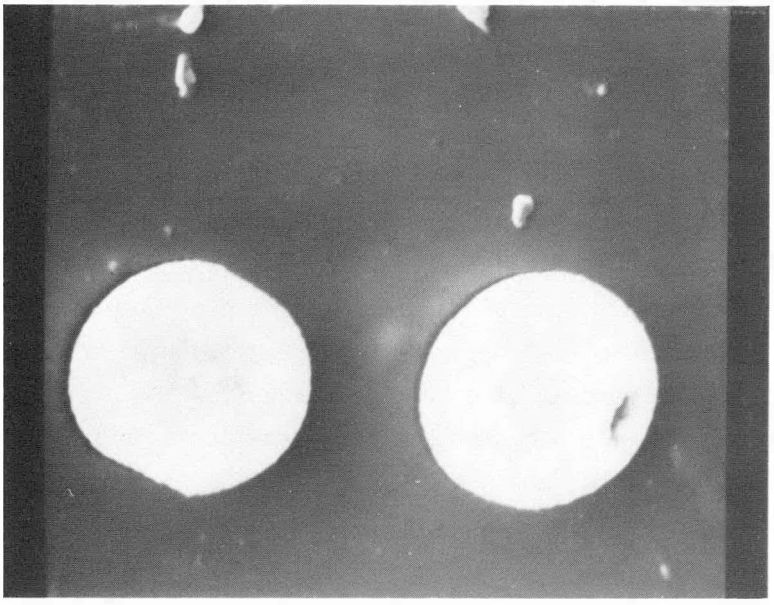

Figure 5-2a. Electron micrograph of 4-μm lithium carbonate shells. Photo courtesy of K.V. Beard and K.H. Leong. (27)

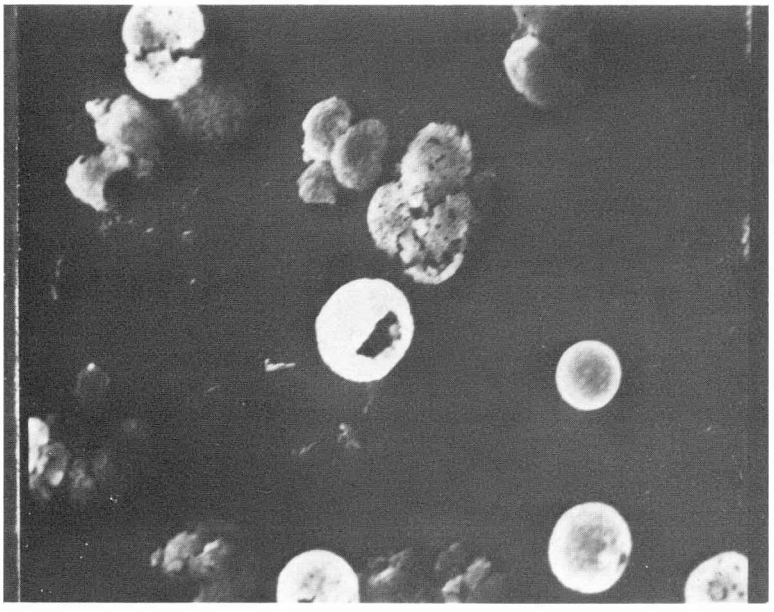

Figure 5-2b. Electron micrograph of fractured lithium carbonate shells. Photo courtesy of K.V. Beard and K.H. Leong. (27)

"Starting at a diameter of nearly one millimeter and a concentration of approximately 20% a drop containing sodium chloride evaporated as a pure liquid drop until cloudy crystals appeared on the side of the drop facing the oncoming air stream. This crystal cap grew rapidly until it covered the whole drop with shiny white crystals. No appreciable change in diameter occurred after the crystal cap covered the surface. The crystal surface soon lost some of its luster, and blowholes into the drop appeared at the downstream side. These holes were attributed to a vaccuum created by the removal of dilute solution from the center, which was relieved by a blowhole through the particle's surface. The picture was the same whether the drop was evaporated in a 200 C hot air stream or in room temperature still dry air, the only difference in the two processes being the time of evaporation, 20 s versus 2000 s."

We refer to this description as the cap scenario of Phase II for reasons which are obvious. Figure 5-1b gives an idealized conceptualization of the cap scenario.

Recent work conducted by the Illinois State Water Survey (27) also lends credence to the existence of spherical caps, although it emphasizes the complexity of final particle formation. Figure 5-2a shows electronmicrographs of the final particles obtained by evaporating 11-μm drops of dilute (1.6 g/liter) lithium carbonate solution. The final particles are indeed porous shells about 0.1 μm thick and 4μm in diameter. Figure 5-2b shows shells which collapsed during capture, from which the very delicate nature of the shell is apparent. Moreover, the shells have large openings at one point on the surface which very well may correspond to the "blowholes" reported by Ranz and Marshall.

Little recognition or theoretical treatment has been given to the cap scenario, although the observations above tend to support it. Our model considers the core and cap scenarios as limiting cases, the core scenario representing the minimum impact of precipitation on evaporation and the cap scenario representing the maximum impact on evaporation.

Phase III represents the equilibrium or asymptotic state of the drop and begins when evaporation ceases either because the rising solute concentration within the drop lowers the vapor concentration at the drop surface to that of the ambient or because the particle becomes dry. (Actually, surface tension and hygroscopic

effects may cause small amounts of water to remain.) Phase III poses no new analytical difficulties, although knowledge of the asymptotic state of Phase II is essential. This point is emphasized in Fig. 5-1b, which illustrates the widely different droplet configurations predicted by the core and cap scenarios for Phase III.

FORMULATION OF DROP SUBMODEL

As previously noted, existing drop submodels are overly simplified in a number of respects, and comparisons we have made illustrate that the differences among various schemes can be quite significant. The drop submodel presented here represents an improvement over existing models in the following respects.

1. The governing equations are integrated numerically, yielding time histories of various drop characteristics. Also, material properties of the drop and its surroundings are carefully treated as functions of temperature and, where necessary, solute concentration. For those cases in which important simplifications can safely be made, they are either implemented automatically by the computer code or are forced by logical switches which the user can set.

2. The model is capable of handling the nonuniform as well as the uniform scenario for Phase I.

3. The model includes a physically sound analysis of Phase II according to the cap scenario. For the sake of comparison, the model also includes an analysis of evaporation according to the core scenario, which the user can select at his discretion. Moreover, the core scenario is formulated in a more thorough manner than in previous models, thus avoiding such anomalies as sudden changes in drop mass or diameter.

4. The model compares favorably with available experimental data for evaporating drops.

Our model does not attempt to analyze all the detailed aspects of drop evaporation, but rather seeks a level of sophistication which provides reliable predictions at reasonable computer and manual setup costs.

TREATMENT OF DYNAMICS

We begin our analysis of drop dynamics by applying Newton's Second Law of Motion for systems of variable mass,

$$\sum \vec{F} = m \frac{d\vec{U}}{dt} - \vec{U}_{rel} \frac{dm}{dt}, \tag{5-1}$$

to a drift drop freely falling in a gaseous environment, as shown in Fig. 5-3. Two external forces are considered to act on the drop: the drag force $\vec{F}_D$, which results from drop motion relative to the surrounding gas, and the weight force $\vec{W}$, which is simply $m\vec{g}$. In all three phases of evaporation, the magnitude of the drag force is calculated from the drag coefficient C_D, defined as

$$C_D \equiv F_D/(\tfrac{1}{2}\rho_g V^2 A_c), \tag{5-2}$$

where C_D is determined as a function of drop Reynolds number ($Re=Vd/\nu$) from the data of Gunn and Kinzer (16). Although Gunn and Kinzer's data are for drops at terminal velocity, Dunn (21) has concluded that they may be used to predict the drag on accelerating drops as well. The direction of the drag force, denoted by unit vector $\vec{e}_D$, is the same as that of the relative motion of the air with respect to the drop, i.e.,

$$\vec{e}_D = (\vec{U}_a - \vec{U}) \,/\, V. \tag{5-3}$$

Finally, if we assume that the mass which evaporates from the drop is accelerated instantaneously to the ambient air velocity, then $\vec{U}_{rel}$, the velocity of mass leaving the drop relative to the drop, is

$$\vec{U}_{rel} = \vec{U}_a - \vec{U}. \tag{5-4}$$

With these intermediate results, Eq. (5-1) may be rearranged to give, in vector form,

$$\frac{d\vec{U}}{dt} = (C_D \rho_g A_s V/8 + \frac{dm}{dt})\ (\vec{U}_a - \vec{U})/m - g\vec{k}, \tag{5-5}$$

or, in component form,

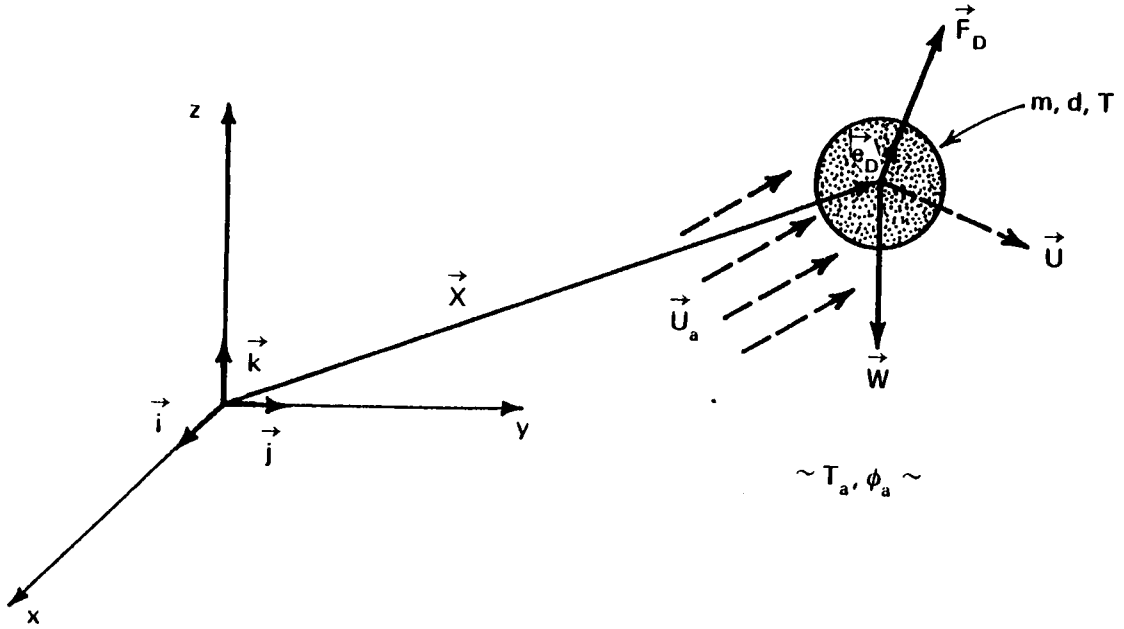

Figure 5-3. Schematic for dynamic analysis of a freely falling solution droplet.

$$\frac{du}{dt} = (C_D \rho_g A_s V/8 + \frac{dm}{dt})\ (u_a - u)/m \qquad (5\text{-}6a)$$

$$\frac{dv}{dt} = (C_D \rho_g A_s V/8 + \frac{dm}{dt})\ (v_a - v)/m \qquad (5\text{-}6b)$$

$$\frac{dw}{dt} = (C_D \rho_g A_s V/8 + \frac{dm}{dt})\ (w_a - w)/m - g. \qquad (5\text{-}6c)$$

We integrate these equations numerically once to obtain drop velocity components (u,v,w) as functions of time and once again to obtain drop position components (x,y,z) as functions of time.

TREATMENT OF HEAT TRANSFER

Our droplet energy analysis is predicated on the assumption that drop temperature varies with time but not with position within the drop. We justify this assumption of temperature uniformity by noting that for small drops the Biot number (a measure of the conductive resistance to heat transfer within the drop relative to the convective resistance to heat transfer at the drop surface) is very small, whereas for large drops, internal circulation tends to homogenize the temperature distribution. The presence of a solute cap around the drop does not alter this situation significantly, as we have found that the thermal resistance of such a cap is negligible.

We perform an energy balance on the drop in order to obtain a differential equation for droplet temperature as a function of time:

[rate of change of drop internal energy] = [rate of heat convection drop from surroundings] + [rate of heat liberation by crystallization] - [rate of latent heat release]

or mathematically,

$$m\overline{c_p}(dT/dt) = h_k A_s (T_a - T) + \lambda(dm_c/dt) - h_{fg}(-dm/dt). \qquad (5\text{-}7)$$

The specific heat $\overline{c_p}$ is obtained by mass-averaging the specific heats of liquid solution ($c_{p\ell}$) and dry solute (c_{ps}):

$$\overline{c_p} = [1-(m_c/m)]\ c_{p\ell} + (m_c/m)\ c_{ps}. \qquad (5\text{-}8)$$

Note that Eqs. (5-7) and (5-8) reduce to the appropriate forms for a drop composed entirely of liquid solution when m_c and dm_c/dt are set to zero, which is the case in Phase I. Regardless of evaporation phase, the convective heat transfer coefficient (h_k) is calculated from the correlation developed by Ranz and Marshall (18, 19),

$$Nu = \frac{h_k d}{k} = 2.0 + 0.6\ Re^{1/2} Pr^{1/3}, \tag{5-9}$$

which, following Dunn [21], we apply under transient as well as steady-state conditions.

TREATMENT OF MASS TRANSFER

PHASE I

Mass transfer in Phase I is governed by the vapor concentration difference between the drop surface and the surroundings, i.e.,

$$dm/dt = -h_D A_s\ (C_{vs} - C_{va}), \tag{5-10}$$

where we calculate C_{vs} and C_{va} from the ideal gas law:

$$C_{vs} = MP_s(\alpha_s, T)/R_u T \tag{5-11a}$$

$$C_{va} = \phi_a MP_v(T_a)/R_u T_a. \tag{5-11b}$$

The Ranz and Marshall (18, 19) mass transfer correlation analogous to Eq. (5-9) is used to determine the convective mass transfer coefficient (h_D):

$$Sh = \frac{h_D d}{D_v} = 2.0 + 0.6\ Re^{1/2} Sc^{1/3}. \tag{5-12}$$

As before, in accordance with Dunn (21), we apply Eq. (5-12) during transient as well as steady-state evaporation.

We note from Eq. (5-11a) that the surface vapor pressure P_s, and hence the evaporation rate, depends not only on temperature but also on the surface solute mass fraction α_s. It is in the calculation of α_s that we distinguish between the two scenarios for Phase I discussed above.

1. Uniform Scenario. If evaporation according to the uniform scenario is selected, then the model neglects solute concentration gradients within the drop and sets the surface solute mass fraction equal to the average solute mass fraction. Thus,

$$\alpha_s = \bar{\alpha} = m_s/m. \tag{5-13}$$

2. Nonuniform Scenario. In analyzing this case, we have applied the spherically symmetric form of the diffusion equation to the drop in an attempt to account for nonuniformity of the solute concentration profile. Assuming a hyperbolic sinusoidal distribution of solute concentration C with radial position in the drop, we have found that the surface-to-average solute concentration ratio may be calculated from

$$C_s/\bar{C} = \beta^2/3G, \tag{5-14a}$$

where

$$\beta\coth\beta = 1+G \tag{5-14b}$$

and

$$G = -(d/4D_s)\ (dd/dt). \tag{5-14c}$$

Details of the derivation of these results may be found in (25). The variation of $C_s/\bar{C}$ with G as predicted by Eqs. (5-14) is very similar to that derived by Gardner (24) using a different approach.

Once C_s is determined from Eqs. (5-14), α_s is calculated iteratively from

$$C_s = \alpha_s\rho(\alpha_s,T), \tag{5-15}$$

where ρ is the solution density as a function of salt concentration and temperature.

PHASE II

Transition to Phase II is assumed to occur when

$$\alpha_s = (\sigma+1)\alpha_{sat}(T), \tag{5-16}$$

where σ is the absolute supersaturation. Generally, some amount of supersaturation ($\sigma>0$) must occur in order to allow nucleation, i.e., formation of tiny crystalline particles on which large-scale crystallization can occur. For drift drops, σ will probably be small, as such drops will likely contain impurities, which facilitate crystallization by serving as nucleation sites.

For both the cap and core scenarios, crystallization of solute from solution during Phase II is assumed to follow the so-called diffusion theory of crystallization, the governing equation for which is given by Mullin (28):

$$dm_c/dt = k_c A_c (\bar{\alpha}-\alpha_{sat})^{n_c}. \qquad (5\text{-}17)$$

In Eq. (17), A_c is the area of the surface on which crystallization is occurring (πd_c^2 for the core scenario, πd_l^2 for the cap scenario); $\bar{\alpha}$ is the average solute mass fraction in the remaining solution, calculated from

$$\bar{\alpha} = (m_s-m_c)/(m-m_c); \qquad (5\text{-}18)$$

and k_c and n_c are empirical crystallization coefficients, which are taken as given. Eq. (5-17) states that the driving force for crystallization is the amount by which the solute mass fraction in solution exceeds saturation, i.e., $\bar{\alpha}-\alpha_{sat}$. Recent studies, e.g., (29-31), have pointed out that the physically correct driving force for crystallization is the chemical potential difference between the solute in solution and the crystalline solute. Nevertheless, the diffusion theory as expressed by Eq. 5-(17), perhaps because of its simplicity, still dominates the literature (e.g., (32)); we feel it represents a level of complexity consistent with the purposes of this study.

The treatment of mass transfer depends on whether the core or cap scenario is assumed.

1. Core Scenario. In this case, the governing equation for mass transfer is the same as in Phase I, i.e., Eq. (5-10); and, as in Phase I, the drop outside diameter shrinks as liquid is evaporated. Crystallized solute is assumed to reside in a spherical ball of diameter d_c and density ρ_s, the density of dry solute, at the center of the drop (recall Fig. 5-1b). With m_c given by Eq. (5-17), d_c is then calculated using

$$d_c = (6m_c/\pi\rho_s)^{1/3}. \qquad (5\text{-}19)$$

2. Cap Scenario. For the cap scenario, which we again emphasize is closer than the core scenario to the experimentally observed behavior of drops in Phase II, we propose that a vapor concentration difference is still the driving force for evaporation but that the cap acts as an additional resistance in the transfer path. To model this effect, we assume that the liquid in the core of the drop is in contact with, but does not infiltrate, the porous solute cap and that vapor evaporated from the liquid core must diffuse through the porous cap before being convected into the surrounding gas. Assuming that this diffusion process is quasi-steady, we have followed an analysis similar to that given by Bird et al. (33) in connection with porous catalyst particles to obtain the following relationship governing mass transfer according to the cap scenario of Phase II:

$$dm/dt = (C_{vs} - C_{va})/(R_c+R_d), \tag{5-20a}$$

where R_c, the convective mass transfer resistance at the cap outer surface, is

$$R_c = 1/h_D A_s, \tag{5-20b}$$

and R_d, the diffusion resistance of the cap, is

$$R_d = (1/d_i - 1/d_o) \; / \; 2\pi D_{eff}. \tag{5-20c}$$

C_{vs} is the vapor concentration at the surface of the liquid core and is determined from Eq.(5-11a) assuming $\alpha_s = \bar{\alpha}$. With m_c given by Eq.(5-17), the solute cap inside diameter d_i is then calculated using

$$d_i = (d_o^3 - 6m_c/\pi\rho_c)^{1/3}, \tag{5-21}$$

where ρ_c is the solute cap density (not necessarily equal to ρ_s, since the cap is porous). d_o, the cap outside diameter, is assumed constant throughout Phase II and equal to the drop diameter at transition to Phase II. Since the density of the solute cap is usually greater than the concentration of salt in a saturated solution, the volume of liquid left in the drop is insufficient to completely fill the volume enclosed by the solute cap. In accordance with experimental observations made by Charlesworth (34), our model assumes that the remaining volume is occupied by a gas bubble of negligible mass and diameter d_v given by

$$d_v = [d_i^3 - 6(m-m_c)/\pi\rho(\bar{\alpha},T)]^{1/3}, \qquad (5\text{-}22)$$

which resides at the center of the liquid core (recall Figure 5-1b).

One missing link in the analysis remains: specification of D_{eff}, the effective diffusivity of vapor through the gas-filled pores of the solute cap. Ideally, D_{eff} should be measured experimentally. However, such experimental data are rarely available. We must therefore resort to estimation of D_{eff}. To aid in this process, consider diffusion in an infinitesimal porous solute shell of thickness dr. Observe that although we model diffusion as if it occurred radially, vapor actually follows a tortuous path through the pores in the shell. Thus, we might write

$$\begin{Bmatrix}\text{vapor}\\ \text{mass}\\ \text{flowrate}\end{Bmatrix} = \begin{Bmatrix}\text{effective}\\ \text{diffusivity}\end{Bmatrix} \times \begin{Bmatrix}\text{radial}\\ \text{area}\end{Bmatrix} \times \begin{Bmatrix}\text{radial}\\ \text{concentration}\\ \text{gradient}\end{Bmatrix}$$

$$\dot{m}_v = D_{eff} \times 4\pi r^2 \times dC_v/dr \qquad (5\text{-}23)$$

$$= \begin{Bmatrix}\text{actual}\\ \text{diffusivity}\end{Bmatrix} \times \begin{Bmatrix}\text{actual}\\ \text{area}\end{Bmatrix} \times -\begin{Bmatrix}\text{actual}\\ \text{concentration}\\ \text{gradient}\end{Bmatrix}$$

$$= D_v \times f_A(4\pi r^2) \times dC_v/dL,$$

where f_A is the fraction of the radial area occupied by pore openings and dL is the infinitesimal tortuous path length. If we assume that dL = p dr, p>1, i.e., that the tortuous path length is always proportionately larger than the radial path length, then Eq. (5-23) yields

$$D_{eff} = (f_A/p)D_v. \qquad (5\text{-}24)$$

But the volume fraction of pores in the cap, f_v, is approximately given by pf_A, so that

$$D_{eff} = (f_v/p^2)D_v; \qquad (5\text{-}25)$$

we may calculate f_v from the cap density ρ_c and the solid crystalline solute density ρ_s using

$$f_v = 1-\rho_c/\rho_s. \qquad (5\text{-}26)$$

Thus, Eq.(5-25) becomes

$$D_{eff} = [(1-\rho_c/\rho_s)/p^2]D_v. \qquad (5\text{-}27)$$

Finally, then, our analysis of Phase II requires that we specify values for two parameters: ρ_c and p. Upper and lower bounds on ρ_c do exist: ρ_c cannot be greater than ρ_s and cannot be smaller than the value ($6\ m_s/\pi d_o^3$) which results in a dry particle with no air space in the center. Theoretically, p can take on any value greater than one.

PHASE III

Our analysis treats only drop dynamics in Phase III; heat and mass transfer are neglected.

COMPUTER PROGRAM

The governing differential equations (Eqs.5-6,5-7,5-10,5-17 and 5-20) together with their associated initial conditions constitute an initial value problem. The equations are integrated numerically by computer using the method of Gear (35) for stiff systems of first order ordinary differential equations. The results are in the form of time-histories of relevant drop characteristics. Three of the basic equations (m, m_c, T) are always integrated, while the user can decide whether to integrate all, some, or none of the dynamic equations (x, y, z, u, v, w).

Presently, the computer model is equipped to analyze drops of pure water, aqueous solutions of sodium chloride (NaCl), or aqueous solutions of ammonium nitrate (NH_4NO_3), in an environment of humid air. Since most of the data specific to a given substance are isolated in subroutines, analysis of different combinations of constituents is relatively straightforward, provided the physics of the problem remains unchanged.

The computer program accounts for the temperature dependence of the physical properties of humid air (ν, k, D_v, ρ_q) and pure water (h_{fg}, P_v) using the interpolating formulae given by Dunn (21). The physical properties of NaCl-H_2O and NH_4NO_3-H_2O solutions (P_s, ρ, α_{sat}, $c_{p\ell}$) are calculated as functions of temperature and, where appropriate, solute concentration, using interpolating polynomials fit to experimental data from various sources, e.g., (36, 37, 38).

RESULTS

MODEL/DATA COMPARISONS

The data of Charlesworth (34) and Charlesworth and Marshall (22) are among the few that are sufficiently detailed to use in evaluating the performance of our model. These workers suspended solution droplets with diameters between 1300 and 1800 μm on a fine glass filament in a vertical heated air stream. Drop mass was determined at various intervals during a given experimental run by shielding the drop from the air stream momentarily and measuring the deflection of the glass suspension filament. A thermocouple was used to measure the drop temperature history in a parallel experimental run under similar conditions, as it was infeasible to determine mass and temperature histories in the same run.

We present below detailed comparisons of the predictions of our model with the experimental data of Charlesworth (34) and Charlesworth and Marshall (22). We realize that the ranges of drop size and composition studied by these workers are not particularly relevant to drift modeling. However, we do feel that these data provide an opportunity to assess our model's treatment of the physics of solution droplet evaporation.

Before beginning our comparison, a few comments on the general modeling procedure are in order.

1. In all of the cases presented here, we have neglected concentration gradients in modeling Phase I. We found that accounting for a nonuniform solute distribution in Phase I via Eqs.(5-14) had little impact on results beyond predicting a slightly earlier transition to Phase II. This result is not surprising in view of the small values of evaporation intensity G ($\sim$0.04-0.5) encountered by a drop in the low temperature environments considered in this report.
2. We found that in order to match Charlesworth and Marshall's (22) asymptotic values for drop mass in Phase III, we had to input initial drop diameters to the model that were at most 1.5% smaller than the values specified by the experimenters. This deviation likely resides within the realm of experimental error.
3. Our initial values for the empirical crystallization constants k_c and n_c, 0.15 kg/m^{2}s and 1.6, were selected on the basis of information given by Mullin (28) and led to unrealistically high predictions of supersaturation in Phase II for both the core and cap scenarios. Also, for given values

of k_c and n_c, the core scenario generally predicted significantly larger values of $\bar{\alpha}$ in Phase II than did the cap scenario, probably due to the fact that the surface area available for crystallization in the core scenario (πd_c^2) is much smaller than that available in the cap scenario (πd_i^2). In subsequent runs, for lack of any experimental data on k_c and n_c, we left n_c equal to 1.6 and adjusted k_c to yield reasonable supersaturations for both the cap and core scenarios in Phase II. Our final selections are listed in Table 5-1.

Table 5-1. Values of crystallization constant k_c used in Model.

Solute	k_c (kg/m²s)	
	Core Scenario	Cap Scenario
NH_4NO_3	1.5	0.6
NaCl	0.15	0.015

Figures 5-4 and 5-5 compare model predictions with Charlesworth and Marshall's (22) data for a stationary drop with an initial diameter of 1565 μm and initial composition of 50% water, 50% ammonium nitrate (by mass), evaporating in a dry air stream with velocity 0.97 m/s and temperature 33.9 C. The model shows good agreement with the data in Phase I, and the predicted transition to Phase II lies between the experimentally observed time of appearance of first crystals (denoted by ↑ in the figures) and time of completion of the solute cap (denoted by ↓). Figure 5-4 indicates clearly that the core scenario vastly overpredicts mass transfer in Phase II. As shown in Fig. 5-5, the cap scenario, due to the added diffusion resistance of the solute cap, predicts a decreasing mass transfer rate in Phase II, in agreement with the experimental data. Use of the minimum possible cap density ($\rho_c = 6m_s/\pi d_o^3$) and minimum diffusion path ratio (p = 1.0) results in a shell which is too porous, as indicated by overprediction of the mass transfer rate in Phase II. On the other hand, use of the maximum possible cap density ($\rho_c = \rho_s$), in accordance with Eq.(5-27) shuts off mass transfer completely at the end of Phase I, thus underpredicting mass transfer in Phase II. Good agreement with the data was obtained by using a cap density which is 90% of the density of crystalline solute along with a path ratio of 2.2. These values are physically reasonable, as they lead to prediction of a hollow, thin-walled dry particle in Phase III, which is the configuration experimentally observed in both the Charlesworth and Marshall (22) and Illinois State Water Survey (27) investigations.

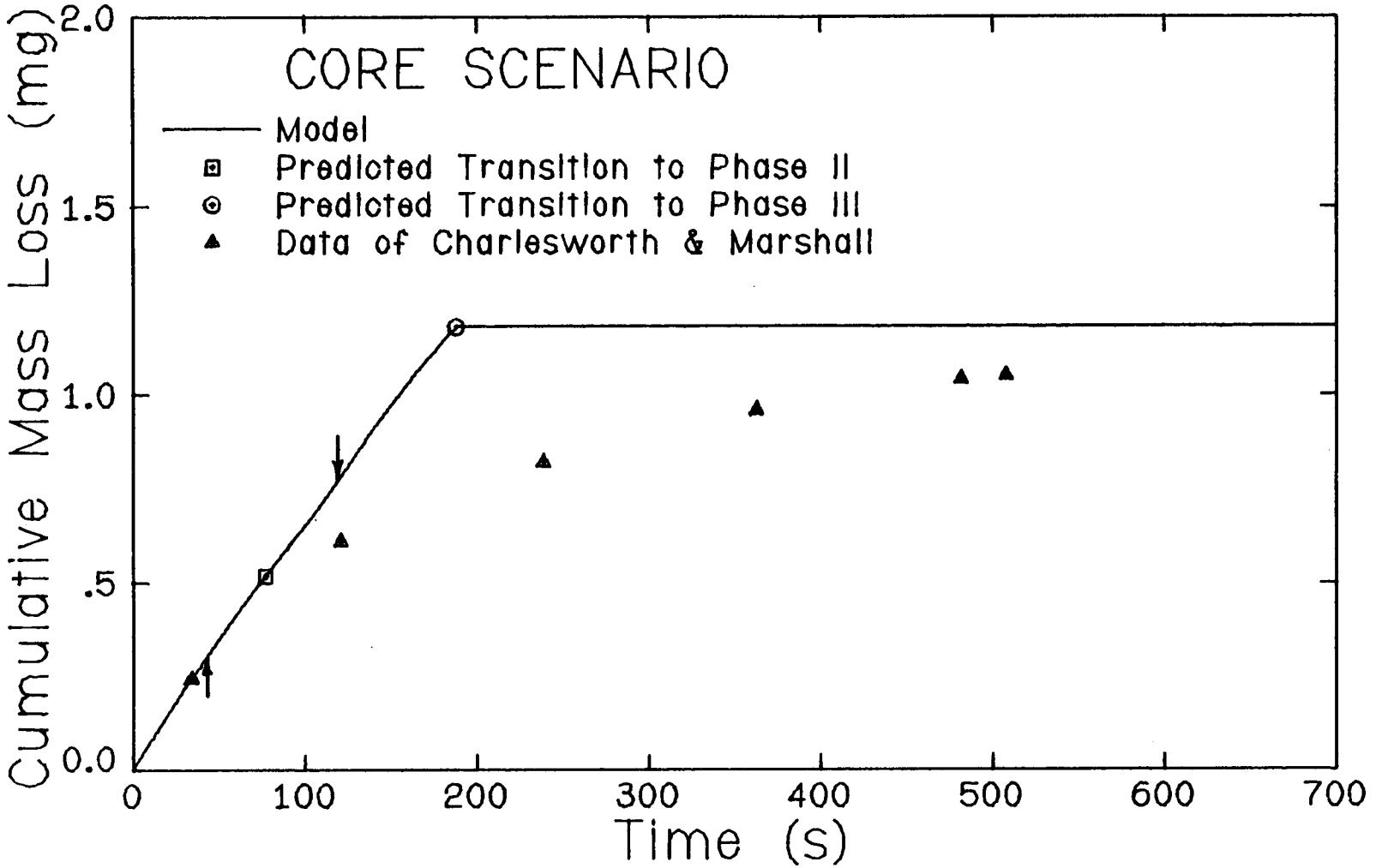

Figure 5-4. Predicted (core scenario) and actual cumulative mass loss histories for d=154μm, α=0.500, solute=NH_4NO_3. Arrows denote experimentally observed time of appearance of first crystals ($\uparrow$) and time of cap completion ($\downarrow$).

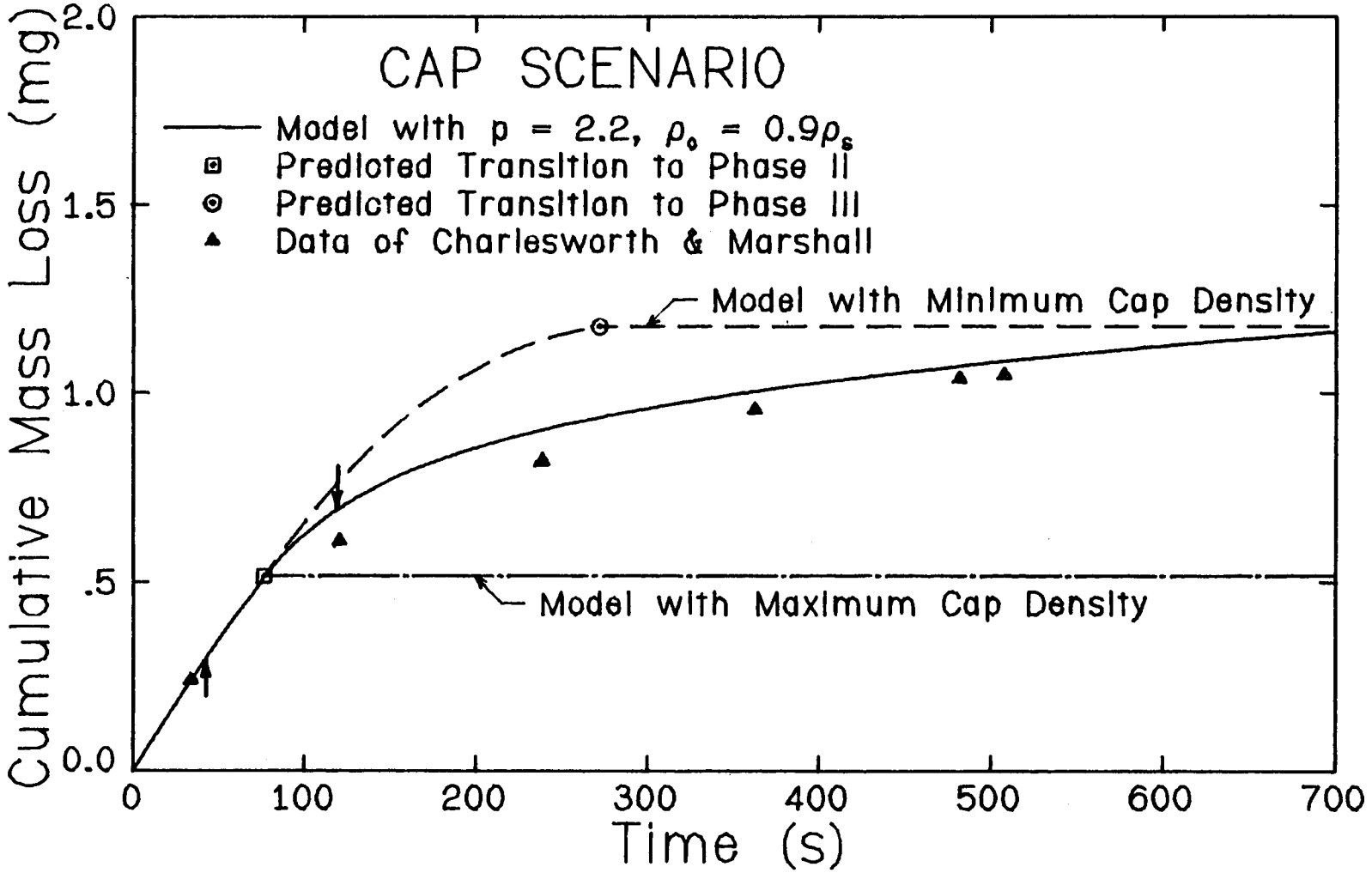

Figure 5-5. Predicted (cap scenario) and actual cumulative mass loss histories for d=1541μm, α=0.500, solute=NH_4NO_3. Arrows denote experimentally observed time of appearance of first crystals (↑) and time of cap completion (↓).

Figure 5-6 shows model/data comparisons for the same size drop and same ambient conditions as before but for initial NH_4NO_3 mass fractions of 0.125 and 0.250. Although the model curves lie slightly below the data for Phase I, transition to Phase II in both cases occurs between the experimentally determined times of crystal appearance and cap completion. Good agreement with the Phase II data was again obtained by using the cap scenario with $\rho_c = 0.9\ \rho_s$ and $p = 2.2$.

Figure 5-7 compares predicted and actual histories of the difference between ambient temperature (T_a) and drop temperature (T) for a 1565-μm drop initially composed of 75% water and 25% NH_4NO_3 evaporating in a dry air stream with velocity 0.97 m/s and temperature 31.7 C. The model correctly predicts a rapid decrease in drop temperature at the start of Phase I (due to latent heat removal as evaporation commences) and a gradual increase in drop temperature towards the end of Phase I (due to a slowing rate of latent heat removal as solute accumulation depresses the surface vapor pressure and slows the evaporation rate). During Phase II, the cap scenario, in qualitative agreement with the data, predicts a gradual rise in drop temperature as the rate of mass transfer slows due to the presence of the cap. The rise in drop temperature predicted by the core scenario at the start of Phase II is also caused by a decrease in mass transfer rate, but in this case mass transfer is slowed by supersaturation of the drop liquid (leading to increased vapor pressure depression) before crystallization can begin in earnest. Once the crystallization rate increases, the supersaturation falls, leading to increased mass transfer and a lower drop temperature, as indicated by the upturn in the core scenario temperature difference curve. This prediction contrasts sharply with the experimentally observed behavior.

In order to emphasize the vastly different physical configurations predicted for the drop by the core and cap scenarios, drop diameter histories according to both scenarios are plotted in Figs. 5-8 and 5-9 even though no experimental data are available for comparison. The drop and ambient conditions for these figures are the same as for Fig. 5-6 with α=0.250. The core scenario (Fig. 5-8) predicts that the drop diameter decreases throughout Phases I and II and that the dry particle in Phase III is a solid, crystalline solute sphere with a diameter of 839 μm. The cap scenario (Fig. 5-9), on the other hand, predicts a decreasing drop outside diameter only through Phase I, after which time the drop is assumed to be covered with a solute cap of fixed outside diameter. In Phase II, the inside diameter of the shell shrinks as solute precipitates until, at transition to Phase III, the drop exists as a hollow, dry, porous solute shell with an outside diameter of 1074 μm and an inside diameter of 836 μm. This structure is consistent with that of the dry particles examined by Charlesworth and Marshall (22).

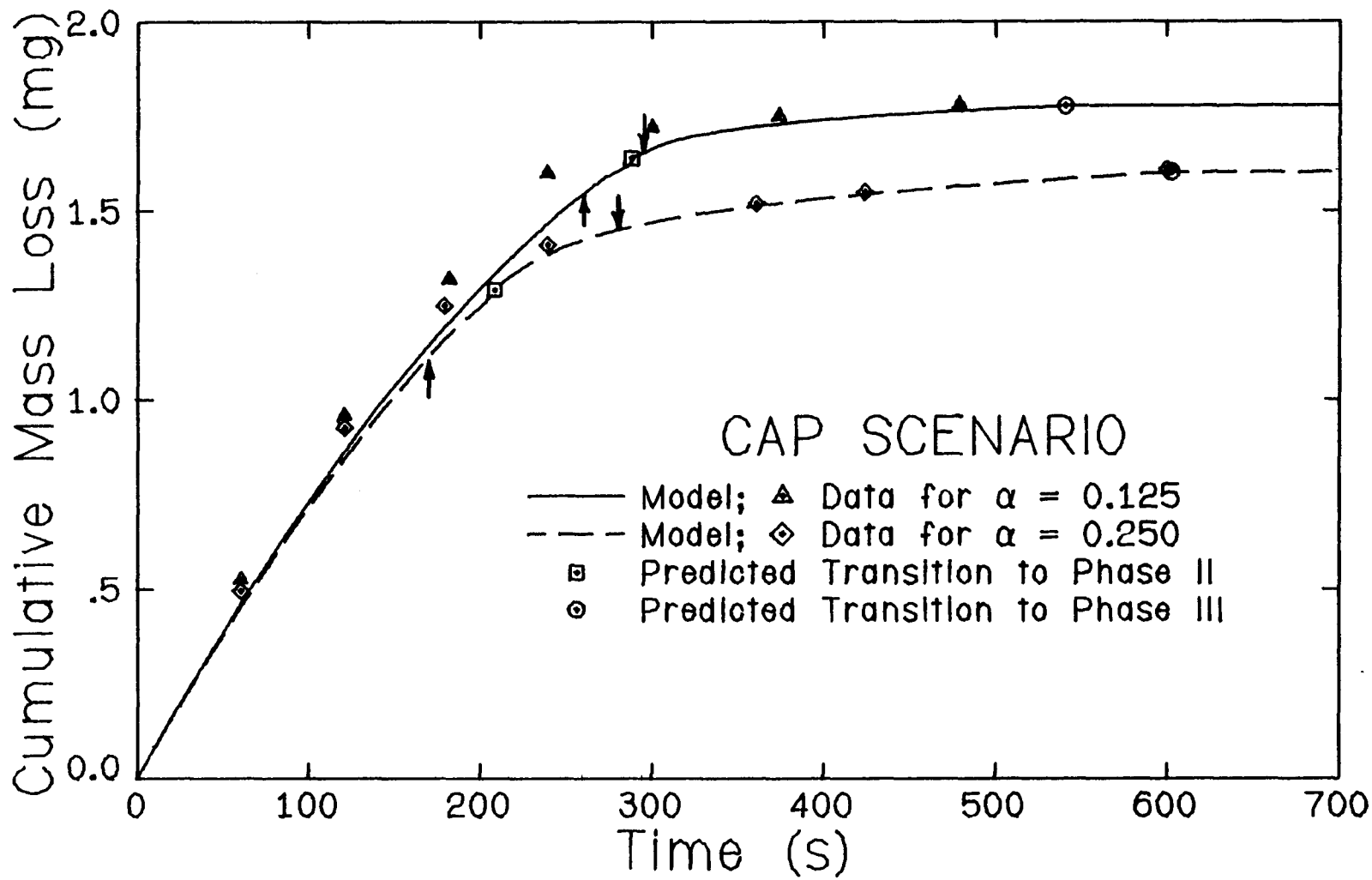

Figure 5-6. Predicted (cap scenario) and actual cumulative mass loss histories for d=1544μm, α=0.125 and 0.250, solute=NH_4NO_3. Arrows denote experimentally observed time of appearance of first crystals (↑) and time of cap completion (↓).

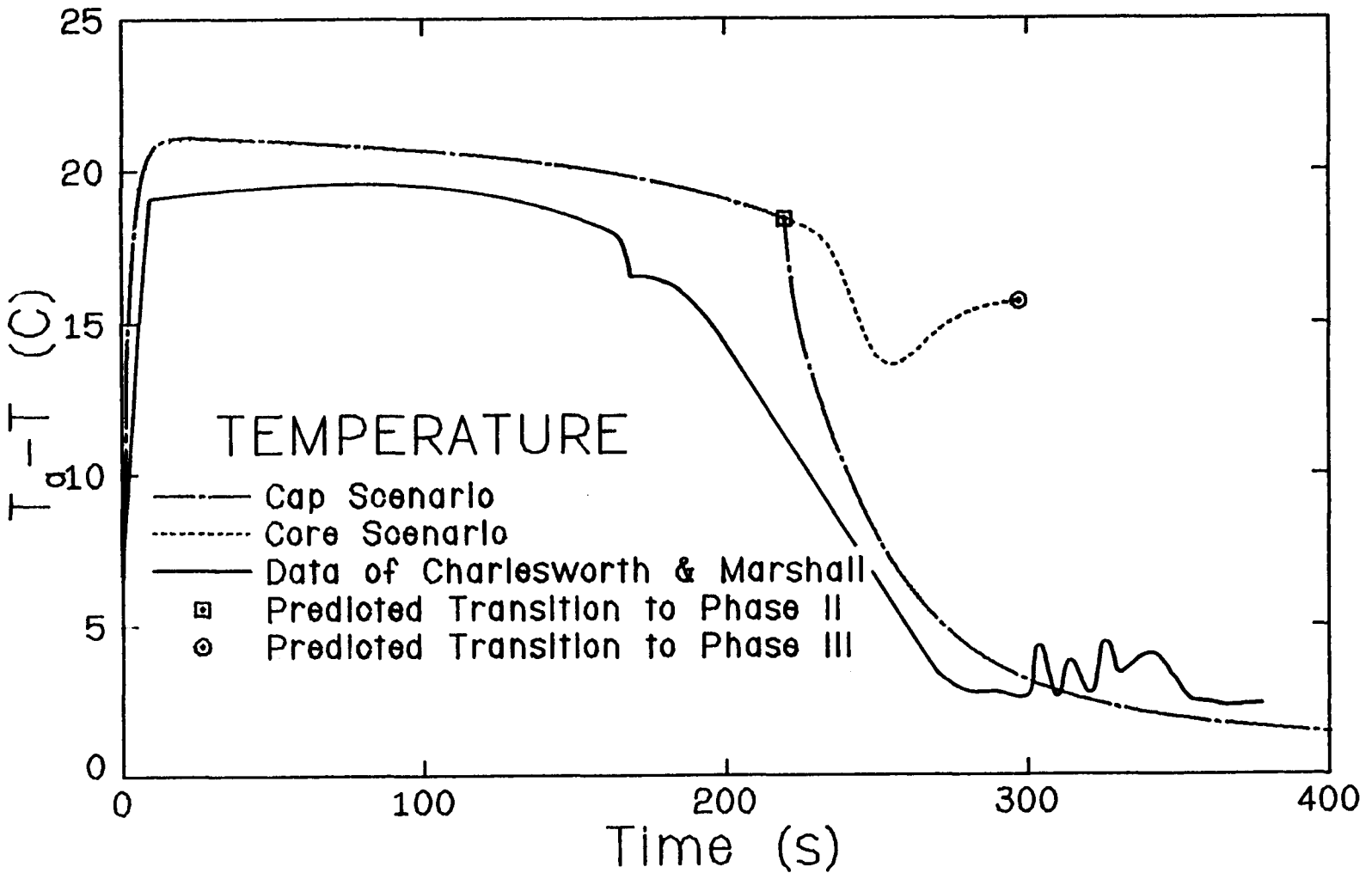

Figure 5-7. Predicted and actual temperature difference histories for d=1544μm, α=0.250, solute=NH_4NO_3.

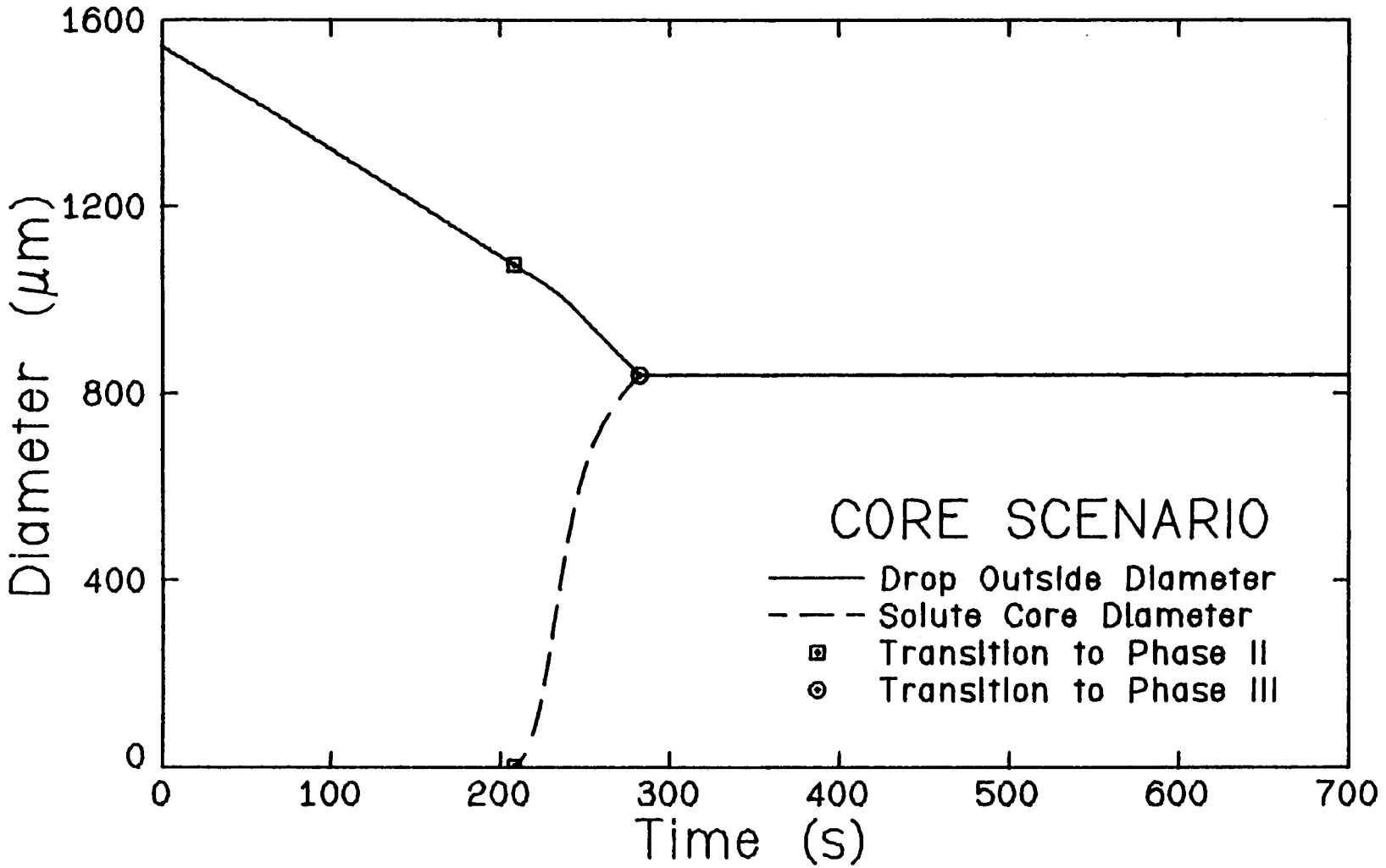

Figure 5-8. Predicted (core scenario) diameter histories for d=1544μm, α=0.250, solute=NH_4NO_3.

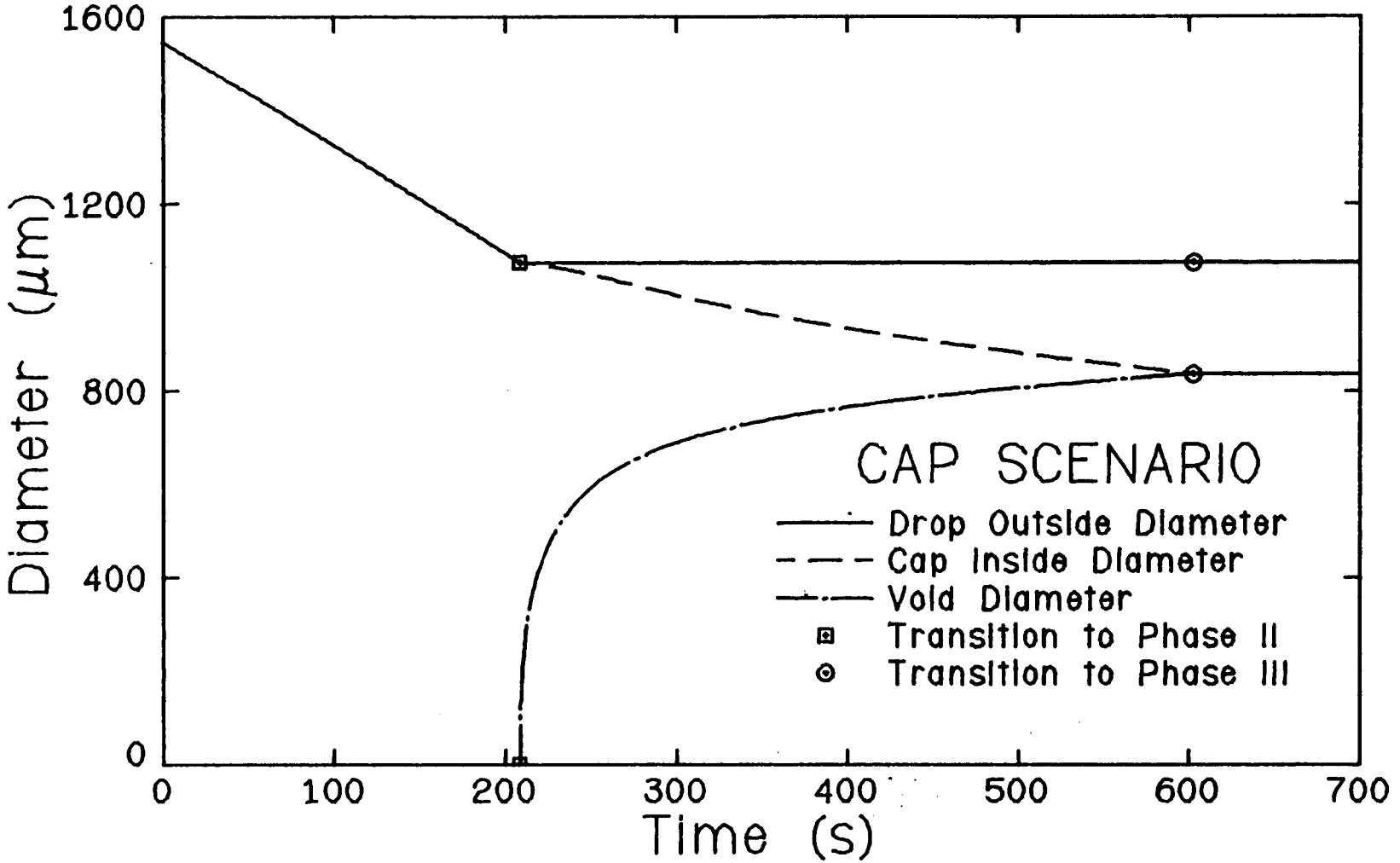

Figure 5-9. Predicted (cap scenario) diameter histories for d=1544μm, α=0.250, solute=NH_4NO_3.

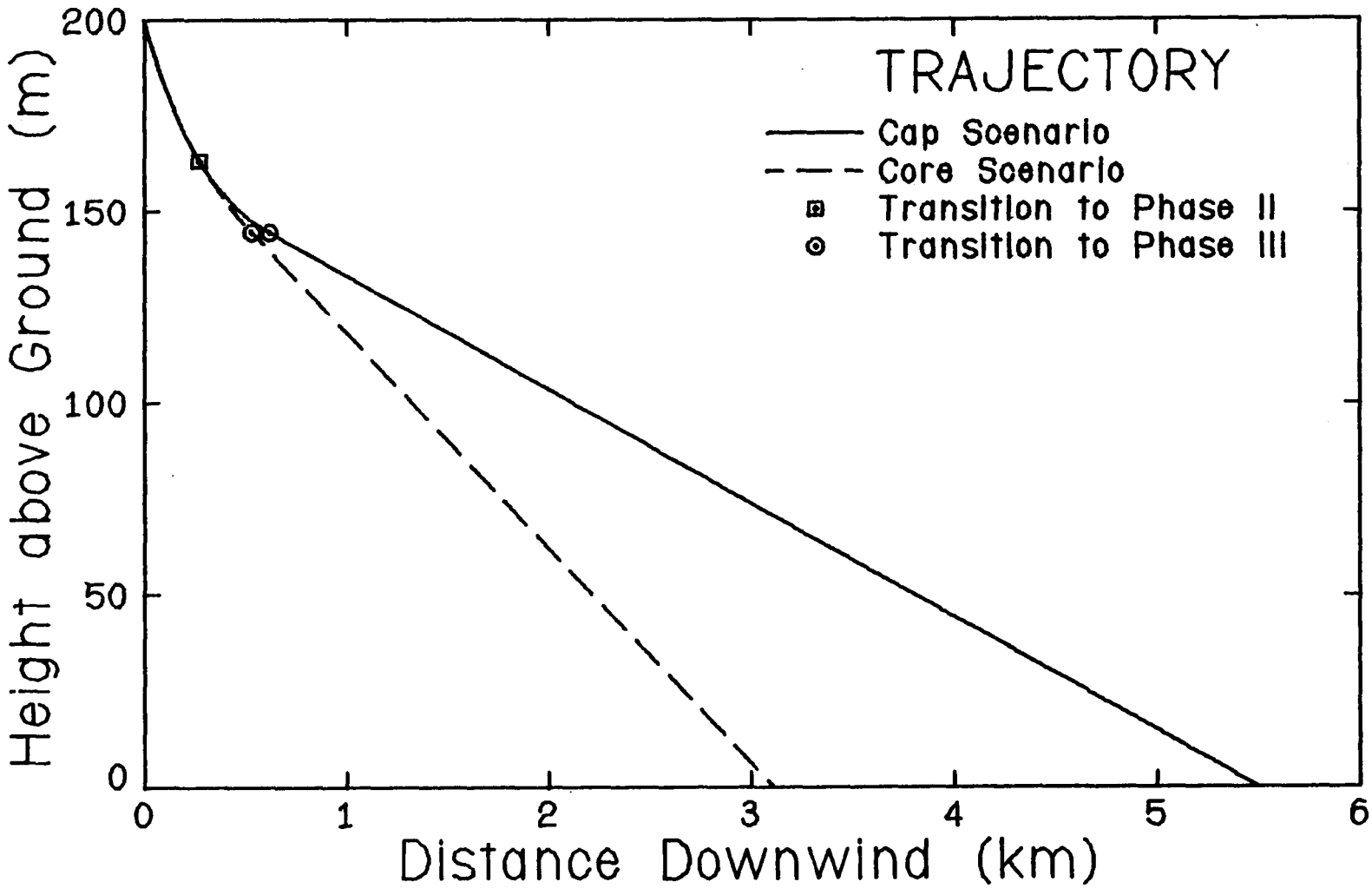

Figure 5-10. Predicted trajectories for d=200μm, α=0.05, solute=NaCl.

The difference in final particle configurations predicted by the cap and core scenarios is of particular importance in drift modeling, as Fig. 5-10 illustrates. This figure shows the trajectories predicted by our model for a drift drop initially 200 μm in diameter and composed of 95% water, 5% sodium chloride (by mass) released from rest into air at 10 C and 60% relative humidity with a wind speed of 4 m/s. The difference between the trajectories predicted by the cap and core scenarios through the end of Phase II is not dramatic, although, as in the cases studied earlier, the core scenario does predict an earlier transition to Phase II. The small, dense dry particle predicted by the core scenario for Phase III, however, falls to deposition much faster than the large, porous dry particle predicted by the cap scenario. The cap scenario predicts deposition at 5.5 km downwind of the release point, a full 77% further downwind than the 3.1 km deposition point predicted by the core scenario.

CONCLUSION

A detailed model of the heat, mass, and momentum transfer processes associated with a solution drop evaporating in gaseous surroundings was presented. Evaluation of model predictions for Phase I, i.e., before the onset of solute crystallization, revealed that solute concentration gradients affect drop behavior only slightly during evaporation in low temperature surroundings, so that adequate modeling of Phase I for the purposes of drift analysis can be accomplished with the assumption of uniform solute concentration. Drop behavior during Phase II, i.e., during solute precipitation, was modeled according to both the cap and core scenarios. The cap scenario, which assumes that solute crystallization occurs on the drop surface and forms a shell around the remaining liquid that impedes further mass transfer, yielded predictions of drop mass and temperature histories and dry particle configuration which were in close agreement with the experimental data of Charlesworth and Marshall (22). The core scenario, which assumes that solute precipitation occurs within the drop, leaving the remaining liquid in contact with the surroundings, overpredicted mass transfer in Phase II and yielded a temperature history and dry particle configuration which were at odds with experimental data. It was demonstrated that these alternative modeling assumptions can have a dramatic impact on the prediction of drift droplet behavior.

Future work in the area of multicomponent droplet evaporation should be primarily experimental, as our ability to model correctly the relevant physical processes is severely limited by the scarcity of detailed experimental data. If possible, future studies should deal with drops free of possibly disruptive

external attachments, such as the suspension filaments used by Charlesworth and Marshall (22), in order to simulate more closely the conditions seen by a freely falling drop.

REFERENCES

1. C.L. Hosler, J. Pena, and R. Pena, "Determination of Salt Deposition Rates from Drift from Evaporative Cooling Towers," J. Eng. Power, 96, 283-291 (1974).

2. Personal communication between G. Schrecker and D. Rutherford, Environmental Systems Corp. (ESC); and W.E. Dunn and A.J. Policastro (Knoxville, Tenn., 1976).

3. P.R. Slawson and T.M.L. Wigley, "Calculation of Cooling Tower Drift Deposition," in Power Generation: Air Pollution Monitoring and Control, ed. K.E. Noll and W.T. Davis, Ch. 8 (Ann Arbor Science Publications, 1976).

4. T. Overcamp, "Sensitivity Analysis and Comparison of Salt Deposition Models for Cooling Towers," Proc. of the Conference on Waste Heat Management and Utilization, 9-11 May, 1977 (Miami Beach, Fla., 1977).

5. Anthony J. Policastro, William E. Dunn, Marvin Breig, and Michael Ratcliff, "Evaluation of Theory and Performance of Salt-Drift Deposition Models for Natural-Draft Cooling Towers," in Environmental Effects of Atmospheric Heat/ Moisture Releases, ed. Kenneth E. Torrance and Robert G. Watts, pp. 27-38 (ASME, 1978).

6. William Dunn, Bruce Boughton, and Anthony Policastro, "Evaluation of Droplet Evaporation Formulations Employed in Drift Deposition Models," Proc. of the Symposium on the Environmental Effects of Cooling Tower Emissions, 2-4 May, 1978 (College Park, Md., 1978).

7. N.H. Fletcher, The Physics of Rainclouds (Oxford: University Press, 1971).

8. B.J. Mason, The Physics of Clouds (Oxford: Clarendon Press, 1971).

9. K. Masters, Spray Drying, 2nd ed. (New York: John Wiley and Sons, 1976).

10. W.A. Sirignano and C.K. Law, "Transient Heating and Liquid-Phase Mass Diffusion in Fuel Droplet Vaporization," ACS Adv. Chem. Ser., #166, 3-26 (1978).

11. Alan Williams, "Combustion of Droplets of Liquid Fuels: A Review," Combustion and Flame, 21, 1-31 (1973).

12. G.M. Faeth, "Current Status of Droplet and Liquid Combustion," Prog. Energy Comb. Sci., 3, 191-224 (1977).

13. Hans R. Pruppacher and James D. Klett, Microphysics of Clouds and Precipitation (Dordrecht: D. Reidel, 1978).

14. R.L. Drake, "A Review and Evaluation of Information on the Thermal Performance of Ultimate Heat Sinks: Spray Ponds and Cooling Ponds," BNWL-B-446, Battelle Pacific Northwest Laboratories (Richland, Wash., 1975).

15. R. Clift, J.R. Grace, and M.E. Weber, Bubbles, Drops, and Particles (New York: Academic Press, 1978).

16. Ross Gunn and Gilbert D. Kinzer, "The Terminal Velocity of Fall for Water Droplets in Stagnant Air," J. Meteorology, 6, 243-248 (1949).

17. K. V. Beard and H.R. Pruppacher, "A Determination of the Terminal Velocity and Drag of Small Water Drops by Means of a Wind Tunnel," J. Atmos. Sci., 26, 1066-1072 (1969).

18. W. E. Ranz and W.R. Marshall, Jr., "Evaporation from Drops-Part I," Chem. Eng. Prog., 48, 141-146 (1952).

19. W. E. Ranz and W.R. Marshall, Jr., "Evaporation from Drops-Part II," Chem. Eng. Prog., 48, 173-180 (1952).

20. K. V. Beard and H. R. Pruppacher, "A Wind Tunnel Investigation of the Rate of Evaporation of Small Water Drops Falling at Terminal Velocity in Air," J. Atmos. Sci., 28, 1455-1464 (1971).

21. W. E. Dunn, "Heat, Mass and Momentum Transfer in Multidrop Systems," Dept. of Mechanical and Industrial Engineering, Report No. UILU-ENG-77-4006, University of Illinois at Urbana-Champaign (Urbana, Ill., 1977).

22. D. H. Charlesworth and W.R. Marshall, Jr., "Evaporation from Drops Containing Dissolved Solids," A. I. Ch. E. Journal, 6, 9-23 (1960).

23. E. U. Schlünder, "Temperatur- und Massenanderung Verdunstender Tropfen aus Reinen Flüssigkeiten und Wässrigen Salzlösungen," Int. J. Heat Mass Transfer, 7, 49-73 (1964).

24. G. C. Gardner, "Asymptotic Concentration Distribution of an Involatile Solute in an Evaporating Drop," Int. J. Heat Mass Transfer, 8, 667-668 (1965).

25. Patrick M. Gavin, "Dynamics and Thermodynamics of an Evaporating Salt-Water Drop," Dept. of Mechanical and Industrial Engineering, Report No. UILU-ENG-78-4015, University of Illinois at Urbana-Champaign (Urbana, Ill., 1978).

26. S. El Golli, J. Bricard, P.-Y. Turpin, and C. Treiner, "The Evaporation of Saline Droplets," J. Aerosol Sci., 5, 273-292 (1974).

27. Personal communication between K.V. Beard and K.H. Leong, University of Illinois Atmospheric Research Lab; and W.E. Dunn and P.M. Gavin (Urbana, Ill., 1980).

28. J.W. Mullin, Crystallization, 2nd ed. (Cleveland: CRC Press, 1972).

29. J.W. Mullin and O. Söhnel, "Expressions of Supersaturation in Crystallization Studies," Chem. Eng. Sci., 32, 683-686 (1977).

30. O. Söhnel and J.W. Mullin, "Expressions of Supersaturation for Systems Containing Hydrates, Partially Dissociated Electrolytes and Mixtures of Electrolytes," Chem. Eng. Sci., 33, 1535-1538 (1978).

31. O. Söhnel and J. Garside, "The Thermodynamic Driving Force for Crystallization from Solution," J. Crystal Growth, 46, 238-240 (1979).

32. I.V. Melikhov and L.B. Berliner, "Crystallization of Salts from Supersaturated Solutions; Diffusion Kinetics," J. Crystal Growth, 46, 79-84 (1979).

33. R. Byron Bird, Warren E. Stewart, and Edwin N. Lightfoot, Transport Phenomena (New York: John Wiley and Sons, 1960).

34. Donald Hector Charlesworth, "Drying of Drops Containing Dissolved Solids," Ph.D. Thesis, Univ. of Wisconsin, Madison, Wis. (1954).

35. C. William Gear, Numerical Initial Value Problems in Ordinary Differential Equations (Englewood Cliffs: Prentice-Hall, 1971).

36. National Research Council of the U.S.A., International Critical Tables of Numerical Data, Physics, Chemistry and Technology (New York: McGraw-Hill, 1927).

37. Handbook of Chemistry and Physics, ed. Robert C. Weast, 57th ed. (Cleveland: CRC Press, 1976).

38. Lange's Handbook of Chemistry, ed. John A. Dean, 11th ed. (New York: McGraw-Hill, 1973).

Section 6

Droplet Deposition Formulation

This section describes the results of ongoing work to improve the treatment of deposition in our drift model. As presently formulated, the drift model developed in the remaining sections of this report does not consider the effects of atmospheric turbulence on the drift drops. Instead, the drift deposition is smeared uniformly over an area defined by a sector angle (usually taken to be 22.5°) and by the distances of deposition predicted by a ballistic analysis for the largest and smallest drops within a given drop size range.

This work is being carried out in five steps as follows.

a. Development of a Monte Carlo methodology for analysis of the atmospheric methodology for analysis of the atmospheric dispersion problem with deposition, settling and evaporation.
b. Verification of the Monte Carlo model with known analytical solutions of atmospheric transport equations.
c. Verification of the Monte Carlo model with field data on ground-level concentration and deposition of pollutants.
d. Development of simple methods which can be used to approximate the results of the Monte Carlo model in most if not all cases of interest in drift model.
e. Inclusion of the deposition methodology into the drift model and verification with available data.

This section deals only with items (a) and (b) above.

The fundamental problem in the formulation of a deposition model is a continuous point release at rate Q (particles per unit time) and height h above the ground. Other source configurations are then treated by superposition. Source dynamics such as buoyant plume rise are also treated in the same framework by specifying an effective release height greater than the actual release height. Thus, the continuous point source release is the prototype problem for study, although the methodology developed herein may be extended to a more general problem.

The mean wind $\bar{u}$ which is the prime factor carrying the drift drops away from the tower may be regarded as constant in time over a period on the order of 20 minutes. Over level terrain free of rising thermals, the mean wind is parallel to the ground and generally increases monotonically with height. Thus, for convenience in our study, we shall assume this idealized behavior for the wind and define a rectangular coordinate system with the x-coordinate in the direction of the mean wind, the y-coordinate in the horizontal crosswind direction and z in the vertical direction as shown in Fig 6-1. The corresponding velocity components are, u, v, and w; an overbar denotes a mean value. Thus, by definition $\bar{v}=\bar{w}=0$.

Superimposed on the mean wind are fluctuating components u', v' and w' which are responsible for turbulent diffusion of the drift particles. The characteristics of these turbulent fluctuations depend strongly on the stability of the atmosphere which, in turn, depends on the vertical gradient of temperature in the atmosphere. The actual vertical temperature gradient must be compared with the dry adiabatic lapse rate,

$$\Gamma = -0.00975 \text{ C/m}, \qquad (6\text{-}1)$$

which is the rate at which temperature would change for a parcel of air raised adiabatically and isentiopically. If the gradient of temperature exceeds the adiabatic lapse rate, a displaced volume of air will return to its original position and the atmosphere is said to be stable. Similarly in an atmosphere whose temperature gradient is less than the adiabatic lapse rate, a displaced volume of air continues to move away from its original position and the atmosphere is said to be unstable.

ATMOSPHERIC TURBULENCE

Definitions of Basic Terms and Concepts

A key step in understanding the random fluid motions of which a turbulent velocity field is composed was made by Reynolds in 1895 when he suggested that the state properties of the fluid be decomposed into mean and fluctuating values. The fluctuating component may then be treated as a random variable and thus characterized using the techniques of probability theory. Following Reynold's suggestion, the velocity components in the x-, y- and z-directions of Fig. 6-1 are written as

$$u = \bar{u} + u' \qquad (6\text{-}2a)$$

$$v = \bar{v} + v', \qquad (6\text{-}2b)$$

and

$$w = \bar{w} + w', \tag{6-2c}$$

where, as before, the overbar denotes an average value and the prime indicates a fluctuating quantity. Thus, by definition $\bar{u}'=\bar{v}'=\bar{w}'=0$.

The averaging process implied in Eqn (6-2) can be performed in a number of different ways depending on the type of turbulent velocity field with which one is dealing. If the flow is steady or can be considered a stationary random process, averaging with respect to time can be used. Mathematically, the time-averaged Eulerian velocity at fixed position x_o is given by

$$\bar{u}(x_o) = \lim_{\Delta t \to \infty} \frac{1}{\Delta t} \int_t^{t+\Delta t} u(x_o,t)\, dt. \tag{6-3}$$

When studying turbulent diffusion the Lagrangian description of motion in which the observer moves with the particle is often more convenient to use. Averaging for a steady or stationary process is then carried out over a large number of particles all of which have the same origin but different starting times.

If the turbulence field is homogeneous, averaging with respect to space can be employed. Mathematically, the space-averaged Eulerian velocity for an instant t_o is given by

$$\bar{u}(t_o) = \lim_{\Delta x \to \infty} \frac{1}{\Delta x} \int_x^{x+\Delta x} u(x,t_o)\, dx. \tag{6-4}$$

In a Lagrangian frame, this process corresponds to averaging over a large number of particles, all of which have the same starting time but different origins. If the flow is neither stationary nor homogeneous then an ensemble average must be used. The ensemble average is an average taken over a large number of experiments each of which has the same initial and boundary conditions. Mathematically, the ensemble-averaged Eulerian velocity is given by

$$\bar{u}(x_o,t_o) = \frac{\sum_{\ell=1}^{M} u_\ell(x_o,t_o)}{M}, \tag{6-5}$$

where M is the number of experiments.

When the turbulence field is both stationary and homogeneous, all three averaging procedures yield the same result and the flow statistics are said to be ergodic.

Many of the measures used to characterize a turbulent velocity field involve

the statistical properties of the probability density distribution of the fluctuating velocities. A majority of the studies of atmospheric turublence (e.g., Sutton (1), Blackadar et al. (2), Pasquill (3)) have shown that the distribution of the fluctuating velocities is very nearly Gaussian, or normal, although deviations from the Gaussian form have been observed particularily near the ground. Further support for the Gaussian assumption can be obtained by appealing to the Central Limit Thereom of probability theory which states that the combined result of a large number of random influences tends toward a Gaussian distribution no matter how the individual influences are distributed. Thus, the probability density function P(u') is given by

$$P(u') = \frac{1}{\sqrt{2\pi}\,\sigma_{u'}} \exp\left(\frac{-u'^2}{2\sigma_{u'}^2}\right), \qquad (6\text{-}6)$$

where $\sigma_{u'} = \sqrt{\overline{u'^2}}$. Similar expressions may be written for v' and w'. Eqn (6-6) represents the distribution of fluctuating velocities at a single point in space at an instant of time. Integrating P(u') between u'_a and u'_b gives the probability of finding u' in the closed interval $[u'_a, u'_b]$.

Statistical Characterization of Turublence

The first statistical characteristic of turbulence we wish to discuss is intensity. The intensity of turbulence is defined as the root-mean-square of the fluctuating velocity and is a measure of the energy of the fluctuating velocities. Since, in the atmosphere, the fluctuating velocities are distributed in a Gaussian fashion, the intensity is equal to the standard deviation of the distribution. Counihan (4) has presented data showing that for neutral atmospheric conditions within the constant shear stress layer near the ground

$$\sqrt{\overline{v'^2}} \;/\; \sqrt{\overline{u'^2}} = 0.75 \qquad (6\text{-}7a)$$

and

$$\sqrt{\overline{w'^2}} \;/\; \sqrt{\overline{u'^2}} = 0.5. \qquad (6\text{-}7b)$$

Thus, the fluctuations in the mean-wind direction contain the most energy, followed by those in the horizontal crosswind direction and finally by the fluctuations in the vertical direction.

We next consider the various correlation coefficients which are used to characterize a turbulent flow. Here, we will only be concerned with the double velocity component correlations, although, in a more general study of turbulence, one must consider higher order velocity component correlations and correlations between velocity components and pressure. In our discussion, definitions will be given in terms of u' with the understanding that similar expressions may be written for v' and w'.

Of most interest to us is the Lagrangian time correlation coefficient defined for a homogeneous flow as

$$R_{L_u}(\xi,t_o) = \frac{\overline{u'(t_o)\, u'(t_o+\xi)}}{\overline{u'(t_o)^2}}, \qquad (6\text{-}8)$$

where the overbar denotes ensemble averaging, $u'(t_o)$ is the velocity of a fluid particle at time t_o and $u'(t_o+\xi)$ is the velocity of the same particle at time $t+\xi$. If the flow is both homogeneous and stationary, then $R_{L_u}(\xi,t_o)$ is independent of the base time t_o and an even function of ξ. In this case, the Lagrangian time correlation is written simply as $R_{L_u}(\xi)$.

Inspecting Eqn (6-8), we observed that for small ξ, $R_{L_u}(\xi,t_o)$ approaches unity, whereas for large ξ, $R_{L_u}(\xi,t_o)$ approaches zero. The general form of the Lagrangian correlation coefficient for $\xi>0$ is shown in Fig 6-2. Determination of the precise functional form of $R_L(\xi,t_o)$ is nearly impossible due to the substantial difficulties encountered when trying to measure fluid particle velocities in the Lagrangian frame.

In a manner analogous to Eqn (6-8), we define the Eulerian time correlation or autocorrelation for a steady or statistically stationary flow as

$$R_{E_u}(\xi,x_o) = \frac{\overline{u'(x_o,t_o)\, u'(x_o,t_o+\xi)}}{\overline{u'(x_o,t_o)^2}}, \qquad (6\text{-}9)$$

where the averaging is with respect to time, $u'(x_o,t_o)$ is the velocity at a fixed point at time t_o and $u'(x_o,t_o+\xi)$ is the velocity at the same point at time $t_o+\xi$. Because of the assumed stationarity, $R_{E_u}(\xi,x_o)$ is an even function of ξ.

In addition to time correlations, we may define space correlations. The Eulerian space correlation coefficient for a steady or stationary turbulent field is defined as

$$R_{E_{u,x}}(x,x_o) = \frac{\overline{u'(x_o,t)\, u'(x_o+x,t)}}{\sqrt{\overline{u'(x_o,t)^2}\;\overline{u'(x_o+x,t)^2}}}, \qquad (6\text{-}10)$$

where the overbar denotes a time average, $u'(x_o,t)$ is the velocity at some point x_o at time t and $u'(x_o+x,t)$ is the velocity at the point x_o+x at time t. If the turbulence is stationary and homogeneous, Eqn (6-10) can be rewritten as

$$R_{E_{u,x}}(x) = \frac{\overline{u'(x_o,t)\ u'(x_o+x,t)}}{\overline{u'(x_o,t)^2}}, \qquad (6\text{-}11)$$

and $R_{E_{u,x}}(x)$ is then an even function of x. The general form of the space correlation is similar to that of the time correlation shown in Fig 6-2.

A statistical characteristic closely related to the correlation coefficient is the integral scale of the turbulence. From the Lagrangian time correlation coefficient, we define the Lagrangian integral time scale as

$$\tau_{L_u} = \int_o^\infty R_{L_u}(\xi,t_o)\ d\xi. \qquad (6\text{-}12)$$

τ_L is a measure of the average time during which a fluid particle moves in a given direction. In the atmosphere, typical values of the Lagrangian integral time scale are on the order of 100 seconds.

Similarly, the Eulerian integral time scale

$$\tau_{E_u} = \int_o^\infty R_{E_u}(\xi,x_o)\ d\xi \qquad (6\text{-}13)$$

can be thought of as the average time during which velocities sampled at a single point are correlated with one another. In the atmosphere, τ_E is on the order of 20 seconds.

From the Eulerian space correlation $R_{E_{u,x}}$, we define the integral length scale

$$L_{u,x} = \int_o^\infty R_{E_{u,x}}(x,x_o)\ dx. \qquad (6\text{-}14)$$

$L_{u,x}$ is a measure of the average distance over which velocities sampled simultaneously are correlated. Additionally, $L_{u,x}$ can be considered a measure of the average size of the "eddies" of which the turbulent field is composed. In this context, the term "eddy" refers to an irregular rolling motion which develops randomly within the flow.

Counihan (4) presents evidence showing that in the atmosphere under neutrally stable conditions the length scale $L_{u,x}$ decreases with increasing surface roughness and increases with height approximately as $\sqrt{z}$ to heights of 200 to 300 meters.

The length scale $L_{w,z}$ is found to be insensitive to changes in surface roughness and increases as z to heights of approximately 100 meters. Thus, since $L_{w,z}$ is a stronger function of height than $L_{u,x}$, we conclude that atmospheric turbulence is less homogeneous in the vertical direction than in the horizontal direction due to the ground.

Another important characteristic of turbulence is the power spectral density or spectrum, which indicates how the energy of the fluctuating velocities varies with scale or, equivalently, how the energy of the fluctuating velocities is distributed among the various eddy sizes. Of key importance here is the spectral function.

The Eulerian spectral function $F_E(f)$, where f is frequency, can be thought of as a relation which gives the fraction of the fluctuating velocity energy contained between frequencies f and f+df, although true physical meaning is attained only after integration. For a homogeneous, stationary flow the spectral density function is defined by the Fourier transform pair

$$F_E(f) = 4\int_0^\infty R_E(\xi) \cos 2\pi f\xi \, d\xi \qquad (6\text{-}15a)$$

and

$$R_E(\xi) = \int_0^\infty F_E(f) \cos 2\pi f\xi \, df \, . \qquad (6\text{-}15b)$$

This relation was first shown by Taylor (5) in 1938. A similar relation can be written relating the Lagrangian spectral density $F_L(f)$ to the Lagrangian time correlation $R_L(\xi)$.

Integrating over all frequencies, we have

$$\int_0^\infty F(f) \, df = 1. \qquad (6\text{-}16)$$

Kaimal et al. (6) have shown that for atmospheric turbulence, a majority of the energy associated with the fluctuations in the mean-wind and horizontal crosswind directions lies in the low frequency range (large eddies) and that these spectra are nearly invariant with height. On the other hand, the scale of eddies associated with the fluctuations in the vertical direction increases with height. Also, a greater fraction of the energy is contained in the high frequency range for the spectrum of the vertical fluctuations as compared with those of the mean wind and horizontal crosswind fluctuations.

As a final comment, we mention that although a great deal of experimental evidence indicates that atmospheric turbulence is neither homogeneous nor stationary, nearly all theoretical work on the diffusion problem assumes a stationary, homogeneous turbulence field. Furthermore, atmospheric turbulence is often taken to be isotropic, i.e., the same in all directions, despite considerable evidence to the contrary.

REVIEW OF PREVIOUS WORK

Presently available analyses of the turbulent diffusion problem have developed along two lines of thought: the gradient transfer approach and the statistical approach. In the first of these, the Eulerian equation of conservation of mass for the diffusing particles is solved using the gradient transport hypothesis as a turbulence model. In the statistical method, the behavior of the diffusing particles is described in terms of the Lagrangian statistical properties of the velocity field.

Although much of the previous work in this area does not allow for settling and/or deposition, insight can be gained by considering the solutions available in the literature. The efforts of previous investigators can be classified according to the following criterion:

1. Whether the source is continuous or instantaneous.
2. Whether the source is a point, a finite line, an infinite line or an area.
3. Whether the source is ground-level or elevated.
4. Whether particle settling is included.
5. Whether particle deposition is considered.

In Table 6-1, the solutions of previous investigators are classified according to these criterion.

Of these, the classification of source type (1 and 2 above) deserves further clarification. The most fundamental source is the instantaneous point source which can be thought of as the instantaneous release of a quantity of matter, Q, at some instant, say t=0 (physically perhaps a puff of smoke formed by an explosion). Since the diffusion problem is linear, solutions for all other types of sources, e.g., the continuously emitting point source, the continuously emitting infinite line source and the area source, can be obtained from the instantaneous point source solution by appropriate integrations. Details of how these integrations are performed can be found in Sutton (1), pp. 134-137. Note that, although solutions for other source types can be derived from the instantaneous point source solution, these solutions can also be obtained independently.

Of greatest interest to us are the continuous point source (a three-dimensional problem) which closely models the emission of pollutants from cooling towers and stacks and the crosswind integrated continuous point source, or equivalently, the continuous infinite line source in the horizontal crosswind direction (a two-dimensional problem) which models point source type emissions when behavior in the horizontal crosswind direction is unimportant. Since the variables in the governing equation are separable, the three-dimensional continuous point source problem concentration distribution can be recovered from the crosswind integrated solution by multiplying by a function of y only.

The Gradient Transfer Approach

To derive the basic equation of the gradient transfer approach, we start with the equation of conservation of mass for passive particles. (Here, passive implies that the presence of the particles does not alter the wind field in any way.). Using indicial notation, the equation is

$$\frac{\partial c}{\partial t} + \frac{\partial}{\partial x_i}(u_i c) = \frac{\partial}{\partial x_i}\left(D \frac{\partial c}{\partial x_i}\right) + S \; ; \qquad (6\text{-}17)$$

where c is the particle concentration, u_i is the component of the fluid velocity in the x_i direction, D is the molecular diffusivity of the particles in the fluid and S is a function describing the distribution of sources of the particles.

For the basic problems discussed above, S is given by:

Instantaneous Point Source

$$S = Q\delta(x_1)\delta(x_2)\delta(x_3-h)\delta(t)$$

Continuous Point Source

$$S = Q\delta(x_1)\delta(x_2)\delta(x_3-h)$$

Crosswind Integrated Point Source

$$S = Q\delta(x_1)\delta(x_3-h)$$

After u_i and c are decomposed into mean and fluctuating components in accordance with our previous discussion of turbulence:

$$u_i = \bar{u}_i + u_i' \quad , \qquad (6\text{-}18a)$$

and

$$c = \bar{c} + c' . \qquad (6\text{-}18b)$$

Substituting into Eqn (6-17) and averaging, we obtain

$$\frac{\partial \bar{c}}{\partial t} + \frac{\partial}{\partial x_i}(\bar{u}_i \bar{c}) + \frac{\partial}{\partial x_i}(u_i' c') = \frac{\partial}{\partial x_i}\left(D \frac{\partial \bar{c}}{\partial x_i}\right) + S. \qquad (6\text{-}19)$$

Making use of the continuity equation for the incompressible flow

$$\frac{\partial \bar{u}_i}{\partial x_i} = 0, \qquad (6\text{-}20)$$

Eqn (6-19) becomes

$$\frac{\partial \bar{c}}{\partial t} + \bar{u}_i \frac{\partial \bar{c}}{\partial x_i} + \frac{\partial}{\partial x_i}(\overline{u_i' c'}) = \frac{\partial}{\partial x_i}\left(D \frac{\partial \bar{c}}{\partial x_i}\right) + S. \qquad (6\text{-}21)$$

Even with a prescribed wind field, Eqn (6-21) is unsolvable due to the presence of the additional unknown quantity $\overline{u_i' c'}$. One of the simplest methods of overcoming this difficulty, known as the closure problem, is the gradient transport hypothesis. Allowing for inhomogeneous and anisotropic turbulence, the hypothesis is

$$\overline{u_i' c'} = -K_{ij} \frac{\partial \bar{c}}{\partial x_j}, \qquad (6\text{-}22)$$

where K_{ij} is the eddy diffusivity tensor and the minus sign indicates that the transport is down the concentration gradient. Notably, the gradient transport hypothesis is a sound physical model only if the scale of the spatial distribution of particles is large compared with the scale of the diffusing action. This condition is most nearly met in the case of vertical diffusion from a ground-level source. A more complete discussion of the limitations of the gradient transport hypothesis is given by Corrsin (7).

Substituting Eqn (6-22) into Eqn (6-21) yields

$$\frac{\partial \bar{c}}{\partial t} + \bar{u}_i \frac{\partial \bar{c}}{\partial x_i} + \frac{\partial}{\partial x_i}\left(-K_{ij} \frac{\partial \bar{c}}{\partial x_j}\right) = \frac{\partial}{\partial x_i}\left(D \frac{\partial \bar{c}}{\partial x_i}\right) + S. \qquad (6\text{-}23)$$

After rearrangement, we obtain

$$\frac{\partial \bar{c}}{\partial t} + \bar{u}_i \frac{\partial \bar{c}}{\partial x_i} = \frac{\partial}{\partial x_i}\left(D \frac{\partial \bar{c}}{\partial x_i} + K_{ij} \frac{\partial \bar{c}}{\partial x_j}\right) + S. \qquad (6\text{-}24)$$

Eqn (6-24) is still too complex for analytical solution except in certain special cases. Therefore, additional simplifying assumptions based on our knowledge of the physics of the problem are required:

1. Molecular diffusion is negligible compared with turbulent diffusion.
2. The eddy diffusivity tensor is diagonal, i.e., we assume a concentration

gradient in the z-direction results in diffusion in the z-direction only and similarly for the x- and y-directions.

3. Diffusion is negligible in the mean wind direction compared with advection.

With these assumptions and reverting to the coordinate system with x in the direction of the mean wind, Eqn (6-24) becomes

$$\frac{\partial \bar{c}}{\partial t} + \bar{u}\frac{\partial \bar{c}}{\partial x} = \frac{\partial}{\partial y}\left(K_y \frac{\partial \bar{c}}{\partial y}\right) + \frac{\partial}{\partial z}\left(K_z \frac{\partial \bar{c}}{\partial z}\right) + S. \qquad (6\text{-}25)$$

Adding the convective term $-w_s\, \partial c/\partial z$, where w_s is the settling velocity (w_s is positive in the negative z-direction), to the left-hand side of Eqn (6-25) to account for gravitational settling, we obtain the final form

$$\frac{\partial \bar{c}}{\partial t} + \bar{u}\frac{\partial \bar{c}}{\partial x} - w_s\frac{\partial \bar{c}}{\partial z} = \frac{\partial}{\partial y}\left(K_y \frac{\partial \bar{c}}{\partial y}\right) + \frac{\partial}{\partial z}\left(K_z \frac{\partial \bar{c}}{\partial z}\right) + S. \qquad (6\text{-}26)$$

Eqn (6-26), known as the atmospheric advective-diffusion equation, is the basic equation of the gradient-transfer approach.

For the crosswind integrated point source or the infinite crosswind line source problem, the governing equation becomes (after integration in y)

$$\frac{\partial \bar{c}}{\partial t} + \bar{u}\frac{\partial \bar{c}}{\partial x} - w_s\frac{\partial \bar{c}}{\partial z} = \frac{\partial}{\partial z}\left(K_z \frac{\partial \bar{c}}{\partial z}\right) + Q\delta(x)\delta(z-h) \qquad (6\text{-}27)$$

Solutions Using the Grandient Transfer Approach.

Analytic Solutions.

One of the first investigators to solve Eqns (6-26) and (6-.27) was Roberts. In 1923 (8), he obtained solutions for the ground-level instantaneous and continuous point sources and the continuous infinite crosswind line source with the mean wind and eddy diffusivities taken as constants.* The inadequacy of this "Fickian" solution to appropriately describe atmospheric diffusion led Roberts later (unpublished, see Sutton (1) to derive a solution for the continuous infinite line source problem with both the mean wind and eddy diffusivity taken as power laws of height.

Rounds (9) obtained solutions for the elevated continuous infinite crosswind line source for neutral atmospheric stability with the mean wind and diffusivity taken as power laws of height based on the profiles of Deacon (10). This solution did include a constant settling velocity. Rounds also obtained solutions of the line source problem for arbitrary atmospheric stability without settling and for area sources infinite in the crosswind direction.

---

*Unless otherwise noted all solutions are for the steady state.

Godson (11), using an approximate method, extended the applicability of Rounds solution with settling to cases of non-neutral atmospheric stability and introduced deposition into the problem. At the ground, the deposition flux j was defined as

$$j(x) = w_s \, \bar{c}(x,o) \tag{6-28}$$

with the boundary condition

$$K_z \frac{\partial \bar{c}}{\partial z} = 0 \quad \text{at } z = 0 \tag{6-29}$$

retained from Rounds' work. Thus, Godson's solution included deposition by merely multiplying the ground-level concentration by the settling velocity. He presented his results in terms of the relative crosswind integrated deposition rate j/Q.

Smith (12), in the context of the point source problem, obtained a solution for the elevated infinite line source using integral transform methods. The mean wind and diffusivity were taken as conjugate power laws of height (Schmidt's conjugate power law)

$$\bar{u} = \bar{u}_o \, z^n \tag{6-30a}$$

and

$$K = K_o \, z^{1-n} \, . \tag{6-30b}$$

Using the infinite line source solution, Smith found an exact solution to the point source problem for the case $n = 1/2$, $K_y = K_z$. Observing that in this case the crosswind concentration distribution was Gaussian, he then assumed a Gaussian, crosswind distribution and obtained a solution in the form of an infinite series for the point source problem for arbitrary n.

In a later paper, Smith (13) obtained solutions for the continuous infinite line source that included both settling and deposition assuming the mean wind was invariant with height. Solutions were presented for various forms of the diffusivity as a function of height including a case which modeled the occurrence of a temperature inversion in the atmosphere. To account for deposition, Smith used the boundary condition proposed by Calder (14)

$$\left(K_z \frac{\partial \bar{c}}{\partial z} + w_s \bar{c}\right)\Big|_{z=0} = w_d c\Big|_{z=0}, \tag{6-31}$$

where w_d is a constant deposition velocity. Thus, particle deposition was assumed to occur at a rate proportional to the ground-level concentration, the factor of proportionality being the deposition velocity w_d. The deposition velocity is a function of particle size, atmospheric stability and terrain roughness and must be determined experimentally. In a recent paper, McMahon and Denison (15) summarized the available empirical atmospheric deposition parameters including deposition velocity data.

Heines and Peters (16), using Laplace transform techniques, obtained solutions for the continuous infinite line and point sources under conditions of a constant mean wind with the eddy diffusivities K_y and K_z taken as power laws of the downwind distance x. They showed that the effect of a temperature inversion was to increase the ground-level concentration and to push the point at which the maximum ground-level concentration occurs further downwind. In a subsequent paper, Heines and Peters (17) re-solved the infinite line and point source problems for a case that included absorption of the diffusing species at the ground.

Yeh and Huang (18), Ermak (19) and Peterson and Seinfeld (20) obtained analytical solutions to the continuous point source problem. Using a Fourier integral transform and the Green's function technique, Yeh and Huang obtained a solution for the case in which the mean wind and vertical diffusivity were power laws of height; the lateral diffusivity was taken as the product of a power law in height and a power law of the downwind distance. Using separation of variables and Laplace transform techniques, Ermak obtained a solution that included both settling and deposition. Deposition was modeled using the boundary condition given in Eqn (6-31). Both eddy diffusivities K_y and K_z were taken as functions of the downwind distance x with the mean wind assumed to be vertically uniform. The settling velocity was taken to be the same functional form of downwind distance as K_z. Petersen and Seinfeld's solution included settling, deposition (as per Eqn (6-31)) and the possibility of removal by a first order chemical reaction. The mean wind and the diffusivities were taken as constants. They applied their solution to a problem in which a conversion from gaseous to particulate matter occurred.

Two rather unique approaches to the diffusion problem were presented by Astarita, Wei and Iorio (21) and Lebedeff and Hameed (22). Astarita, Wei and Iorio developed a solution which described diffusion in the x,y-plane by making a transformation of the independent variables from (x,y) to (ϕ,ψ), where ϕ was the potential function and ψ was the stream function of the two-dimensional incompressible flow in the x,y-plane. Using the (ϕ,ψ) coordinates, they derived a solution applicable to arbitrary source distributions in the x,y-plane. The

solution assumed $K_x = K_y$ = constant and allowed for the occurrence of first order chemical reaction.

Lebedeff and Hameed obtained approximate solutions to the two-dimensional diffusion equation (Eqn (6-26)) for ground-level semi-infinite area and infinite line sources using an integral method more commonly applied in boundary-layer theory (see Schlichting (23)). Essentially the method in this application consists of assuming a form for the solution $\bar{c}(x,z)$ in which the z-dependence is specified, substituting this form into the governing equation and integrating over z to an upper bound g(x) (diffusion is assumed to be limited to the depth g(x)). From this integration, one obtains an ordinary differential equation which can be solved for the ground-level concentration. Lebedeff and Hameed's solution used wind and diffusivity profiles based on the Monin-Obukhov similarity theory.

One of the few unsteady solutions to the diffusion problem was presented by Nunge (24). Nunge solved the problem of dispersion of a cloud, initially of rectangular cross section, within a three-dimensional rectangular region. The boundaries in the vertical and crosswind directions were impenetrable. Particular solutions were presented for two simple wind profiles with the diffusivities taken as constants.

Numerical Solutions.

Many different numerical techniques have been used to solve the atmospheric advective-diffusion equation, the most popular being the finite difference method.

Ragland and Dennis (25), using a finite difference scheme, obtained a solution for the elevated continuous point source problem within a region bounded above by an impenetrable stable layer (temperature inversion) which they called the mixing layer. Deposition and settling were neglected. The functional dependence of the mean wind and eddy diffusivities on height were determined by the height of the mixing layer, the wind speed at the top of the mixing layer, the net heat flux to the air and the surface roughness.

Liu and Goodin (26), assuming that the atmosphere below an inversion was uniformly mixed, integrated the three-dimensional diffusion equation over the depth of the inversion to obtain an equation which described time dependent diffusion in the x,y-plane. This equation was then solved numerically to predict carbon monoxide concentrations in the Los Angeles area. A study was made to test the accuracy of four different finite difference schemes.

Runca and Sardei (27) solved the time dependent infinite line source problem for the case in which the mean wind and eddy diffusivity were functions of height using a mixed Lagrangian-Eulerian finite difference technique. Advection was treated with a Lagrangian procedure while diffusion was handled in the conventional Eulerian fashion. This procedure was employed to avoid the numerical diffusion that may arise when advection is treated with a conventional Eulerian finite difference scheme.

Another hybrid Lagrangian-Eulerian method developed to combat the numerical diffusion problem is the particle-in-cell technique. Basically, the technique solves the advective-diffusion equation by following a number of Lagrangian particles, each particle representing a discrete amount of pollutant, within a fixed Eulerian grid (see Sklarew (28) for details). Shei (29) used this technique to solve the two-dimensional time dependent diffusion equation including settling and thermal coagulation. Coagulation is the removal of small particles from the atmosphere by coalescence with larger particles whose gravitational settling is significant.

A second numerical technique that has been applied to the advective-diffusion equation is the pseudospectral method. Here, space derivatives are computed by means of finite Fourier transforms, i.e., in spectral space, with the products and the time integration evaluated in physical space. Christensen and Prahm (30) modified this method to handle the boundary conditions encountered in atmospheric work. In a later paper, Berkowicz and Prahm (31) used this refined technique to solve the continuous infinite line source problem including deposition. The psuedospectral technique is free from the numerical diffusion problem associated with the finite difference methods.

Finally, we consider the probabilistic or Monte Carlo method of numerically solving the advective-diffusion equation. The technique is Lagrangian in nature, i.e., solutions are obtained by following individual particles as they travel through the atmosphere. The effect of turbulence is simulated by random movements of the particles. The mathematical basis of the method was developed by Chandrasekhar (32) in 1943. He showed that in the limit of a large number of displacements, the probability distribution obtained from a random walk problem is a solution to the advective-diffusion equation. Thus, an equivalence exists between following a large number of particles along random flights and solving the advective-diffusion equation.

Wipperman (33) applied this technique to the continuous point source problem

taking into account the variation of the eddy diffusivity with height by varying the step size of the random walk in the vertical direction. Joynt and Blackman (34) used the method to obtain a time dependent solution of the continuous point source problem with the size of the random particle displacement determined by the intensity of the turbulent velocity fluctuations in the vertical direction and the ratios of the scales of the turbulence in the mean-wind, lateral and vertical directions.

Runchal, Bealer and Seagal (35) used a Monte Carlo model to solve several problems with known analytical solutions. Agreement between the Monte Carlo simulations and the analytical results was good.

The Statistical Approach

The mathematical basis of this approach was developed by Taylor (36) in 1921 in his classic work on diffusion by continuous movements. The analysis proceeds as follows.

Consider a homogeneous and stationary turbulent velocity field. Let X be the deviation of a typical particle from its mean position due to the fluctuating velocity u' at time t = T. From the usual rules governing mean values in a turbulent field, we can write

$$\overline{\frac{dX^2}{dt}} = \frac{\overline{dX^2}}{dt} = 2\overline{X\frac{dX}{dt}} = 2\overline{Xu'(T)} = 2\overline{\int_0^T u'(\zeta)\, d\zeta\, u'(T)},$$

or

$$\overline{\frac{dX^2}{dt}} = 2\int_0^T \overline{u'(\zeta)\, u'(T)}\, d\zeta, \qquad (6\text{-}32)$$

where $\overline{X^2}$ is the mean square deviation (variance) of a large number of particles (ensemble average).

Substituting $\zeta = T+\xi$, where T is a constant, into Eqn (6-32) yields

$$\overline{\frac{dX^2}{dt}} = 2\int_{-T}^{0} \overline{u'(T+\xi)\, u'(T)}\, d\xi. \qquad (6\text{-}33)$$

Using the definition of the Lagrangian correlation coefficient, Eqn (6-8), we obtain

$$\overline{\frac{dX^2}{dt}} = 2\int_{-T}^{0} \overline{u'^2}\, R_{L_u}(\xi)\, d\xi. \qquad (6\text{-}34)$$

Since the field is stationary, $\overline{u'^2}$ is a constant and $R_{L_u}(\xi)$ is an even function of ξ. Therefore, Eqn (6-34) becomes

$$\frac{\overline{dX^2}}{dt} = 2\,\overline{u'^2}\int_0^T R_{L_u}(\xi)\,d\xi. \qquad (6\text{-}35)$$

Integrating Eqn (6-35), we obtain Taylor's important result

$$\overline{X^2} = 2\,\overline{u'^2}\int_0^t\int_0^T R_{L_u}(\xi)\,d\xi\,dT, \qquad (6\text{-}36)$$

where X is now the deviation of a particle at time t.

We now consider the applicability of Taylor's result to the study of diffusion of particles emitted continuously from a source located at a fixed point in a homogeneous, stationary turbulent flow. In the derivation of Eqn (6-36), we considered the statistical properties of a single particle observed a large number of times. In the case of a continuously emitting source, we are concerned with the statistics of a large number of particles as they successively pass a fixed point. However, in a stationary and homogeneous turbulence field, the two are identical. Therefore, Taylor's result is applicable to the diffusion of particles emitted from a continuous source as long as the particles are passive and no relative motion exists between the particles and fluid. Extending Eqn (6-36) to three dimensions, using the usual coordinate system, and allowing for anisotropic turbulence, we have

$$\overline{X^2} = \sigma_x^2(t) = 2\overline{u'^2}\int_0^t\int_0^T R_{L_u}(\xi)\,d\xi\,dT, \qquad (6\text{-}37a)$$

$$\overline{Y^2} = \sigma_y^2(t) = 2\overline{v'^2}\int_0^t\int_0^T R_{L_v}(\xi)\,d\xi\,dT, \qquad (6\text{-}37b)$$

and

$$\overline{Z^2} = \sigma_z^2(t) = 2\overline{w'^2}\int_0^t\int_0^T R_{L_w}(\xi)\,d\xi\,dT, \qquad (6\text{-}37c)$$

where σ is the standard deviation of the diffusing particles. For the case of a constant mean wind, t can be replaced by $x/\bar{u}$, where x is the distance travelled downwind, and the σ's become a function of x.

Eqn (6-37) is significant in that it completely describes the variance of the diffusing particles in any particular direction in a homogeneous, stationary turbulent wind field in terms of only two parameters: the mean square fluctuating velocity component and the Lagrangian correlation coefficient. Thus, for given u'^2, v'^2, w'^2 and R_{L_u}, R_{L_v}, R_{L_w} the task of obtaining solutions describing the diffusion process is reduced to finding functions representing the concentration distribution $\bar{c}(x,y,z,t)$ which satisfy Eqn (6-37) with

$$\sigma_x^2 = \frac{\int_0^\infty x^2\, \bar{c}(x,y,z,t)\, dx}{\int_0^\infty \bar{c}(x,y,z,t)\, dx}, \tag{6-38a}$$

$$\sigma_y^2 = \frac{\int_{-\infty}^\infty y^2 \bar{c}(x,y,z,t)\, dy}{\int_{-\infty}^\infty \bar{c}(x,y,z,t)\, dy}, \tag{6-38b}$$

and

$$\sigma_z^2 = \frac{\int_0^\infty z^2 \bar{c}(x,y,z,t)\, dz}{\int_0^\infty \bar{c}(x,y,z,t)\, dz} - h^2, \tag{6-38c}$$

appropriate boundary conditions and an equation which imposes conservation of mass.

An immediate barrier to obtaining solutions with this technique is deciding upon the functional form of the correlation coefficients. However, we can deduce some valuable information about the diffusion process without making any assumptions regarding R_L. Let us consider only the x direction for the purpose of discussion with similar results applicable to the y and z directions. Knowing only the behavior of R_L for very short and very long diffusion times, we conclude from Eqn (6-37)

$$t \to 0 \quad R_L \to 1 \qquad \sigma_x^2 \to \overline{u'^2}\, t^2 \tag{6-39}$$

and

$$t \to \infty \quad R_L \to 0 \qquad \sigma_x^2 \to 2\, \overline{u'^2} \tau_{L_u}\, t \tag{6-40}$$

Thus, the spread of the diffusing particles, as measured by the standard deviation of their displacements, is proportional to t for short diffusion times and is proportional to $\sqrt{t}$ for long diffusion times. For the case of a constant mean wind, we conclude that the spread is initially proportional to x and ultimately goes as $\sqrt{x}$.

Batchelor (37) has pointed out other useful relations. Performing an integration by parts on Eqn (6-36) gives

$$\sigma_x^2 = 2\overline{u'^2} \int_0^t (t-\xi)\, R_{L_u}(\xi)\, d\xi. \tag{6-41}$$

Eqn (6-41) was first presented by Kampé de Fériet (38) in 1939. Applying the Fourier transform relation between $R_L(\xi)$ and $F_L(f)$ as in Eqn (6-15), Batchelor shows that Eqn (6-41) can be rewritten as

$$\sigma_x^2 = \overline{u'^2} \int_0^\infty F_{L_u}(f)\, \frac{(1-\cos 2\pi f t)}{2\pi^2 f^2}\, df. \tag{6-42}$$

From mathematical analysis of this equation (see Hinze (39), we conclude that for short diffusion times particle velocity fluctuations of all frequencies contribute to the diffusion process, whereas for large values of t a particle's diffusion is dominated by the low frequency fluctuations (large eddies).

Batchelor also derived a relationship between the statistical properties of the dispersion and the eddy diffusivity of the gradient transfer approach. Assuming the probability distribution of the particle displacements was Gaussian, he showed that for the case of an instantaneous point source release in an infinite medium the diffusion process was governed by a differential equation of the form shown in Eqn (6-25) with the diffusivities given by

$$K_x(t) = \frac{1}{2}\frac{d\sigma_x^2}{dt} = \overline{u'^2}\int_0^t R_{L_u}(\xi)\, d\xi. \qquad (6\text{-}43)$$

Using the relations of Eqns (6-39) and (6-40), we see that the turbulent diffusivity should start at zero, increase linearly with time and finally approach a constant value given by $u'^2 \tau_{L_u}$.

Solutions Using the Statistical Approach.

Sutton, while working on problems related to chemical warfare at the Chemical Defense Experimental Station, Porton, Wiltshire, developed solutions to the diffusion problem which form the basis of much of the more recent work employing the statistical approach. In his earliest work, Sutton (40) chose the power law form

$$R_L(\xi) = \left(\frac{a}{\overline{u}\xi}\right)^n \qquad (6\text{-}44)$$

for the Lagrangian correlation coefficient, where a and n are constants determined by comparison with experimental data.

In a later paper (41) the form of Eqn (6-44) was replaced by

$$R_{L_u}(\xi) = \left(\frac{\nu}{\nu+\overline{u'^2}\xi}\right)^n, \qquad (6\text{-}45a)$$

$$R_{L_v}(\xi) = \left(\frac{\nu}{\nu+\overline{v'^2}\xi}\right)^n, \qquad (6\text{-}45b)$$

and

$$R_{L_w}(\xi) = \left(\frac{\nu}{\nu+\overline{w'^2}\xi}\right)^n, \qquad (6\text{-}45c)$$

where ν is the kinematic viscosity of air and the exponent n is determined by matching the observed wind profile to the power law

$$\bar{u} = \bar{u}_1 \left(\frac{z}{z_1}\right)^{\frac{n}{2-n}} \quad , \quad 0 \leq n \leq 1 \ . \tag{6-46}$$

Sutton obtained Eqn (6-46) using von Karman's mixing length hypothesis and assuming similarity between vertical momentum transport and diffusion. Eqn (6-45) was considered valid for neutrally stable atmospheric conditions over smooth terrain. A value of n = 1/4, which corresponds to a 1/7 power law wind profile, was selected as the best fit to experimental data. Sutton (1) later extended the applicability of Eqn (6-45) to fully rough surfaces by replacing the kinematic viscosity by the macroviscosity u*k, where u* is the friction velocity and k the roughness height. (k can be interpreted as a roughness length characterizing the surface, although by definition it is the height at which the mean wind $\bar{u}$ goes to zero. Values of k range from 10^{-4} m for smooth ice to 1 m for forested or city areas (see Pasquill (3).) We should note that Sutton's solutions considered the wind invariant with height, although the power law form, Eqn (6-46), was used to determine n.

Substituting Eqn (6-45) into Eqn (6-37) and integrating, Sutton obtained

$$\sigma_x^2 = \frac{1}{2} C_x^2 \, (\bar{u}t)^{2-n}, \tag{6-47}$$

where C_x is a constant defined by

$$C_x^2 = \frac{4\nu^n}{(1-n)(2-n)\bar{u}^n} \left(\frac{\overline{u'^2}}{\bar{u}^2}\right)^{1-n} \tag{6-48}$$

with similar expressions defined for σ_y and σ_z.

Assuming a Gaussian concentration distribution in all three coordinate directions and a constant mean wind, Sutton derived a function describing the diffusion of particles released from a ground-level, instantaneous point source located at the origin which satisfied:

1. the boundary conditions

$$\begin{aligned} t &\to 0 \qquad \bar{c} \to 0 \text{ except at the origin} \\ t &\to \infty \qquad \bar{c} \to 0 \end{aligned} \tag{6-49}$$

2. the continuity relation

$$\int_{-\infty}^{\infty} \bar{c}(x,y,z,t)\, dx\, dy\, dz = Q \qquad (6\text{-}50)$$

3. Eqn (6-47) with variances calculated using Eqn (6-38).

By performing appropriate integrations, the following solutions were obtained for ground-level continuous point and infinite crosswind line sources. Continuous Point Source:

$$\bar{c}(x,y,z) = \frac{Q}{\pi C_y C_z \bar{u} x^{2-n}} \exp\left\{\frac{-1}{x^{2-n}}\left(\frac{y^2}{C_y{}^2} + \frac{z^2}{C_z{}^2}\right)\right\} \qquad (6\text{-}51)$$

Continuous Infinite Crosswind Line Source:

$$\bar{c}(x,z) = \frac{Q}{\sqrt{\pi}\, C_z \bar{u} x^{1-n/2}} \exp\left\{\frac{-z^2}{C_z{}^2 x^{2-n}}\right\} \qquad (6\text{-}52)$$

For the continuous point source, the continuity condition used was

$$\int_{-\infty}^{\infty} \bar{u}\, \bar{c}(x,y,z)\, dy\, dz = Q. \qquad (6\text{-}53)$$

Sutton points out that his solutions are not unique in that distributions of concentration other than the Gaussian form could have been used and that, in fact, any distribution of the form $\bar{c} \alpha \exp(-y^p - z^q)$ with $p,q>1$ would work equally well. Using this fact, Sutton modified his solution to the infinite line source problem by changing the exponent of z to 2/(2-n) in an attempt to more accurately take into account the variation of wind with height.

In a third paper, Sutton (42) extended his previous work on the continuous point source problem to treat the case of an elevated source. Imposing the conditions of complete reflection of the particles at the ground, which implied

$$\int_0^{\infty}\int_{-\infty}^{\infty} \bar{u}\, \bar{c}(x,y,z)\, dy\, dz = Q \qquad (6\text{-}54)$$

and using the previously derived solution, Eqn (6-51), as a starting point the required solution was obtained by employing the method of images. Thus,

$$\bar{c}(x,y,z) = \frac{Q}{\pi C_y C_z \bar{u} x^{2-n}} \exp\left\{\frac{-y^2}{C_y x^{2-n}}\right\}\left[\exp\left\{\frac{-(z-h)^2}{C_z{}^2 x^{2-n}}\right\} + \exp\left\{\frac{-(z+h)^2}{C_z{}^2 x^{2-n}}\right\}\right], \qquad (6\text{-}55)$$

where the first exponential term in the large bracket represents the diffusion of particles released at a height h and the second is the image term which describes diffusion of particles released from a height -h.

Sutton's work, particularly Eqn. (6-55), is of extreme importance because it forms the basis of what is now called the Gaussian plume theory. To obtain the Gaussian plume solutions from Sutton's results, we simply express his solution in terms of the particles standard deviation functions. Thus, in Eqn (6-55) we make the substitutions from Eqn (6-47)

$$\sigma_y^2 = \frac{1}{2} C_y^2 x^{2-n}, \tag{6-56a}$$

and

$$\sigma_z^2 = \frac{1}{2} C_z^2 x^{2-n}, \tag{6-56b}$$

and obtain

$$\bar{c}(x,y,z) = \frac{Q}{2\pi \bar{u} \sigma_y \sigma_z} \exp\left\{\frac{-y^2}{2\sigma_y^2}\right\} \left[\exp\left\{\frac{-(z-h)^2}{2\sigma_z^2}\right\} + \exp\left\{\frac{-(z+h)^2}{2\sigma_z^2}\right\}\right] . \tag{6-57}$$

Using Eqn (6-57), particle concentrations can be calculated for more general cases in which the functional form of the standard deviation functions are not limited to those of Eqn (6-56).

Baron, Gerhard and Johnstone (43) modified Sutton's point source solution (Eqn (6-55)) to take into account particle settling and deposition. Deposition was modeled by multiplying the strength of the image term (the second term in square brackets) by a factor α_o which was a function of the fraction deposited at any point downwind of the source. However, no explicit solution was obtained.

Later, Csanady (44) developed a closed-form solution for the image multiplier α_o (at ground level) and thus obtained a solution based on Sutton's point source equation which included both settling and deposition. The fractional multiplier $\alpha_o(x)$ was adjusted such that, at ground level, the boundary condition

$$j(x,y) = w_s \bar{c}(x,y,o) \tag{6-58}$$

(the three-dimensional form of Eqn (6-28)) was satisfied.

Settling was accounted for by employing what is now called the "sinking plume assumption." Here, the mean motion of the particles is taken to be in the direction given by the vectoral sum of the mean wind $\bar{u}$ and the constant settling velocity w_s. Compensation for settling is then made by replacing the source height h with $h-w_s x/\bar{u}$ in Eqn (6-57).

In a second paper, Csanady (45) extended his earlier work to include (a) a release height which was a function of downwind distance, as a means of modeling thermal rise, and (b) to allow for arbitrary forms of the particle standard deviation functions. The ground-level concentration distribution for a constant source height given by Csanady is

$$\bar{c}(x,y,o) = \frac{Q(1+\alpha_o(x))}{2\pi\bar{u}\sigma_y\sigma_z} \exp\left\{\frac{-y^2}{2\sigma_y^2}\right\} \exp\left\{\frac{-(h-w_s x/\bar{u})^2}{2\sigma_z^2}\right\} \qquad (6\text{-}59)$$

where

$$\alpha_o(x) = 1 - \frac{2w_s}{2w_s + \frac{(\bar{u}h-\bar{w}_s x)}{\sigma_z}\frac{d\sigma_z}{dz}} \qquad (6\text{-}60)$$

The deposition flux was then calculated from the ground-level concentration using Eqn (6-58). Csanady discusses the validity of the substitution $h \to h-w_s x/\bar{u}$ as a means of accounting for settling and also points out that the introduction of the multiplier α_o can interfere with conservation of mass and cause total deposition to exceed emission. He notes that his solution is only an approximate solution to the advective-diffusion equation with the diffusivities taken as suggested by Batchelor (37) (Eqn (6-43)).

Overcamp (46) extended Csanady's solution to cover the case in which the deposition velocity does not equal the settling velocity. Thus, the boundary condition at the ground was no longer given by Eqn (6-58) but was

$$j(x,y) = w_d\, \bar{c}(x,y,o) \quad . \qquad (6\text{-}61)$$

Overcamp obtained a solution with the ground-level concentration given by Eqn (6-59) but with

$$\alpha_o(x) = 1 - \frac{2w_d}{w_s+w_d+\frac{(\bar{u}h-w_s x)}{\sigma_z}\frac{d\sigma_z}{dx}} \qquad (6\text{-}62)$$

which reduces to Eqn (6-60) for the case $w_d = w_s$.

Chamberlain (47) presented a technique, known as the source depletion method, which extended Sutton's solutions to include deposition. This approach reduces the source strength Q in the Gaussian plume formula to account for deposition yielding an effective source strength Q'(x) which decreases with increasing downwind distance. The deposition flux is calculated using Eqn (6-61). Van der Hoven (48) points out that a major drawback of the source depletion method is that it retains the Gaussian shape of the concentration profile despite deposition at the ground. Thus, the effect of ground-level deposition is instantaneously distributed throughout the entire vertical extent of the concentration profile.

Horst (49) developed a technique, called the surface depletion method, in which deposition was represented as a particle sink at the point of deposition. The starting point for the analysis was the standard Gaussian plume solution to the continuous point source problem for nondepositing particles (i.e., reflecting boundary condition solution) Eqn (6-57). The concentration distribution at any point was then calculated as the sum of the nondepositing solution and the diffusion from all of the upwind surface sinks which accounted for deposition. Horst's solution satisfied the boundary condition of Eqn (6-61) and the advective-diffusion equation when the diffusivities were given by Eqn (6-43).

Two final solutions based on the sinking Gaussian plume model are those of Schrecker and Slinn (see Policastro et al. (50)). In his analysis, Schrecker uses only the real source of the sinking Gaussian plume model. Thus,

$$\bar{c}(x,y,z) = \frac{Q}{2\pi\bar{u}\sigma_y\sigma_z} \exp\left\{\frac{-y^2}{2\sigma_y^2}\right\} \exp\left\{\frac{-(z-h+w_s x/\bar{u})^2}{2\sigma_z^2}\right\}. \qquad (6\text{-}63)$$

The net deposition rate J(x) is determined by calculating the total mass of the particles "below the ground plane" as shown in Fig 6-3. Performing the integration we obtain

$$J(x) = \frac{Q}{2}\left[1 - \text{erf}\left\{\frac{h-w_s x/\bar{u}}{\sqrt{2}\sigma_z}\right\}\right] \qquad (6\text{-}64)$$

The deposition flux j is obtained by differentiating Eqn (6-64) with respect to x.

Slinn developed a model which was intended to provide an upper bound on the distance to deposition. The ground-level concentration used by Slinn is given by

$$\bar{c}(x,y,o) = \frac{1}{4\pi\bar{u}\sigma_y\sigma_z} \exp\left\{\frac{-y^2}{2\sigma_y^2}\right\}\left[\exp\left\{\frac{-(h-w_s x/\bar{u})^2}{2\sigma_z^2}\right\} + \exp\left\{\frac{-(h+w_s x/\bar{u})^2}{2\sigma_z^2}\right\}\right]. \qquad (6\text{-}65)$$

Deposition is calculated using Eqn (6-61).

SCOPE OF PRESENT WORK

Despite a great deal of work on the atmospheric diffusion problem, very few of the presently available solutions can treat the situation in which both particle settling and deposition occur. Analytic solutions of the gradient transfer approach are limited by the mathematical complexities that arise when the diffusivity and settling velocity are anything but simple functions. All solutions based on the gradient transfer hypothesis, whether analytical or numerical, have limited applicability in that the basic concept of the turbulent flux being related to the mean concentration gradient is physically realistic only when the scale of the transporting mechanism is small compared to the spatial scale of the distribution. In addition to the obvious problem of determining the form of the Lagrangian correlation coefficient, the statistically based solutions commonly fail to conserve mass because the functional form of the concentration distribution is selected rather arbitrarily (only the second moments of the distribution are specified by Taylor's result) and a form which is mass conserving and satisfies the appropriate boundary conditions is not readily available.

Due to the shortcomings of both the gradient transfer and statistical approaches, we have developed a technique which combines the mass conserving property of the gradient transfer solutions with the probabilistic appeal of the statistical approach. The basis of our model is the fact that turbulent diffusion may be treated as a stochastic process and therefore can be accurately simulated by a Lagrangian probabilistic or, equivalently, a Monte Carlo model. The model determines deposition by tracking a large number of particles from release to deposition. The particle's lifetime is divided into finite intervals or time steps. At each time step, the particle's motion is further broken into deterministic and stochastic components. Advection by the mean wind and gravitational settling are carried out deterministically with the stochastic component simulating the random movement of the particle caused by turbulence.

Advantages of this modeling technique are: (a) realistic functional forms of the mean wind and settling velocity can be used, (b) mass conservation is inherent, (c) the statistical properties of the turbulent velocity field can be used when determining the stochastic step size and (d) solutions of either the gradient transfer or statistical approach can be readily obtained.

In as much as the prime objective of this work is to uncover the key patterns of deposition behavior, we shall for the sake of simplicity restrict our analysis in the remainder of this chapter to the crosswind-integrated problem. This simplification, which reduces the problem from three to two (x and z) dimensions, is possible because diffusion in the lateral direction is not affected by settling, deposition or the prescence of the ground. Moreover, the approach described herein is easily extended to the three-dimensonal case, if desired.

THE MONTE CARLO MODEL

This chapter describes the formulation of our Monte Carlo simulation of turbulent atmospheric transport with settling, evaporation and deposition. The model can, in principle, handle any arbitrary set of ambient conditions, include any drop or particle model for evaporation and incorporate any of the available turbulent transport hypotheses. However, we shall present the formulation here in terms of simple yet physically sound conceptualizations in order to gain insight into the problem and to better identify major regimes of deposition behavior.

Specific Modeling Considerations

The Mean Wind.

The results of numerous studies of the wind profile in the atmosphere indicate that the mean wind $\bar{u}$ can be taken as a function of only the vertical coordinate z. For neutral atmospheric conditions within the constant shear stress layer, the generally accepted form for $\bar{u}(z)$ is the logarithmic-law

$$\bar{u}(z) = \frac{u^*}{\kappa} \ln\left(\frac{z}{k}\right), \tag{6-66}$$

where κ is von Karmon's constant, usually taken to be 0.4, and κ is roughness length. Panofsky (51) and, more recently, Panofsky and Peterson (52) have suggested that the average depth of the constant shear layer in which the mean wind profile follows the logarithmic-law can be taken as approximately 100 m.

Although the logarithmic-law of Eqn (6-66) is considered the most appropriate formula for neutrally stable atmospheric conditions, many investigators (e.g., Sverdrup (53), Frost (54), Deacon (55) and Slade (56) have shown that the wind profile under most atmospheric stability conditions and to heights of 400 meters can be accurately represented by a power-law of the form

$$\bar{u}(z) = \bar{u}_o\left(\frac{z}{z_o}\right)^m, \tag{6-67}$$

where $\bar{u}_o$ is the mean wind speed at the height z_o. The power-law exponent m is a function of both atmospheric stability and surface roughness. Irwin (57) gives values of the exponent ranging from 0.05 for unstable atmospheric conditions (Pasquill stability class A) and a roughness length of 0.01 meters to 0.69 for stable atmospheric conditions (class F) and a roughness length of 3.00 meters. Average values of the exponent for neutral conditions suggested by Counihan (4) are 0.143 for rural areas, 0.22 for suburban areas and 0.28 for urban areas.

Because the wind profile of Eqn (6-67) has found considerable acceptance in the literature, we shall adopt it for our use.

Particle Settling.

The problem of turbulent transport is considerably simplified if the following assumptions can be reasonably made.

1. The fluctuating velocity of a particle of the size of principal interest is essentially that of the surrounding fluid; damping of fluctuations due to particle inertia is very small.

2. The difference between the settling velocity of an evaporating drop and that of a nonevaporating particle of equal mass and size is negligible.

The convenience afforded by these assumptions is the ability to write the particle velocity as the vector sum of the instantaneous settling and local fluid velocities.

To fully justify the above assumptions requires a detailed analysis of the equations of motion of the particle, a study beyond the focus of the present work. We can, however, intuitively justify the assumptions on the basis of the following arguments of scale.

Inertial effects are obviously greatest for the largest drops. Although these large drops (over 1000 μm diameter) do not respond to the fluid velocity as a first order system, a definite relaxation behavior is apparent. The "time constant" of this relaxation is approximately given by w_s/g. Even for a particle of 5000 μm diameter, the inertial time constant is less than 1 second which is well below the 100 second Lagrangian time scale of atmospheric turbulence. Our criterion then for accepting the first assumption is

$$g\tau_{L_w}/w_s >> 1, \tag{6-68}$$

which is satisfied for all drop sizes of practical interest. For a more detailed discussion of heavy particle diffusion see Yudine (58) or Csanady (59).

The amount by which the actual particle velocity lags the settling velocity of a nonevaporating particle of equal mass and diameter is determined by the ratio

$$\frac{(dw_s/dt)_{ev}}{g}, \tag{6-69}$$

where $(dw_s/dt)_{ev}$ is the rate at which the particle settling velocity (as a function of drop size alone) is changing due to evaporation. For all drop sizes of practical interest and for all ambient conditions characteristic of the atmosphere, the above ratio is well below 5×10^{-3}. Thus, the particle velocity can be assumed to depend only on the instantaneous particle size.

Evaporation

The particle settling velocity must be considered a function of time to accurately model the diffusion of evaporating drift particles. The Monte Carlo model itself does not place any restrictions on how the settling velocity varies with time. In fact, a droplet evaporation model could be used in conjunction with the Monte Carlo model to provide a very accurate treatment of particle settling. However, in accordance with the primary objective of this work we wish to employ a simple, yet physically realistic, functional representation for the settling velocity. Thus, for modeling purposes, we have selected the quadratic form

$$w_s(t) = \begin{cases} a_1 + a_2 t + a_3 t^2, & t < t_{evap} \quad (6\text{-}70a) \\ w_{s,evap}, & t \geq t_{evap} \quad (6\text{-}70b) \end{cases}$$

where the constants a_1, a_2 and a_3 are determined by imposing the three conditions:

$$w_s(o) = w_{s,init}, \quad (6\text{-}71a)$$

$$w_s(t_{evap}) = w_{s,evap} \quad (6\text{-}71b)$$

and

$$\int_0^{t_{\ell,det}} w_s(t)\, dt = h. \quad (6\text{-}71c)$$

In Eqns (6-70) and (6-71), $w_{s,init}$ is the particle's initial settling velocity, $w_{s,evap}$ is its settling velocity after evaporation, t_{evap} is the time at which the particle completes evaporation and $t_{\ell,det}$ is the lifetime of a particle which follows a deterministic or simple ballistic trajectory. Note that for a given set of ambient conditions, $w_{s,evap}$ is the asymptotic settling velocity the particle would attain if the release height was such that the final evaporated state (either a dry particle or a solution drop in equilibrium with the ambient) could be reached. For solute containing drops, $w_{s,evap}$ is a positive non-zero quantity. For pure liquid drops, $w_{s,evap}$ is zero.

The quadratic form is supported by theoretical studies of droplet evaporation For example, Fuchs (60) has shown that for pure liquid drops if drop diameter squared is plotted against evaporation time the result is a straight line of constant slope.

For small Reynold's numbers, when Stoke's Law applies, the settling velocity is proportional to d^2. Consequently, in this case for pure liquid drops the settling velocity is a linear function of time and Eqn (6-70) is exact with $a_3 = 0$. Moreover, a numerical analysis of the evaporation problem in the more general situation of solute containing drops and arbitrary Reynold's number shows that the quadratic form is a good approximation to the true behavior.

Turbulence

As seen in REVIEW OF PREVIOUS WORK, alternative turbulence models lead to completely different approaches to the entire atmospheric diffusion-deposition problem. The eddy diffusivity model leads to the gradient transfer analysis and the necessary solution of a partial differential equation which expresses conservation of mass. Modeling turbulence along the lines of Taylor's hypothesis, i.e., using the Lagrangian time correlation to obtain the variances of the particle distribution, the so-called Gaussian plume dispersion parameters, leads to the statistical approach. In this method, solutions to particular problems are developed from the knowledge of the second moments of the particle concentration distribution, appropriate boundary conditions and a continuity relation.

Efforts have been made to reconcile these two alternatives. For example, Batchelor's (37) result, Eqn (6-43), relates the diffusivity to the variances of the particle distribution for the case of an instantaneous point source release of non-settling particles in an infinite medium.

For the case of a continuous point source in a turbulence field with a constant mean wind, Eqn (6-43) with the substitution $t = x/\bar{u}$ becomes

$$K_z(x) = \frac{\bar{u}}{2} \frac{d\sigma_z^2}{dx}. \qquad (6\text{-}72)$$

The generality of this result, however, for more realistic situations in which particle settling or the presence of the ground must be accounted for is unknown.

Taylor (61) points out a rather serious problem for cases in which the diffusivity is taken as a function of diffusion time or downwind distance. Consider, for example, a situation in which two point sources, one located upstream of the other, are continuously emitting particles into the atmosphere. By the linearity of the diffusion problem the combined solution can be obtained by simple superposition of the separate point source solutions. The difficulty arises in that at points where the individual distributions overlap, two different diffusivities must be

applied at the same time and same point in space. Therefore, we see that the indiscriminate use of a diffusivity which varies as time or distance downwind can lead to anomalous results. On the other hand, the constant asymptotic value of the diffusivity for diffusion times which are large compared to the Lagrangian time scale, i.e., $K_z(t>\tau_{L_w}) = w'^2\tau_{L_w}$, is a physically meaningful property of the turbulence field.

In practice, the most common turbulence modeling approach is the use of Gaussian plume dispersion parameters defined as functions of x, the distance downwind from a point source, parameterized by routinely available meteorlogical data such as insolation, cloud cover, surface mean wind speed and the extent of the fluctuations in the wind direction. Investigators that have developed such stability classification schemes and presented graphs of σ_z versus x include Pasquill (3,62,63), Gifford (64,65), Cramer (66,67), Briggs (68), Calder (69) and Singer and Smith (70,71). The work of Pasquill and Gifford has found the greatest recognition and acceptance and hence, many times the charts relating the dispersion parameters to downwind distance are called Pasquill-Gifford curves. As an example of a dispersion parameter model, Table 6-2 shows the Pasquill (62) stability classification scheme and Figure 6-4 gives the corresponding dispersion parameters as a function of downwind distance as presented in Turner (72).

Reasons for the formulation of such curves include: the general acceptance of the Gaussian plume formula as a means of estimating particle concentrations, the need to compensate for the inadequacies of the statistical theory which, being based on a homogeneous, stationary turbulence field, breaks down in atmospheric applications (compensation is made by adjusting the functional form of the dispersion parameters and therefore, typical Pasquill-Gifford curves do not even possess the theoretically predicted asymptotic behaviors) and perhaps, the relative ease of experimentally obtaining the dispersion parameter as compared to the Lagrangian correlation coefficient or eddy diffusivity.

The principal inadequacies in the use of the Gaussian dispersion parameters as a means of modeling turbulence are a consequence of the dissimilarities between the physical situations to be modeled and the experiments from which they were derived. Included among the deficiencies are: (a) most of the experimental studies from which the dispersion parameters were calculated were of low level releases, (b) the studies involved particles which behaved as gases (no settling), (c) calculations performed upon the experimental data to obtain the dispersion parameters assumed a constant mean wind, (d) most experiments were over rather

smooth (k ≃ 3 cm), level terrain, (e) the curves for large downwind distances are extrapolations and (f) the estimates of σ_z apply only to release times greater than the time required for the vertical particle distribution to respond to the entire spectrum of the vertical component of turbulence. Pasquill (63) suggests that for the dispersion parameters presented in Fig 6-4 this limiting sampling time be taken as 10 min for source heights greater than or equal to 100 m and be given by (h/10) min for h less than 100 m. Adjustments to the curves, in the form of correction factors, to compensate for some of the other points listed above are also given by Pasquill.

Since it is not the purpose of this study to develop a turbulence model, for simplicity and to make model comparisons possible, we shall use the Gaussian dispersion parameters as a means of modeling turbulence despite their known shortcomings. Specifically, we shall use power-law fits of the revised σ_z curves developed by Smith (see Pasquill (3,63)). Thus, we have

$$\sigma_z = ax^s, \quad 0.5 \leq s \leq 1 \tag{6-73}$$

where the constants a and s are determined by surface roughness and atmospheric stability. These revised estimates of the dispersion parameter differ from those presented in Fig 6-4 in two respects: (a) adjustments for roughnesses differing from that of grassland (k = 3 cm) have been added and (b) the accelerated growth of σ_z with downwind distance for the more unstable stability classes no longer appears. Values of the coefficient a and power-law index s for a roughness length of 10 cm and three different stability classes are shown in Table 6-3.

It must be emphasized, however, that the Monte Carlo model has the capability of using any turbulence model which can be cast into a statistical framework as discussed below.

The Monte Carlo Equations

The equations governing the movement of a particle are

$$x^{i+1} = x^i + \bar{u}^i_{avg} \, \Delta t \tag{6-74}$$

and

$$z^{i+1} = |z^i + \sigma^i r_{nd}| - w^i_{s_{avg}} \, \Delta t, \tag{6-75}$$

where

$$\bar{u}^i_{avg} = \frac{1}{\Delta t} \int_{t^{i-1}}^{t^i} \bar{u}(z(t)) \, dt \tag{6-76}$$

and

$$w_{s_{avg}}^{i} = \frac{1}{\Delta t}\int_{t^{i-1}}^{t^{i}} w_s(t)\, dt \qquad (6\text{-}77)$$

along with the initial conditions

$$x^0 = 0 \quad \text{at} \quad t^0 = 0 \qquad (6\text{-}78a)$$

and

$$z^0 = h \quad \text{at} \quad t^0 = 0. \qquad (6\text{-}78b)$$

Eqn (6-78) simply implies that the source is located at the point x = 0, z = h. Here, the superscript i indicates a value at time i, x is the position of the particle in the direction of the mean wind, z is the vertical coordinate of the particle and Δt is the time step. The meaning of the remaining terms will be described below.

Eqn (6-74) represents the completely deterministic movement of the particle in the direction of the mean wind. Diffusion has been neglected relative to advection, a realistic assumption since for typical atmospheric conditions $\sqrt{\overline{u'^2}}/\bar{u}$ is on the order of 0.1. Thus, at each time step the particle is simply advected a distance $\bar{u}_{avg}^{i}\ \Delta t$ by the mean wind.

On the other hand, Eqn (6-75) is composed of two distinct components: the deterministic movement $-w_{s,avg}^{i}\ \Delta t$ which is very similar to the advection by the mean wind, representing the particle's settling and the stochastic component $\sigma^i r_{nd}$ which models the random movement of the particles caused by turbulence. For our simulations, we chose the r_{nd} from a population of normally distributed random numbers with mean zero and standard deviation one, although random numbers from any other distribution could have been used just as easily. This choice was made because of both the probabilistic arguments based on the Central Limit Theorem and the experimental evidence indicating that the fluctuating velocity w' is distributed in a Gaussian manner. Both the partial and total correlations between the random numbers used at different "time steps" were zero, so that each random displacement was independent. This independence, however, does not limit the applicability of our method since it can be shown that random movements with any specified correlation, e.g., Taylor's (36) Markov process, can be attained using independent random variables by appropriately selecting the σ^i.

σ^i is the standard deviation of the particle's stochastic movement at time i and thus can be considered a measure of the diffusing power of the turbulence at time step i. The specific form given to σ^i is dependent upon the turbulence model

employed. Thus, the only requirement placed on the turbulence model in the Monte Carlo simulation is that an equation in some form, algebraic, differential, or integral, can be written for σ^i. Here, we shall show how σ^i can be related to the statistical properties of the turbulence through Taylor's result, the eddy diffusivity and the Gaussian plume dispersion parameters.

Taylor's result, Eqn (6-36), which has been rewritten here for convenience, relates the variance of the particle distribution to the root mean square of the fluctuating velocity and the Lagrangian time correlation.

$$\sigma_z^2(t) = \overline{2w'^2} \int_o^t \int_o^T R_{L_w}(\xi)\, d\xi\, dt \tag{6-36}$$

Since the random numbers are all independent,

$$\sigma_z^2 = \sum_{i=1}^{N} (\sigma^i)^2, \tag{6-79}$$

where $N=t/\Delta t$ is the number of steps. Combining this result with Eqn (6-36) we obtain

$$(\sigma^i)^2 = \overline{2w'^2} \int_{t^{i-1}}^{t^i} \int_o^T R_{L_w}(\xi)\, d\xi\, dT \tag{6-80}$$

which can be rewritten as

$$(\sigma^i)^2 = \overline{2w'^2}\, \tau_{L_w} \int_{t^{i-1}}^{t^i} r(T)\, dT; \tag{6-81}$$

where

$$r(t) = \frac{1}{\tau_{L_w}} \int_o^t R_{L_w}(\xi)\, d\xi. \tag{6-82}$$

Expressing σ^i in this form shows clearly that as t becomes large, σ^i approaches a constant asymptotic value given by $2w'^2\, \tau_{L_w}\, \Delta t$. The function r(t) corresponding to the correlation coefficient presented in Fig 6-2 is shown in Fig. 6-5.

Given an eddy diffusivity as a function of downwind distance, as suggested by Batchelor's result for the continuous point source, the appropriate equation relating σ^i to the diffusivity is

$$(\sigma^i)^2 = 2\, K_{z,avg}^i\, \Delta t, \tag{6-83}$$

where

$$K_{z,avg}^i = \frac{1}{\Delta t} \int_{t^{i-1}}^{t^i} K_z(x(t))\, dt. \tag{6-84}$$

When using the Gaussian plume dispersion parameters as a means of modeling turbulence, σ^i takes the form

$$(\sigma^i)^2 = \sigma_z^2(x(t^i)) - \sigma_z^2(x(t^{i-1})). \tag{6-85}$$

Returning to the Monte Carlo equations, we next point out that the absolute value in Eqn (6-75) is necessary to simulate the no-turbulent-flux boundary condition at the ground,

$$\frac{\partial \bar{c}}{\partial z} = 0 \quad \text{at} \quad z = 0. \tag{6-86}$$

This boundary condition was chosen over the deposition velocity form as given in Eqn (6-31) to avoid the mathematical difficulties and anomalous behavior associated with the deposition form. Like the turbulence treatment itself, many unresolved issues surround the treatment of turbulent deposition. Both of these matters will be addressed more fully in future work. In the Monte Carlo simulation, Eqn (6-86) is invoked by reflecting any particle that would strike or move through the ground on a stochastic step back into the diffusing field.

Summarizing, we have shown that, in the Monte Carlo model, the turbulent diffusion process is simulated using Eqns (6-74) and (6-75) and either Eqn (6-81) when a Lagrangian time correlation coefficient is specified, as in the statistical approach, Eqn (6-83) when an eddy diffusivity is given, as in the gradient transfer solutions or Eqn (6-85) when employing the Gaussian plume dispersion parameters.

Nondimensionalization of the Diffusion Problem

We seek a nondimensionalization of the problem with a minimum number of parameters. Analysis of the Monte Carlo equations, Eqns (6-74) and (6-75) yields the following

$$x_* = \frac{T_{sc}x}{\bar{u}_r h^2} \quad , \quad z_* = \frac{z}{h} \quad , \quad t_* = \frac{T_{sc}t}{h^2} \quad , \quad \sigma_* = \frac{\sigma}{h} \quad ,$$

$$h_* = \frac{w_{s_c} h}{T_{sc}} \quad , \quad \alpha = \frac{t_{evap}}{t_{\ell,det}} \quad , \quad \beta = \frac{w_{s_{init}}}{w_{s_c}} \quad , \quad \gamma = \frac{w_{s_{evap}}}{w_{s_c}} \quad , \tag{6-87}$$

$$\bar{u}_*(z_*) = \frac{\bar{u}(z)}{\bar{u}_r} \quad , \quad w_{s_*}(t_*) = \frac{w_s(t)}{w_{s_c}} \quad , \quad c_* = \frac{c\bar{u}_r h}{Q} \quad , \text{ and } j_* = \frac{j\bar{u}_r h}{T_{sc}Q} \quad ,$$

where $\bar{u}_r$ is a reference value of the mean wind, T_{sc} is a turbulence scale whose specific form depends on the turbulence model employed, w_{s_c} is a characteristic settling velocity defined by

$$w_{sc} = \frac{h}{t_{\ell,det}} \tag{6-88}$$

and j is the deposition flux .

The advantage in using a settling velocity scale as defined in Eqn (6-88) is that w_{sc} is weighted according to the fraction of the total particle lifetime spent evaporating. Thus, as $t_{evap}/t_{\ell,det}$ approaches zero (small particles), w_{sc} approaches $w_{s,evap}$ and for the case of a constant settling velocity ($\beta = 1$) or for cases in which $t_{evap}/t_{\ell,det}$ approaches infinity (large particles), w_{sc} approaches $w_{s,init}$.

Dividing Eqn (6-70) by w_{s_c} and imposing the conditions given in Eqn (6-71) yields the following expression for the nondimensional settling velocity w_{s_*}.

$$w_{s_*}(\eta) = \begin{cases} \beta + b_1\eta + b_2\eta^2, & \eta<\alpha \quad (6\text{-}89a) \\ \gamma, & \eta\geq\alpha \quad (6\text{-}89b) \end{cases}$$

where $\eta=h_*t_*=t/t_{\ell,det}$. The constants b_1 and b_2 are given by

$\alpha<1$:

$$b_1 = \frac{-4\alpha(\beta-\gamma) + 6(1-\gamma)}{\alpha^2} \tag{6-90a}$$

$$b_2 = \frac{3\alpha(\beta-\gamma) - 6(1-\gamma)}{\alpha^3} \tag{6-90b}$$

$\alpha\geq 1$:

$$b_1 = \frac{2(\beta-\gamma) - 6\alpha^2(\beta-1)}{\alpha(3\alpha-2)} \tag{6-91a}$$

$$b_2 = \frac{6\alpha(\beta-1) - 3(\beta-\gamma)}{\alpha(3\alpha-2)} \tag{6-91b}$$

The particular expressions for T_{sc} corresponding to each of the turbulence models discussed in Turbulence are shown in Table 6-4 along with the appropriate expression for σ^i.

Dividing Eqn (6-67) by $\bar{u}_r$, we obtain the nondimensional wind velocity profile. Thus,

$$\bar{u}_*(z_*) = z_*^m, \tag{6-92}$$

where $\bar{u}_r$ is given by

$$\bar{u}_r = \frac{\bar{u}_o}{z_{o*}^m}. \tag{6-93}$$

The nondimensional dispersion parameter σ_{z_*} is obtained by dividing Eqn (6-73) by h. Thus,

$$\sigma_{z_*} = z_*^s, \tag{6-94}$$

where

$$T_{sc} = \left(\frac{a}{h}\right)^{\frac{1}{s}} \bar{u}_r h^2 \tag{6-95}$$

which implies the reference value x_r has been taken as

$$x_r = \left(\frac{1}{s}\right)^{\frac{1}{2s-1}} \left(\frac{h}{a}\right)^{\frac{1}{s}} . \tag{6-96}$$

Substitution of the nondimensional variables into the Monte Carlo equations gives

$$x_*^{i+1} = x_*^i + \bar{u}_*^i, \text{ avg} \tag{6-97}$$

and

$$z_*^{i+1} = |z_*^i + \sigma_*^i r_{nd}| - h_* w_{s_*,\text{avg}}^i \Delta t_*, \tag{6-98}$$

where

$$\bar{u}_*^i,\text{avg} = \frac{1}{\Delta t_*}\int_{t_*^{i-1}}^{t_*^i} \bar{u}_* (z_*(t_*))\, dt_* \tag{6-99}$$

and

$$w_{s_*,\text{avg}}^i = \frac{1}{\Delta t_*}\int_{t_*^{i-1}}^{t_*^i} w_{s_*}(t_*)\, dt_* . \tag{6-100}$$

The dimensionless initial conditions are

$$x_*^0 = 0 \quad \text{at} \quad t_*^0 = 0 \tag{6-101a}$$

and

$$z_*^0 = 1 \quad \text{at} \quad t_*^0 = 0. \tag{6-101b}$$

From Eqns (6-97) and (6-98) we conclude that

$$C_* = C_*(x_*, z_*, t_*; h_*, s, \alpha, \beta, \gamma, m) \tag{6-102a}$$

and

$$J_* = J_*(x_*, z_*, t_*; h_* s, \alpha, \beta, \gamma, m). \tag{6-102b}$$

Thus, in the most general situations, the diffusion problem is characterized by six parameters, namely, h_*, s, α, β, γ, and m. However, usually only two or three of these parameters are needed to characterize a problem; in many cases, only the parameters h_* and s are significant.

To the characterizing parameters we attach the following physical interpretations.

a. h_* relates the stability of the atmosphere to the rate of settling and deposition and can be thought of as the ratio of the characteristic settling

velocity. w_s to the mean turbulent transport velocity T_{sc}/h. In the case of a diffusing gas or for extremely unstable atmospheric conditions h_* approaches zero. Conversely, for large particles or very stable atmospheric conditions h_* approaches infinity. For the diffusion of drift particles under typical atmospheric conditions, h_* falls into the range $0 \leq h_* \leq 1000$.

b. α is the ratio of the total evaporation time to the lifetime of a drop following a deterministic trajectory. For very large drops, α approaches infinity whereas α goes to zero for small drops.

c. β is ratio of the particle's initial settling velocity to the characteristic settling velocity. For the case of a constant settling velocity, $\beta = 1$. As α becomes large, β approaches unity.

d. γ is the ratio of the particle's settling velocity after evaporation to the characteristic settling velocity. For cases in which α approaches zero, γ approaches unity.

As a final point, we note that when comparing cases in which different turbulence models have been employed equal values of the parameters s, h_*, α, β, γ and m will generally not yield the same dimensional results because of the different meanings of the various turbulence scales T_{sc}.

General Description of the Computer Program

A Fortran program MONTEC was written to perform the Monte Carlo simulations. All calculations are made using the nondimensional equations presented earlier. The execution time of MONTEC ranges from 3 to 20 seconds on a CYBER 175, depending on the number of particles required and the complexity of the case. Considered below are two important features of the program: (a) the generation of the normally distributed random numbers and (b) the criterion for selecting the size of the time step.

The normally distributed random numbers were generated using an algorithm, called the polar method, due to Box and Muller (73) as outlined in Knuth (74). The method has essentially perfect accuracy, i.e., the statistical properties of the random numbers so obtained are essentially those of the normal distribution. We compared the speed of generation of the polar method to that of a technique developed by Marsaglia, MacLaren and Bray (75), one of the few methods which like the polar method gives essentially perfect accuracy, and found the polar method to be faster in terms of computation time. The latter algorithm requires

machine dependent operations (masking and shifting of bits). Consequently, the polar method has the added advantage of code portability.

Since the Monte Carlo technique is free from numerical instability in the usual sense, the size of the time step is selected to assure that the effect of turbulence is adequately simulated. Thus, the time step Δt_* is calculated using

$$\Delta t_* = 1/(N_{steps} h) \ , \tag{6-103}$$

where N_{step} is usually taken to be 20-100 depending on the value of h_*. Use of Eqn (6-103) guarantees that on average a particle will experience approximately N_{step} stochastic movements before striking the ground. (A particle following a deterministic trajectory is deposited at time $t_* = 1/h_*$ for the case of a constant mean wind.)

MONTEC is supported by a supplemental program PLTMONT which calculates and plots the nondimensional deposition flux $j_*(x_*)$. The basis of the calculation is the continuity relation

$$\int_0^\infty j(x)\, dx = Q \tag{6-104}$$

which in nondimensional form is

$$\int_0^\infty j_*(x_*)\, dx_* = 1. \tag{6-105}$$

Physically, Eqn (6-105) simply states that all particles must eventually be deposited.

The nondimensional net deposition rate $J_*(x_*)$, the ratio of the number of particles deposited to the total number released, is defined as

$$J_*(x_*) = \int_0^{x_*} j_*(\xi_*)\, d\xi_*. \tag{6-106}$$

From Eqns (6-106) and (6-105), we observe that $J_*(x_*)$ is a nondecreasing function of x_* with asymptotic values

$$J_*(0) = 0 \tag{6-107a}$$

and

$$J_*(\infty) = 1. \tag{6-107b}$$

Additionally, differentiating Eqn (6-106) we have

$$j_*(x_*) = \frac{dJ_*}{dx_*}(x_*). \tag{6-107c}$$

Thus, $J_*(x_*)$ can be considered a cumulative distribution function with $j_*(x_*)$ the associated probability density function.

The cumulative distribution function cannot be determined exactly from the Monte Carlo simulation since only a finite number of particles are used. However, an estimate of $J_*(x_*)$ can be obtained from the x_* coordinates of the deposited particles using the relation

$$J_{*est}(x_*) = \frac{(\text{number of particles deposited at distances} \leq x_*)}{N_{rel}} \tag{6-108}$$

where N_{rel} is the number of particles released.

Parzen (76) shows that $J_{*,est}(x_*)$ is essentially a binomially distributed random variable with mean and variance given by

$$E\left\{J_{*,est}(x_*)\right\} = J_*(x_*) \tag{6-109}$$

and

$$Var\left\{J_{*,est}(x_*)\right\} = \frac{J_*(x_*)\,[1-J(x_*)]}{N_{rel}}, \tag{6-110}$$

where E implies an expected value in the usual probability sense. Thus, as anticipated, as the number of particles released becomes large, $J_{*,est}(x_*)$ converges to $J_*(x_*)$.

Numerous techniques exist which can be employed to obtain an estimate of the probability density function (see e.g., Parzen (75), Wegman (77, 78), Whittle (79), Rosenblatt (80). The method we have selected uses a least-squares routine to fit the cumulative distribution function estimate $J_{*,est}(x_*)$ with a function which can be differentiated analytically.

As a measure of the "goodness" of the density function estimate, we used the average square error criterion as defined in Wegman (77),

$$A.S.E. = \frac{1}{N_{dep}} \sum_{i=1}^{N_{dep}} \left[j_{*,est}(x_*) - j_*(x_{*i})\right]^2, \tag{6-111}$$

where N_{dep} is the number of particles deposited. Using this criterion, we compared our method with several techniques discussed in Wegman (78) for a few simple cases in which the exact solution (density) is known. The accuracy of our technique was found to be comparable to the "best" methods cited in Wegman. A very important advantage of our method is that, unlike many of the alternative techniques, no unknown "smoothing" parameters are required.

RESULTS OF THE MONTE CARLO MODEL

The results of the Monte Carlo model presented here are limited to verification of the model by comparison with analytical solutions of the transport problem. Table 6-5 summarizes the various cases to be considered, indicating relevant parameters for each case.

Ongoing work includes:

(a) The comparison of the Monte Carlo model with other models for transport with deposition and constant settling velocity. (Only h_* and s are important.)

(b) The comparison of the Monte Carlo model with other models for transport with deposition and evaporation.

Verification of the Monte Carlo Model

The Monte Carlo turbulence modeling scheme was verified by comparing the Monte Carlo calculated dispersion parameter σ_{z*} with the analytical expression given by Pasquill (3) (Eqn (6-96)). To reproduce the analytical dispersion parameter, the continuous point source problem without settling or deposition must be solved. The analytical solution to this problem which satisfies the zero gradient condition at the ground is simply the Gaussian plume formula (Eqn (6-57)). Thus, by comparing the analytical and Monte Carlo calculated dispersion parameters, we are essentially testing if the Monte Carlo model can reproduce the Gaussian plume solution.

Figure 6-6 shows the analytical and Monte Carlo calculated nondimensional parameter σ_{z*} plotted against downwind distance x_* for the neutrally stable case listed in Table 6-3. The Monte Carlo values were obtained by using the discrete analog of Eqn (6-38c). Agreement between the Monte Carlo and analytical results is good. Similar results were obtained for the other stability classes.

The results of the Monte Carlo model were compared to those of Ermak (19) to test the Monte Carlo treatment of deposition and settling. Recall that Ermak's solution is an exact solution to the gradient transfer equation for the continuous point

source problem with settling and deposition. However, the physically unrealistic assumption that the settling velocity and eddy diffusivity have the same functional form must be made, i.e.

$$w_s(x)/K_2(x) = \text{constant.} \tag{6-112}$$

Since Ermak expresses his solution in terms of the Gaussian plume dispersion parameters σ_y and σ_z by employing Batchelor's result (Eqn (6-72)), Eqn (6-112) becomes

$$w_s(x)/(d\sigma_z^2/dx) = \text{constant.} \tag{6-113}$$

After substituting for σ_z and converting to nondimensional form, we have

$$w_{s*}(x_*) = 2s(h_* x_*)^{2s-1}. \tag{6-114}$$

This form is very restrictive and totally unrepresentative of typical settling velocities, except, for perhaps, the special case of $2 = 1/2$ and $w_{s_*} = 1$, This implies constant settling velocity and constant eddy diffusivity.

Ermak's solution satisfies the deposition velocity boundary condition given in Eqn (6-31). However, by imposing the condition

$$w_d = w_s, \tag{6-116}$$

the solution can be made to satisfy the zero gradient condition used in the Monte Carlo model.

Invoking Eqn (6-116), the nondimensional ground-level concentration for the crosswind-integrated point source as given by Ermak is

$$c_*(x_*,0) = \frac{\sqrt{2}}{\sigma_{z_*}\sqrt{\pi}} \exp\left\{\frac{-(h_*^{2s}\sigma_{z_*}^{2} - 1)^2}{2\sigma_{z_*}^{2}}\right\}$$
$$-h_*^{2s} \exp\left(2h_*^{2s}\right) \operatorname{erfc}\left\{\frac{h_*^{2s}\sigma_{z_*}^{2}+1}{\sqrt{2}\sigma_{z_*}}\right\}. \tag{6-117}$$

For this case, the nondimensional deposition flux is

$$j_*(x_*) = 2s\, h_*^{2s}\, x_*^{2s-1}\, c_*(x_*,0). \qquad (6\text{-}118)$$

In Figures 6-7 through 6-12, the Monte Carlo† and Ermak nondimensional net deposition rate J_* and deposition flux j_* are compared for three representative cases. Agreement between the Monte Carlo results and Ermak's exact solution is good over the full range of h_*. Moreover, the Monte Carlo model does well for both constant settling velocity cases ($s = 0.5$) and cases in which the settling velocity is a function of time ($s = 0.76$). The plots of j_* give an indication of the accuracy of the density estimation technique we have employed. Agreement between the analytical and Monte Carlo results also shows that the zero-turbulent-flux condition at the ground is handled correctly in the Monte Carlo program.

The deposition pattern of Fig 6-10 is typical of large h_* cases. As h_* approaches infinity, the j_* density approaches a Gaussian form with mean and variance given by

$$\text{mean} = \frac{1}{h_*} \qquad (6\text{-}119a)$$

and

$$\text{variance} = \frac{1}{h_*^{2(s+1)}}\ . \qquad (6\text{-}119b)$$

The ability to draw more incisive conclusions concerning the general behavior of the deposition rate is severely limited by the restrictive form required by the Ermak analysis.

In summary, we have shown:

1. The Monte Carlo results are in good agreement with analytical solutions over the full range of h_*.
2. Turbulence, deposition, settling and the boundary condition at the ground are treated correctly.
3. As h_* becomes large, the ground-level deposition flux j_* becomes Gaussian with mean and variance given by Eqn (6-119).

†For convenience the est subscript has been dropped from the Monte Carlo J_{*est} and j_{*est} results.

REFERENCES

1. Sutton, O.G., Micrometeorology, McGraw-Hill, New York (1953).

2. Blackadar, A.K., J.A. Dutton, H.A. Panofsky and A. Chaplin, Investigation of the turbulence wind field below 150 m altitude at the Eastern test range, N.A.S.A. Contractor Rep. NASA-CE-1410 (1969).

3. Pasquill, F., Atmospheric Diffusion, 2nd Ed., John Wiley & Sons, New York (1974).

4. Counihan, J., Adiabatic atmospheric boundary layers: a review and analysis of data from the period 1880-1972, Atmos. Envir., 9, 871 (1975).

5. Taylor, G.I., The spectrum of turbulence, Proc. Roy. Soc., A, 164, 476 (1938).

6. Kaimal, J.C., J.C. Wyngaard, Y. Izumi and O.R. Coté, Spectral characteristics of surface layer turbulence, Quart. J. R. Met. Soc., 98, 417 (1972).

7. Corrsin, S., Limitations of gradient transport models in random walks and in turbulence, Advances in Geophs., 18A, 25 (1974).

8. Roberts, O.F.T., The theoretical scattering of smoke in a turbulent atmosphere, Proc. Roy. Soc., A, 104, 640 (1923).

9. Rounds, W., Solutions of the two-dimensional diffusion equations, Trans. Amer. Geoph. Union, 36, 395 (1955).

10. Deacon, E.L., Vertical diffusion in the lowest layers of the atmosphere, Quart. J. R. Met. Soc., 75, 89 (1949).

11. Godson, W.L., The diffusion of particulate matter from an elevated source, Archiv f. Met. und Biokl., A, 10, 305 (1958).

12. Smith, F.B., The diffusion of smoke from a continuous elevated point-source into a turbulent atmosphere, J. Fluid Mech., 2, 49 (1957).

13. Smith, F.B., The problem of deposition in atmospheric diffusion of particulate matter, J. Atmos. Sci., 19, 429 (1962).

14. Calder, K.L., Atmospheric diffusion of particulate material considered as a boundary value problem, J. Met., 18, 413 (1961).

15. McMahon, T.A. and P.J. Denison, Empirical atmospheric deposition parameters-a survey, Atmos. Envir., 13, 571 (1979).

16. Heines, T.S. and L.K. Peters, The effect of a horizontal impervious layer caused by a temperature inversion aloft on the dispersion of pollutants in the atmosphere, Atmos. Envir., 7, 39 (1973).

17. Heines, T.S. and L.K. Peters, The effect of ground level absorption on the dispersion of pollutants in the atmosphere, Atmos. Envir., 8, 1143 (1974).

18. Yeh, G.T. and C.H. Huang, Three-dimensional air pollutant modeling in the lower atmosphere, Boundary-Layer Met., 9, 381 (1975).

19. Ermak, D.L., An analytical model for air pollutant transport and deposition from a point source, Atmos. Envir., 11, 231 (1977).

20. Peterson, T.W. and J.H. Seinfeld, Mathematical model for transport, inter-conversion, and removal of gaseous and particulate air pollutants - application to the urban plume, Atmos. Envir., 11, 1171 (1977).

21. Astarita, G., J. Wei and G. Iorio, Theory of dispersion, transformation and deposition of atmospheric pollution using modified Green's functions, Atmos. Envir., 13, 239 (1979).

22. Lebedeff, S.A. and S. Hameed, Laws of effluent dispersion in the steady-state atmospheric surface layer in stable and unstable conditions, J. Appl. Met., 11, 326 (1976).

23. Schlichting, H., Boundary-Layer Theory, 6th Ed., McGraw-Hill, New York (1968).

24. Nunge, R.J., Application of an analytical solution for unsteady, advective-diffusion to dispersion in the atmosphere - I - II, Atmos. Envir., 8, 969 (1974).

25. Ragland, K.W. and R.L. Dennis, Point source atmospheric diffusion model with variable wind and diffusivity profiles, Atmos. Envir., 9, 175 (1975).

26. Liu, C.Y. and W.R. Goodin, A two-dimensional model for the transport of pollutants in an urban basin, Atmos. Envir., 10, 513 (1976).

27. Runca, E. and F. Sardei, Numerical treatment of time dependent advection and diffusion of air pollutants, Atmos. Envir., 9, 69 (1975).

28. Sklarew, R.C., A new approach: the grid model of urban air pollution, J. Air Pollut. Control Assoc., 20, 79 (1970).

29. Sheih, C.M., Mathematical modeling of particulate thermal coagulation and transport downstream of an urban area source, Atmos. Envir., 11, 1185 (1977).

30. Christensen, O. and L.P. Prahm, A pseudospectral model for dispersion of atmospheric pollutants, J. Appl. Met., 15, 1284 (1976).

31. Berkowicz, R. and L.P. Prahm, Pseudospectral simulation of dry deposition from a point source, Atmos. Envir., 12, 379 (1978).

32. Chandrasekhar, S., Stochastic problems in physics and astronomy, Rev. Modern Phys., 15, (1943).

33. Wippermann, F.K., On turbulent diffusion in an arbitrarily stratified atmosphere, J. Appl. Met., 5, 640 (1966).

34. Joynt, R.C. and D.R. Blackman, A numerical model of pollutant transport, Atmos. Envir., 10, 433 (1976).

35. Runchal, A.K., A.W. Bealer and G.S. Segal, A completely Lagrangian random-walk model for atmospheric dispersion, Proc. of the Thirteenth Sym. on Atmos. Pol., Paris, April 26-28 (1978).

36. Taylor, G.I., Diffusion by continuous movements, Proc. London Math. Soc., 20, 196 (1921).

37. Batchelor, G.K., Diffusion in a field of homogeneous turbulence, I. Eulerian analysis, Aust. J. Sci. Res., 2, 437 (1949).

38. Kampé de Fériet, M.J., Les fonctions aléatoires stationnaires et la théorie statistique de la turbulence homogène, Ann. Soc. Sci. Brux., 59, 145 (1939).

39. Hinze, J.O., Turbulence, 2nd Ed., McGraw-Hill, New York (1975).

40. Sutton, O.G., A theory of eddy diffusion in the atmosphere, Proc. Roy. Soc., A, 135, 143 (1932).

41. Sutton, O.G., The problem of diffusion in the lower atmosphere, Quart. J. R. Met. Soc., 73, 257 (1947).

42. Sutton, O.G., The theoretical distribution of airborne pollution from factory chinmeys, Quart. J. R. Met. Soc., 73, 426 (1947).

43. Baron, T., E.R. Gerhard and H.F., Johnstone, Dissemination of aerosol particles dispersed from stacks, Ind. Eng. Chem., 41, 2403 (1949).

44. Csanady, G.T., Dispersal of dust particles from elevated sources, Aust. J. Phys., 8, 545 (1955).

45. Csanady, G.T., Dispersal of dust particles from elevated sources, II. Limitations of the approximate theory, Aust J. Phys., 10, 558 (1957).

46. Overcamp, T.J., A general Gaussian diffusion-deposition model for elevated point sources, J. Appl. Met., 15, 1167 (1976).

47. Chamberlain, A.C., Aspects of travel and deposition of aerosol and vapour clouds, A.E.R.E., HP/R-1261, H.M.S.O. (1953)

48. Van der Hoven, I., Deposition of particles and gases, Met. and Atomic Energy, U.S.A.E.C., TID-24190 (1968).

49. Horst, T.W., A surface depletion model for deposition from a Gaussian plume, Atmos. Envir., 11, 41 (1977).

50. Policastro, A.J., W.E. Dunn, M.L. Breig and J.P. Ziebarth, Evaluation of mathematical models for characterizing plume behavior from cooling towers, NUREG/CR-1581, 2, (1980).

51. Panofsky, H.A., The structure of atmospheric shear flows-review, A.G.A.R.D., C.P. 48 (1969).

52. Panofsky, H.A. and E.L. Peterson, Wind profiles and change of terrain roughness at Riso, Quart. J. R. Met. Soc., 98, 418 (1972).

53. Sverdrup, H.U., Note on the log-law of wind structure near the ground, Quart. J. R. Met. Soc., 62, 461 (1936).

54. Frost, R., The velocity profile in the lowest 400 feet, Met. Mag. London, 76, 14 (1947).

55. Deacon, E.L., Gust variation with height up to 150 m., Quart. J. R. Met. Soc., 81, 562 (1955).

56. Slade, D.H., Wind measurements on a tall tower in rough and inhomogeneous terrain, J. Appl. Met., 8, 293 (1969).

57. Irwin, J.S., A theoretical variation of the wind profile power-law exponent as a function of surface roughness and stability, Atmos. Envir., 13, 191 (1979).

58. Yudine, M.I., Physical considerations on heavy-particle diffusion, Advances in Geophs., 6, 185 (1959).

59. Csanady, G.T., Turbulent diffusion of heavy particles in the atmosphere, J. Atmos. Sci., 20, 201 (1963).

60. Fuchs, N., Concerning the velocity of evaporation of small droplets in a gas atmosphere, National Advisory Committee for Aeronautics, TM 1160 (1947).

61. Taylor, G.I., The present position in the theory of turbulent diffusion, Advances in Geophs., 6, 101 (1959).

62. Pasquill, F., The estimation of the dispersion of windborne material, Met. Mag., 90, 33 (1961).

63. Pasquill, F., Atmospheric dispersion parameters in Gaussian plume modeling, Part II. Possible requirements for change in the Turner workbook values, EPA-600/4-76-030b (1976).

64. Gifford, F.A., Atmospheric dispersion, Nucl. Safety, 1 (3), 56 (1960).

65. Gifford, F.A., Use of routine meteorological observations for estimating atmospheric dispersion, Nucl. Safety, 2 (4), 47 (1961).

66. Cramer, H.E., Engineering estimates of atmospheric dispersal capacity, Amer. Ind. Hyg. Assoc. J., 20, 183 (1959).

67. Cramer, H.E., A brief survey of the meteorological aspects of atmospheric pollution, Bull. Amer. Met. Soc., 40 (4), 165 (1959).

68. Briggs, G.A., Diffusion estimation for small emissions, Air Resources Atmospheric Turbulence and Diffusion Laboratory 1973 Annual Report, USAEC ATDL-106, National Oceanic and Atmospheric Administration (1974).

69. Calder, K.L., A climatological model for multiple source urban air pollution, User's Guide for the Climatological Dispersion Model, Appendix E, U.S. EPA R4-73-024 (1973).

70. Singer, I.A. and M.E. Smith, Relation of gustiness to other meteorological parameters, J. Met., 10, 121 (1953).

71. Singer, I.A. and M.E. Smith, Atmospheric dispersion at Brookhaven National Laboratory, Int. J. Air Water Poll., 10, 125 (1966).

72. Turner, D.B., Workbook of Atmospheric Dispersion Estimates, revised, U.S. EPA, AP-26, Government Printing Office, Washington, DC (1970).

73. Box, G.E.P. and M.E. Muller, A note on the generation of random normal deviates, Ann. Math. Statist., 29, 610 (1958).

74. Knuth, D.E., The Art of Computer Programming, Vol. 2, Addison-Wesley, Reading, Mass. (1968).

75. Marsaglia, G., M.D. MacLaren and T.A. Bray, A fast procedure for generating normal random variables, CACM, 7, 4 (1964).

76. Parzen, E., On estimation of a probability density function and model, Ann. Math. Stat., 33, 1065 (1962).

77. Wegman, E.J., Nonparametric probability density estimation: II. A comparison of density estimation methods, J. Statist. Comput. Simul., 1, 225 (1972).

78. Wegman, E.J., Nonparametric probability density estimation: I. A summary of available methods, Technometrics, 14, 533 (1972).

79. Whittle, P., On the smoothing of probability density functions, J. R. Stat. Soc., B, 20, 334 (1958).

80. Rosenblatt, M., Remarks on some nonparametric estimates of a density function, Ann. Math. Stat., 27, 832 (1956).

Table 6-1

GRADIENT TRANSPORT

Investigator/ Year	instantaneous	continuous	point	finite line	infinite line	area	ground-level	elevated	settling	deposition	evaporation	unsteady	numerical
Roberts 1923	X	X	X		X		X						
Rounds 1955		X			X	X		X	X				
Godson 1958		X			X			X	X	X			
Smith 1957		X	X		X		X	X					
Smith 1962		X			X		X	X	X	X			
Heines & Peters 1973		X	X		X			X					
Heines & Peters 1974		X	X		X			X		X			
Yeh & Huang 1975		X	X		X			X		X			
Ermak 1977		X	X					X	X	X			
Peterson & Seinfeld 1977		X	X					X	X	X			
Astarita, Wei & Ioria 1979		X	X				X						
Lebedeff & Hameed 1976		X			X	X	X						
Nunge 1974	X				X		X					X	
Ragland & Dennis 1975		X	X				X						X
Liu & Goodin 1976		X			X	X						X	X
Sheih 1977		X	X					X	X			X	X
Berkowicz & Prahm 1978		X			X			X		X		X	X

Table 6-1 continued

Investigator/ Year	instantaneous	continuous	point	finite line	infinite line	area	ground-level	elevated	settling	deposition	evaporation	unsteady	numerical
Wipperman 1966		X	X				X						
Joynt & Blackman 1976		X	X				X					X	X
Runchal, Bealer & Segal 1978	X	X	X		X		X						X
Sutton 1932	X	X	X	X	X		X						
Sutton 1947		X	X		X			X					
Baron, Gerhard & Johnstone 1949		X	X					X	X				
Csanady 1955, 1957		X	X					X	X	X			
Overcamp 1976		X	X					X	X	X	X		
Chamberlain 1953		X	X				X	X		X			
Van der Hoven 1968		X	X					X		X			
Horst 1977		X	X					X		X			
Schrecker		X	X					X	X	X	X		
Slinn		X	X					X	X	X	X		

STATISTICAL

Table 6-2

Key to stability categories

Surface wind speed (m/sec)	Insolation			Night	
	Strong	Moderate	Slight	Thinly overcast or ≥ 4/8 low cloud	≤ 3/8 cloud
<2	A	A-B	B	-	-
2-3	A-B	B	C	E	F
3-5	B	B-C	C	D	E
5-6	C	C-D	D	D	D
>6	C	D	D	D	D

(for A-B take average of values for A and B etc.)

Table 6-3

Stability class	Coefficient a	Index S
A (very unstable)	0.279	0.90
D (neutral)	0.199	0.76
F (moderately stable)	0.117	0.67

x and σ_z in meters. This power-law approximation good only for $x \leq 10{,}000$ m

Table 6-4

Model	Basic Quantities	$\sigma^{i}{}_{z}^{2}$	T_{sc}
Statistical Approach	$\overline{w'^2}$, τ_{L_W}	$2\overline{w'^2}\,\tau_{L_W}\int_{t^{i-1}}^{t^{i}} r(t)\,dT$, $r(t) = \frac{1}{\tau_{L_W}}\int_{o}^{t} R_{L_W}(\xi)\,d\xi$	$\overline{w'^2}\,\tau_{L_W}$
Gradient Transfer	$k(x)$	$2\,K^{i}_{avg}\,\Delta t$, $K^{i}_{avg} = \frac{1}{\Delta t}\int_{t^{i-1}}^{t^{i}} K(x(t))\,dt$	K_r +
Gaussian Plume Dispersion Parameters	$\sigma_z(x)$	$\sigma_z^2(x(t^i)) - \sigma_z^2(x(t^{i-1}))$	$\frac{\bar{u}_r}{2}\left.\frac{d\sigma_z^2}{dx}\right\|_r$ +

+The subscript r indicates evaluation at some convenient reference point.

Table 6-5

Figure number	m	s	h_*	α	β	γ	number of particles
6-6	0	0.76	0	-	-	-	4000
6-7, 6-8	0	0.5	5	-	-	-	4000
6-9, 6-10	0	0.5	80	-	-	-	4000
6-11, 6-12	0	0.76	1.0	-	-	-	4000

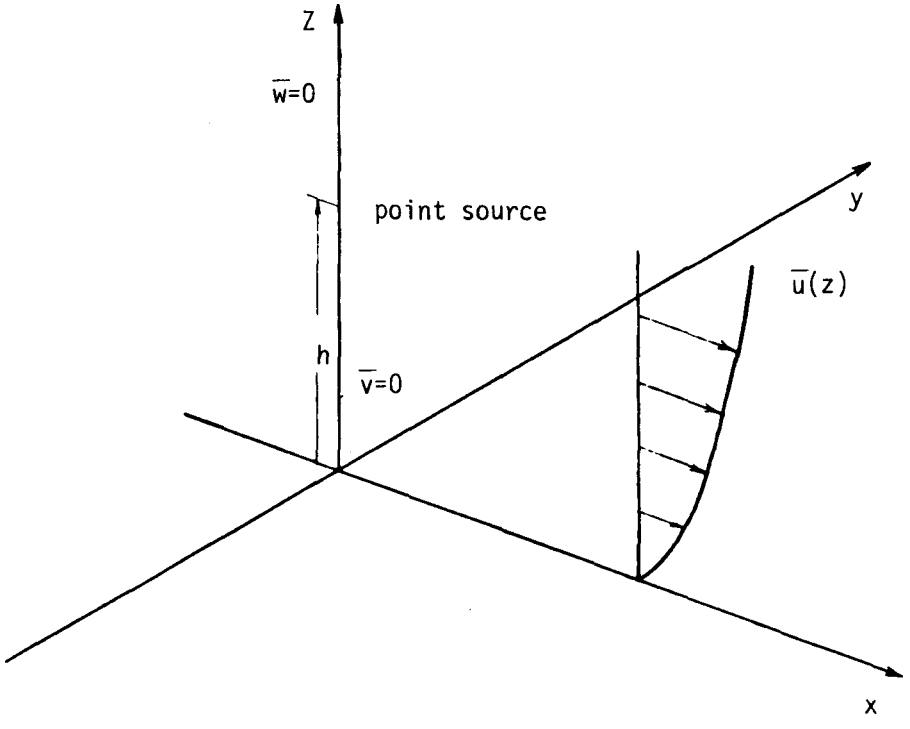

Figure 6-1. Coordinate system

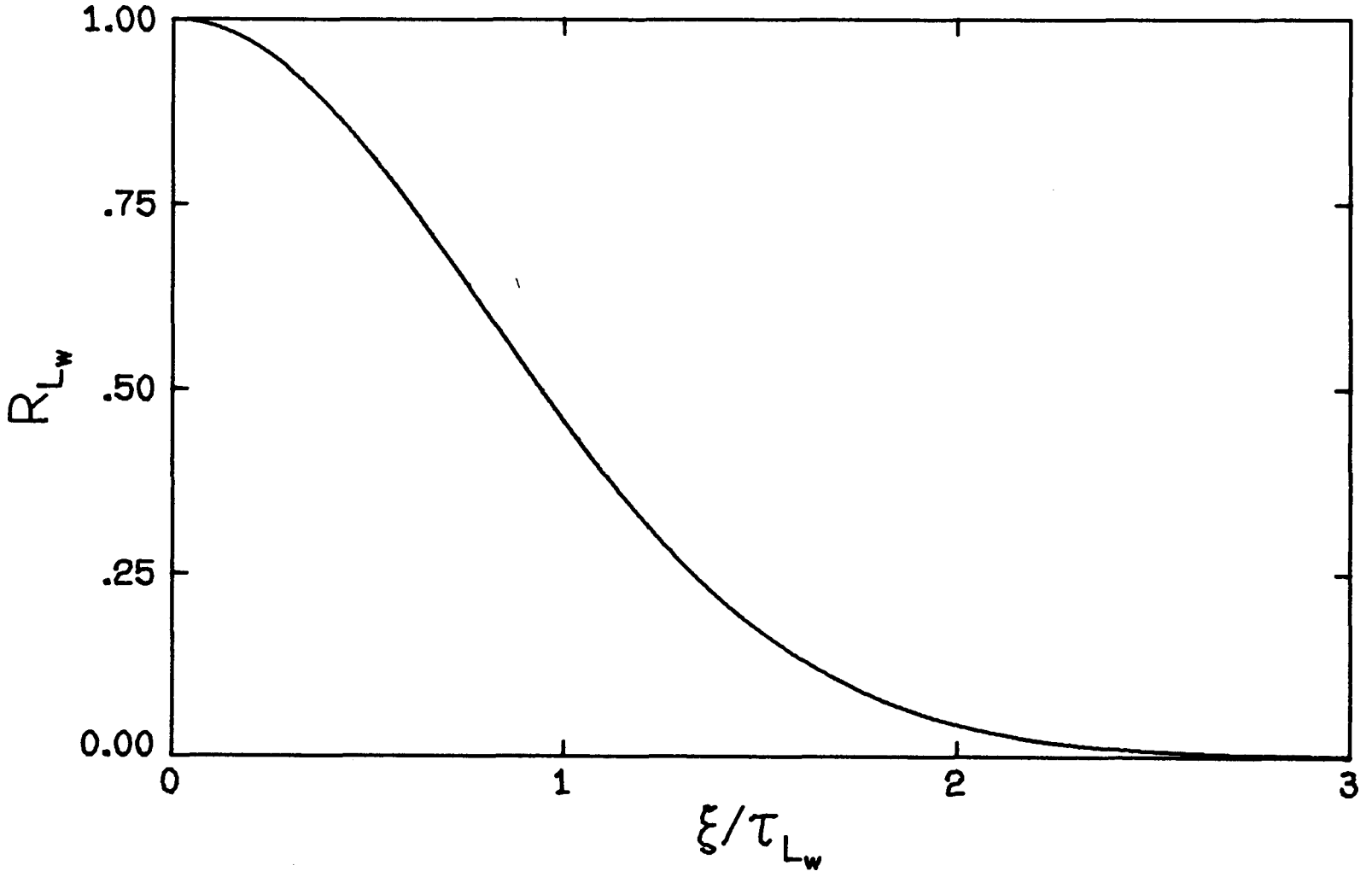

Figure 6-2. Typical form of the Lagrangian correlation coefficient.

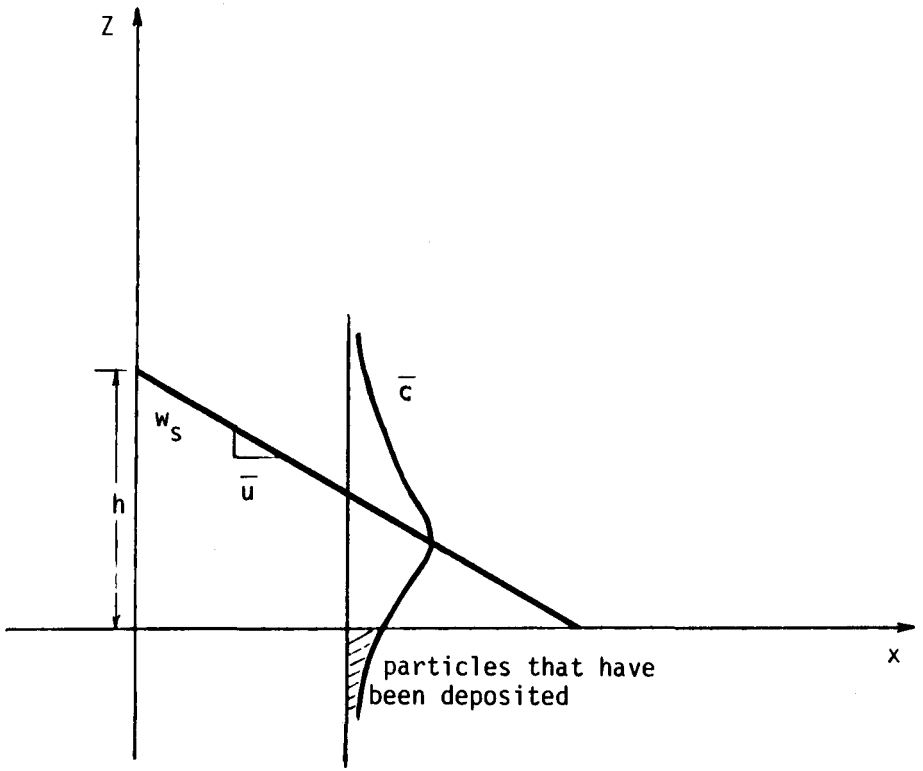

Figure 6-3. Pictoral representation of the Schrecker method of calculating the net deposition rate.

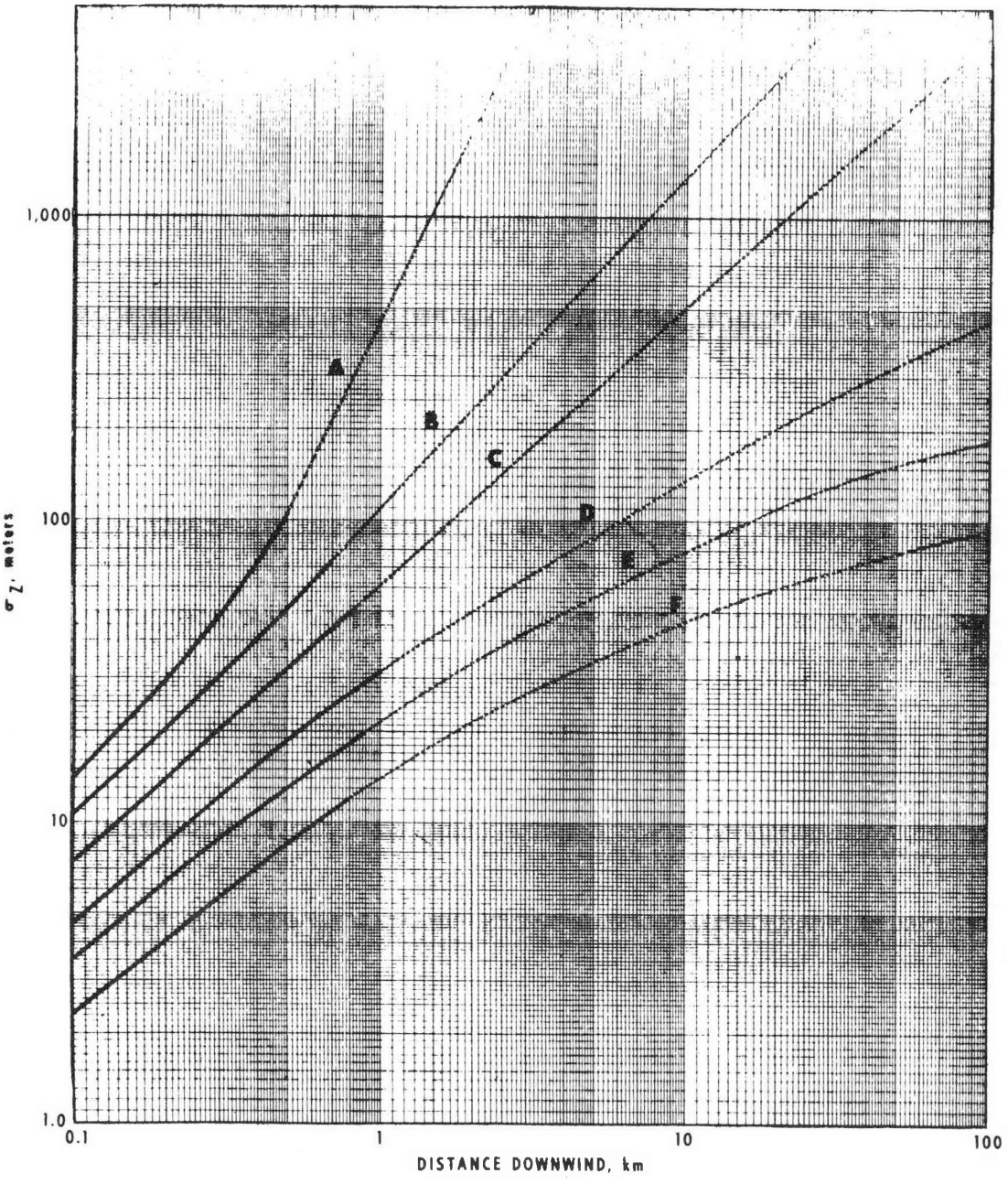

Figure 6-4. Vertical dispersion coefficient as a function of downwind distance from the source.

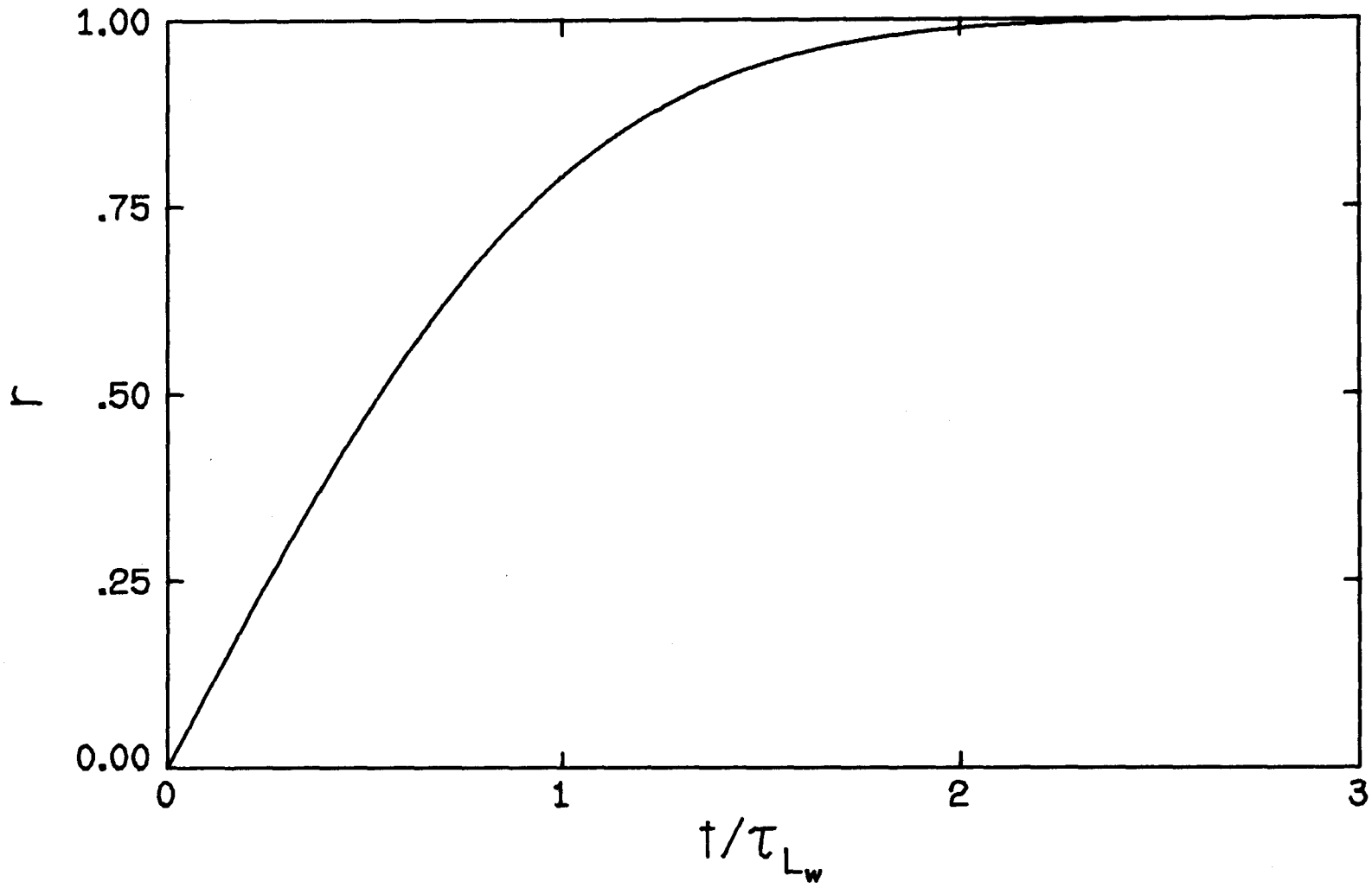

Figure 6-5. The function r used to calculate $\sum_i$ for cases in which a Lagrangian correlation coefficient is specified.

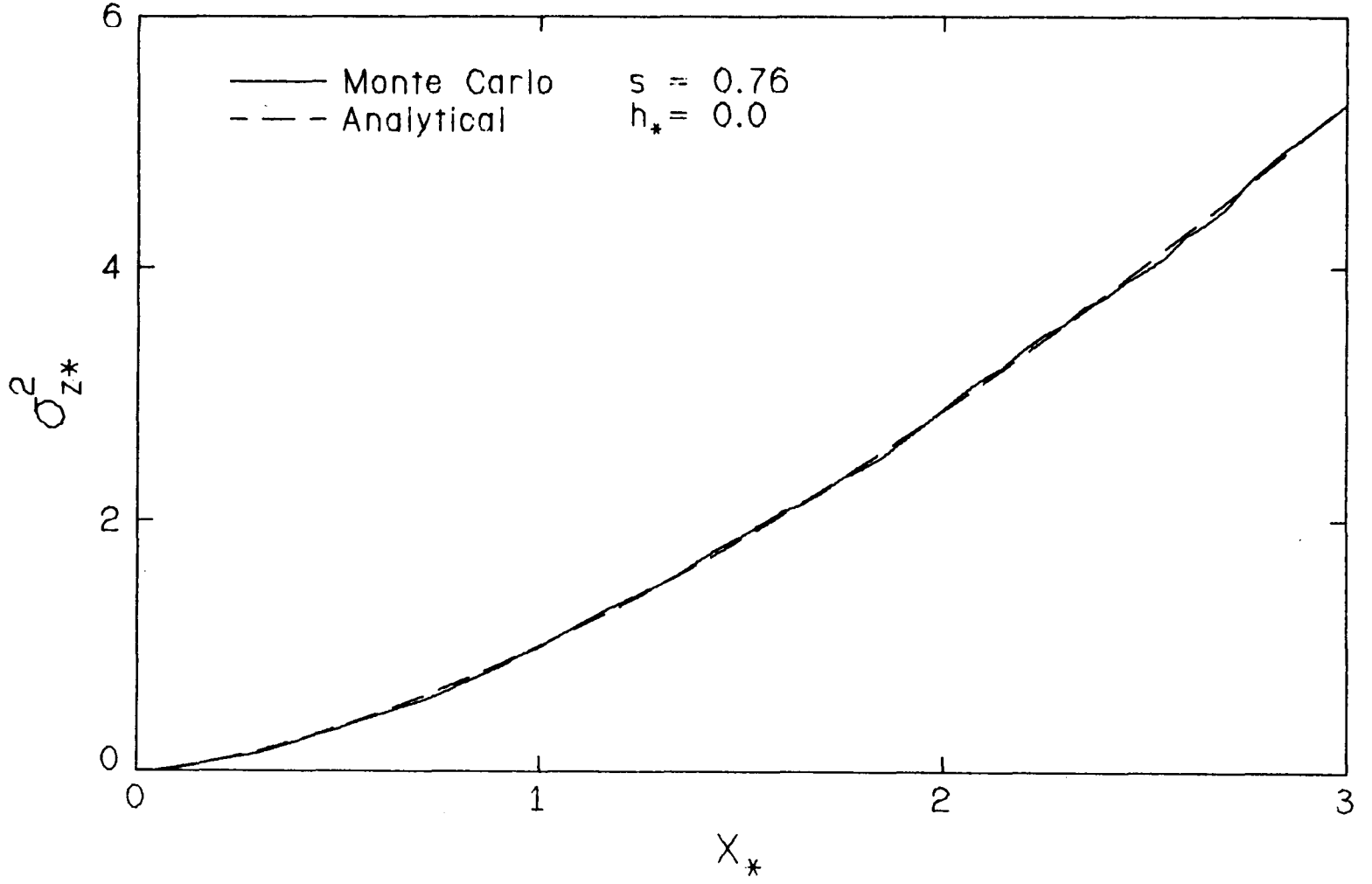

Figure 6-6. Comparison of Monte Carlo calculated and analytical dispersion parameters for stability class D.

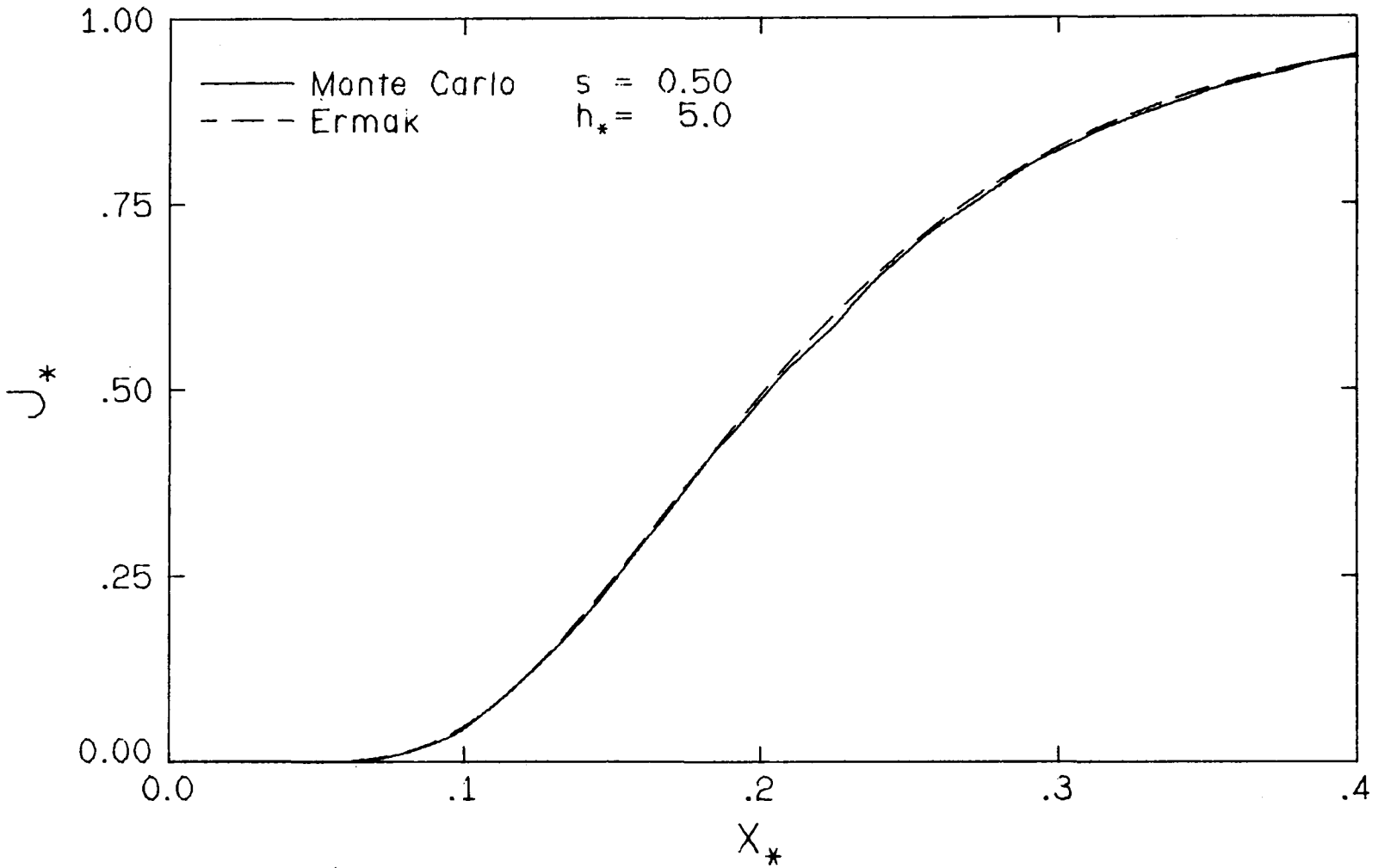

Figure 6-7. Comparison of Monte Carlo and Ermak nondimensional net deposition rate.

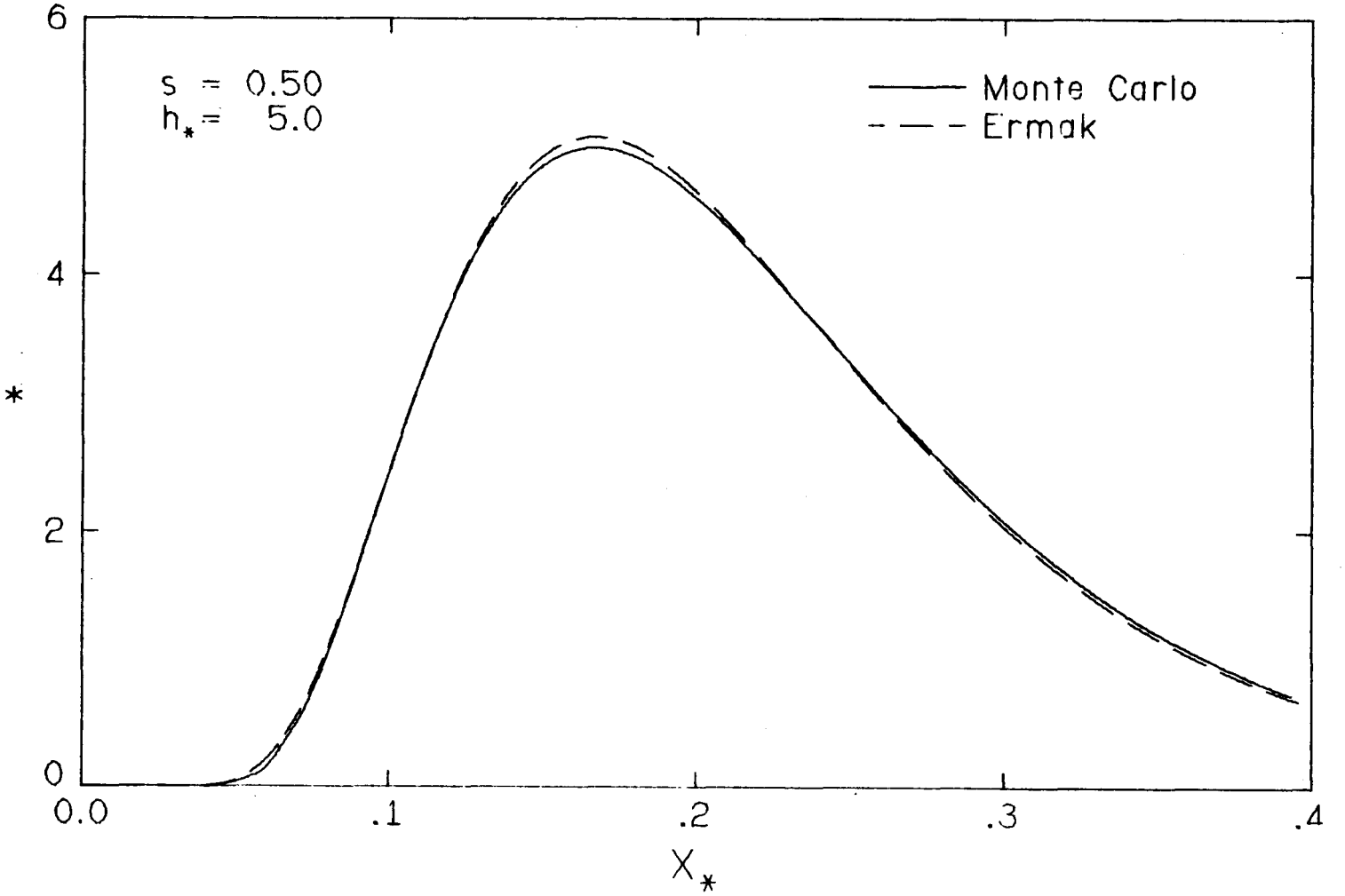

Figure 6-8. Comparison of Monte Carlo and Ermak nondimensional deposition flux.

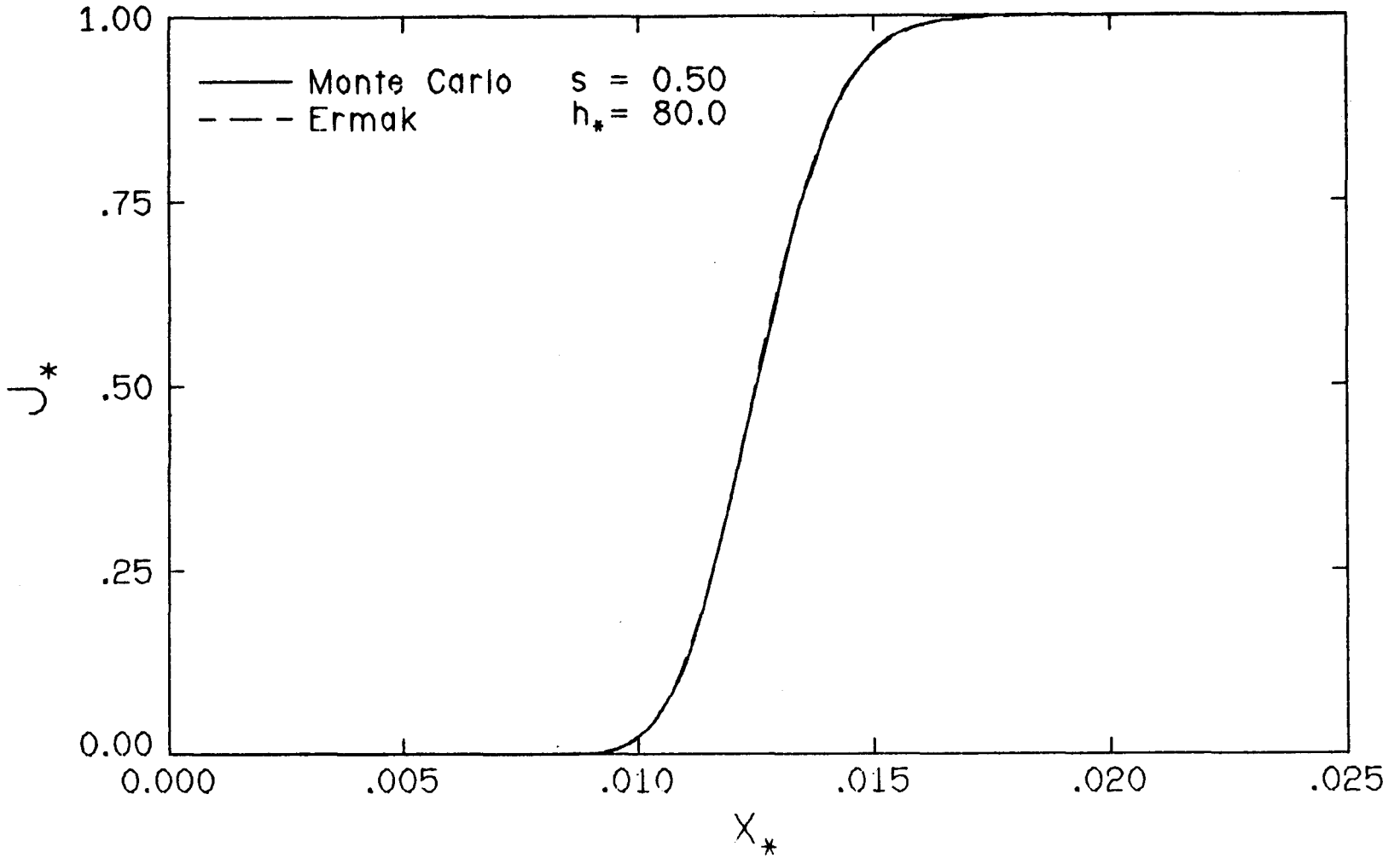

Figure 6-9. Comparison of Monte Carlo and Ermak nondimensional net deposition rate.

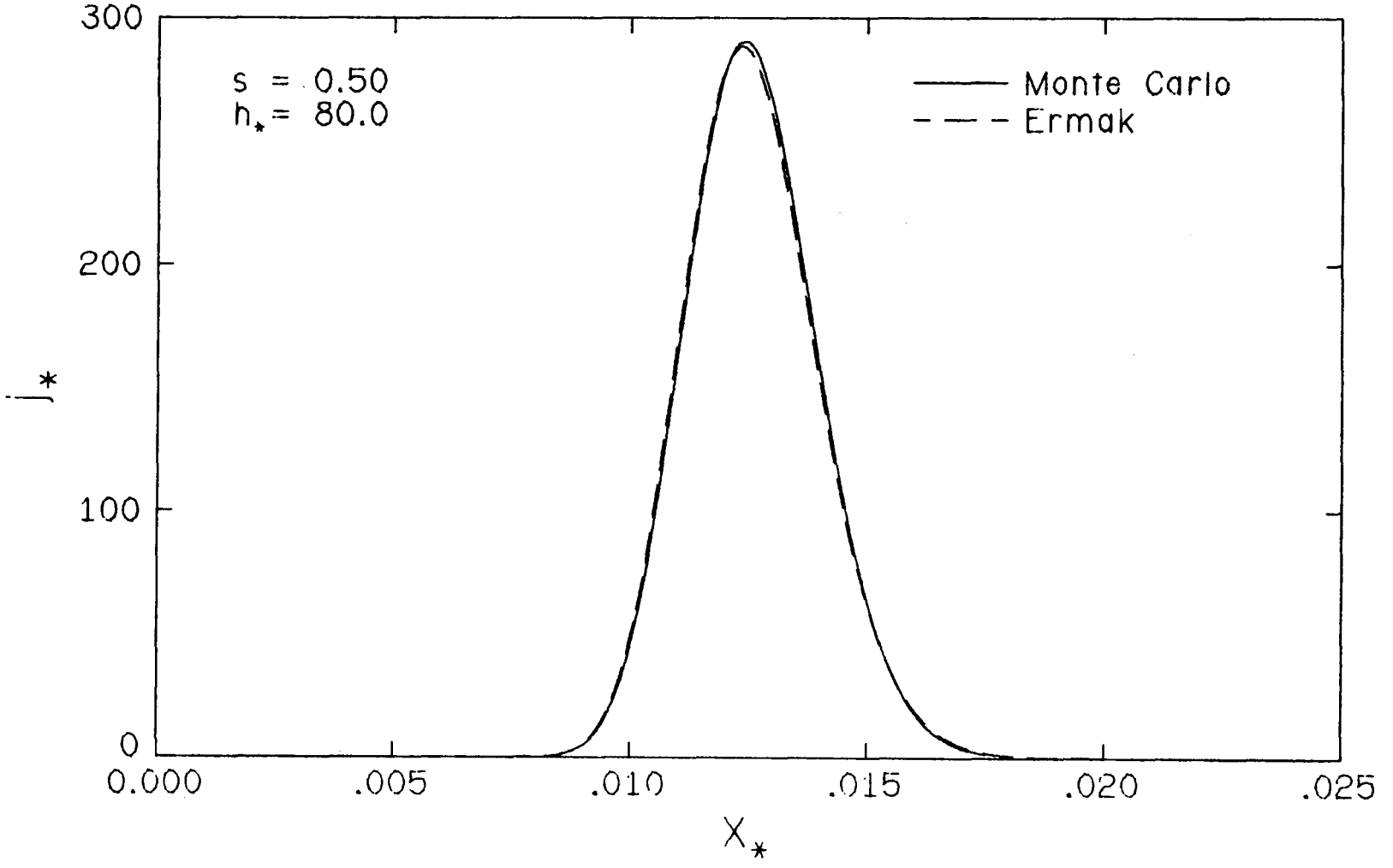

Figure 6-10. Comparison of Monte Carlo and Ermak nondimensional deposition flux.

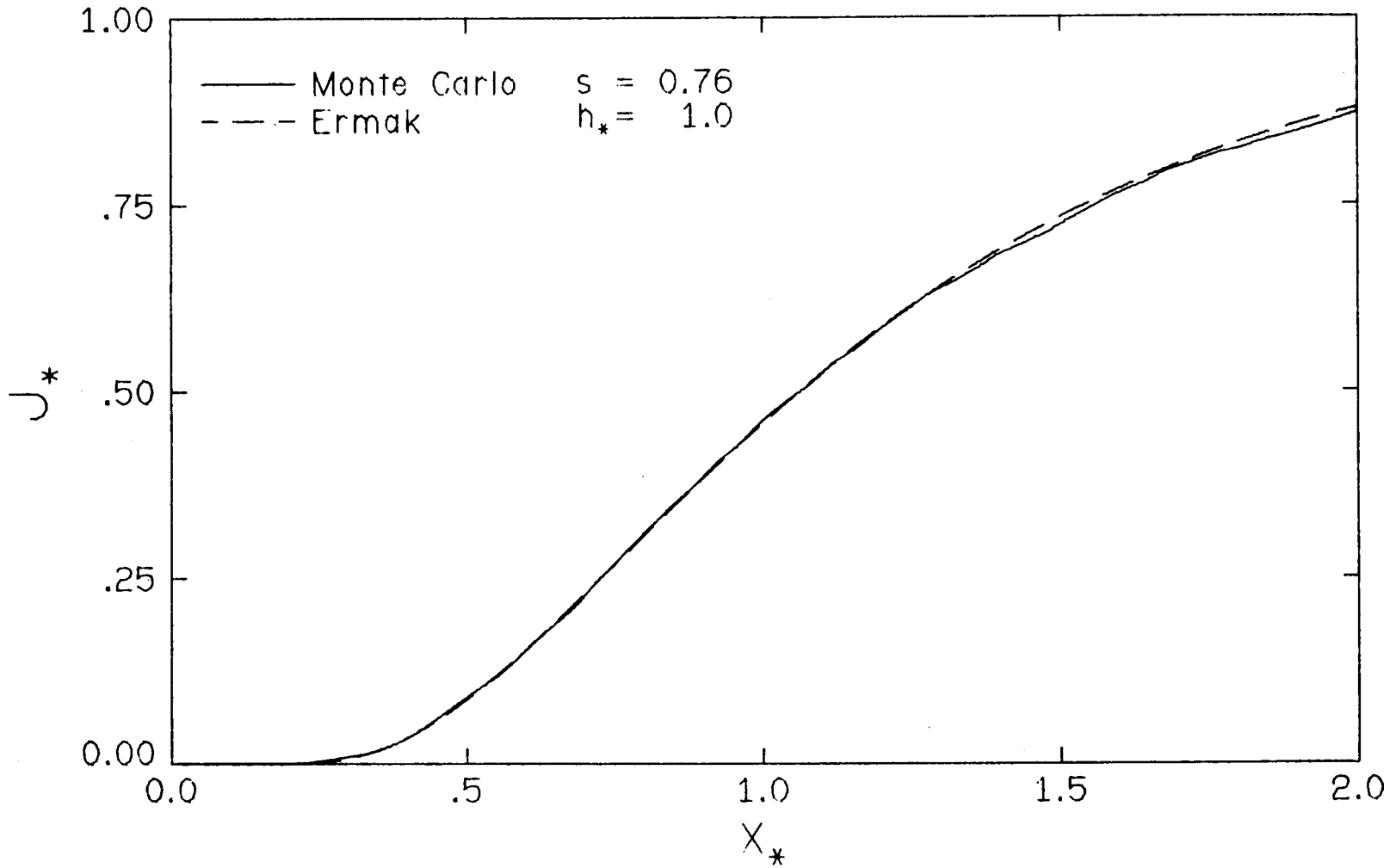

Figure 6-11. Comparison of Monte Carlo and Ermak nondimensional net deposition rate.

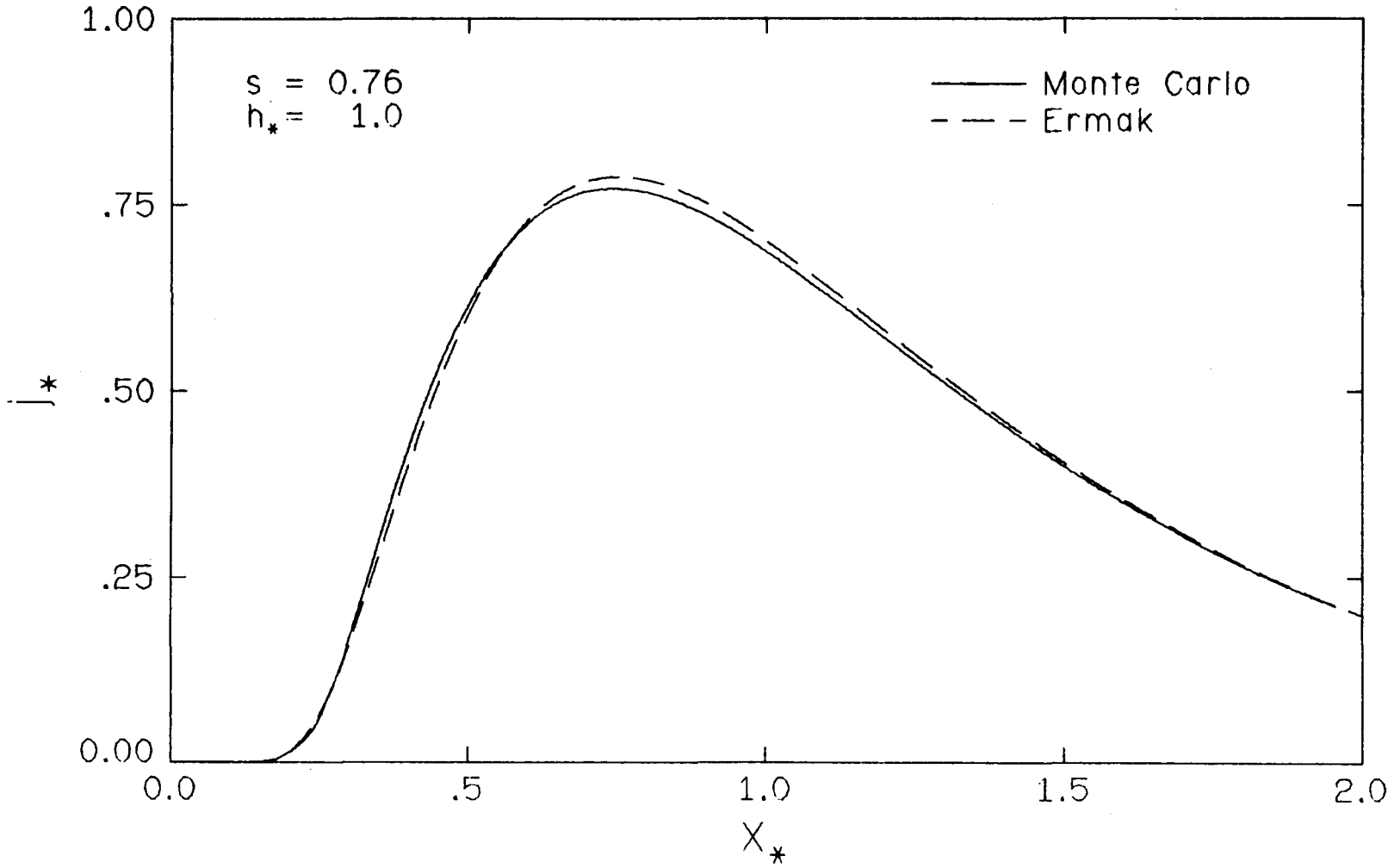

Figure 6-12. Comparison of Monte Carlo and Ermak nondimensional deposition flux.

Blank

Section 7

SENSITIVITY STUDY OF DRIFT MODEL PREDICTIONS TO CHOICE OF BREAKAWAY METHOD

INTRODUCTION

At this point in our program to develop a drift model for single natural-draft cooling towers, we have completed (a) a calibrated and validated plume rise model, and (b) an improved droplet evaporation submodel. Our decision to use the ballistic method at present requires only a choice in breakaway criterion. Lack of experimental data on the precise way in which drift droplets break away from a cooling-tower plume has led us to test the four most popular methods in addition to one method we developed. Our testing included:

1. a sensitivity study to assess the actual differences that result from use of the various breakaway criteria, and

2. evaluation of our drift model through model/data comparisons to field data taken at Chalk Point.

Results from the sensitivity study and the model/data comparison study appear in Sections 7 and 8, respectively. Our final choice of breakaway method among the five tested will depend upon the results of those two studies.

FORMULATION OF SENSITIVITY STUDY ON BREAKAWAY CRITERIA

As noted above, our single-tower drift model is put together in piecewise fashion by combining the NDCT plume model with the droplet evaporation model through the breakaway criterion. The breakaway criteria being studied are:

1. droplet settling velocity becomes just greater than the updraft velocity at the plume centerline. This breakaway criterion is used in the Overcamp-Israel (1) and ESC/Schrecker Models (2) ...Criterion #1.

2. droplet vertical fall in the plume just becomes larger than the local plume radius measured vertically. The Wigley-Slawson (3) and Hanna Models (4) use this method ...Criterion #2.

3. lateral droplet displacement from the plume centerline just becomes equal to the initial plume radius measured at the tower top. This

criterion is used in the Wolf I and II Models (5) ...Criterion #3.

4. modification of Criterion #2 in that the drop never actually breaks away from the plume but is under the influence of a Gaussian distribution in vertical velocity, vapor concentration, and temperature centered about the plume centerline. See Table 7-1 for a listing of the equations used to describe the method. This method was developed at the University of Illinois...Criterion #4.

5. fraction of droplets of each size range breaks away from the plume (at each downwind ΔX) dependent on settling velocity, wind speed, and local plume radius. This method is used in the recent Hanna drift model (6) ...Criterion #5.

We begin our parametric study by choosing a set of representative conditions at the Chalk Point natural-draft cooling tower. In the study we follow the trajectory and physical characteristics of one droplet through the plume and to final deposition. For each case calculated, only one ambient or initial droplet characteristic is changed in order to study the effect that change had on droplet path and character. Our standard case is represented by the following:

- Tower geometry and exit conditions:
  - -- height of tower 124.1m
  - -- exit diameter of tower 54.9m
  - -- exit velocity of tower 4.0 m/s
  - -- exit temperature of tower 30.0°C
- Ambient conditions:
  - -- wind speed 4 m/s (uniform)
  - -- dry-bulb temperature 10°C (uniform)
  - -- relative humidity 70% (uniform)
- Droplet conditions:
  - -- diameter 200 microns
  - -- salt concentration 0.005 g NaCl/g soln.

Note that the ambient environment has constant properties...wind speed, dry-bulb temperature, and relative humidity. The ambient atmosphere being of uniform temperature is therefore isothermal and stable. We consider this situation as our standard case. Computations are made with our drift model for the 200 μm drop only and we seek the following information:

1. path of the droplet while in the plume, through breakaway and to the ground.

2. the height above ground and downwind location of the drop upon breakaway from the plume.

3. deposition distance downwind from the tower and the diameter of the droplet as it strikes the ground.

This information for the standard and other cases will be presented in graphical as well as tabular form for easy interpretation. We are interested in the effects on the above-listed quantities due to changes in the following parameters:

- droplet diameter:
  -- from 200 μm to 50, 100, 300, 400, 500, 600, 700, 800, 900, 1000 μm
- ambient temperature:
  -- from 10°C to -10°, 0°, 20°C.
- ambient relative humidity:
  -- from 70% to 30, 80, 90%.
- ambient wind speed:
  -- from 4 m/s to 1, 5, 10, 20 m/s.
- droplet salt concentration:
  -- from 0.005 g/g to 0.05 g/g.

Note that in each case, only one parameter is changed at a time from the standard case and that we are always following just one droplet. In order to test the effect of our assumption of uniform ambient conditions, we set up three more cases to study. Each of these three fictitious cases allows only for average ambient conditions over plume height to equal 10°C, 4 m/s, and 70% relative humidity except that we have ambient variations with height which represent neutral, moderately unstable and moderately stable environments. The precise definition of these environments is given in Table 7-2. With these three variations, we will be able to determine the difference in drop path and drop characteristics between (a) variable environmental conditions and (b) averages of those variations representing uniform profiles for temperature, humidity, and wind speed.

Recall again that the model we are testing is a combination of the ANL single tower plume model (from Vol. 2) with the University of Illinois droplet evaporation model, linked together by a choice of any of the above five breakaway criteria. No droplet evaporation or condensation is assumed to occur during the droplet's traverse through the plume (except Criteria #4).

RESULTS OF SENSITIVITY STUDY

Graphical results of the calculations described above are presented in (Figure 7-1 to 7-30). At times two different scales are employed to focus in on (a) the drop trajectory within the plume, and then (b) the drop trajectory after breakaway. The results in (Figure 7-1 to 7-30) are summarized in terms of key information in

(Figure 7-1 to 7-30) and Table 7-3. The effect of parametric variation on breakaway criterion #5 (new Hanna method) is presented in Table 7-4 only. Clearly, Criteria #1, 2, and 3 provide only one breakaway location in the plume for any drop. Criterion #4 provides no point of breakaway for any droplet since it allows for a continuous transition between drop environment and ambient environment. Within any droplet size range, the new Hanna method provides for a fraction of the droplet mass emission to break away from the plume at each ΔX downwind. The method attempts to account for plume turbulence in dispersing drops within the plume by allowing a certain fraction of droplets to break away at any ΔX. The effects of such a breakaway criterion is difficult to plot due to the large number of trajectories that result from any droplet size class; consequently, we present the results in only tabular form giving the fraction of initial mass flux of that droplet size that breaks away between downwind locations X_i and $X_i-\Delta X$.

The effects of droplet diameter variation are quite interesting (Figure 7-1 to 7-11) and Table 7-3. For the small diameters, 50 μm and less, the heights of release from the plume are essentially at the plume centerline at the downwind location where the plume enters the diffusion phase. Actually, we inserted logic into our drift code to assure that if a droplet did not release from the plume before the beginning of the diffusion phase, it would necessarily be released at that cross-section. That assumption is common to all drift models. Beginning at D_o = 100 μm and continuing to larger drop diameters, we notice differences in the effects of the different breakaway criteria. We notice that for all diameters between 100 and 800 μm, Criterion #1 (settling velocity greater than or equal to the local centerline vertical velocity) provides the latest and highest locations of droplet release from the plume. The earliest release in each case occurs for Criterion #3 (horizontal drop deviation from plume centerline greater than or equal to the initial plume radius). We expect the relationship between release points for Criteria #2 and 3 since the local plume radius measured vertically is nearly always larger than the initial radius. Consequently, a criterion based on initial plume radius should lead to earlier breakaway. Apparently, the difference between horizontal deviation of drop location from the centerline and a vertical deviation with respect to the centerline (which is a secondary difference between Criteria #2 and 3) is not very important.

In general, for drop diameters between 100 and 600 μm, Criterion #4 leads to apparent breakaway before Criterion #2 yet after Criterion #3. Earlier breakaway than Criterion #2 here is probably due to the simulation of the vertical plume

velocity (in Criterion #4) as Gaussian-shaped (more attenuated vertically) rather than top-hat.

Another interesting feature shown in (Figure 7-1 to 7-11) and Table 7-3 is that Criterion #2 releases drops from the plume slightly further downwind than Criterion #1 for drop diameters 50 μm - 300 μm. This is due to the fact that those drops generally release at the downwind plane where diffusion begins and this plane is tilted with respect to the horizontal (the criterion for the beginning of the diffusion phase in our plume model is the centerline location where the local densimetric Froude number of the plume is zero, not where the plume has leveled off). Since the final plane of calculation is tilted, there is the possibility that drops have fallen below the jet centerline and have become displaced downwind a little further than is the centerline location. It should be noted that it is the vertical deviation of droplet release points from one another that is most crucial in determining relative deposition distances (since the wind speed acting horizontally is usually much greater than the drop settling velocity acting vertically) rather than the horizontal deviations that are presented at breakaway points.

For drop diameters 600 μm - 900 μm, we find that the drop release points, in terms of height above ground and downwind location, find themselves in the order 1, 4, 2, 3 in terms of magnitude. For D_o = 1000 μm, all criteria lead to the drop falling back into the tower (except Criteria #4); for Criteria #2 and 3, the drop actually rises a little but falls below tower height for $X < R_o$, the tower exit radius, and hence drops into the tower. Criteria #4 starts a drop on the plume centerline at the tower edge, therefore it will not predict a drop falling back into the tower.

It is interesting to determine the relative impact these criteria have on deposition location and character. From (Figure 7-1 to 7-11) and Table 7-3, we see that for $D \leq 100$ μm, the criteria have essentially the same effect both in downwind distance to deposition and in final drop diameter.

Final distance to deposition as determined from the four breakaway criteria for drops sized 200 μm - 900 μm differ among them from 50% to a factor of four for the diameters tested. However, the more common breakaway methods, Criteria #1 and 2 differ generally by 50-70% in terms of computed downwind deposition distance. This difference is not very large. In terms of actual distances, the breakaway

criteria lead to the greatest sensitivity in predictions for the smaller drops that strike the ground at large distances. We note from Table 7-3 that the final size of the droplets as they strike the ground hardly change among the four criteria for $D_o \leq 300$ μm. Clearly, these drops have evaporated to their final state and are in Phase III of their evaporation history. Table 7-3 shows that the final sizes of the droplets are not significantly different from any of the breakaway criteria tested (except for the 400 μm droplet).

The next set of sensitivity tests involves droplet concentration for D_o = 200 μm, our standard drop size (Figure 7-12 and 7-13). For Criteria #1, 2, and 3, no change occurs in location of breakaway since our drift model does not assume any evaporation or condensation within the plume. Criterion #4 does allow droplet evaporation to occur while the drop is in the plume; however, only negligible differences are present. Thus, plume and breakaway predictions are essentially independent of droplet salt concentration. However, the effect of droplet concentration is very significant on the location and final diameter at deposition. Clearly, the larger salt concentration within the drop reduces evaporation after breakaway and leads to a large (and heavier) drop state.

The effect of ambient relative humidity variation is noticeable but not significant on the location at breakaway (Figure 7-14 to 7-17). The location of drop breakaway is affected through the relative humidity influence on the plume. The increase in ambient atmospheric moisture leads to a more moist and therefore more buoyant plume as it entrains additional moisture from the ambient air. The associated increase in plume buoyancy leads to a higher rising plume and therefore higher breakaway locations for those higher relative humidity cases. The difference in ground deposition character (distance and final diameter) depends largely on evaporation characteristics of the drop after breakaway. Note that the final diameter has been reached in the 30% and 70% relative humidity cases. Even though the drop under 30% relative humidity evaporated more rapidly, traveling a longer time with a smaller settling velocity (leading to a larger distance to deposition), not much difference is noted between the ambient relative humidities of 30% and 70% in terms of deposition distance. However, for the larger relative humidities, 80% and 90%, drop evaporation is more inhibited leading to a significantly shorter distance to deposition in these cases.

The effect of changes in ambient temperature (Figure 7-18 to 7-21) provide only small effects in drop breakaway locations and these effects are due to changes in

plume characteristics. It should be noted that for each ambient temperature chosen, T = -10, 0, 10, 20°C, we assumed that the tower would add an additional 20°C to provide the exit temperature. The exit velocity was assumed unchanged. [A more detailed study would employ a tower model to actually predict the exit temperature and velocity for those ambient conditions. We felt that this kind of detail was not warranted for the purposes of our study.] Note that the final diameter in each case is unchanged because our 200 μm drop deposited at its final state in each case tested. The effect of a variable ambient profile with the same averages over maximum plume height as our uniform profile case reveals sharp differences (Figure 7-22 to 7-25). The more unstable the atmosphere, the higher the plume rises and consequently the higher and further the drop gets released. The precise distance to deposition is a more complicated function of the conditions tested.

The effect of wind velocity is very significant (Figure 7-26 to 7-30). Clearly, the larger the wind speed, the more bent-over the plume is and the lower the breakaway location will be. The distance to the release point is not so predictable. Several factors have significant interplay:

1. the larger the wind speed, the greater the tendency for the droplet to be transported downwind before breakaway (note the effects of U = 1, 4, 5, 10 m/s on Criteria #1, 2 as increased wind speed increases the downwind distance to breakaway).

2. the larger the wind, the greater the deviation a drop has from the plume centerline (see effects of U = 1, 4, 5, 10, 20 m/s on Criteria #3 leading to faster breakaway as wind speed increases).

3. for the largest winds, U = 20 m/s, the increased mixing effect of the tower wake causes rapid dilution and reduction in plume centerline velocity to the point where the downwind location to breakaway for U = 20 m/s is significantly shortened (compared to the cases U = 1, 4, 5, 10 m/s) for Criterion #1.

Note that the distance to deposition does not always increase for the larger winds. The special cases (U = 20 m/s for Criteria #1, 2) reflect the lower release heights for those cases as compared to lower wind runs. Also notable is that for U = 1, 4, 5, 10, 20 m/s, the drop evaporated to its final state which was identical for all cases. Clearly, our drop size was kept at 200 μm, the ambient environment was otherwise unchanged, and the drops in each case had sufficient time to evaporate to final state.

We finally focus attention to Table 7-4 which presents, for Criterion #5, the distribution of fractions for breakaway at different distances downwind. In each

case, these fractions are presented for different distance increments downwind. For the standard case, for instance, the fraction of 200 micron drops which leaves the plume in the downwind distance range 0-100 m is 0.435. For the distance 100-200 m, the fraction of mass of 200 μm drops falling from the plume is 0.130. At a distance 740 m downwind of the tower, all the mass of 200 μm drops emitted from the tower has dropped from the plume. Sum totals are given for each run. Comparisons of breakaway fractions computed from this distribution method may be made with the results given in Table 7-3 for the other breakaway criteria. The results of those comparisons show the following:

1. In the cases of drop diameters 500-1000 μm, the new Hanna method (Criterion #5) predicts breakaway earlier than Criteria #1, 2, 3, and 4 do. The same is true, but less emphatically, for drop sizes 300-400 μm where the new Hanna breakaway criterion predicts a majority of mass fallen away before the other methods release their drop mass at one location. For drop sizes 50 μm and 100 μm, Criteria #1, 2, 3, and 4 release their mass earlier than the new Hanna criterion does; actually some of the Criterion #5 mass is released earlier than predicted by the other methods but that mass fraction is quite small for the 50 and 100 μm drops.

2. For the cases where drop concentration, ambient relative humidity, ambient temperature, and ambient profile distribution were varied, we see essentially no changes. For drop concentration variation, there indeed were no changes. Indeed, for Criteria #1, 2, 3, and 4, changes were present but were insignificant. For Criterion #5, the formulation for mass fraction breaking away depends only on local plume radius; this plume radius is not significantly affected by our changes in ambient relative humidity and ambient dry bult temperature. Surprisingly, the effect of changing the vertical ambient profile showed insignificant effects as compared to Criteria #1, 2, and 4. In our opinion, this insensitivity of Criteria #3 and 5 to such significant ambient changes indicates a lack of physical representation.

3. The effect of wind speed is very interesting. When the wind is increased from 1 m/s to 4, 5, 10, and 20 m/s, the mass fraction released from the plume between 0-100 m is greater than the 1 m/s case. The mass fractions then decrease (compared to the U = 1 m/s case) from 100 m to about 400 m. At 400 m, all the mass of 200 μm drops has been emitted from the plume for U = 1 m/s. However, beyond 400 m, mass is still released up to a larger distance depending on wind speed. The effect of wind speed is not as great for Criterion #5 as it was for Criteria #1, 2, 3, and 4.

CONCLUSIONS

It is clear from the above study that the five breakaway criteria tested provide significantly different predictions of droplet breakaway locations and resulting drop deposition distances for the intermediate range of droplet sizes, 100-850 μm.

The breakaway criteria are least sensitive for the smallest (D_o < 100 μm) and largest droplets (D_o > 850 μm). Other than initial droplet size, the second most important parameter in determining breakaway location and deposition distance is ambient wind speed, not only on its effect on the plume (and therefore the drop), but also its effect on drop trajectory after breakaway. Surprisingly, Criteria #3 and 5 show a level of insensitivity to some important variations such as ambient profile chosen (neutral, unstable, or stable) and wind speed for Criterion #5.

Our assessment of which criterion is superior will have to await the completion of our comparisons of our drift model predictions (all five breakaway criterion to be tested) with Chalk Point Dye Study Data.

REFERENCES

1. G. Israel and T. Overcamp. "Drift Deposition Model for Natural-Draft Cooling Towers." IN: Cooling Tower Environment - 1974. Ed. S. R. Hanna and J. Pell. Technical Information Center. U.S. ERDA Conf-740302. 1975.

2. G. Schrecker and D. Rutherford. Personal Communication. Environmental Systems Corporation. Knoxville, Tennessee. 1976.

3. P. R. Slawson and T. M. L. Wigley. "Calculation of Cooling Tower Drift Deposition." Chapter 8 IN: Power Generation: Air Pollution Monitoring and Control. Ed. K. E. Noll and W. T. Davis. Ann Arbor Science Publishers. 1976.

4. S. R. Hanna. "Meteorological Effects of the Mechanical-Draft Cooling Towers of the Oak Ridge Gaseous Diffusion Plant": IN: Cooling-Tower Environment - 1974. Eds. J. Pell and S. Hanna. p. 291-306. 1974.

5. M. Wolf. Personal Communication. Letter of July 7, 1976. Battelle Pacific Northwest Laboratories. Richland, Washington. July 1976.

6. S. R. Hanna. "A Simple Deposition Model Applied to the Chalk Point Dye Tracer Experiment." Atmospheric Turbulence and Diffusion Laboratory. Oak Ridge, Tennessee. IN: Cooling-Tower Environment - 1978 Proceedings. Power Plant Siting Program. Maryland Department of Natural Resources. PPSP-CPCTP-22. WRRC Special Report No. 9. May 1978.

Table 7-1

Summary of Formulas for Breakaway Criterion #4

Vapor Concentration in Environs of Droplet

$$C_a = C_a(Z) + \left(\overline{C}_a - C_a(Z)\right) \exp\left[\frac{-2(Z-Z_c)^2}{R_{tw}^2}\right]$$

$$C_d = C_a + 2\,(C-\overline{C}_a) \exp\left[\frac{-2(Z-Z_c)^2}{R_{pm}^2}\right]$$

where

R_{tw} = radius of tower

R_{pm} = moisture radius of plume at local drop position

$C_a(Z)$ = ambient vapor concentration calculated from the local ambient temperature and humidity at elevation Z

$\overline{C}_a$ = ambient vapor concentration averaged over ambient encompassing plume cross-section

C = plume vapor concentration averaged across plume (top hat value) above drop calculated from plume temperature and plume mixing ratio

C_d = vapor concentration "seen" by drop

Z = vertical elevation (of drop)

Z_c = vertical elevation of plume centerline

Temperature in Environs of Droplet

$$T_a = T_a(Z) + \left(\overline{T}_a - T_a(Z)\right) \exp\left[\frac{-2(Z-Z_c)^2}{R_{tw}^2}\right]$$

$$T_d = T_a + 2\,(T-\overline{T}_a) \exp\left[\frac{-2(Z-Z_c)^2}{R_{pt}^2}\right]$$

where

R_{tw} = radius of tower

R_{pt} = temperature radius of plume at local drop position

$T_a(Z)$ = ambient temperature at elevation Z of drop

$\overline{T}_a$ = ambient temperature averaged over plume cross-section

T = plume temperature averaged across plume cross section (top hat value)

T_d = "ambient" temperature that drop "sees"

Z = vertical elevation (of drop)

Z_c = vertical elevation of plume centerline

Table 7-1 (Continued)

Summary of Formulas for Breakaway Criterion #4

Vertical Velocity of Drop

$$W = W_p \exp\left[\frac{-2(Z-Z_c)^2}{R_{pm}^2}\right]$$

where

W = upward velocity acting on drop from influence of plume

W_p = plume centerline velocity above drop (top-hat value)

R_{pm} = momentum radius of plume

Z = vertical elevation (of drop)

Z_c = vertical elevation of plume centerline

Note: An iterative scheme is used to check whether the computed vapor concentration and temperature "seen" by the drop lead to supersaturated conditions. If so, a correction is made to assume only saturation conditions.

Table 7-2

Variable Ambient Conditions Tested in the Parametric Study
on the Effects of Different Breakaway Criteria

NEUTRAL:

$$\begin{cases} T(z) = T(10m) - 0.01\,[z - 10] \\ U(z) = U(10m) \cdot \left[\frac{z}{10}\right]^{1/7} \\ q = \text{Constant} \end{cases}$$

MODERATELY STABLE:

$$\begin{cases} T(z) = T(10m) + 0.028\,[z - 10] \\ U(z) = U(10m) \cdot \left[\frac{z}{10}\right]^{0.45} \\ q = \text{Constant} \end{cases}$$

MODERATELY UNSTABLE:

$$\begin{cases} T(z) = T(10m) - 0.018\,[z - 10] \\ U(z) = U(10m) \cdot \left[\frac{z}{10}\right]^{0.1} \\ q = \text{Constant} \end{cases}$$

Note: The value of q is the mixing ratio at T = 10°C, RH = 70%.

Note: The average temperature and wind speed (averaged from ground level to the height where the plume enters the diffusion phase) for each of the three profiles is equal to t = 10°C, U = 4 m/s. These latter values are the constant ambient variables for our standard case. Fully-mixed conditions (q = Constant) is assumed for each of the three profiles and is the same mixing ratio as for our uniform profile standard case.

Table 7-3

Comparison of Droplet Characteristics at Breakaway and at Deposition Predicted from the ANL Drift Model under Different Breakaway Criteria

		Diameter (μm)														
		D=50	D=100	D=200	D=300	D=400	D=500	D=600	D=700	D=800	D=900	D=1000	Standard	Stable	Neutral	Unstable
Height of Release (Km)	1	.319	.319	.319	.318	.302	.274	.250	.229	.209	.189	.124	.319	.256	.485	.563
	2	.318	.301	.270	.234	.203	.174	.155	.138	.131	.127	.124	.270	.239	.368	.448
	3	.318	.273	.218	.185	.167	.155	.144	.136	.131	.128	.124	.218	.234	.219	.218
Distance to Release Point (Km)	1	.307	.305	.303	.299	.254	.192	.147	.116	.089	.065	0.0	.303	.154	.770	.742
	2	.308	.308	.308	.308	.216	.117	.077	.049	.039	.033	0.0	.308	.157	.783	.749
	3	.308	.218	.127	.089	.069	.058	.048	.039	.035	.031	0.0	.127	.136	.128	.128
Distance to Deposition (Km)	1	823.	203.	43.8	12.7	1.33	.794	.577	.499	.351	.276	0.0	43.8	26.8	65.6	39.0
	2	820.	191.	36.0	6.70	.816	.478	.339	.247	.202	.174	0.0	36.0	23.1	48.5	37.2
	3	820.	173.	27.5	2.99	.542	.379	.290	.233	.199	.172	0.0	27.5	21.9	25.2	26.2
	4	795.	169.	32.9	6.06	.708	.473	.369	.308	.265	.234	.212	32.0	3.02	44.3	34.3
Final Diameter (μm)	1	11.9	23.8	47.1	71.2	162.	386.	524.	644.	757.	866.	*	47.1	47.6	47.6	47.6
	2	11.9	23.8	47.1	71.2	276.	433.	554.	666.	773.	877.	*	47.1	47.5	47.5	47.6
	3	11.9	23.8	47.1	71.2	304.	440.	557.	667.	773.	877.	*	47.1	47.4	47.6	47.6
	4	11.8	23.7	47.4	71.2	264.	414.	533.	643.	750.	854.	956.	47.4	99.1	47.4	47.0

*-Fell into tower
1-Criterion #1...drop settling velocity greater than updraft velocity of plume
2-Criterion #2...vertical fall of droplet greater than plume radius measured vertically
3-Criterion #3...horizontal deviation of droplet from plume centerline equals initial plume radius
4-Criterion #4...combined method in which drop undergoes a continuous transition between plume and ambient conditions

Table 7-3 (Continued)

Comparison of Droplet Characteristics at Breakaway and at Deposition Predicted from the ANL Drift Model under Different Breakaway Criteria

		Ambient Relative Humidity				Ambient Temperature				Wind Velocity				Drop Salt Concentration	
		RH=.30	RH=.70	RH=.80	RH=.90	T=-10	T=0	T=10	T=20	U=1.0	U=4.0	U=5.0	U=10.0	U=20.0	C=.005	C=.05
Height of Release (Km)	1	.318	.319	.320	.334	.307	.311	.319	.328	.568	.319	.285	.188	.130	.319	.319
	2	.265	.270	.273	.284	.258	.263	.270	.278	.553	.270	.234	.145	.083	.270	.270
	3	.211	.218	.219	.219	.205	.209	.218	.222	.553	.218	.185	.141	.129	.218	.218
Distance to Release Point (Km)	1	.325	.303	.291	.307	.299	.296	.303	.308	.087	.303	.387	.577	.060	.303	.303
	2	.331	.308	.296	.311	.304	.301	.308	.313	.089	.308	.394	.970	2.10	.308	.308
	3	.119	.127	.128	.129	.119	.120	.127	.128	.089	.127	.118	.089	.065	.127	.127
Distance to Deposition (Km)	1	48.7	43.8	10.9	7.05	28.1	38.0	43.8	49.0	21.1	43.8	48.6	57.7	67.7	43.8	9.33
	2	40.2	36.0	9.03	5.56	20.6	30.4	36.0	40.6	20.5	36.0	38.1	41.0	31.6	36.0	7.67
	3	31.2	27.5	6.67	3.46	12.4	21.7	27.5	31.3	20.5	27.5	28.1	38.2	66.8	27.5	5.73
	4	39.6	32.0	7.46	3.89	14.7	25.2	32.0	37.1	9.0	32.0	34.7	47.1	66.0	32.0	6.26
Final Diameter (μm)	1	47.6	47.1	51.8	62.5	47.5	47.6	47.1	47.5	47.5	47.1	47.5	47.6	47.6	47.1	104.
	2	47.6	47.1	51.8	62.5	47.5	47.6	47.1	47.5	47.5	47.1	47.5	47.6	47.6	47.1	104.
	3	47.6	47.1	51.8	62.5	47.5	47.6	47.1	47.5	47.5	47.1	47.5	47.6	47.6	47.1	104.
	4	47.5	47.4	51.7	63.2	47.5	47.4	47.4	47.4	47.2	47.4	47.3	47.3	47.5	47.4	103.

1-Criterion #1...drop settling velocity greater than updraft velocity of plume
2-Criterion #2...vertical fall of droplet greater than plume radius measured vertically
3-Criterion #3...horizontal deviation of droplet from plume centerline equals initial plume radius
4-Criterion #4...combined method in which drop undergoes a continuous transition between plume and ambient conditions

Table 7-4

Composition of Drop Characteristics at Breakaway and at Deposition Predicted from the ANL Drift Model under Breakaway Criterion #5 (New Hanna)

Downwind Distance (m)	D=50	D=100	D=200	...	C=.05	RH=.3	RH=.8	RH=.9	T=-10	T=0	T=20	U=1	U=5	U=10	U=20	Stable	Neutral	Unstable
100	.042	.162	.435	...	.435	.434	.435	.435	.444	.440	.428	.333	.438	.419	.392	.405	.431	.435
200	.011	.042	.130	...	.130	.140	.137	.136	.141	.139	.136	.356	.126	.097	.067	.134	.133	.134
300	.01	.032	.099	...	.099	.100	.098	.097	.101	.099	.098	.210	.091	.073	.049	.111	.094	.093
400	.007	.026	.085	...	.085	.085	.085	.082	.086	.085	.082	.101 to 360	.076	.061	.041	.102	.076	.074
500	.006	.023	.078	...	.078	.077	.076	.075	.080	.079	.076		.067	.054	.036	.095	.065	.062
600	.006	.022	.073	...	.073	.075	.073	.071	.075	.074	.072		.064	.048	.033	.089	.057	.053
700	.005	.021	.069	...	.069	.069	.068	.067	.071	.070	.068		.061	.045	.030	.064 to 680	.051	.046
800	.005	.019	.023 to 740	...	.023 to 740	.02 to 740	.028 to 740	.037 to 770	.002 to 710	.014 to 720	.04 to 770		.058	.042	.028		.047	.043
900	.005	.019		...									.019 to 840	.039	.027		.044	.039
1000	.004	.017		...										.037	.025		.002 to 910	.024 to 960
1100	.004	.017		...										.035	.025			
1200	.004	.016		...										.034	.025			
1300	.004	.015		...										.016 to 1250	.025			
1400	.003	.014		...											.024			
1500	.003	.014		...											.024			
2000	.016	.060		...											.11			
2500	.002 to 2070	.008 to 2070		...											.039 to 2250			
3000				...														
3500				...														
Sum	.137 at 2070	.527 at 2070	1.0 at 740	...	1.0 at 740	1.0 at 740	1.0 at 740	1.0 at 770	1.0 at 710	1.0 at 720	1.0 at 770	1.0 at 360	1.0 at 840	1.0 at 1250	1.0 at 2250	1.0 at 680	1.0 at 910	1.0 at 960

Table 7-4 (Continued)

		D=300	D=400	D=500	D=600	D=700	D=800	D=900	D=1000
	10	.302	.409	.512	.614	.717	.819	.921	1.0
	20	.099	.134	.168	.202	.235	.181	.079	
	30	.059	.08	.100	.120	.048			
	40	.047	.064	.080	.064				
	50	.043	.058	.073					
	60	.040	.054	.067					
Downwind	70	.036	.049						
Distance	80	.034	.046						
(m)	90	.032	.043						
	100	.030	.110						
	150	.126	.002 to 110						
	200	.102							
	250	.05 to 230							
	300								
	350								
	Sum	1.0 at 230	1.0 at 110	1.0 at 60	1.0 at 40	1.0 at 30	1.0 at 20	1.0 at 20	1.0 at 10

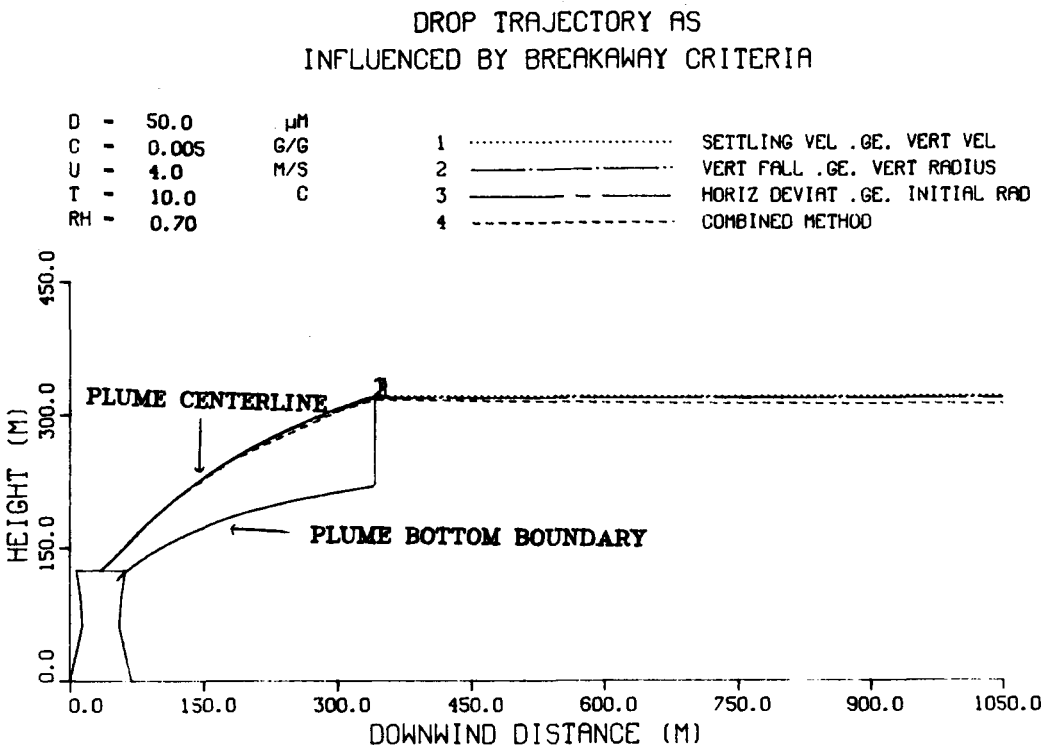

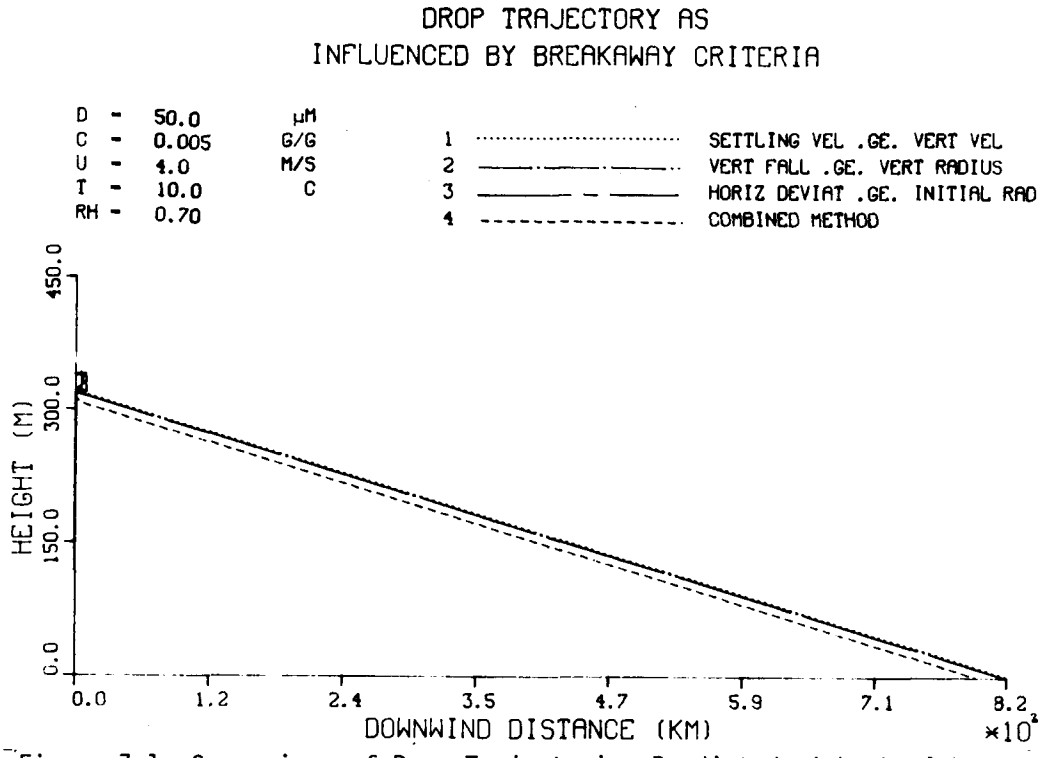

Figure 7-1 Comparison of Drop Trajectories Predicted with the ANL Drift Model under Different Breakaway Criteria

... D=50 μm

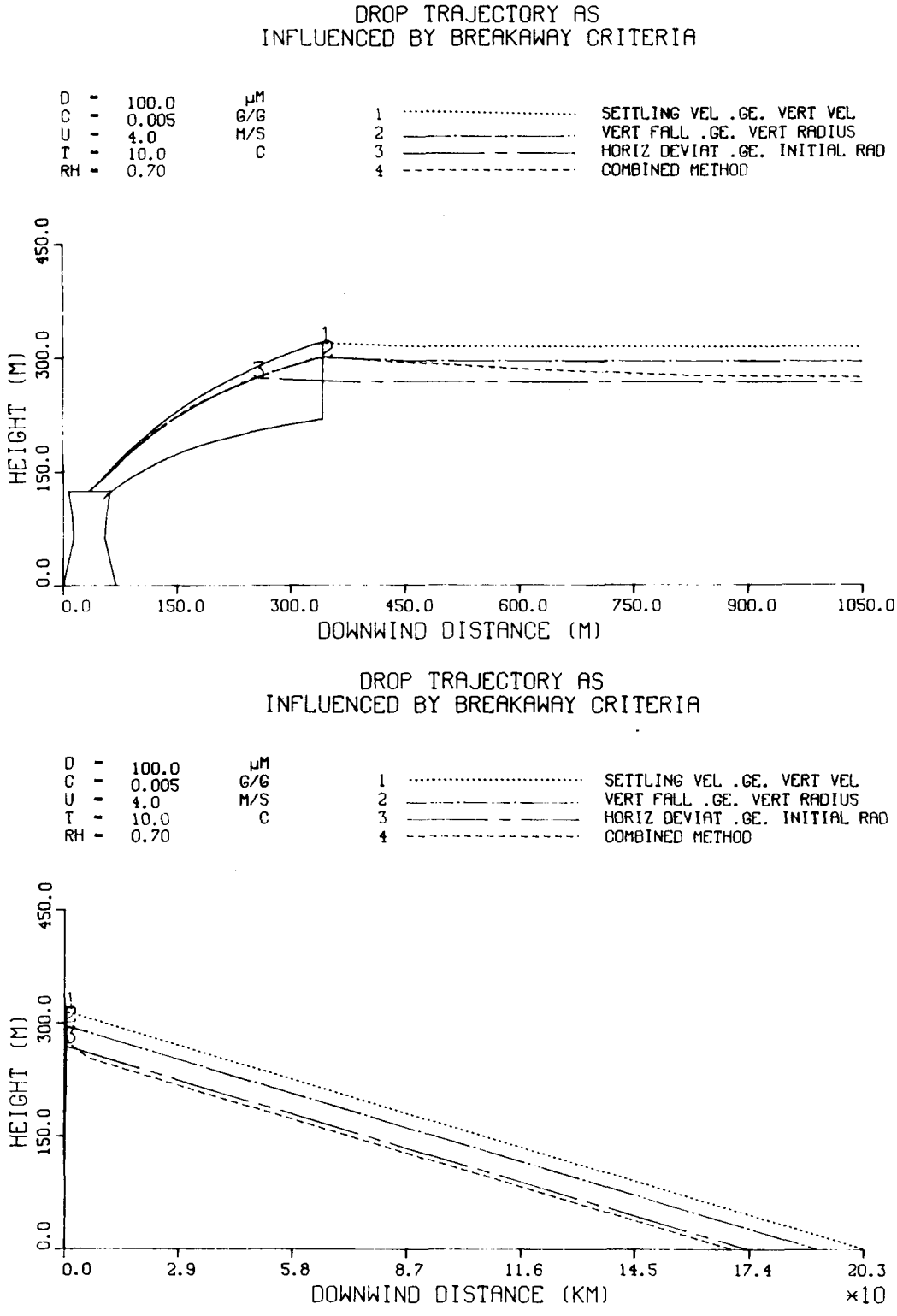

Figure 7-2 Comparison of Drop Trajectories Predicted with the ANL Drift Model under Different Breakaway Criteria

... D=100 µm

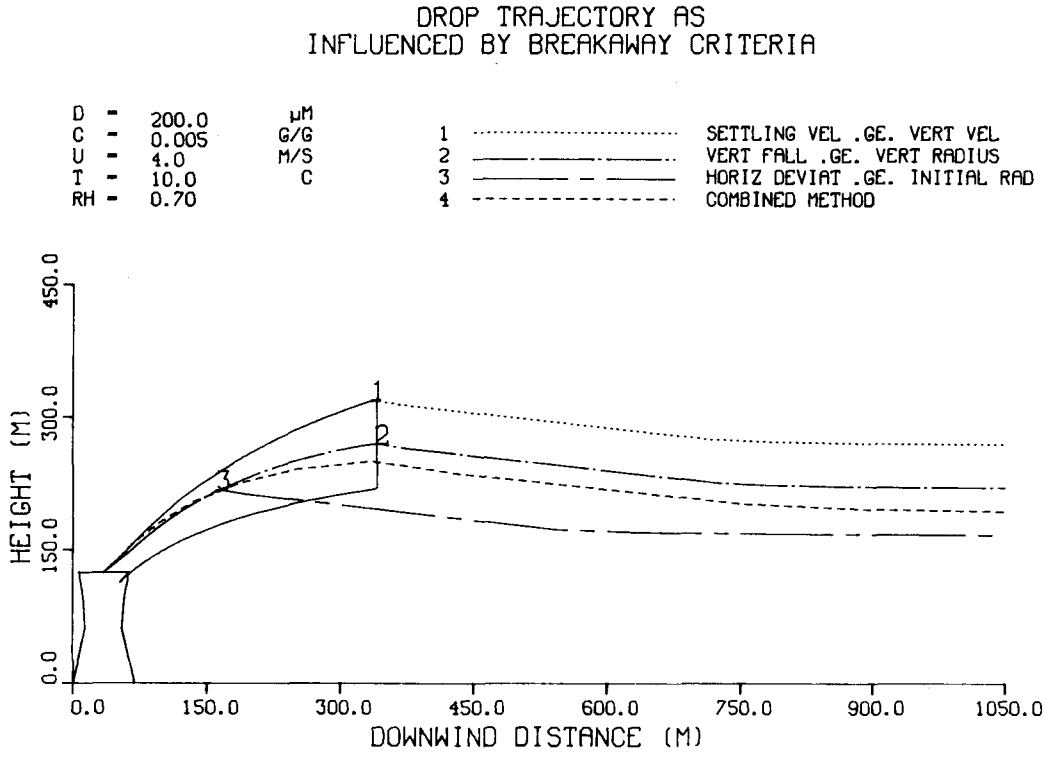

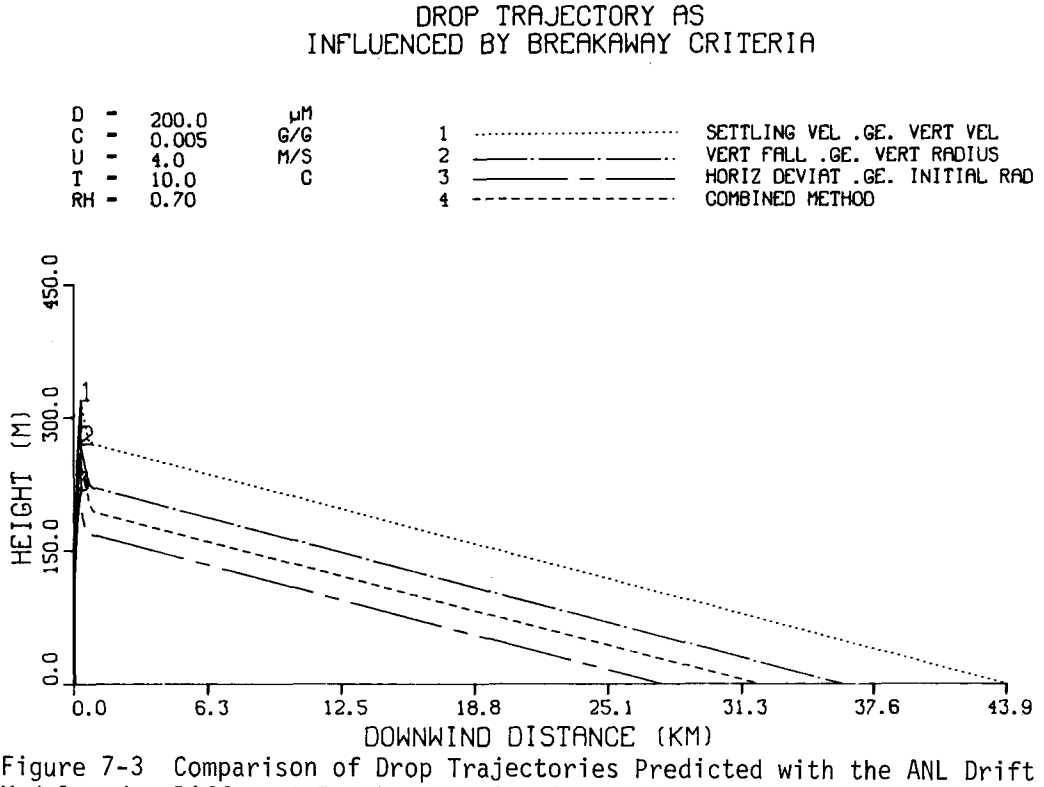

Figure 7-3 Comparison of Drop Trajectories Predicted with the ANL Drift Model under Different Breakaway Criteria

... Standard Case
... D=200 µm

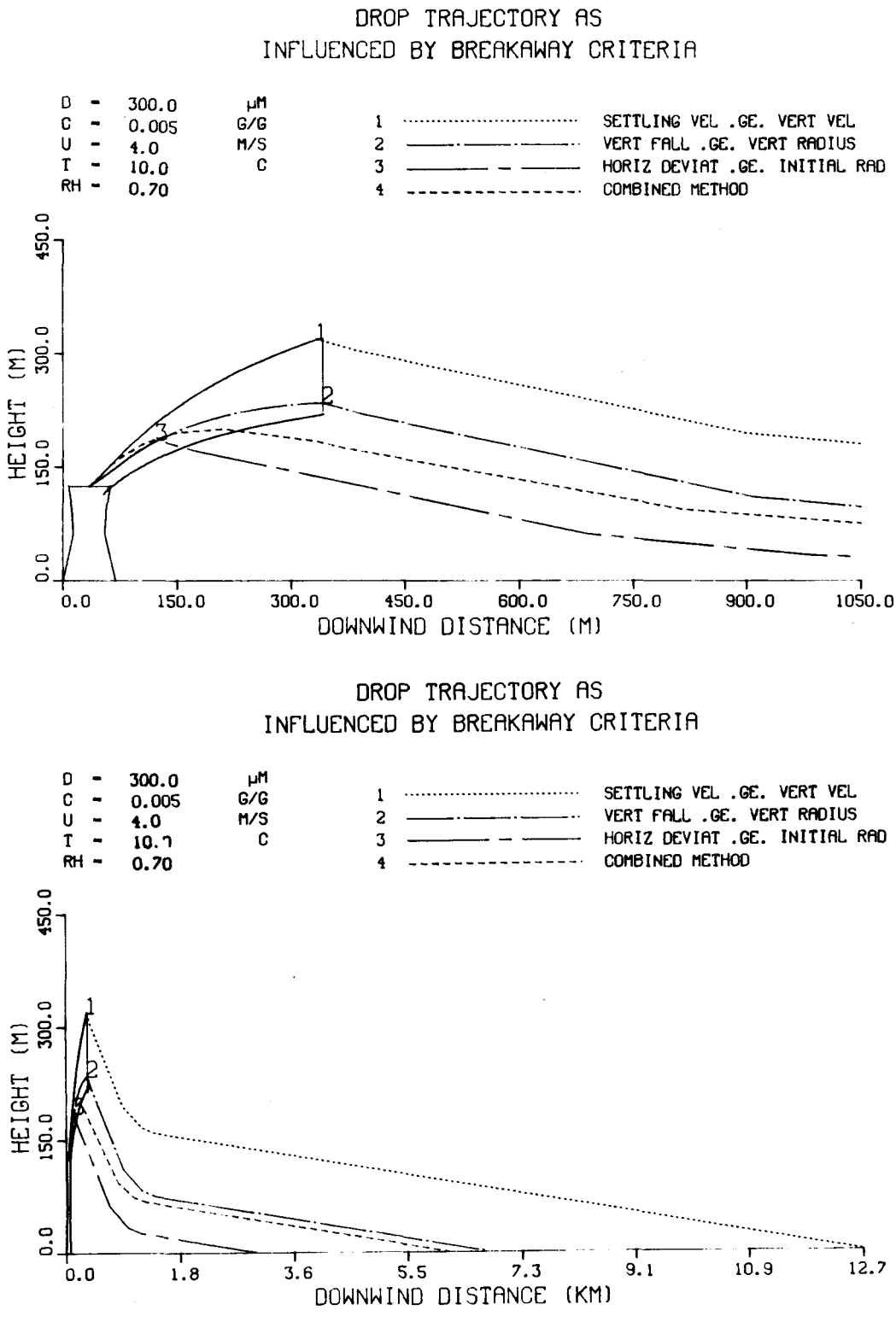

Figure 7-4 Comparison of Drop Trajectories Predicted with the ANL Drift Model under Different Breakaway Criteria

... D=300 µm

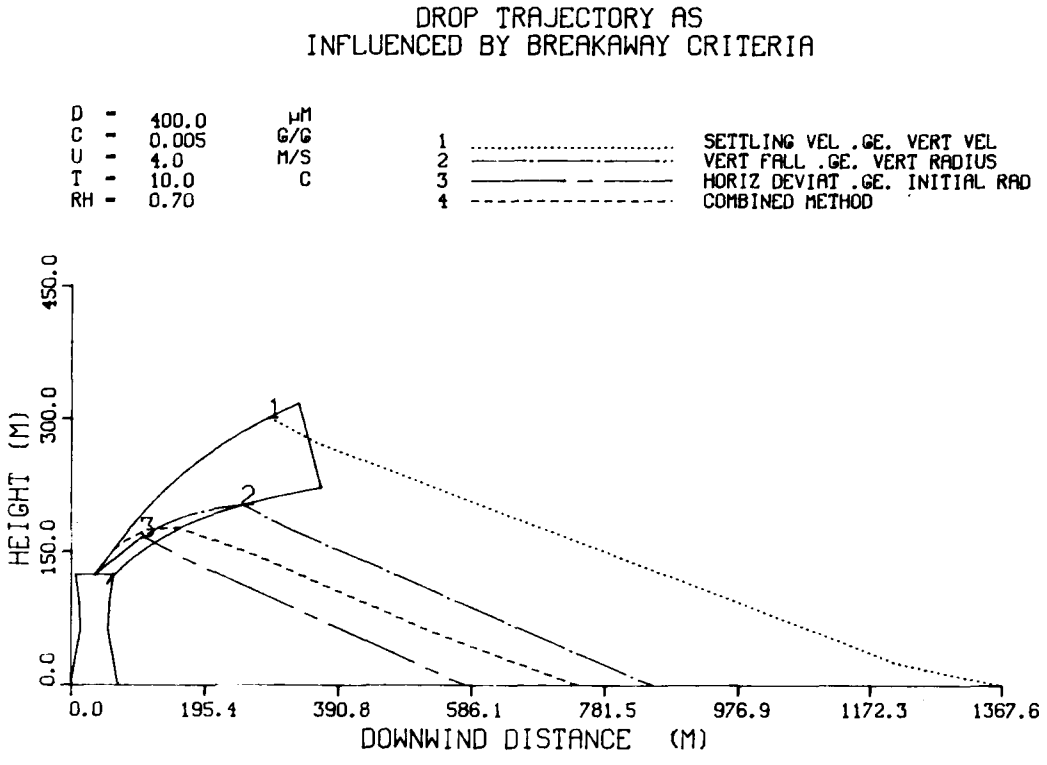

Figure 7-5 Comparison of Drop Trajectories Predicted with the ANL Drift Model under Different Breakaway Criteria

... D=400 µm

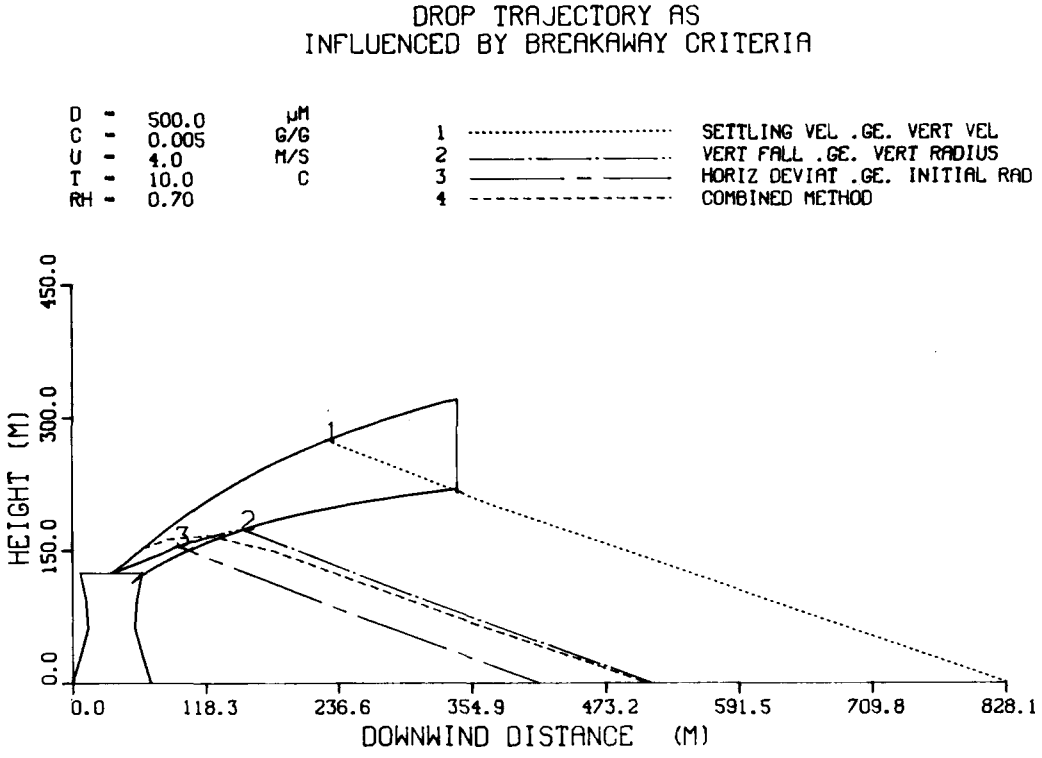

Figure 7-6. Comparison of Drop Trajectories Predicted with the ANL Drift Model under Different Breakaway Criteria

... D=500 µm

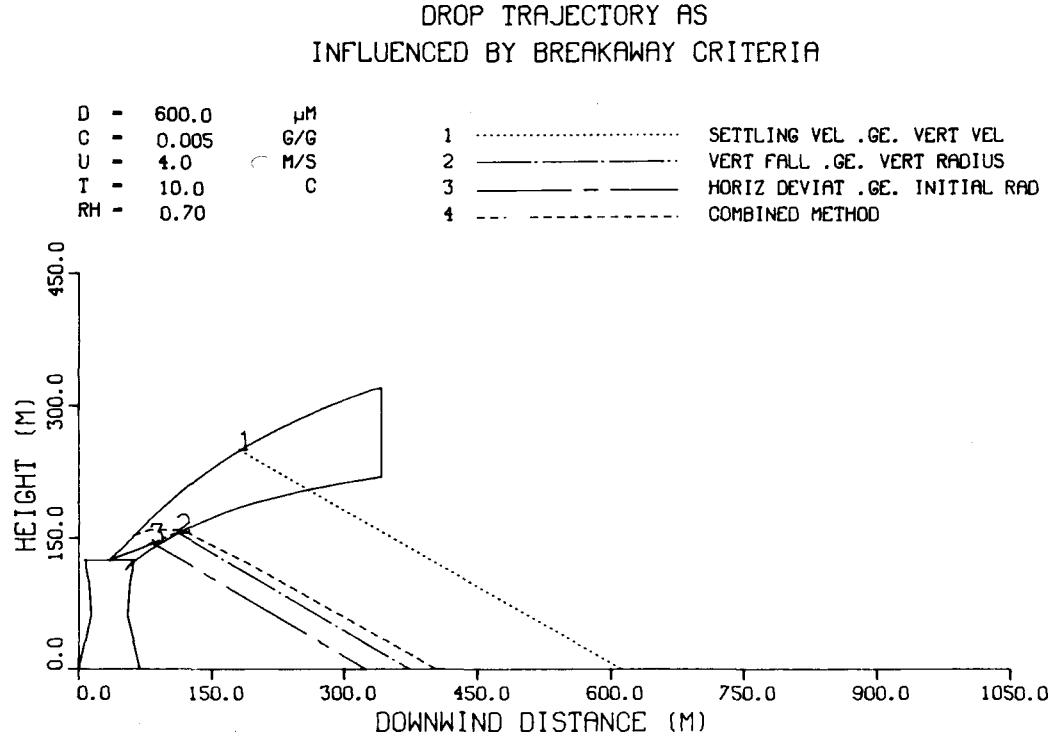

Figure 7-6. Comparison of Drop Trajectories Predicted with the ANL Drift Model under Different Breakaway Criteria

... D=600 µm

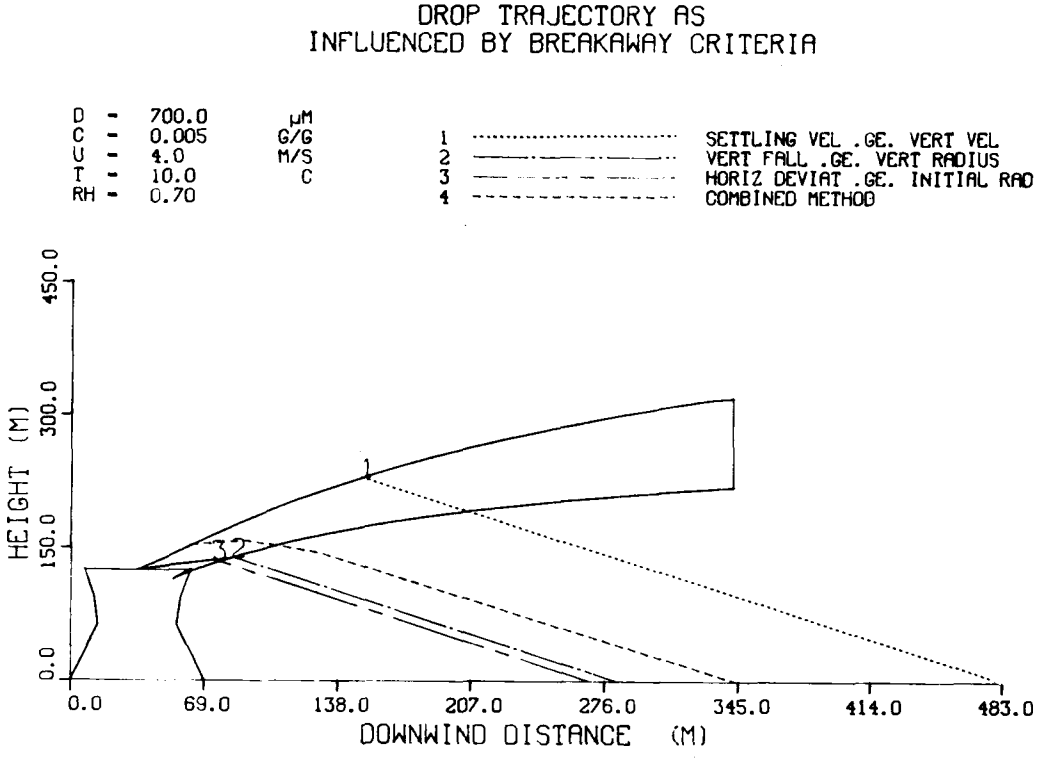

Figure 7-7 Comparison of Drop Trajectories Predicted with the ANL Drift Model under Different Breakaway Criteria

... D=700 μm

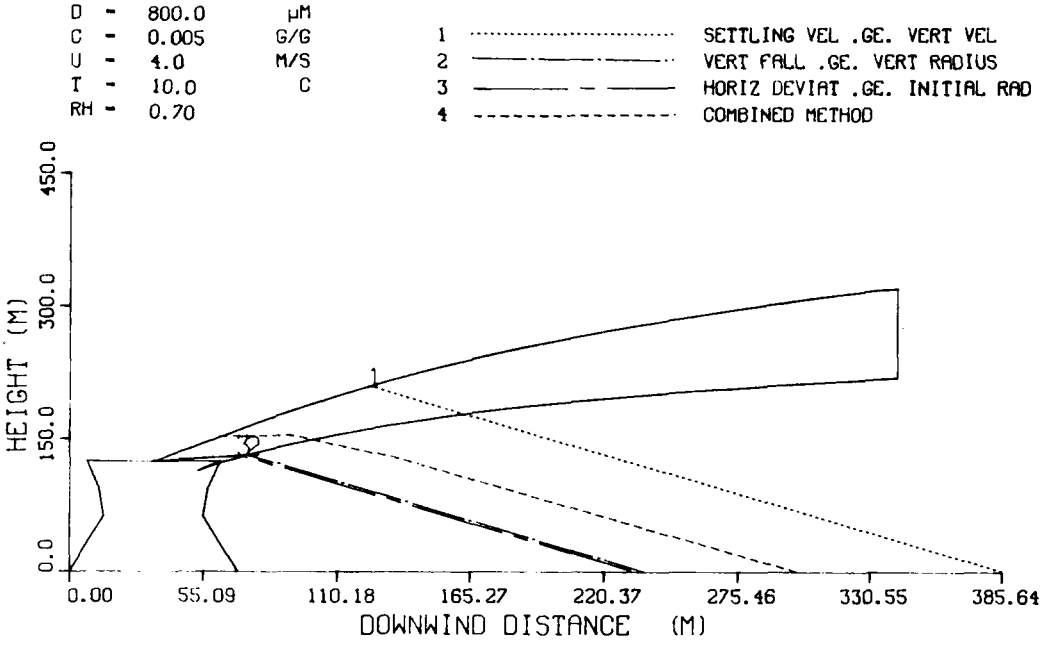

Figure 7-7. Comparison of Drop Trajectories Predicted with the ANL Drift Model under Different Breakaway Criteria

... D=800 μm

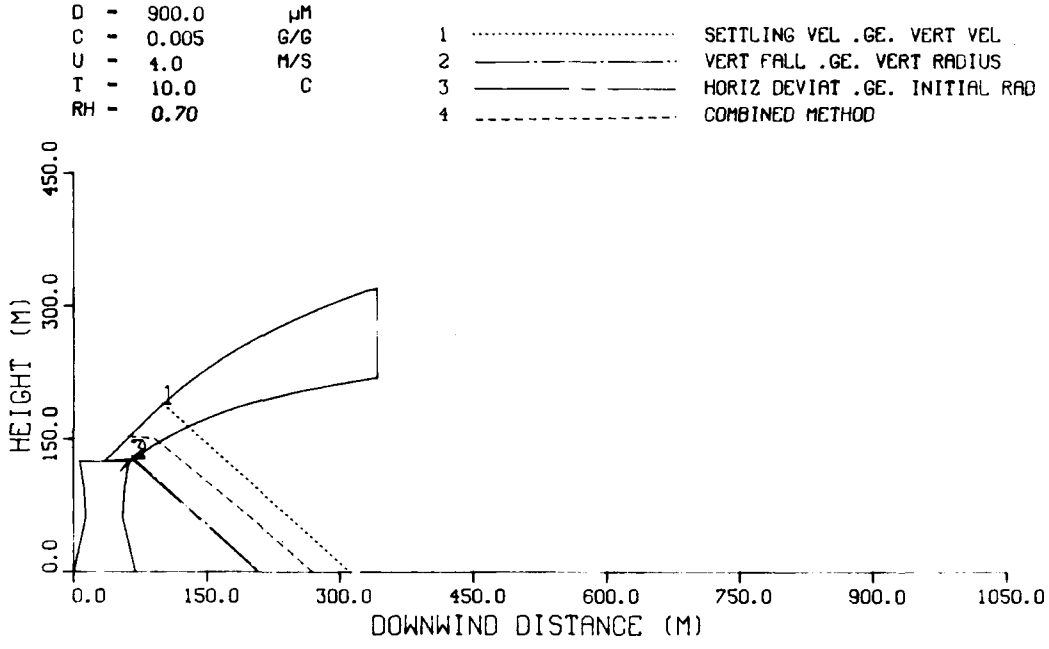

Figure 7-8 Comparison of Drop Trajectories Predicted with the ANL Drift Model under Different Breakaway Criteria

... D=900 μm

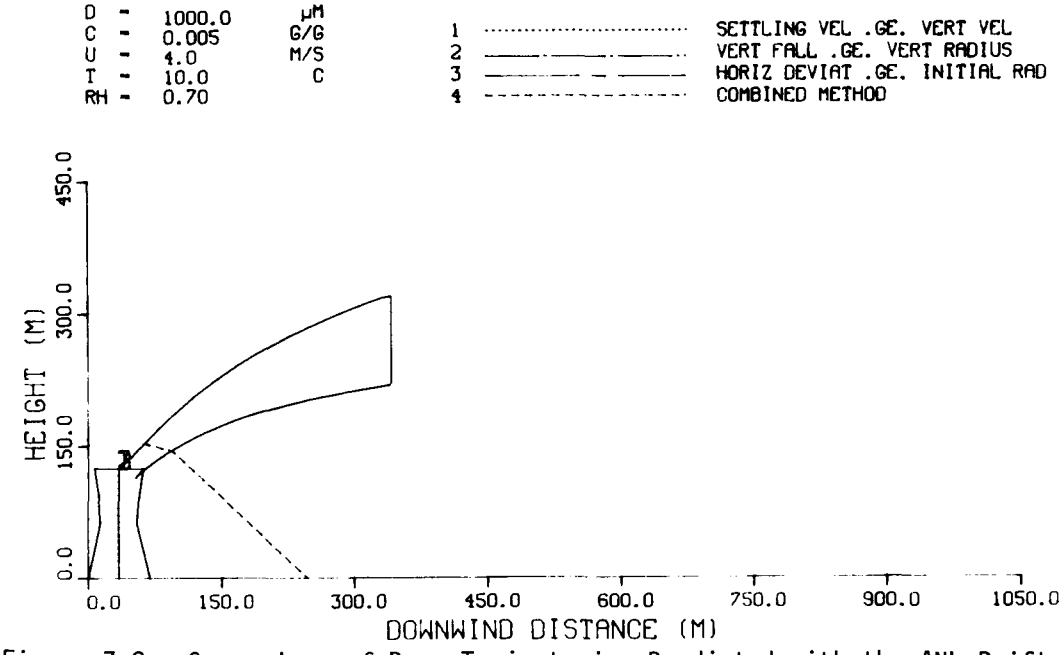

Figure 7-8. Comparison of Drop Trajectories Predicted with the ANL Drift Model under Different Breakaway Criteria

... D=1000 μm

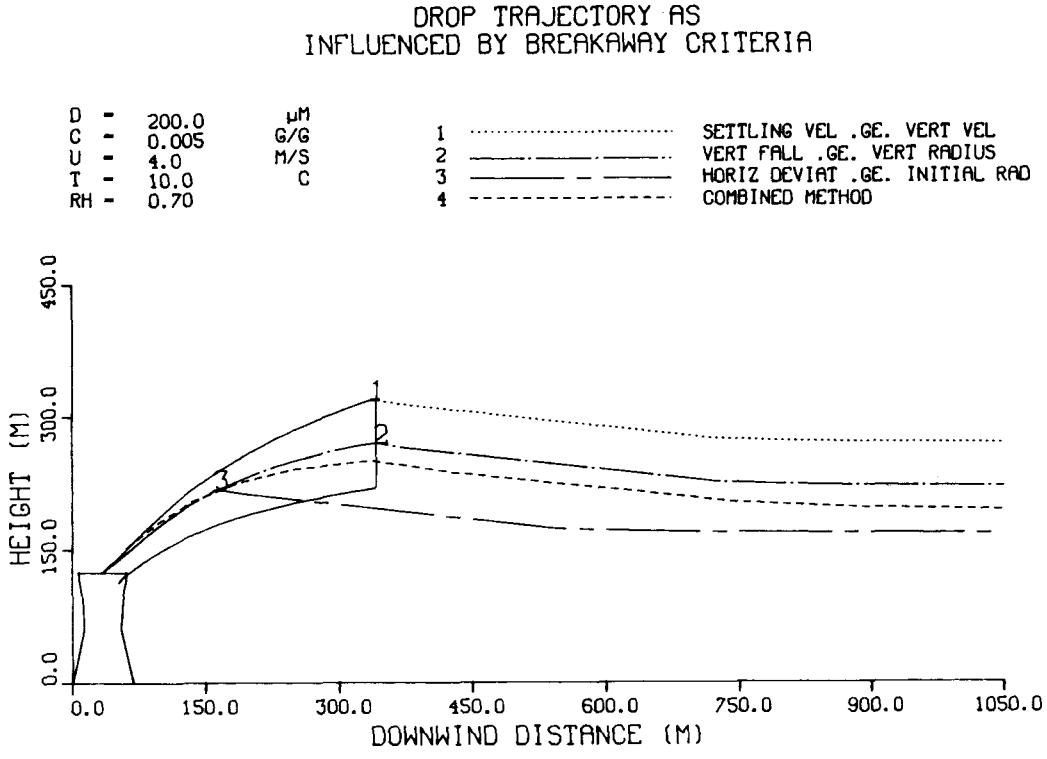

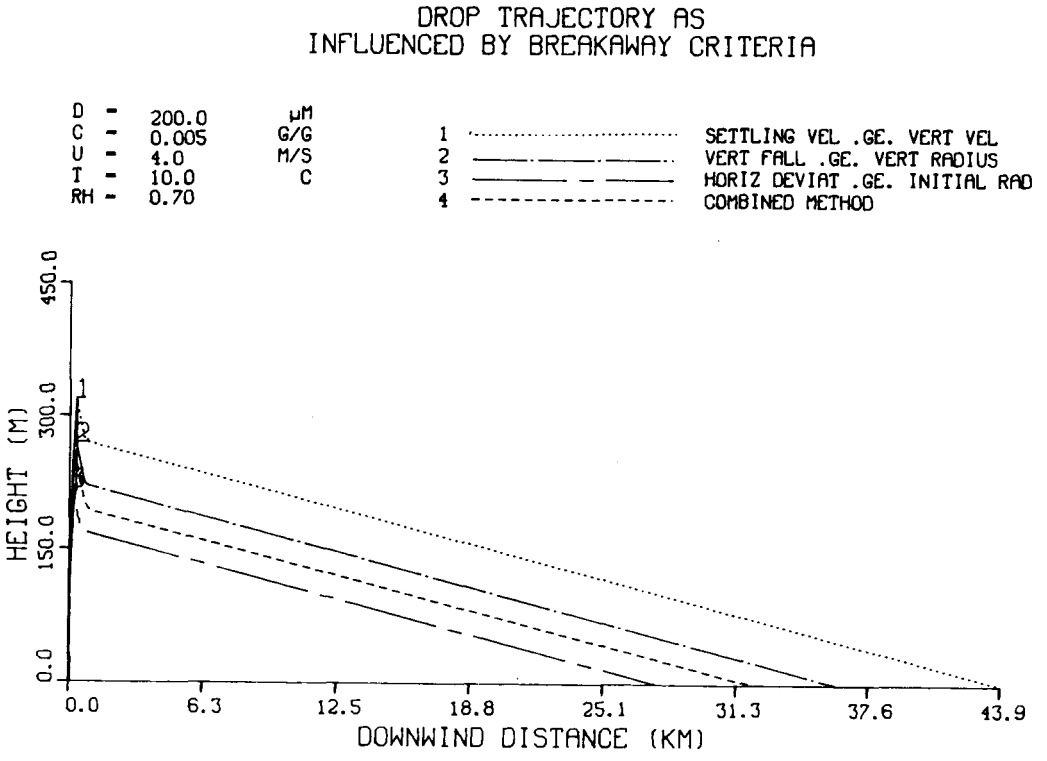

Figure 7-9. Comparison of Drop Trajectories Predicted with the ANL Drift Model under Different Breakaway Criteria

... Standard Case
... D=0.005

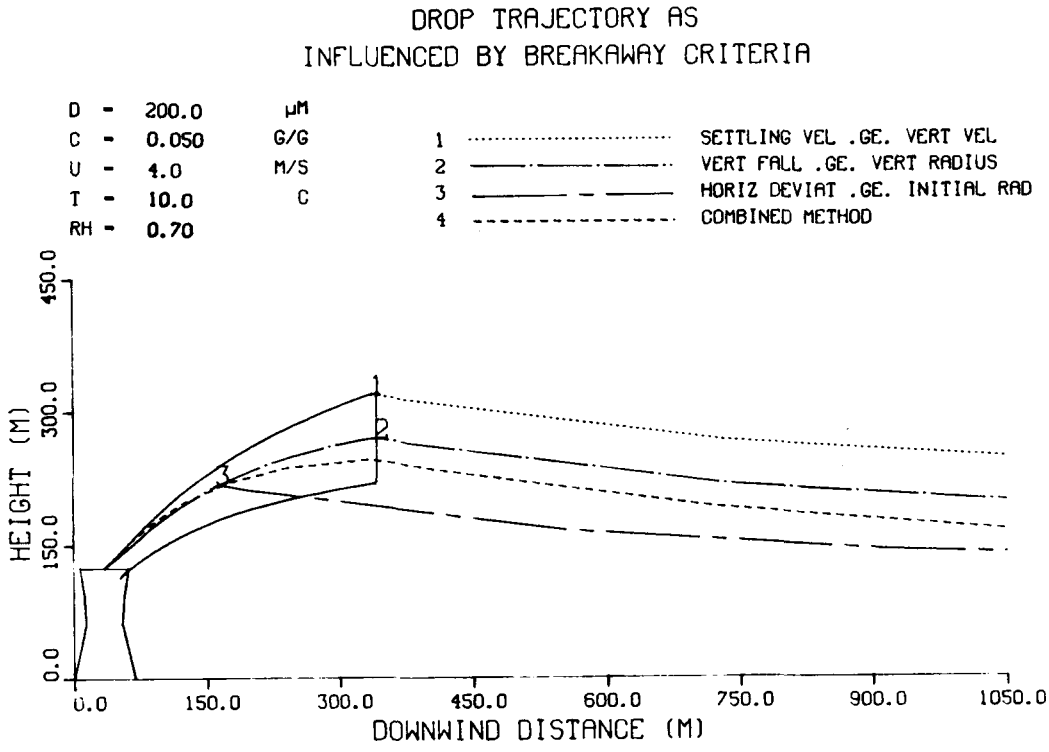

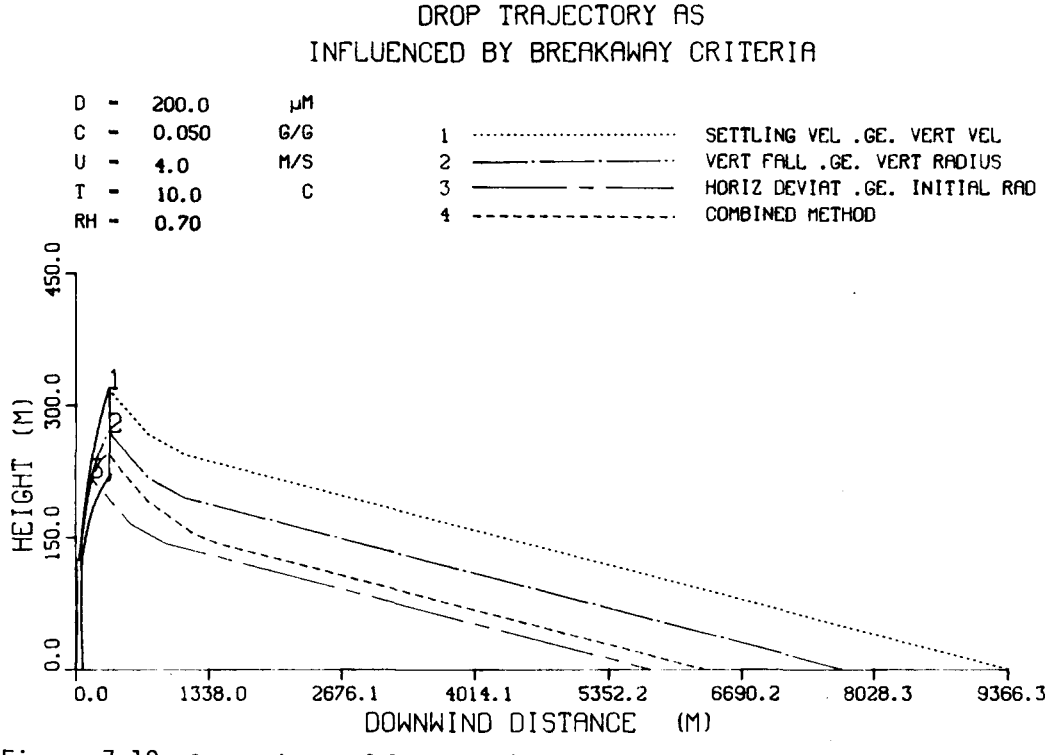

Figure 7-10. Comparison of Drop Trajectories Predicted with the ANL Drift Model under Different Breakaway Criteria

... C=.05

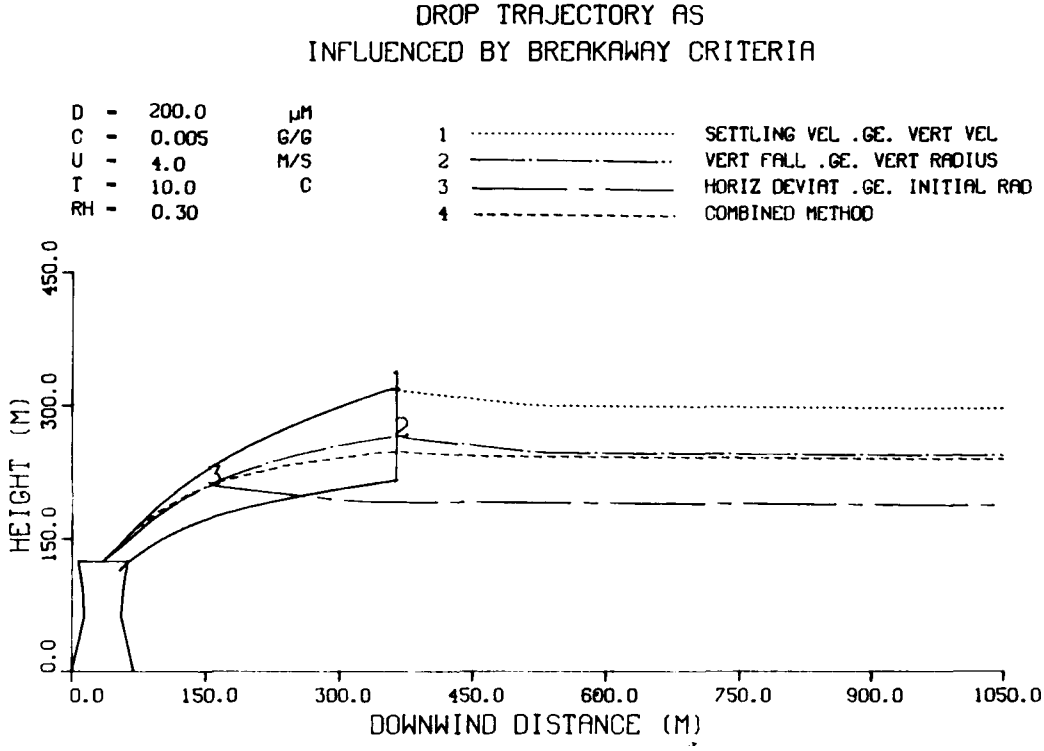

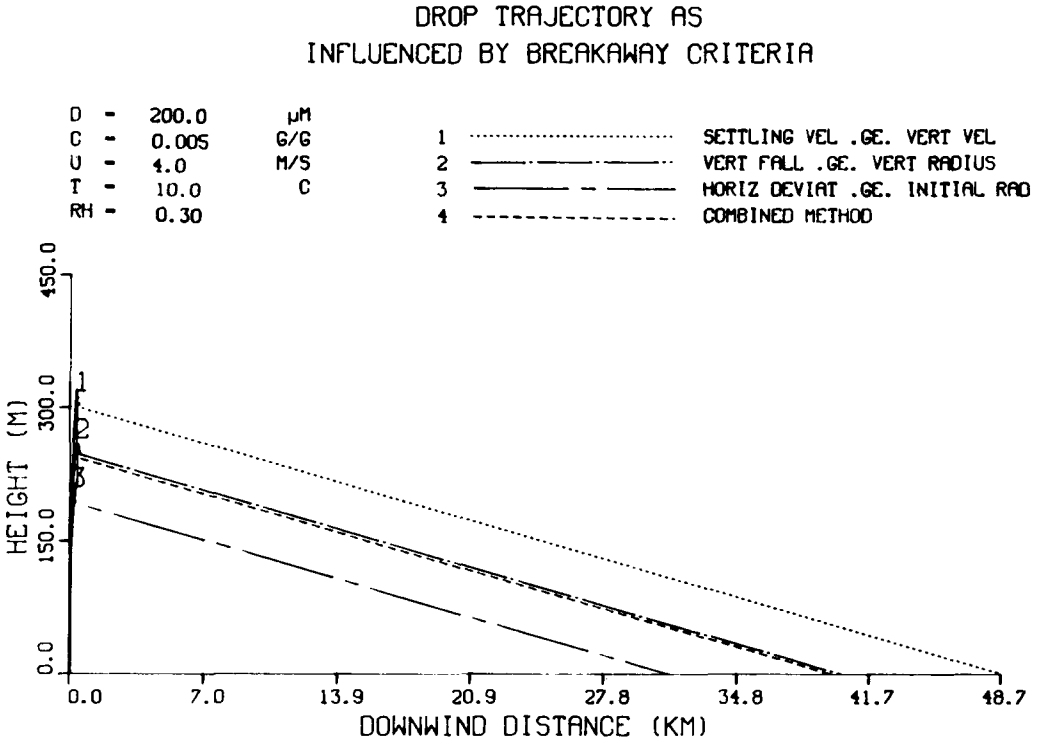

Figure 7-11. Comparison of Drop Trajectories Predicted with the ANL Drift Model under Different Breakaway Criteria

... RH=.30

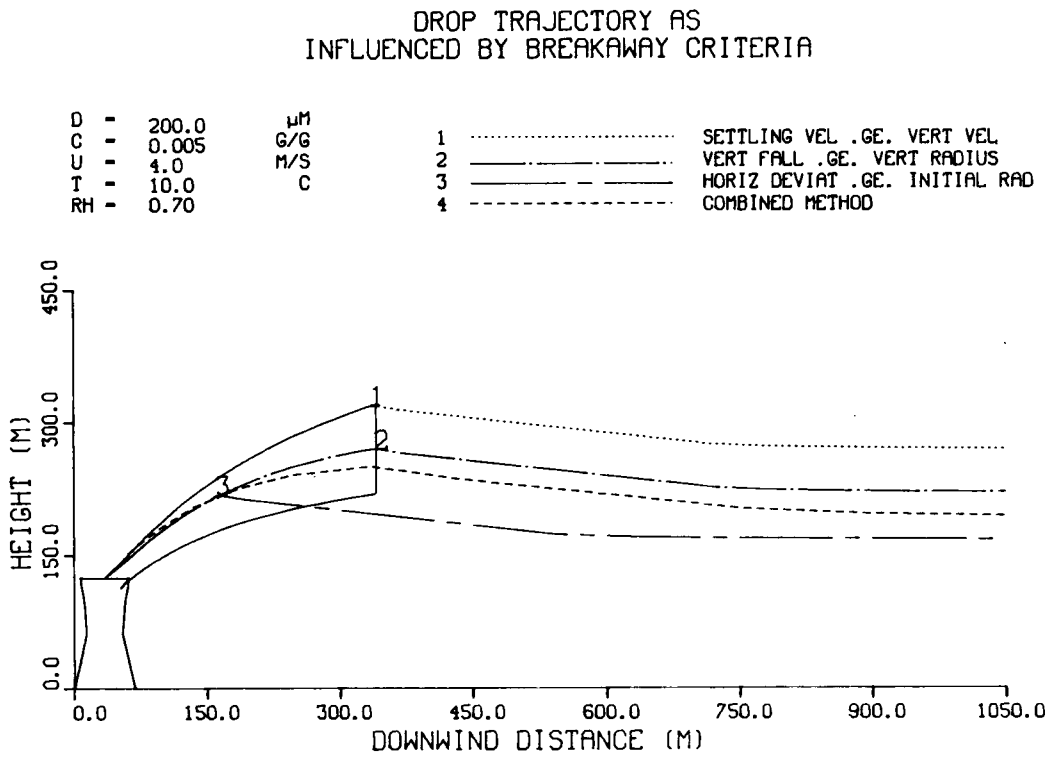

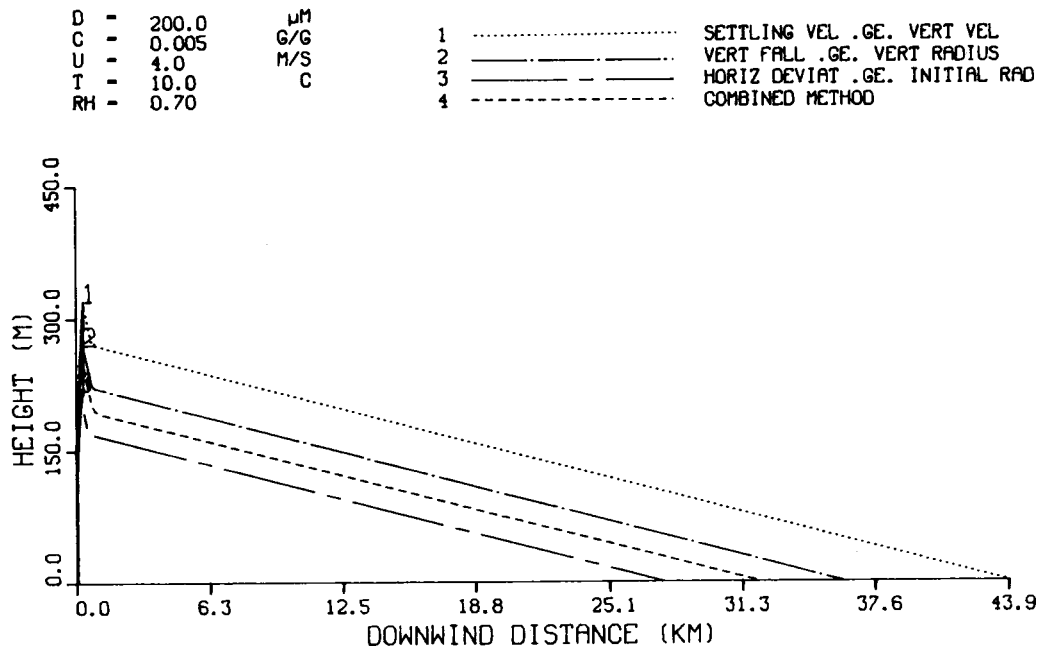

Figure 7-12. Comparison of Drop Trajectories Predicted with the ANL Drift Model under Different Breakaway Criteria

... Standard Case
... RH=.70

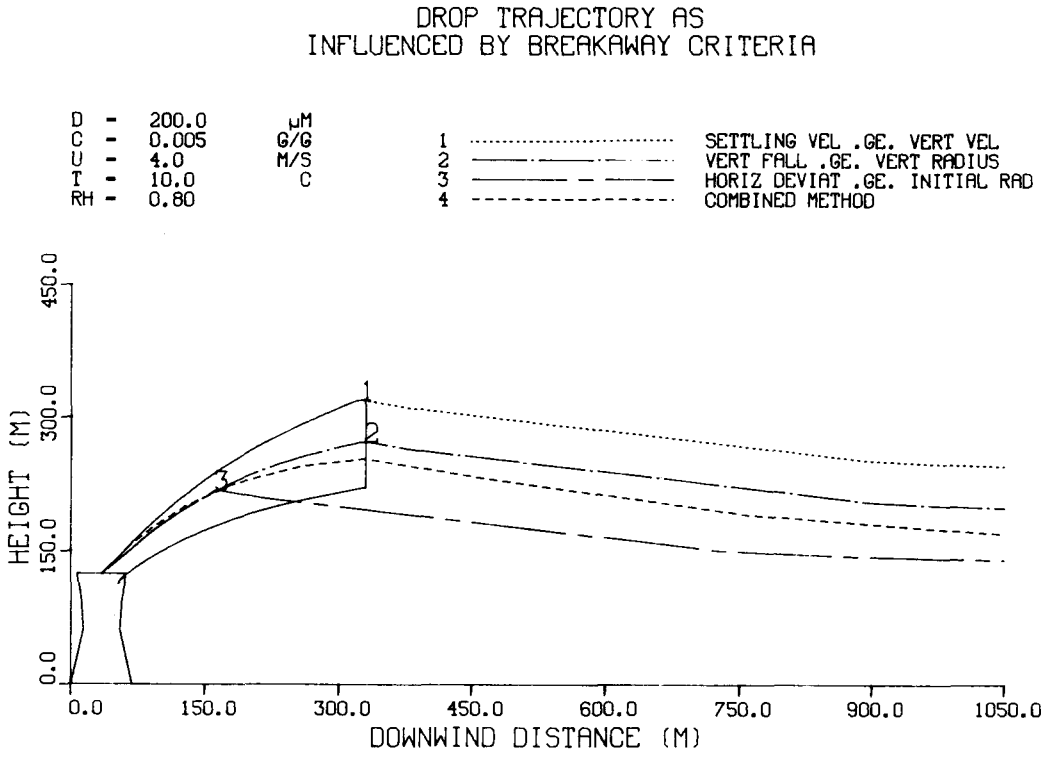

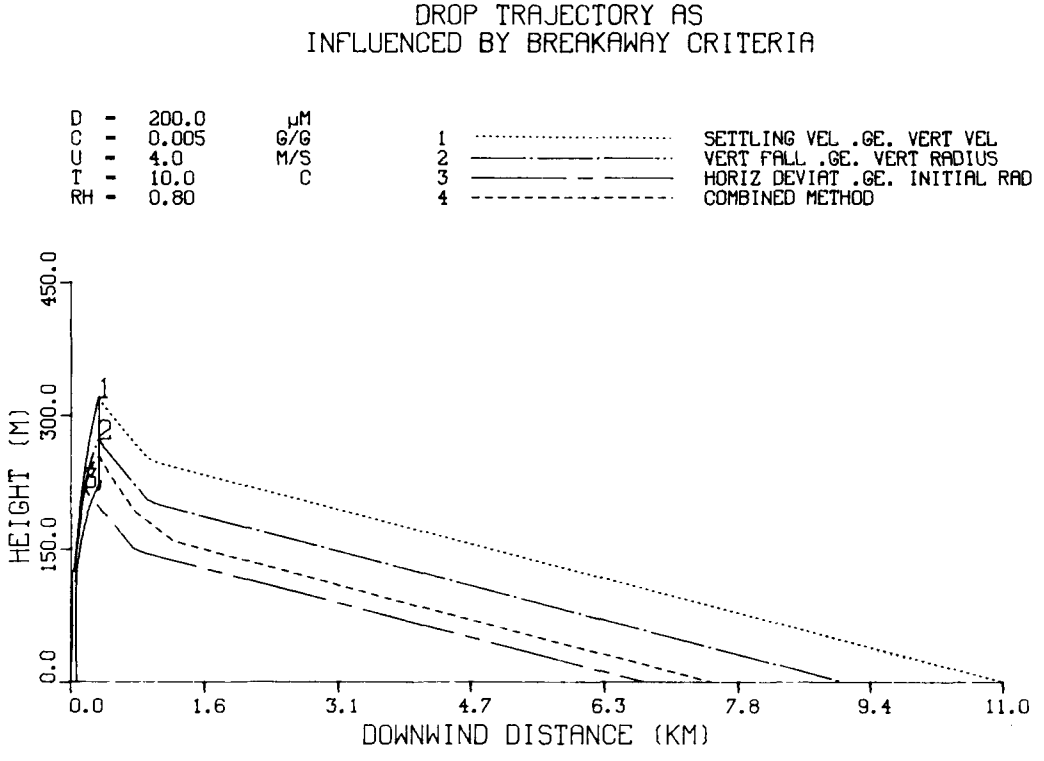

Figure 7-13. Comparison of Drop Trajectories Predicted with the ANL Drift Model under Different Breakaway Criteria

... RH=.80

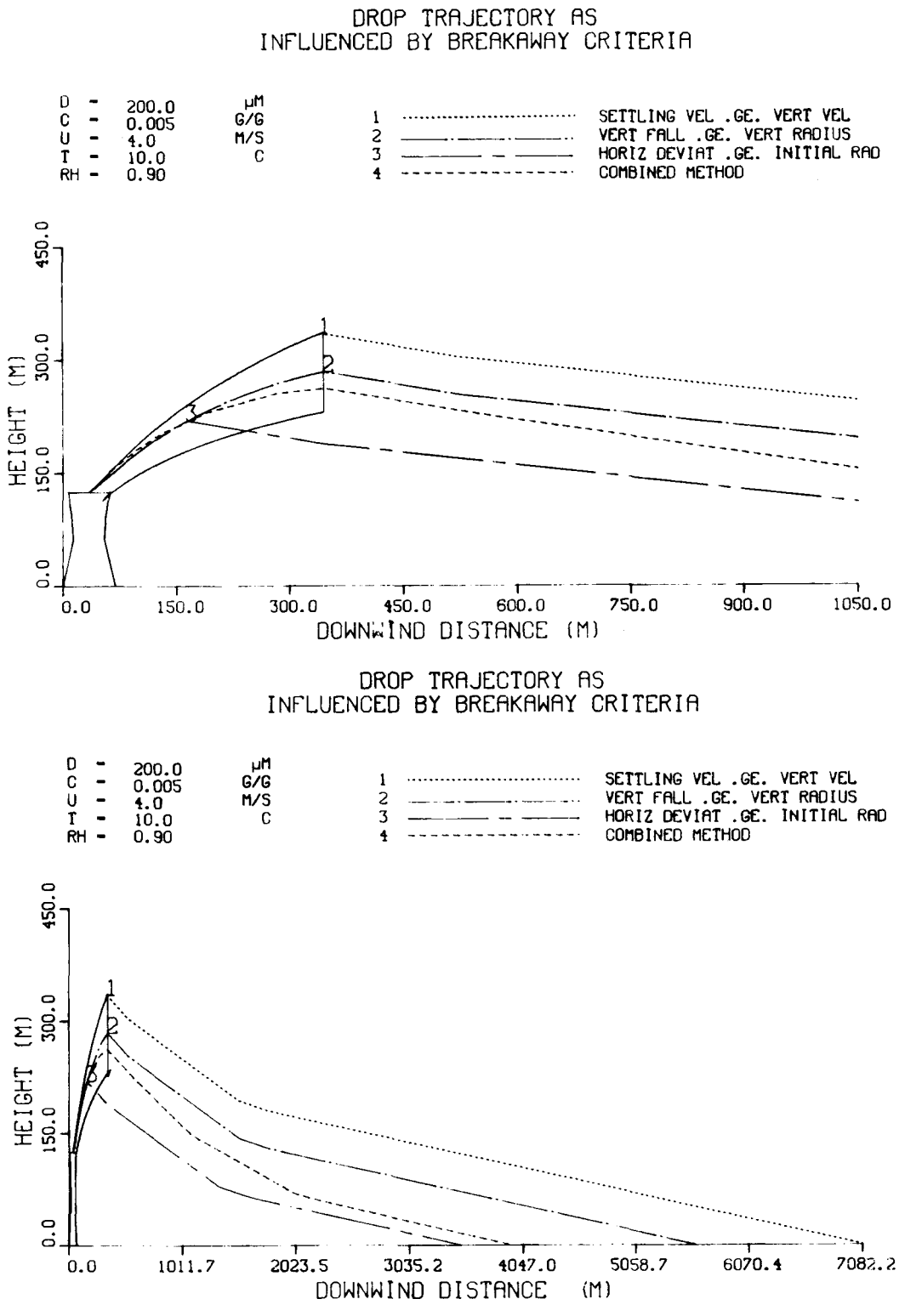

Figure 7-14. Comparison of Drop Trajectories Predicted with the ANL Drift Model under Different Breakaway Criteria

... RH=.90

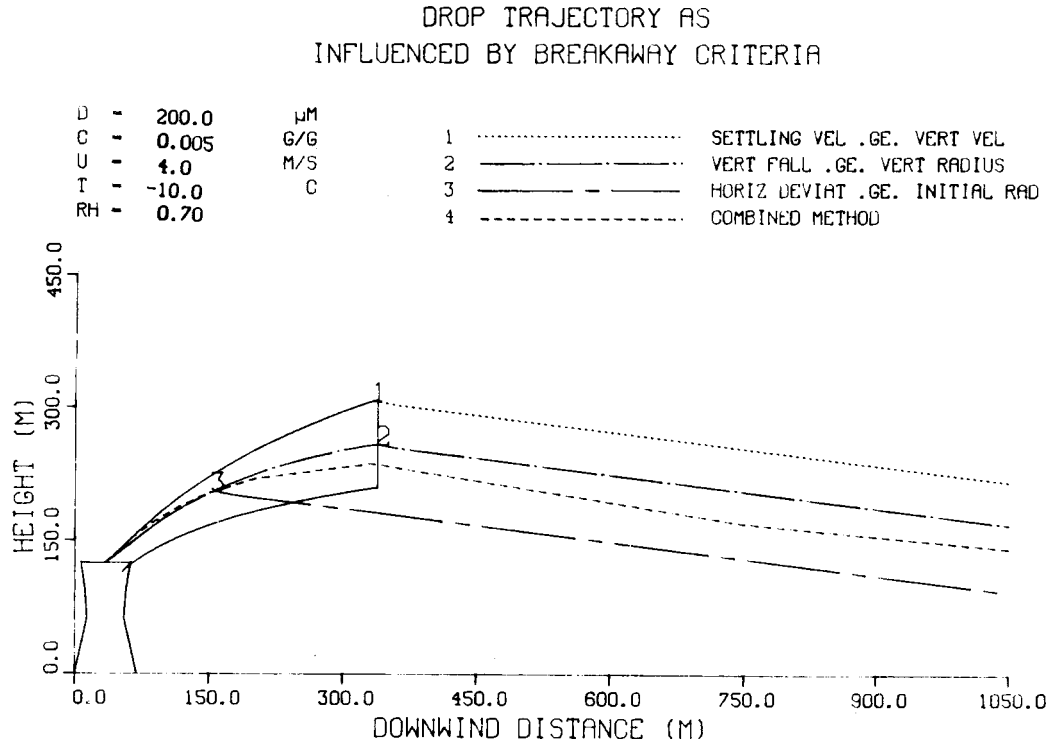

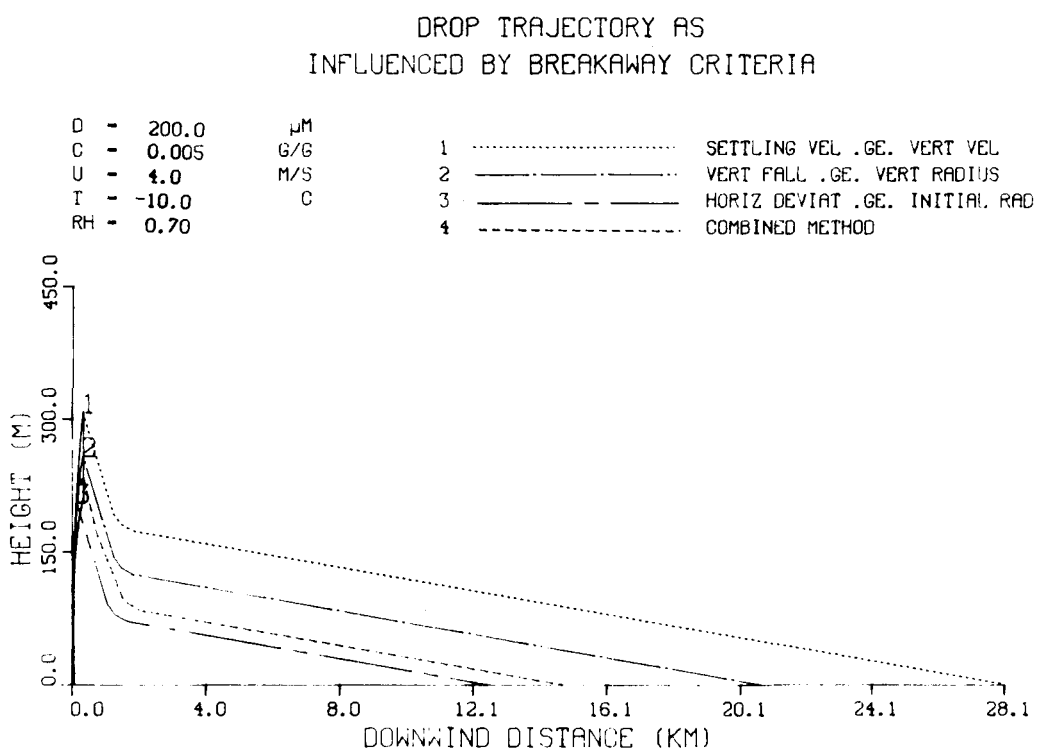

Figure 7-15. Comparison of Drop Trajectories Predicted with the ANL Drift Model under Different Breakaway Criteria

... T=-10°C

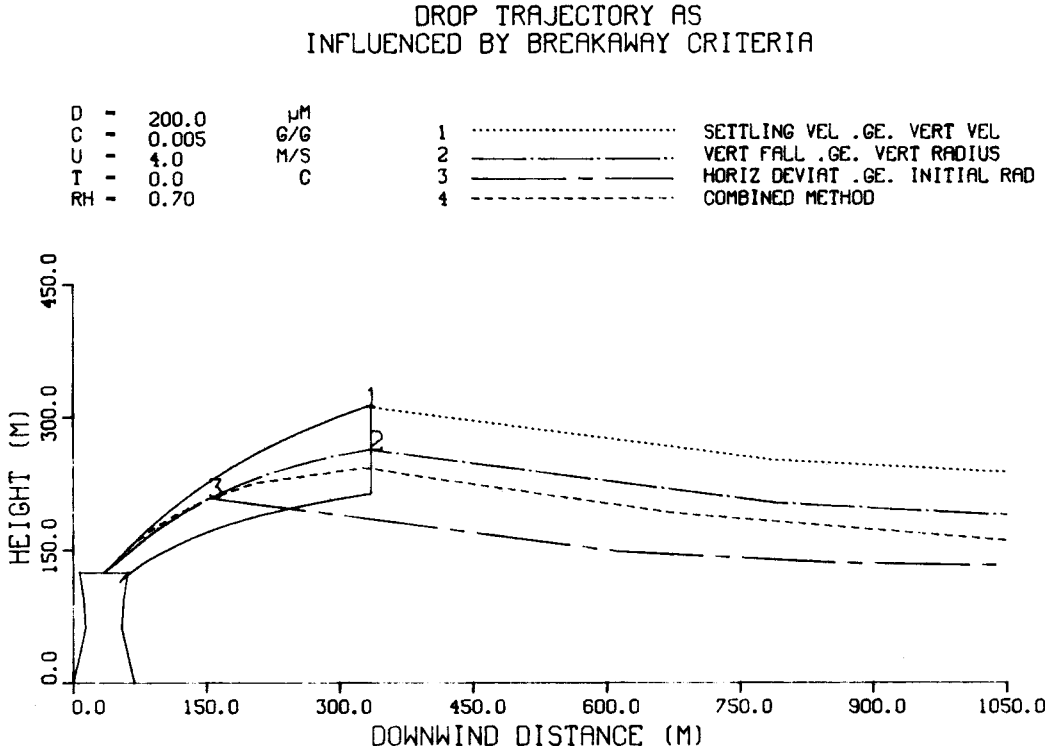

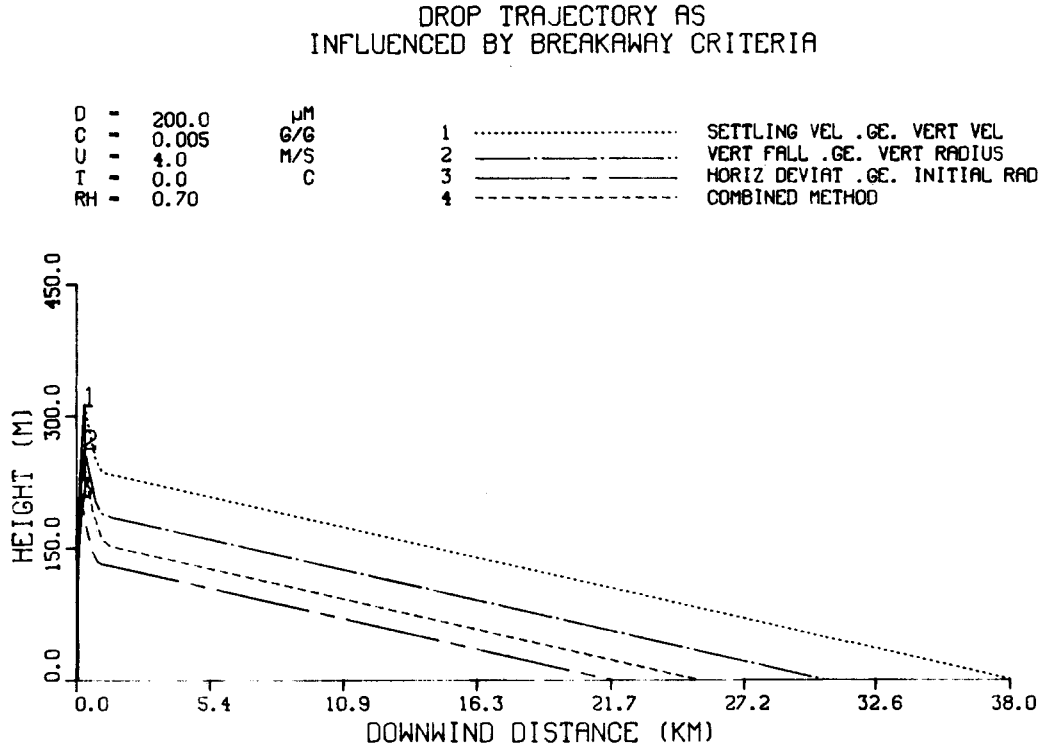

Figure 7-16. Comparison of Drop Trajectories Predicted with the ANL Drift Model under Different Breakaway Criteria

... T=0°C

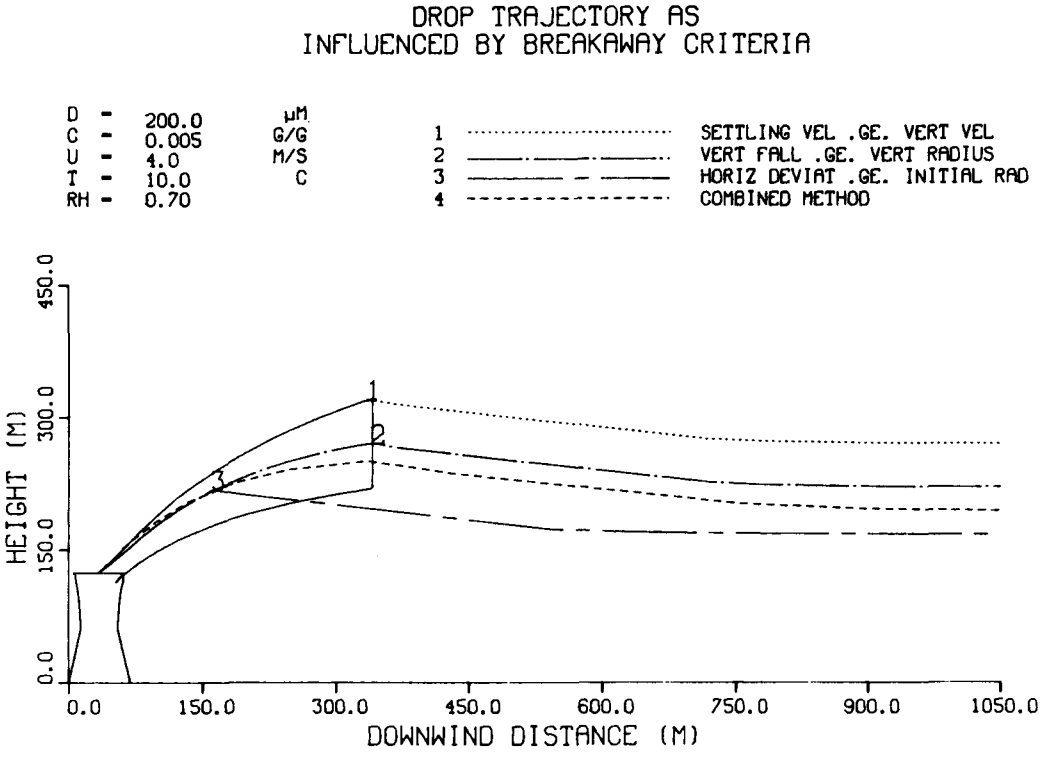

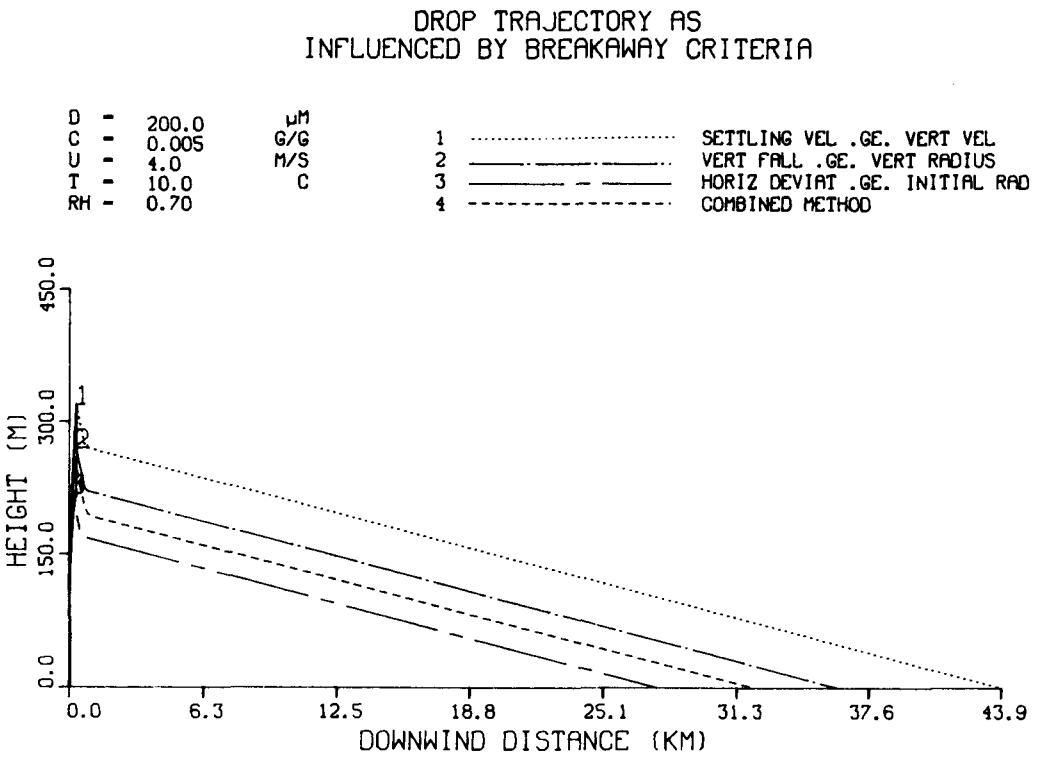

Figure 7-17. Comparison of Drop Trajectories Predicted with the ANL Drift Model under Different Breakaway Criteria

... Standard Case
... T=10°C

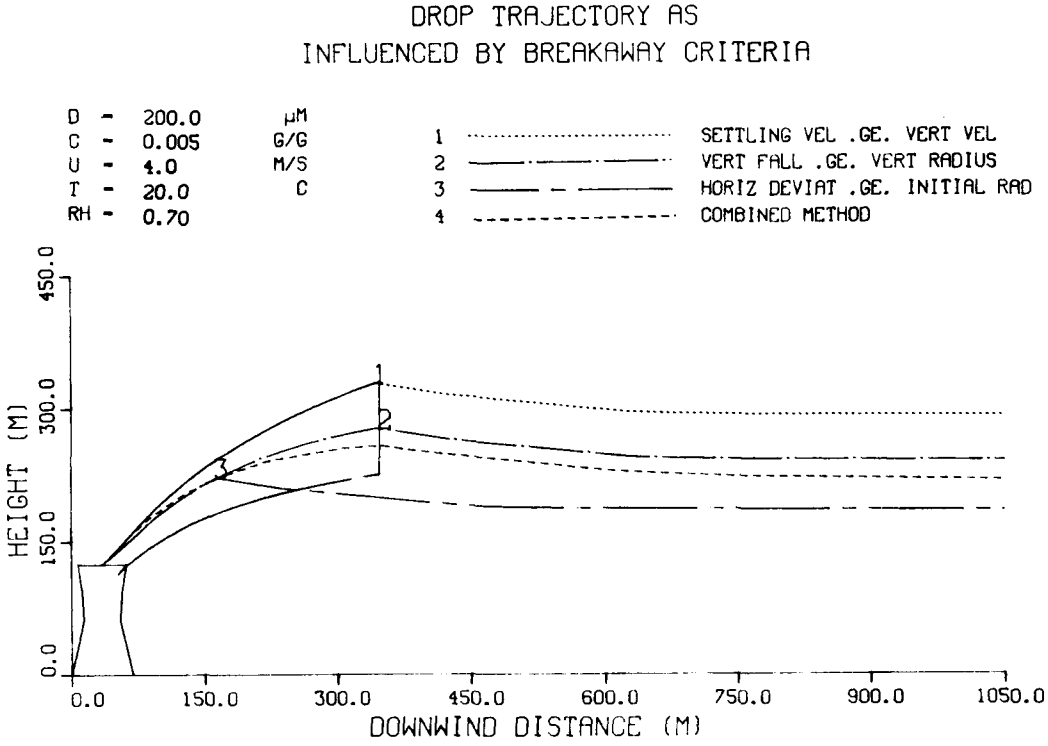

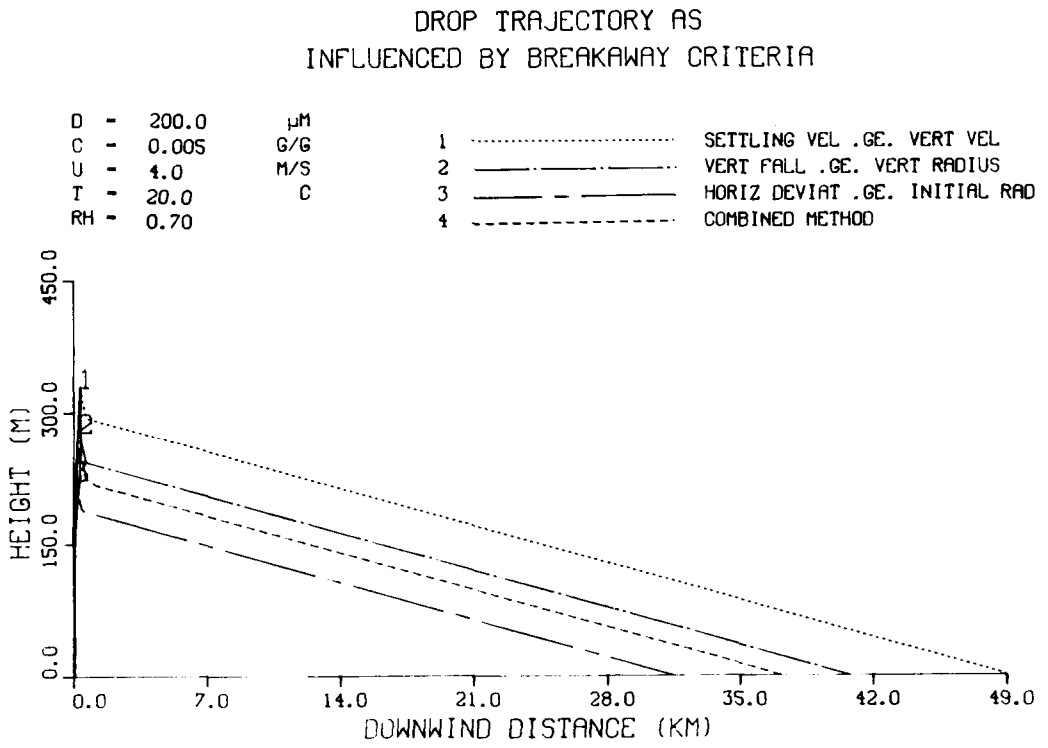

Figure 7-18. Comparison of Drop Trajectories Predicted with the ANL Drift Model under Different Breakaway Criteria

... T=20°C

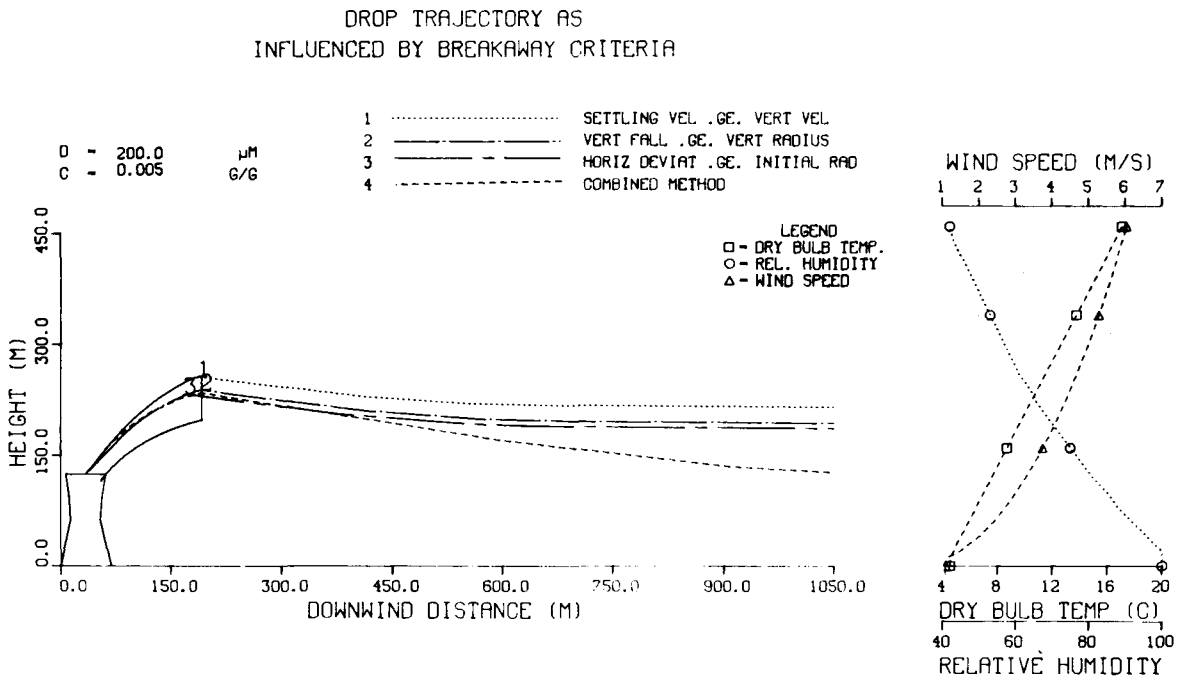

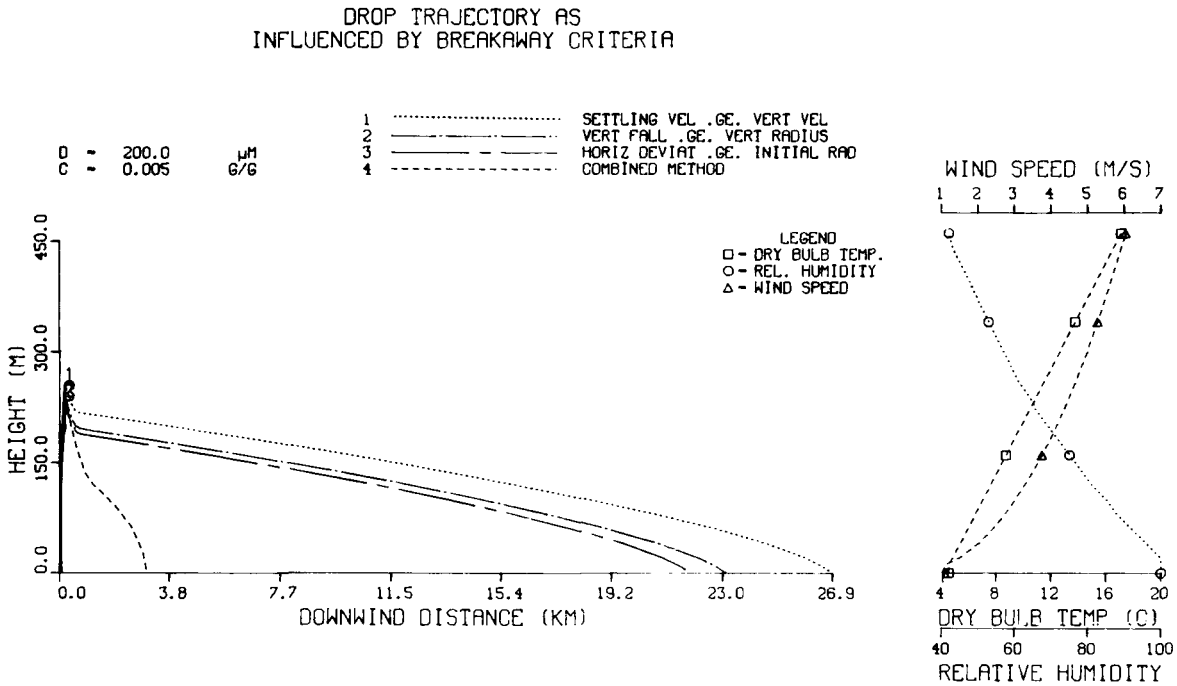

Figure 7-19. Comparison of Drop Trajectories Predicted with the ANL Drift Model under Different Breakaway Criteria

... Stable Conditions

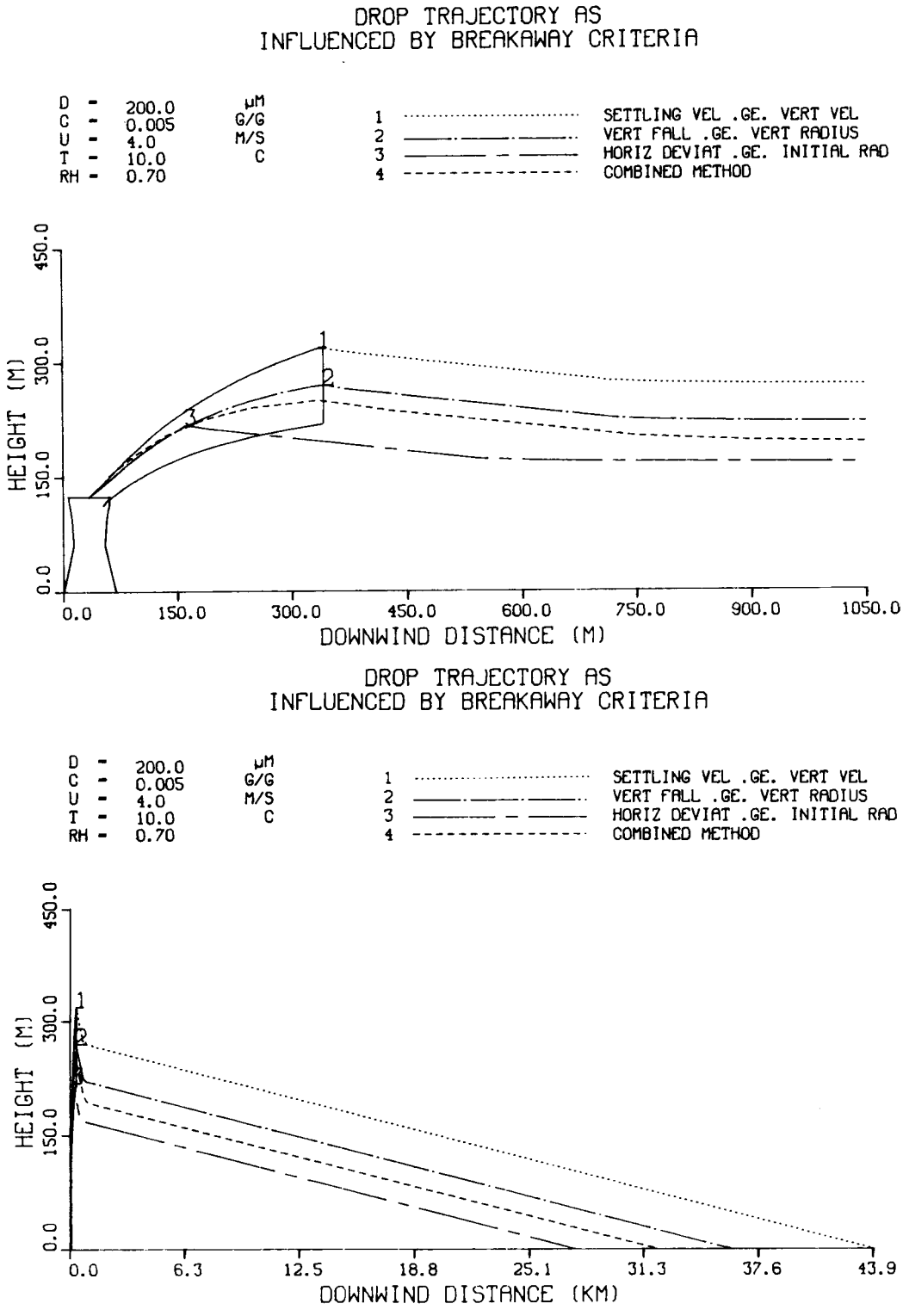

Figure 7-20. Comparison of Drop Trajectories Predicted with the ANL Drift Model under Different Breakaway Criteria

... Standard Case
... Constant Conditions

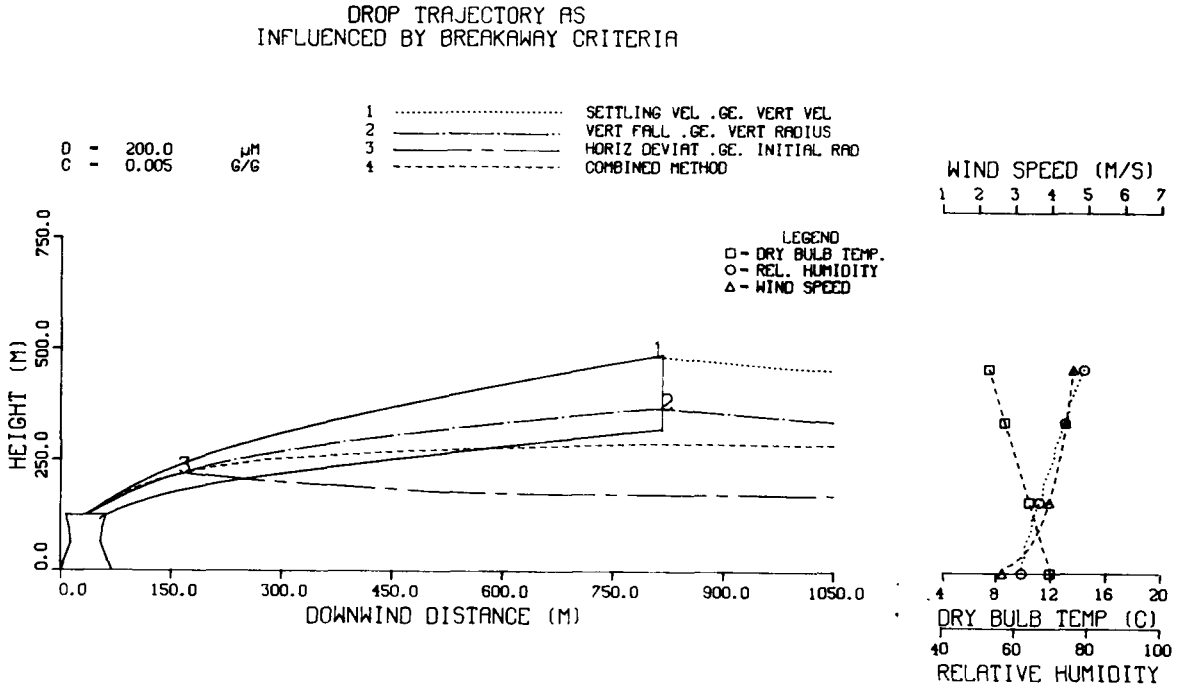

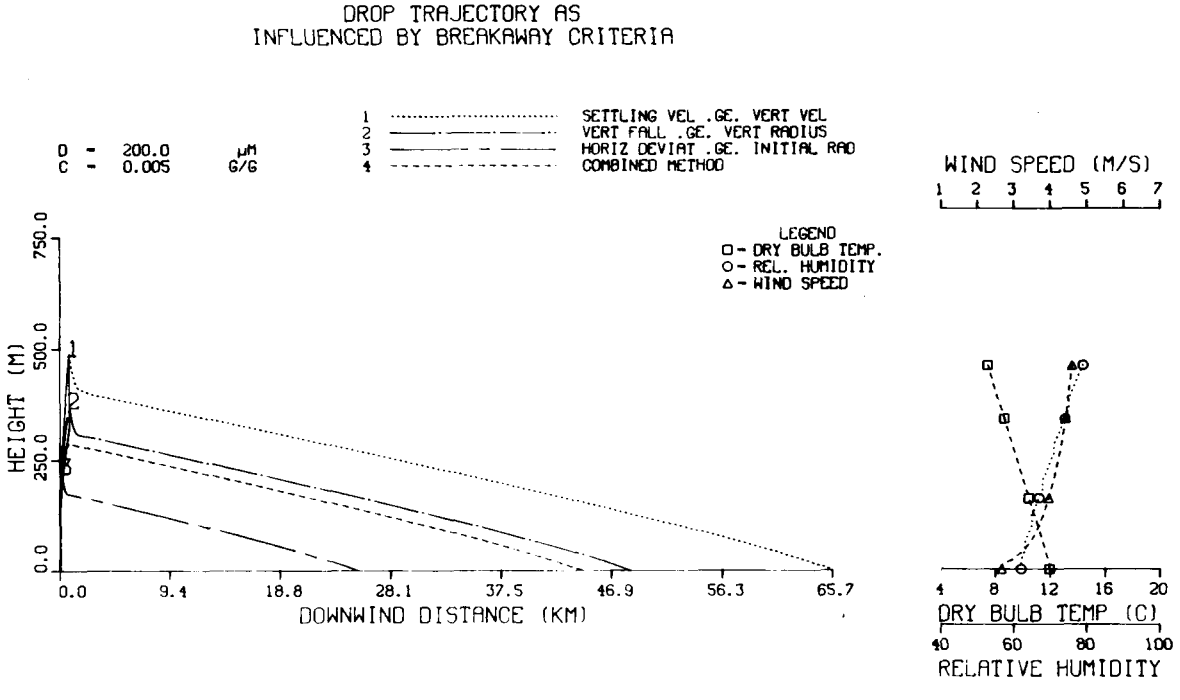

Figure 7-21. Comparison of Drop Trajectories Predicted with the ANL Drift Model under Different Breakaway Criteria

... Neutral Conditions

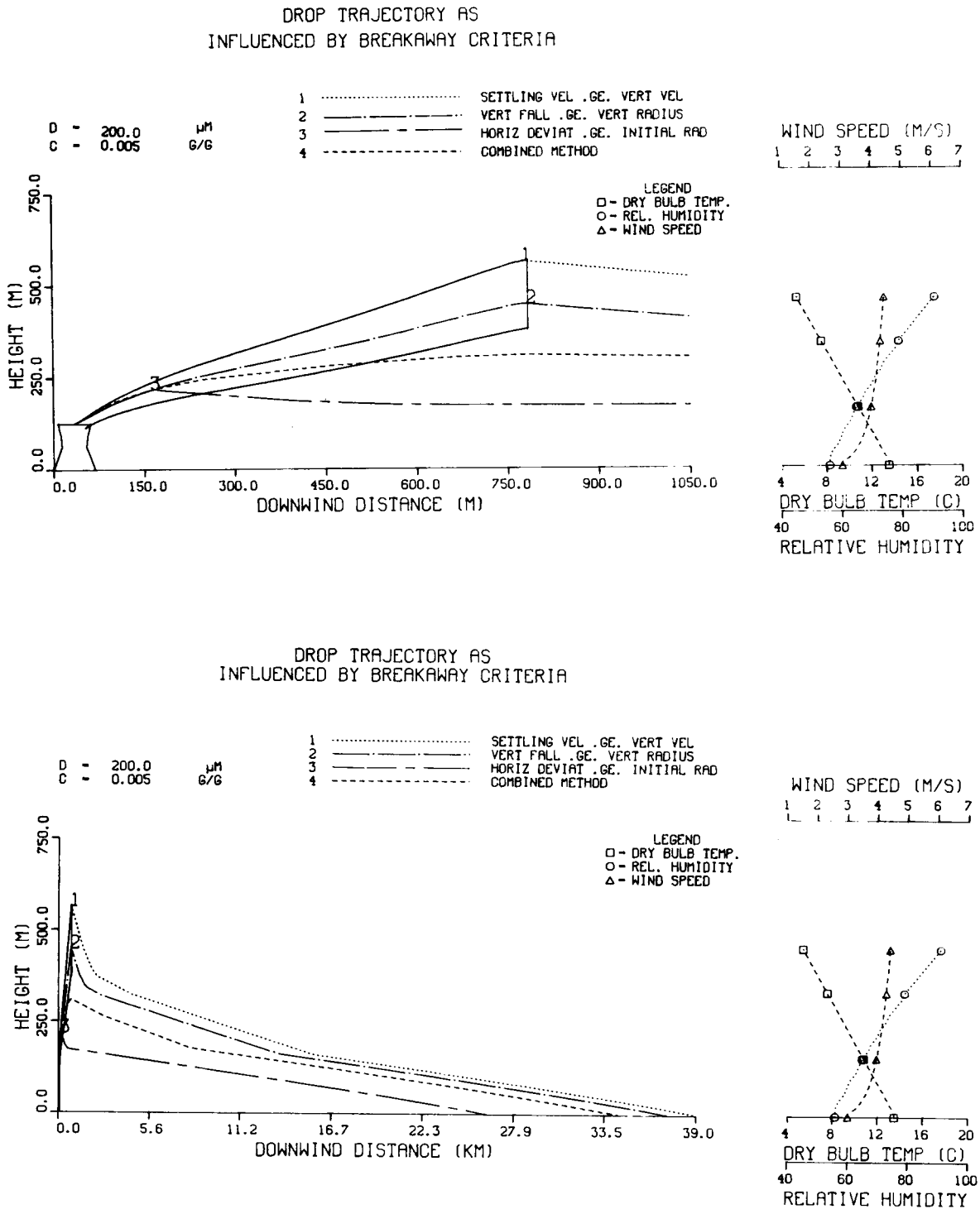

Figure 7-22. Comparison of Drop Trajectories Predicted with the ANL Drift Model under Different Breakaway Criteria

... Unstable Conditions

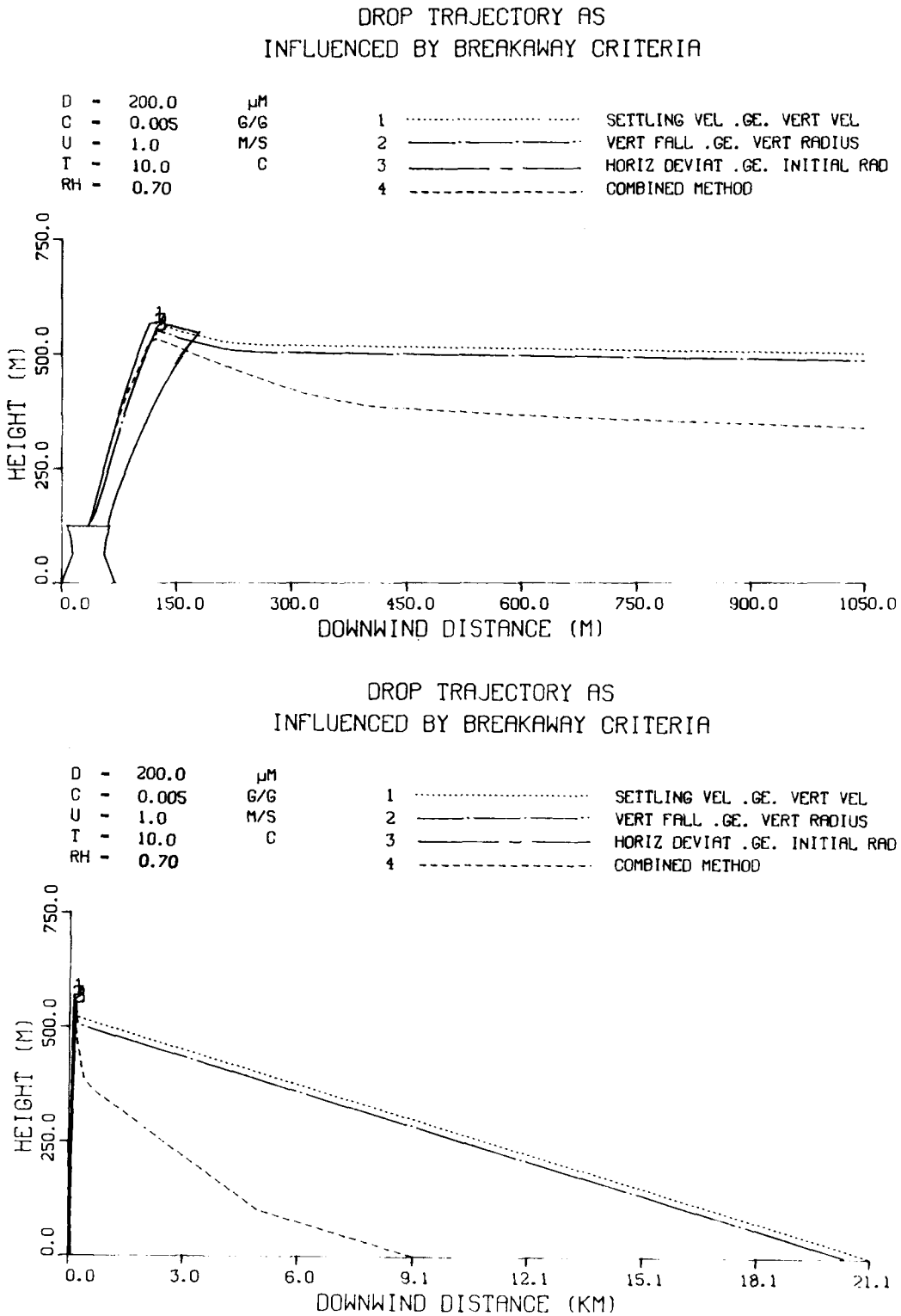

Figure 7-23. Comparison of Drop Trajectories Predicted with the ANL Drift Model under Different Breakaway Criteria

... U=1.0 m/s

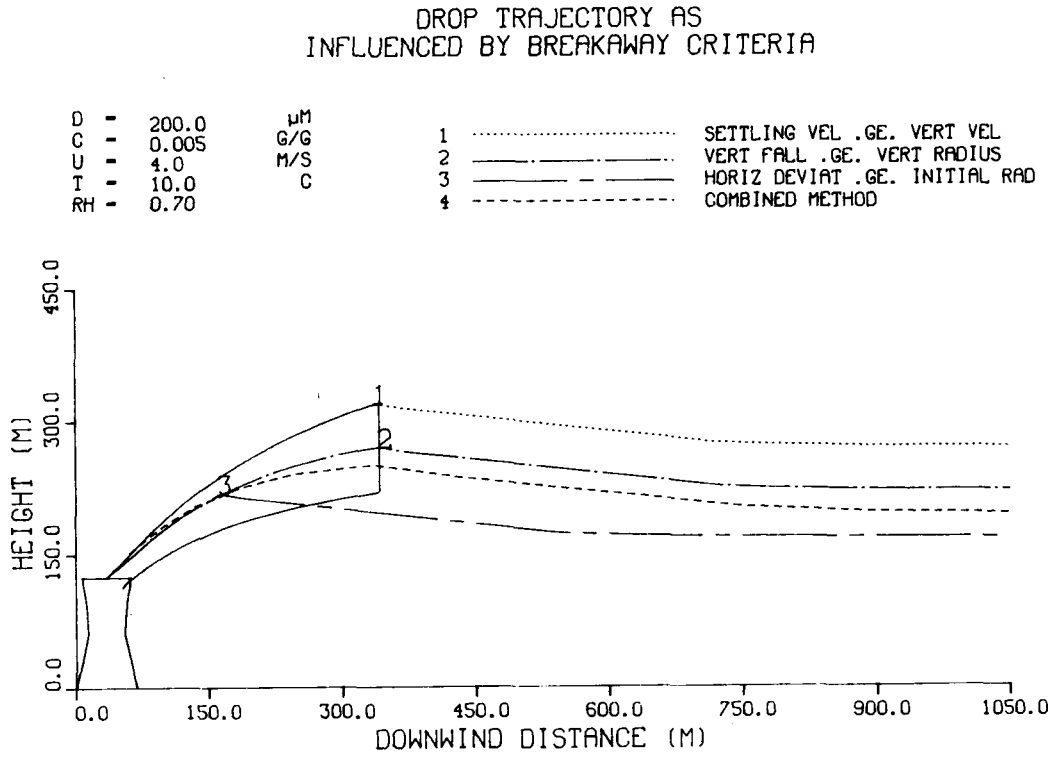

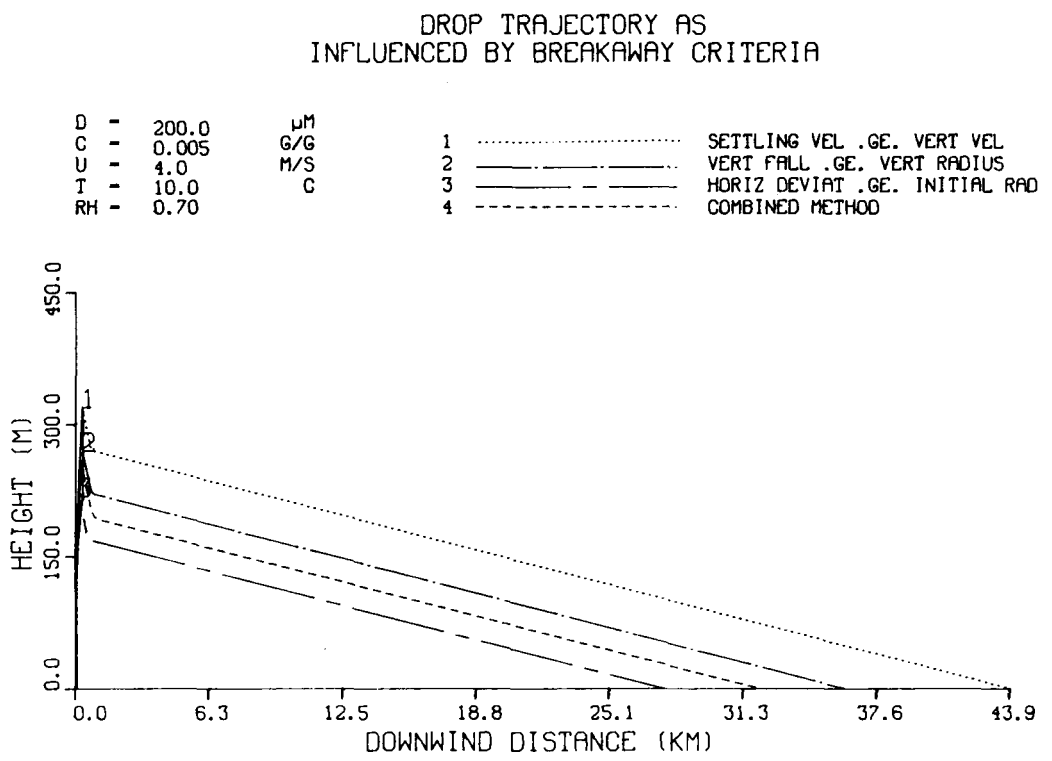

Figure 7-24. Comparison of Drop Trajectories Predicted with the ANL Drift Model under Different Breakaway Criteria

... Standard Case
... U=4 m/s

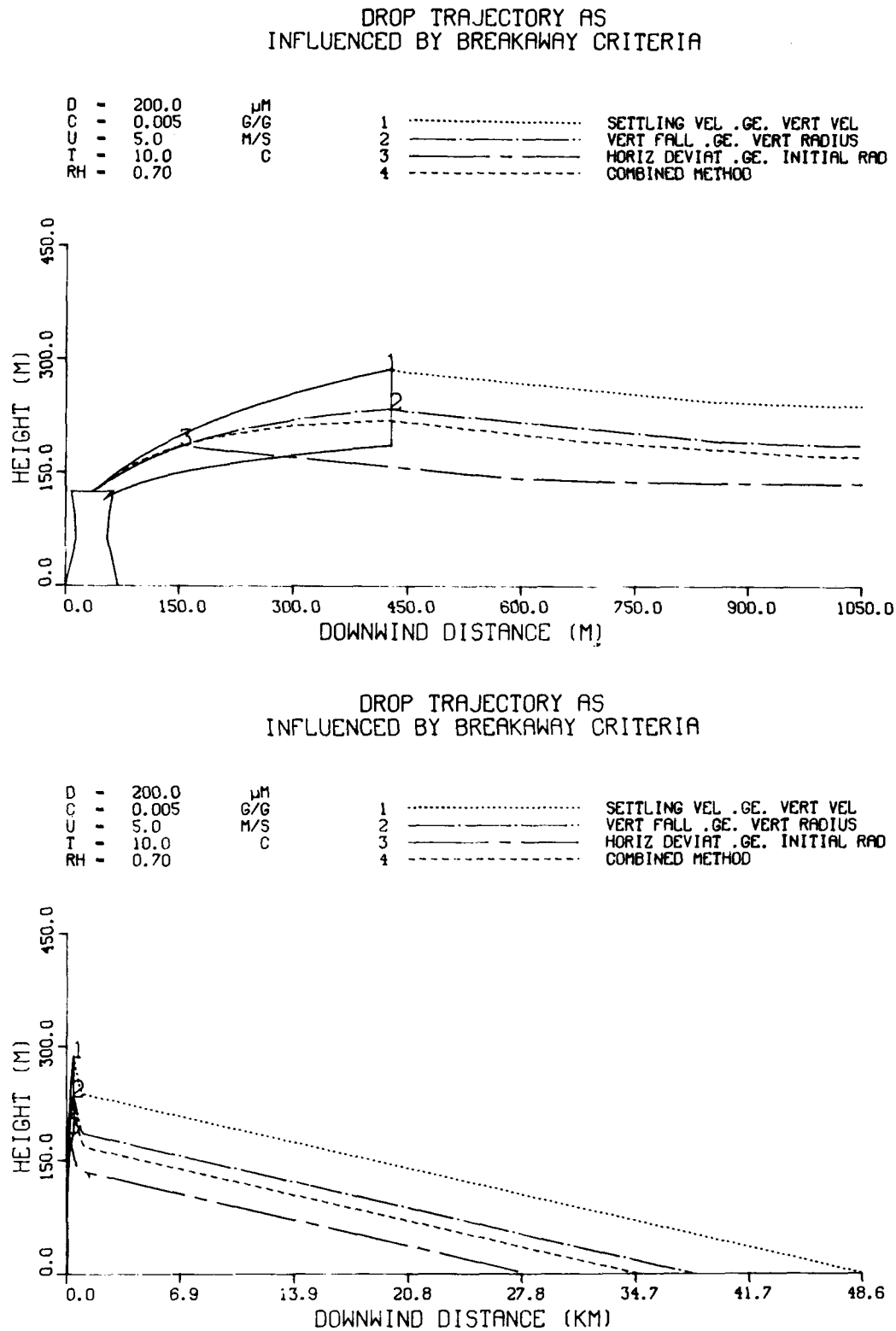

Figure 7-25. Comparison of Drop Trajectories Predicted with the ANL Drift Model under Different Breakaway Criteria

... U=5.0 m/s

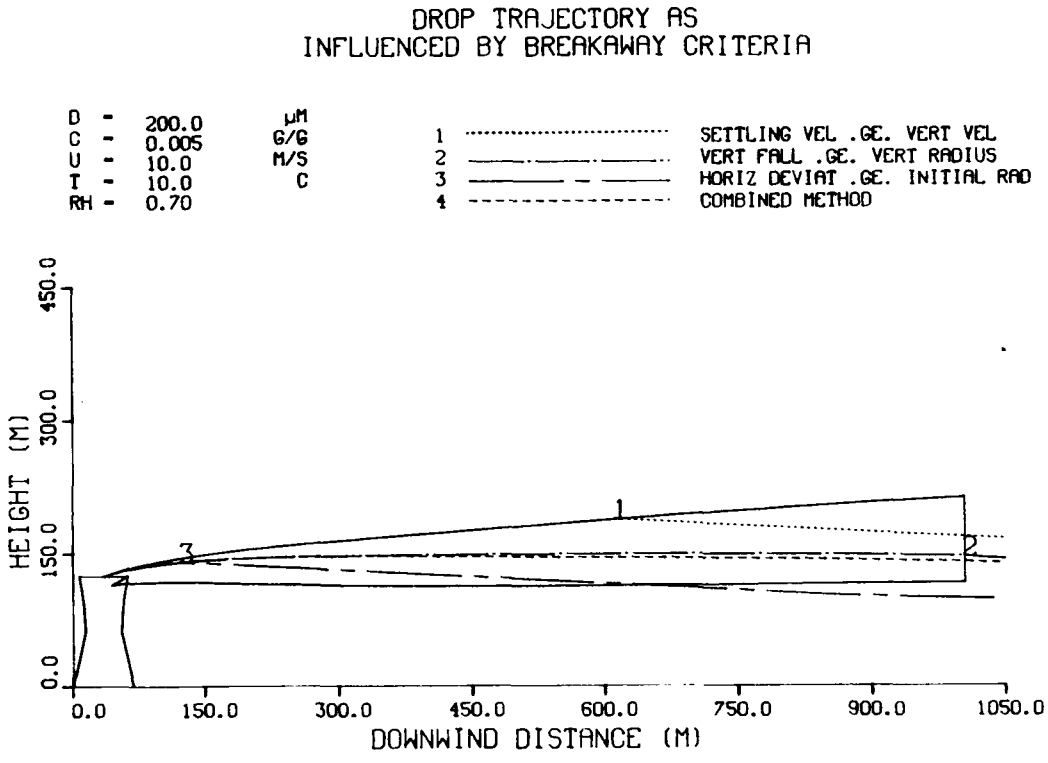

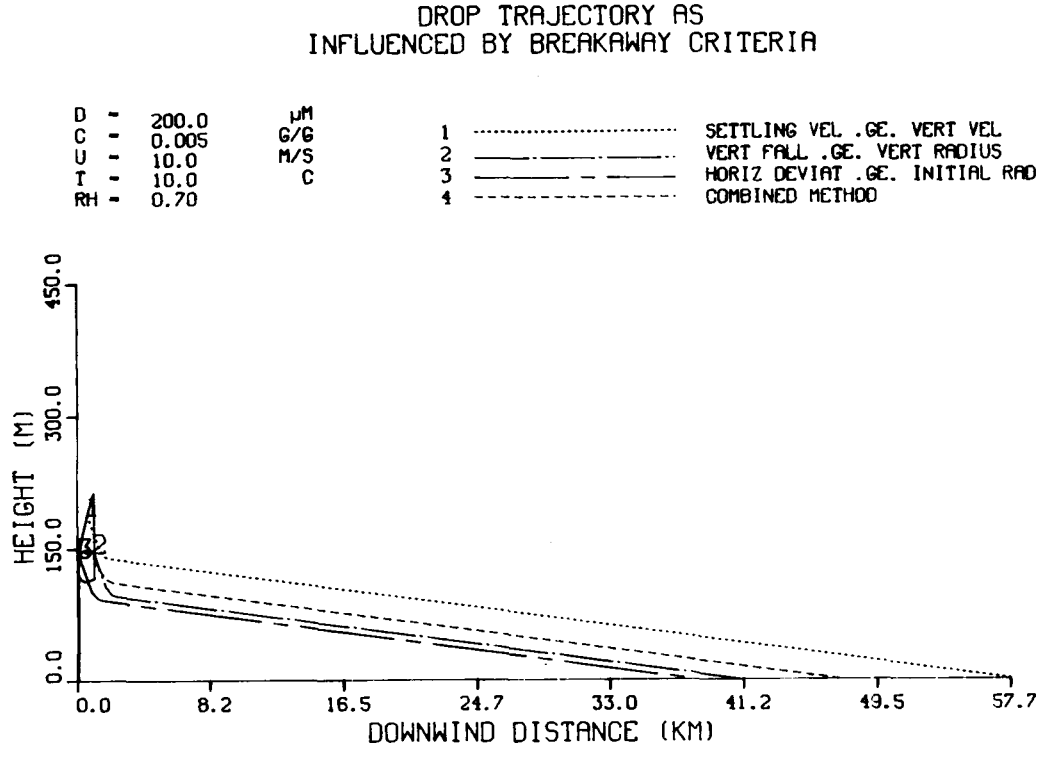

Figure 7-26. Comparison of Drop Trajectories Predicted with the ANL Drift Model under Different Breakaway Criteria

... U=10.0 m/s

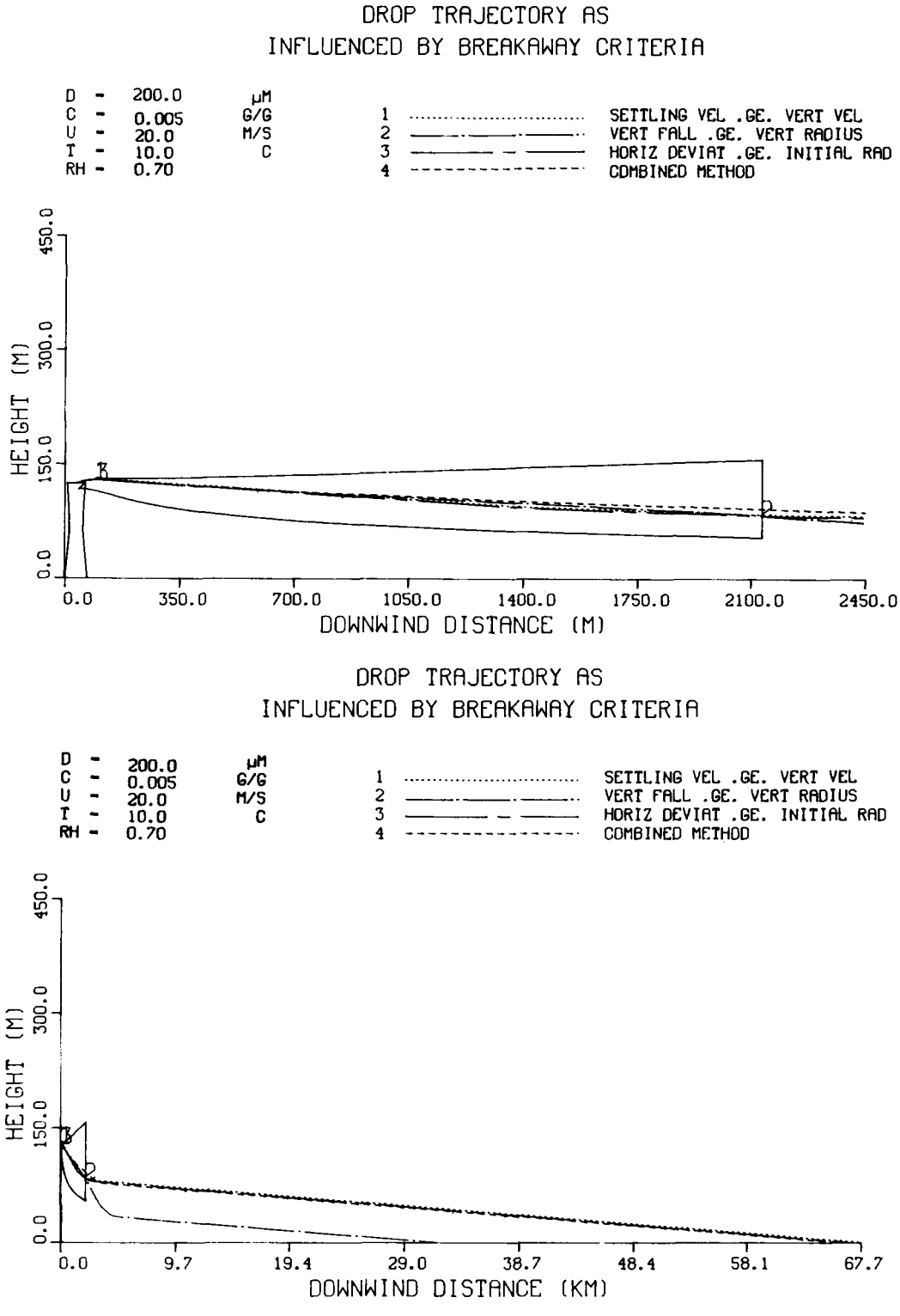

Figure 7-27. Comparison of Drop Trajectories Predicted with the ANL Drift Model under Different Breakaway Criteria

... U=20.0 m/s

Blank

Section 8

Performance of ANL Drift Model with Chalk Point Dye Study Data

At this point in the development of our drift model, we have combined our ANL single tower plume model with the University of Illinois droplet evaporation submodel through a choice of any of five breakaway methodologies. A ballistic method for deposition is used at present. The sensitivity study carried out in Section 7 revealed the kinds of differences that one can expect from the various choices in breakaway methods. Section 7 also provided some insight into which of the breakaway methods appeared to provide the most physically reasonable behavior when key parameters were varied.

This section provides an important test of the ANL model with the different breakaway methods. Here ANL Model predictions are presented for the 1977 Chalk Point Dye Study. Details of the field program, data analysis, and comparisons with predictions of existing models appears in Section 4 of this report. The reader is referred to that section for background details.

Results of predictions of our model (with the breakaway method alternatives) are compared to the 1977 Chalk Point Dye data in Table 8-1 and Figures 8-1 and 8-2. The method of preparing the ANL model's predictions follows the methodology presented in Section 4 for the remaining of the other 12 models tested in Section 4. We see from examining Table 8-1 and Figures 8-1 and 8-2 that Method 5 largely underpredicts drift deposition in nearly all categories except average diameter at 0.5 and 1.0 km distances. Method 3 largely overpredicts sodium deposition at 1.0 km. Methods 2 and 4 perform best with Method 4 providing overall better performance. Method 4 breakaway (also Method 2) in the ANL Model provides as good a performance as any of the other models tested in Section 4 of this report. In terms of model/data comparisons alone it is on par with the ESC/Schrecker Model which performed best with this 1977 Chalk Point data.

It is useful to view the ANL model/data comparisons just presented for this 1977 Chalk Point Dye data in the light of the model/data comparisons presented in Section 4 for 12 existing models. Here we present a simple statistic as a simple measure of model performance: a model succeeds in its prediction of drift at a given sampler if that prediction is within a factor of three of the measured data. Success within a factor of three means that the prediction is within the range encompassed by one-third and three times the measured value. Samples where either the measured value is zero or the model prediction is zero are not counted. Other statistics can be used but it is thought that this simple one provides a quick assessment of comparative model performances. The same statistic is used with some success in Volume 5 to assess the performance of the ANL multiple-source drift model with field data.

Tables 8-2 to 8-4 present the results of our factor-of-three comparisons. Success within a factor-of-three is indicated with a "Y" (yes) while failure is represented with an "N" (no). A "-" refers to either (a) a prediction or data value of zero, or (b) the inability of the model to predict that quantity used for comparison purposes. Comparison tables are presented for sodium deposition flux, drop number flux, average diameter, and liquid mass deposition flux. If we do not distinguish between successes and failures among different deposition indicators, we arrive at the following dichotomy in model performances

1. only one failure in prediction over entire measured data:
   ANL Model (Breakaway Criterion #2)
   ANL Model (Breakaway Criterion #4)
   Wolf I
   Wolf II
2. two failures in prediction over entire measured data:
   Hosler-Pena-Pena (ANL)
   MRI
   Wigley-Slawson
   Wigley-Slawson (profiles)
3. three failures in prediction over entire measured data:
   ANL Model (Breakaway Criterion #1)
   ANL Model (Breakaway Criterion #3)
   ANL Model (Breakaway Criterion #5)
   ESC Schrecker
   ESC Schrecker (limited)

Clearly, this statistic of model performance as applied to the 1977 Chalk Point data is a rather crude one and does not underscore the important differences that exist among the models. However, it does identify the better performing models and they are the ones we expected to perform well from analysis of the graphs of model/data comparisons. We know that the ESC/Schrecker (limited) model is not as

theoretically sound as the original ESC/Schrecker Model. Theoretical considerations indicate the superiority of the Wigley-Slawson (profiles) version as compared to the Wigley-Slawson model. The MRI and Wolf II models have significant theoretical limitations (1). As a result, we reaffirm our conclusions as to the identity of the superior drift models and the good performance of the ANL Model with these 1977 Chalk Point Dye data.

It must be recognized that this data set does not provide a general test of models since (a) it is only one set of measurements, and (b) the data represent very special conditions: moderate-to-large wind speed, high ambient relative humidity, and strongly stable ambient stratification. Under these specialized conditions, a large portion of a drift model becomes untested. For instance, the above ambient conditions imply a minimum effect of evaporation (due to high ambient relative humidity) and ambient turbulence effects (due to the closeness of the samples to the tower and the large drops that must strike there).

These data also represent the only high quality drift data available from a single natural-draft tower. Consequently, true validation for any of these models requires a much larger quantity of high-quality field data taken under a variety of ambient and tower conditions. Due to the unavailability of this kind of data, we must rely heavily on models with more correct theoretical assumptions. We can only say then that the ANL model (with breakaway Method 2 or 4) is of stronger theoretical development in terms of plume rise and droplet evaporation submodels than the models we previously evaluated in Sections 2-4 and therefore can be generally expected to provide better performances in new applications with new data. The final judgment on our model can be made only upon the acquisition of high-quality data taken under widely-varying conditions and the testing of our model with that data. Until then, we must be satisfied with a model with as strong a theory as possible but with validation limited to available data.

REFERENCES

1. A. J. Policastro, W. E. Dunn, M. L. Breig, J. P. Ziebarth. Evaluation of Mathematical Models for Characterizing Plume Behavior from Cooling Towers. Vol. 2. Salt Drift Deposition from Natural Draft Cooling Towers. U.S. Nuclear Regulatory Commission Report NUREG/CR-1591. February 1979.

Sampler		JHU Dye Data June 16-17, 1977 Sodium Deposition Flux Tower mg/m^2-4 Hours					
Distance (m)	Dir.	OBS.	1	2	3	4	5
1000	340	1.4 ± .4	.68	1.15	3.12	1.40	1.20
1000	342.5	3.6 ± .9	.69	1.17	3.16	1.94	1.20
1000	345.0	2.4 ± .4	1.5	2.19	6.21	3.31	2.00
1000	347.5	3.3 ± .8	2.6	2.86	7.82	4.20	2.79
1000	350.0	2.4 ± 1.2	2.7	2.28	6.10	3.10	2.25
1000	352.5	2.4 ± 1.2	2.7	2.29	6.14	3.10	2.26
1000	355.0	1.2 ± .3	3.3	2.86	6.86	3.73	2.59
1000	357.5	1.2 ± .3	2.5	1.73	3.66	2.24	1.78
1000	0.0	1.4 ± .4	.83	0.66	1.25	0.83	0.58
1000	5.0	.51 ± .1	.67	1.02	2.31	1.36	0.75
1000	7.5	0.0	1.12	1.72	3.40	2.29	1.27
1000	10.0	.55 ± .2	1.05	1.71	4.00	2.29	1.27

Table 8-1.

Comparison of predictions of ANL drift model to ground-level measurements of sodium deposition flux, number drop deposition flux, average deposited diameter, and liquid mass deposition flux testing five breakaway methods (see text)...cooling tower contribution at JHU samplers.

Sampler		JHU Dye Data June 16-17, 1977 Tower					
Distance (m)	Dir.	OBS.	1	2	3	4	5
# Drops/m^2-Hour							
500	355	6300	3126	2607	8777	3006	680
1000	350	7208	2771	2368	16900	3791	4627
Average Diameter (μm)							
500	355	310	438	457	331	442	349
1000	350	241	288	291	198	262	213
Liquid Mass Deposition Flux mg/m^2-4 Hours							
500	355	393	215	182	163	190	17
1000	350	204	47	44	80	45	16

Sampler		JHU Dye Data June 16-17, 1977 Sodium Deposition Flux Tower mg/m^2-4 Hours					
Distance (m)	Dir.	OBS.	1	2	3	4	5
500	330	1.9 ± .5	0.0	0.00	0.00	0.00	0.00
500	335	2.7 ± .7	.37	0.40	0.71	0.52	0.15
500	340	4.7 ± 2.1	3.7	3.97	7.03	5.14	1.49
500	345	8.9 ± 2.6	6.2	6.55	11.07	8.40	2.31
500	350	10.9 ± 2.7	6.9	7.26	10.11	8.75	1.32
500	355	7.7 ± 2.5	9.4	9.30	13.20	10.90	1.39
500	0.	6.1 ± 2.4	1.5	1.47	1.90	1.66	0.07
500	5.	1.9 ± .8	2.0	2.28	4.60	3.00	0.44

Table 8-2.

Summary Table showing whether model predictions of sodium deposition flux from 12 existing models and 5 versions of the ANL model are within a factor of 3 of field data measured at Chalk Point (500 m distance from the tower).

Sampler		JHU Dye Data June 16-17, 1977 Sodium Deposition Flux Tower																	
		Existing Models													ANL Model with Breakaway Criterion #				
Distance (m)	Dir.	1	2	3	4	5	6	7	8	9	10	11	12		1	2	3	4	5
500	330	-	-	-	-	-	-	-	-	-	-	-	-		-	-	-	-	-
500	335	Y	Y	N	Y	N	-	Y	Y	Y	Y	Y	Y		N	N	Y	N	N
500	340	Y	Y	N	Y	N	-	Y	Y	Y	Y	Y	Y		Y	Y	Y	Y	Y
500	345	Y	Y	N	Y	Y	-	Y	Y	Y	Y	Y	Y		Y	Y	Y	Y	Y
500	350	Y	Y	N	Y	N	-	Y	Y	Y	Y	Y	Y		Y	Y	Y	Y	Y
500	355	Y	Y	Y	Y	Y	-	Y	Y	Y	Y	Y	Y		Y	Y	Y	Y	N
500	0.0	Y	Y	Y	Y	Y	-	Y	Y	Y	Y	Y	Y		Y	Y	Y	Y	N
500	5.0	Y	Y	Y	Y	Y	-	Y	Y	Y	Y	Y	Y		Y	Y	Y	Y	Y

meaning of symbols: Y = model prediction is within a factor of 3 of observation
N = model prediction is not within a factor of 3 of deposition
- = model prediction or observation is zero; or model cannot predict this quantity.

LEGEND
1. Hanna
2. Hosler-Pena-Pena
3. Overcamp-Israel
4. Wigley-Slawson (profiles)
5. Slinn I
6. Slinn II
7. Wolf I
8. Wolf II
9. ESC/Schrecker
10. MRI
11. Wigley-Slawson
12. ESC/Schrecker (limited)

Table 8-3.

Summary Table showing whether model predictions of sodium deposition flux from 12 existing models and 5 versions of the ANL model are within a factor of 3 of field data measured at Chalk Point (1000 m distance from the tower).

Sampler		JHU June 16-17, 1977 Sodium Deposition Flux Tower																
		Existing Models												ANL Model with Breakaway Criterion #				
Distance (m)	Dir.	1	2	3	4	5	6	7	8	9	10	11	12	1	2	3	4	5
1000	340	Y	Y	Y	Y	Y	Y	Y	Y	Y	Y	Y	Y	Y	Y	Y	Y	Y
1000	342.5	N	Y	Y	Y	Y	N	Y	Y	N	Y	N	Y	N	Y	Y	Y	Y
1000	345.0	Y	Y	Y	Y	Y	N	Y	Y	Y	Y	Y	Y	Y	Y	Y	Y	Y
1000	347.5	Y	Y	Y	Y	Y	N	Y	Y	Y	Y	Y	Y	Y	Y	Y	Y	Y
1000	350.0	Y	Y	Y	Y	N	N	Y	Y	Y	Y	Y	Y	Y	Y	Y	Y	Y
1000	352.5	Y	Y	Y	Y	Y	N	Y	Y	Y	Y	Y	Y	Y	Y	Y	Y	Y
1000	355.0	Y	Y	Y	Y	N	N	N	Y	Y	Y	Y	N	Y	Y	N	Y	Y
1000	357.5	Y	Y	Y	Y	N	N	Y	Y	Y	Y	Y	N	Y	Y	Y	Y	Y
1000	0.0	Y	Y	Y	Y	N	N	Y	Y	Y	Y	Y	N	Y	Y	Y	Y	Y
1000	5.0	N	N	N	Y	Y	N	Y	Y	Y	Y	Y	Y	Y	Y	N	Y	Y
1000	7.5	-	-	-	-	-	-	-	-	-	-	-	-	-	-	-	-	-
1000	10.0	-	-	-	-	-	-	-	-	-	-	-	-	Y	Y	N	Y	Y

LEGEND

1. Hanna
2. Hosler-Pena-Pena
3. Overcamp-Israel
4. Wigley-Slawson (profiles)
5. Slinn I
6. Slinn II
7. Wolf I
8. Wolf II
9. ESC/Schrecker
10. MRI
11. Wigley-Slawson
12. ESC/Schrecker (limited)

meaning of symbols: Y = model prediction is within a factor of 3 of observation
N = model prediction is not within a factor of 3 of deposition
- = model prediction or observation is zero; or model cannot predict this quantity

Table 8-4

Summary Table showing whether model predictions of sodium deposition flux from 12 existing models and 5 versions of the ANL model are within a factor of 3 of field data measured at Chalk Point.

Sampler		JHU Dye Data June 16-17, 1977 Tower																
		Existing Models												ANL Model with Breakaway Criterion #				
Distance (m)	Dir.	1	2	3	4	5	6	7	8	9	10	11	12	1	2	3	4	5
		# Drops/m^2-hour																
500	355	N	Y	N	Y	Y	-	Y	Y	Y	N	Y	Y	Y	Y	Y	Y	N
1000	350	N	N	N	N	N	-	Y	Y	N	N	N	Y	N	Y	Y	Y	Y
		Average Diameter																
500	355	Y	-	Y	Y	Y	-	Y	Y	Y	-	Y	Y	Y	Y	Y	Y	Y
1000	350	Y	-	Y	Y	Y	-	Y	Y	Y	-	Y	Y	Y	Y	Y	Y	Y
		Liquid Mass Deposition Flux																
500	355	Y	-	Y	Y	N	-	Y	Y	Y	-	Y	Y	Y	Y	Y	Y	N
1000	350	N	-	Y	Y	N	-	Y	N	N	-	Y	Y	N	N	Y	N	N

LEGEND

1. Hanna
2. Hosler-Pena-Pena
3. Overcamp-Israel
4. Wigley-Slawson (profiles)
5. Slinn I
6. Slinn II
7. Wolf I
8. Wolf II
9. ESC/Schrecker
10. MRI
11. Wigley-Slawson
12. ESC/Schrecker (limited)

meaning of symbols: Y = model prediction is within a factor of 3 of observation
N = model prediction is not within a factor of 3 of deposition
- = model prediction or observation is zero or model cannot predict this quantity

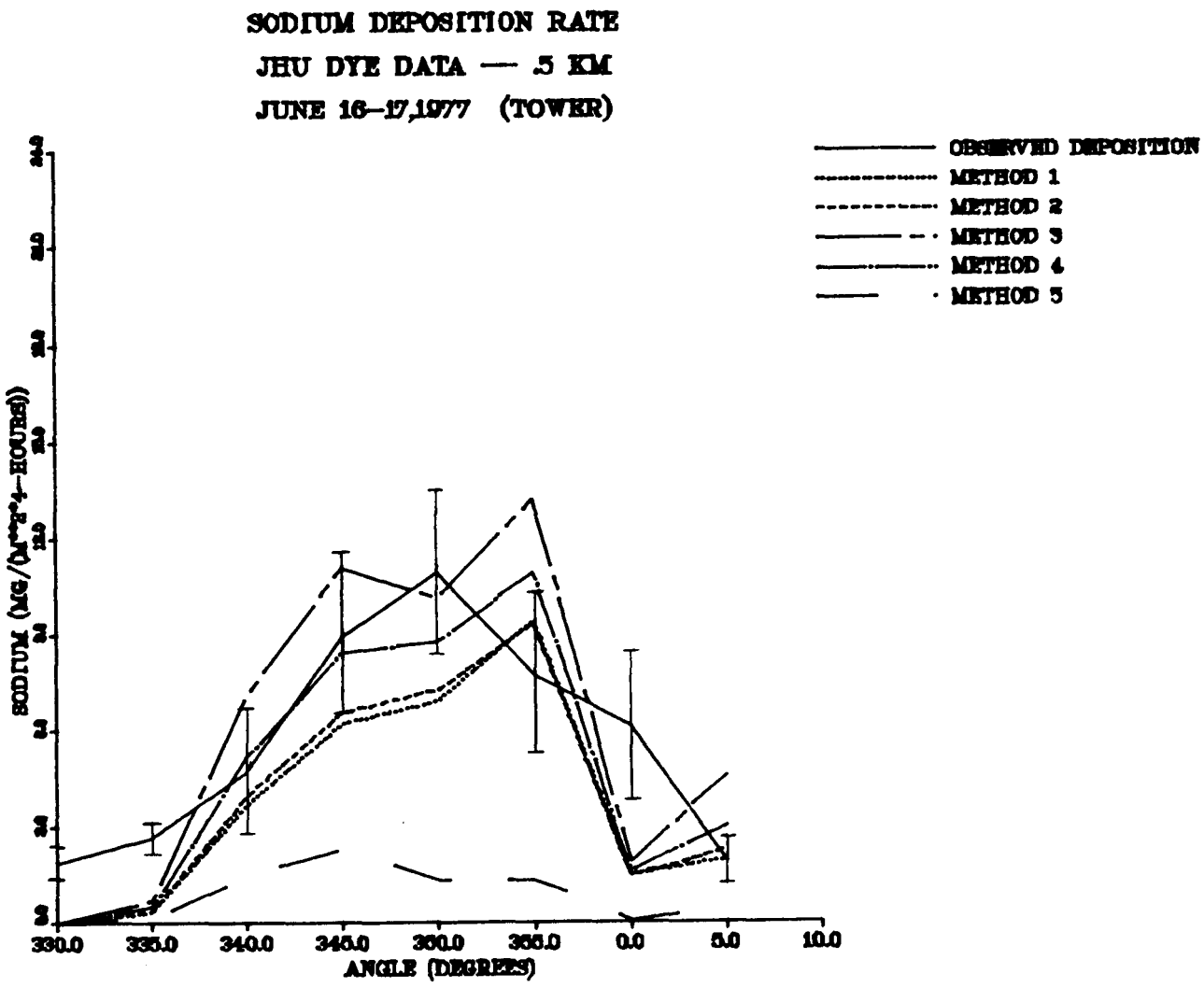

Figure 8-1. Comparison of ANL Model Predictions of Drift Deposition to Sodium Deposition Flux Measurements at Fixed Locations Along a 0.5 km Arc. (Methods 1-5 refer to Drop Breakaway Assumptions Described in Text.)

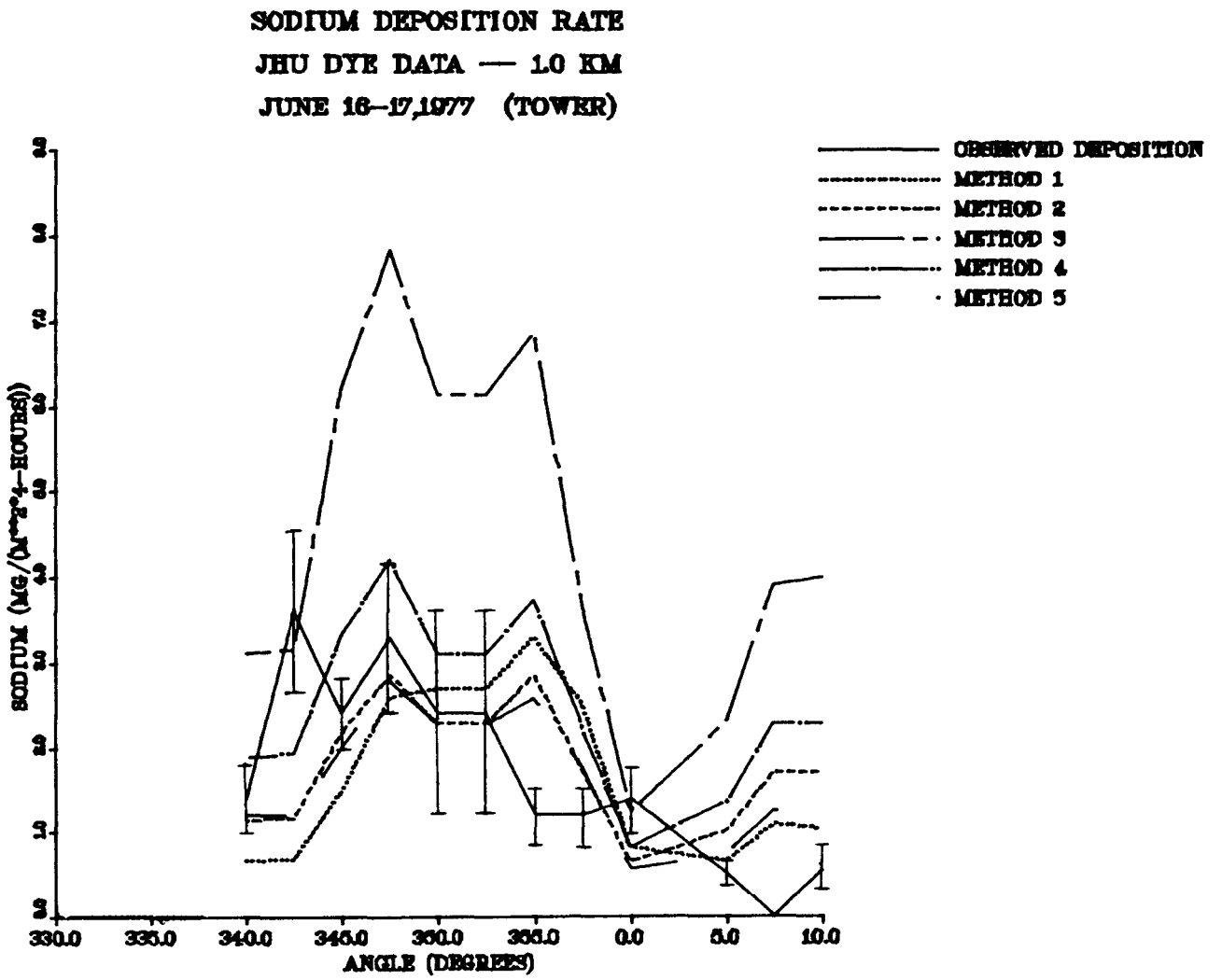

Figure 8-2. Comparison of ANL Model Predictions of Drift Deposition to Sodium Deposition Flux Measurements at Fixed Locations Along a 1.0 km Arc. (Methods 1-5 refer to Drop Breakaway Assumptions Described in Text.)